processes

Special Issue Reprint

Extraction, Utilization and Conversion of Woody Biomass

Edited by
Ali Umut Şen, Catarina Pereira Nobre and Terencio Rebello de Aguiar Junior

mdpi.com/journal/processes

MDPI

Extraction, Utilization and Conversion of Woody Biomass

Extraction, Utilization and Conversion of Woody Biomass

Guest Editors

Ali Umut Şen
Catarina Pereira Nobre
Terencio Rebello de Aguiar Junior

MDPI

Basel • Beijing • Wuhan • Barcelona • Belgrade • Novi Sad • Cluj • Manchester

Guest Editors

Ali Umut Şen
Department of Energy Systems Engineering
Izmir Institute of Technology
Izmir
Turkey

Catarina Pereira Nobre
CoLAB BIOREF-Collaborative Laboratory for Biorefineries
S. Mamede Infesta
Portugal

Terencio Rebello de Aguiar Junior
Polytechnic School
Federal University of Bahia
Salvador
Brazil

Editorial Office
MDPI AG
Grosspeteranlage 5
4052 Basel, Switzerland

This is a reprint of the Special Issue, published open access by the journal *Processes* (ISSN 2227-9717), freely accessible at: https://www.mdpi.com/journal/processes/special_issues/utilization_woody_biomass.

For citation purposes, cite each article independently as indicated on the article page online and as indicated below:

Lastname, A.A.; Lastname, B.B. Article Title. *Journal Name* **Year**, *Volume Number*, Page Range.

ISBN 978-3-7258-6003-6 (Hbk)
ISBN 978-3-7258-6004-3 (PDF)
https://doi.org/10.3390/books978-3-7258-6004-3

Contents

About the Editors

Ali Umut Şen

Ali Umut Şen holds an integrated MSc in Chemical Engineering and a PhD in Forest Products Chemistry from Technical University of Lisbon (Portugal), specializing in wood chemistry and biomass valorization. He is currently an Assistant Professor at Izmir Institute of Technology (Turkey), where he teaches courses in Mass and Energy Balances, Waste-to-Energy systems, and Biomass Energy and Technologies. He also supervises both undergraduate and graduate theses. During his PhD and postdoctoral research at University of Lisbon, he focused on lignocellulosic biomass valorization, with extensive work on the pyrolysis kinetics, extractive chemistry, and advanced characterization of barks and other underutilized biomasses. His research interests include thermochemical conversion processes (pyrolysis, gasification, combustion), kinetic modeling and reactor design, biochar and activated carbon production, and the extraction and valorization of bioactive compounds from diverse biomass sources. He has published extensively in international journals and is the author of more than 60 journal articles and conference papers and actively participates in national and international projects, including EU collaboration networks. ORCID: 0000-0003-3734-466X

Catarina Pereira Nobre

Catarina Pereira Nobre holds a degree in Biochemistry, a MSc, and a PhD in Energy and Bioenergy from NOVA School of Science and Technology (NOVA-SST, Portugal), where she also carried out postdoctoral research on effluent bioremediation. During her PhD, she collaborated with companies in the bioenergy and waste management sectors, taught graduate courses on biomass energy and biofuels, and co-supervised several MSc theses. From 2020 to 2022, she was a researcher and team leader at CoLAB BIOREF, focusing on project development and industry-oriented services. She is currently an Auxiliary Researcher at VALORIZA – Research Center for Endogenous Resource Valorization, at Portalegre Polytechnic University (PPU, Portugal), where she participates in ten international projects, coordinating one of them, and also serves as Science Communication Coordinator of the WIRE COST Action (CA20127). At PPU, she lectures in postgraduate programs on hydrogen and renewable energies. Her research interests include thermochemical conversion processes such as gasification, pyrolysis, and hydrothermal treatments of lignocellulosic biomass and waste-derived fuels, as well as the production of renewable gases like hydrogen and biomethane. She is the author of more than 90 scientific outputs, including journal articles, book chapters, and conference papers. ORCID: 0000-0001-5733-902X

Terencio Rebello de Aguiar Junior

Terencio Rebello de Aguiar Junior is a researcher with a bachelor's degree in Biological Sciences and a master's in Natural Resources Management. He holds a doctorate in River Ecosystem Restoration and Management from the University of Lisbon, with a sandwich period in Environmental Sciences at the University of California/Polytechnic University of Madrid, in addition to a postdoctoral fellowship in Toxicology. His experience covers water resource contamination, watershed management, ecology, and toxicology. Currently, he is a collaborating professor at the Federal University of Bahia, a researcher at the Technical University of Lisbon, and a public servant in Porto Seguro. He is the author of several scientific publications and serves as a reviewer for international journals. ORCID: 0000-0002-7080-1618

processes

MDPI

Review

Life Cycle Assessment (LCA) of Biochar Production from a Circular Economy Perspective

Joana Carvalho [1,2], Lucas Nascimento [1,2], Margarida Soares [1], Nádia Valério [1,2], André Ribeiro [1,2], Luciana Faria [1], André Silva [1], Nuno Pacheco [1,2], Jorge Araújo [1] and Cândida Vilarinho [2,*]

[1] CVR—Centre for Waste Valorisation, University of Minho, 4800042 Guimarães, Portugal
[2] MEtRICs—Mechanical Engineering and Resource Sustainability Center, Campus de Azurém, Universidade do Minho, 4800058 Guimarães, Portugal
* Correspondence: candida@dem.uminho.pt

Highlights:

Among several approaches to circular economy and zero-waste concepts, biochar production is a great example and might be a way to push the economy to a carbon-neutral balance. Overall, despite all the differences in assumptions and methodologies adopted, LCA proved that biochar is a very promising way of contributing to carbon-efficient resource circulation, mitigation of climate change, and economic sustainability.

What are the main findings?

- Biochar is considered a black porous and carbon-rich matter;
- Biochar is a promising source of alternative energy.

What is the implication of the main finding?

- It can be concluded that the costs are closely related to the technologies used in biochar production and also to the feedstock used.

Abstract: Climate change and environmental sustainability are among the most prominent issues of today. It is increasingly fundamental and urgent to develop a sustainable economy, capable of change the linear paradigm, actively promoting the efficient use of resources, highlighting product, component and material reuse. Among the many approaches to circular economy and zero-waste concepts, biochar is a great example and might be a way to push the economy to neutralize carbon balance. Biochar is a solid material produced during thermochemical decomposition of biomass in an oxygen-limited environment. Several authors have used life cycle assessment (LCA) method to evaluate the environmental impact of biochar production. Based on these studies, this work intends to critically analyze the LCA of biochar production from different sources using different technologies. Although these studies reveal differences in the contexts and characteristics of production, preventing direct comparison of results, a clear trend appears. It was proven, through combining life cycle assessment and circular economy modelling, that the application of biochar is a very promising way of contributing to carbon-efficient resource circulation, mitigation of climate change, and economic sustainability.

Keywords: life cycle assessment (LCA); biochar; biomass; circular economy

1. Introduction

As climate change is threatening the world and society grows exponentially, with more and more waste being generated, environmental sustainability is being questioned. It has been proven that linear models promote huge negative impacts on the environment. This occurs by extraction and landfilling at the end-of-life, and also in the economy, since not only when discarded is the economic value of products zero, but the value of finite resources also increases [1,2]. The transition to a circular economy is connected to great

expectations of ecological and economic benefits, helping in the clear separation between economic growth and the use of resources, the building block of the linear economy and its respective impacts, and additionally promoting the perspective of sustainable growth and egalitarian society. The circular models can potentially improve the efficiency of using primary raw materials and allow the waste to return to production as high-quality secondary raw materials [1,3]. In addition, a circular economy can also provide a platform for pioneering methodologies, technologies and business models that create improved economic value from limited natural resources, helping industry to become more resilient to external impacts and improve its global competitiveness.

Among several approaches to circular economy and zero-waste concepts, biochar production is a great example and might be a way to push the economy to a carbon neutral balance [4]. The assembly and appliance of biochar has been widely developed all over the world. Biochar is a solid material formed during the thermochemical decomposition of biomass in an oxygen-limited environment. It is defined, by the International Biochar Initiative, as "a solid material obtained from the carbonization of biomass" [5,6]. Biochar can be produced through several techniques, such as pyrolysis, torrefaction, and gasification. It can also be obtained by various biomass feedstocks, such as wood, agro-residues, or wastewater sludge.

Several studies report the environmental benefits of using biochar in the most diverse industrial areas. However, the safest way to affirm this is through LCA studies that assess the most diverse environmental impacts such as climate change and ozone layer degradation, among others. LCA methodology is a technical tool that allows the systematic analysis and assessment of the environmental aspects and potential impacts associated with products or services throughout its life cycle. In this context, the aim of this work is to perform an overview on biochar concepts and applications and mostly on LCA of biochar production, analyzing several study cases, from the perspective of circular economy.

2. Biochar

Biochar is considered a black porous and carbon-rich matter. This material can be produced with little or unavailable air, through a thermochemical conversion of biomass. Chemical, biological and physical properties of biochar make it a great material with many purposes [7]. The following Figure 1 presents some benefits of biochar.

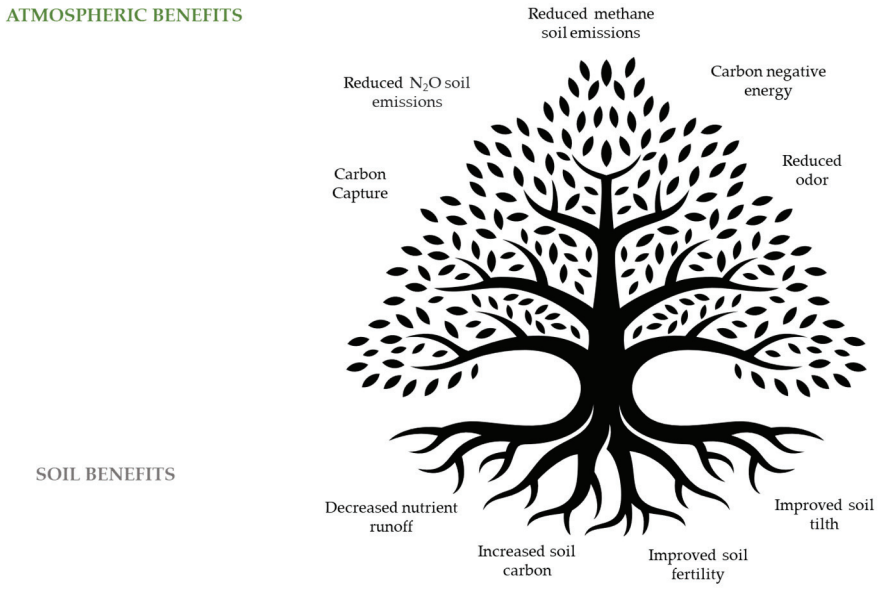

Figure 1. Biochar benefits (adapted from [6]).

2.1. Biochar Production

For biochar production, several thermochemical processes are used based on different reaction conditions (amount of oxygen available) including pyrolysis, gasification, and torrefaction. In this way, several types of reactors were developed for biomass production, with the objective of achieving the highest quality and yield of the product. These reactors differ in certain thermochemical parameters, such as oxygen availability, temperature, and the rate of heating itself. Thus, these parameters vary the physical and chemical properties of the biochar [8]. The following Figure 2 shows these several methods [8].

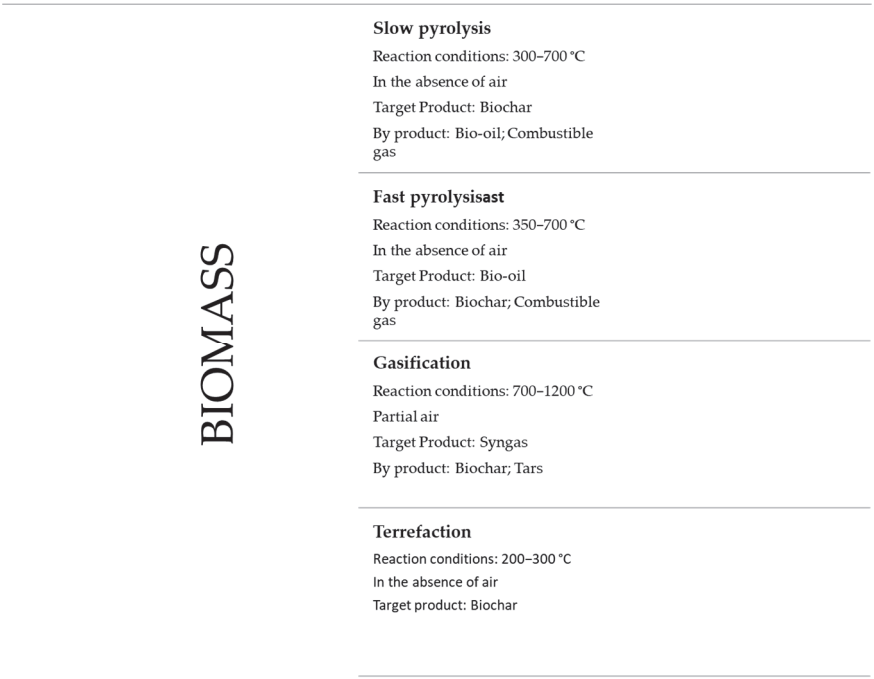

Figure 2. Biomass thermochemical conversion technologies for biochar production (adapted from [8]).

Biochar production quality heavily depends on the biomass' compositions and properties. These parameters define the application fields, production, quality and toxicity of biochar. Their stability is influenced by pyrolysis temperature, this being the main parameter [9]. Biochar production involves a complex biochemical reaction process where biomass undertakes decomposition, depolymerization and condensation in anoxic high temperature conditions [4,8,10]. Several factors define the quality of biochar, such as pH, specific surface area, porosity, nutrients, and carbon content, the latter being one of the main factors. High carbon content is directly linked to a high-quality biochar [11].

2.1.1. Slow Pyrolysis and Fast Pyrolysis

Different studies have demonstrated that slow pyrolysis allows the production of a quality biochar. This technique is characterized by using moderate temperatures (350–500 °C) and low heating rates [8]. In addition, other operational parameters strongly influence this type of pyrolysis, such as particle size, the atmosphere itself, the use of a catalyst, etc. Veses et al. (2015), stated that improving the residence time of the raw material and the pyrolysis vapor in contact, as well as the particle size and the ratio of catalyst in the biomass can favor the quality and production yield of biochar. Furthermore, it was mentioned that higher pyrolysis temperatures are very important for improving the quality of biochar (expanding carbon content), and reduced heating rate can increase its production in this type of pyrolysis [12].

Unlike the slow process, fast pyrolysis is characterized by the application of high heating rates, temperatures around 500 °C, and residence times shorter than 2 s, with rapid decomposition of the biomass [13]. As mentioned above, higher pyrolysis temperatures

increase the carbon content of the product and its specific surface area [14]. However, Chen et al. (2016), mentioned that increases in pyrolysis temperature, such as an increase in the heating rate, reduces the production yield due to the release of volatile gases. Since there is a shorter residence time, the amount of carbon deposition is reduced too [8].

2.1.2. Gasification

Regarding gasification, this process involves an incomplete combustion of biomass using several gasifying agents (air, pure oxygen, steam) that occur at 700–1000 °C [8]. Briefly, the process involves three main reactions: the devolatilization of the biomass, the combustion, and the gasification itself. Char from gasification is different from that obtained through pyrolysis, essentially due to the oxidizing environment of the gasifier. This environment affects the physical, chemical and morphological properties of biochar [15]. As mentioned above, the quality of biochar is directly related to the carbon content present, which is essentially affected by gasification conditions. The main parameters are the equivalence ratio, the properties of the raw material, pressure and the gasifying agent [16]. Several studies have shown that production yield decreases with increasing equivalence ratio, since the gasification temperature increases and carbon content also decreases [17,18].

2.1.3. Torrefaction

In turn, the torrefaction process is a modern method of obtaining biochar from biomass. This process is considered a mild pyrolysis, carried out at temperatures between 200–300 °C, under anaerobic conditions [18]. This method uses low heating rates and long residence times [8]. As for fast pyrolysis, increasing the processing temperature leads to a reduction in production yield. However, it is possible to achieve an energetically denser material, correlated with larger destruction of the structural elements. In turn, increasing the process time increases the calorific value of the biomass and has positive effects on carbon content [19,20]. The structure and biomass composition have influence on the process. For example, the size particles and the presence of heavy metals affect the torrefaction mechanism [20].

In short, the higher the carbon content, the more superior the quality of the biochar. In turn, the carbon content is higher when all volatile compounds are released from the biomass. This occurs when slow pyrolysis is carried out, being considered a deeper pyrolysis, using moderate temperatures over a long period of time. In this way, slow pyrolysis yields a high-quality biochar [8]. In torrefaction, the biochar undergoes only a lighter pyrolysis, with a low content of volatile compounds released, and there are not so many chemical reactions [21].

2.2. Biochar Applications

The interest in conversion of biomass waste from agriculture and forestry to energy production and carbon sequestration has been growing [22–24]. Carbon and energy content in these wastes make them potential candidates for thermochemical process to produce bioenergy and bioproducts [24]. In general, the many approaches to using biochar facilitate zero waste and the interest of circular economy values [25]. Pyrolysis of biomass waste produces biochar with great capacity in agricultural, industrial and construction applications. In addition, a bio-oil that can be burned to generate hot water, steam and/or electricity, is also produced in the process, thus reducing amount of waste discarded [4]. Recently, the manufacture and use of biochar has been widely developed worldwide. However, there are great uncertainties surrounding the operations, costs and emissions associated with wood processing [26].

As already mentioned, raw material quality, production technology and method conditions mainly define the efficiency, quality and biochar toxicity, and thus affect the subsequent biochar application strategy [4,27,28]. The physicochemical characteristic of biochar reveal its distinct application perspectives, involving soil conditioning, composting additive, building material, activated carbon, promoting anaerobic digestion and a list

of potential uses that continues to expand [5,29–32]. As the number of biochar purposes increases, so does the number of producers. However, it is neither financially nor energetically viable to generate and apply biochar without standards or regulations for its production and application [4]. To solve this problem, many countries are developing their own standards. So far, the International Biochar Initiative (IBI) in the United States of America and the European Biochar Certificate (EBC) are the most-usually used standards all over the world. These two standards were built helping to decrease the health and environmental risks correlated with the production and use of biochar, particularly in agriculture. However, the two standards are voluntary industry guidelines. As biochar has excellent potential for sustainability in several industries, these two guidelines appear to be unsatisfactory to regulate the quality of biochar manufactured as a whole. With the growing importance in biochar, many countries have their individual biochar policies in line with IBI and EBC standards. Other nations, which presently do not have a biochar standard, are controlling biochar usage with fertilizer or compost specifications [4].

Figure 3 shows some examples of promising biochar applications.

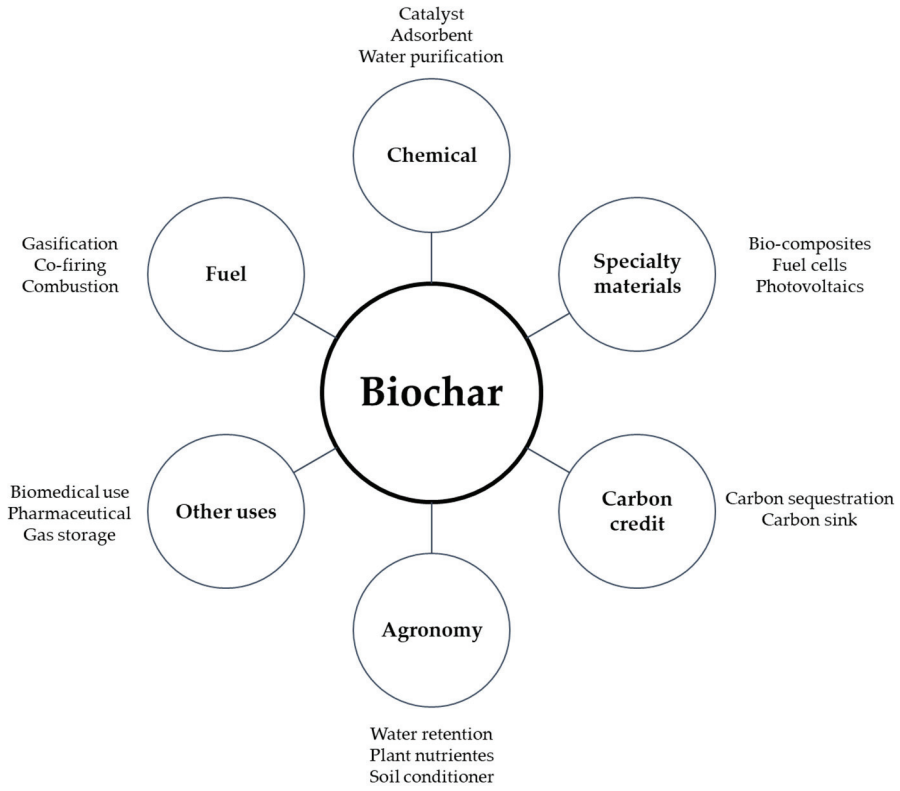

Figure 3. Promising applications of biochar (adapted from [33]).

2.2.1. Agriculture

Biochar application in agriculture has been extensively tested in the laboratory and field, and it has been usually employed as a chemical component [34–36], or as a soil corrective to enhance crop production, increasing nutrient availability [35,36], water retention capacity [36] and soil microbial activity [37]. Biochar can increase the pH of highly acidic soils [38–40] and mitigate the release of heavy metals into the soil [40–42]. Several studies have shown the advantages of biochar application as a soil conditioner and have demonstrated its potential in that respect. Some of the main benefits are the decreasing of greenhouse gas emissions and the mitigation soil infertility and desertification, improving soil quality and crop yield [43]. This is justified by the inorganic content present in biochar that acts as a nutrient and aids in fertilization [44]. As previously mentioned, biochar is produced by the thermal decomposition of biomass in an oxygen-limited ecosystem while composting is the natural biodegradation of organic material by the microbial commu-

nity in aerobic conditions. Carbon-based compounds in compost degrades rapidly and mineralizes so its valuable effects are quite short-lived, which is distinct from biochar, which can endure in soil for a long time [45]. Biochar has also been applied as an additive to enhance the composting rate e.g., a combination of 35% over mushroom compost with 20% biochar has been demonstrated to decrease the composting time to 24 days in comparison to the more common 90–270 days [46]. The elevated porosity of biochar can also enhance microbial development in the compost stockpile and consequently speed up nutrient recovery [47]. The incorporation of biochar in poultry manure for composting condensed the thermophilic stage and increased the highest temperature reached [48]. To manage the quality of biochar, it is extremely essential to determine its organic and inorganic pollutions [49]. General organic and inorganic contaminants that affect biochar quality are polycyclic aromatic hydrocarbons (PAHs), polychlorinated biphenols (PCBs), dioxins, furans and heavy metals [50]. In addition to biochar contaminations, it is also necessary to guarantee that biochar brings more advantages to its applications, such as cation exchange capacity, moisture retention, nutrient retention, plant growth promotion, heavy metals stabilization from soil or construction material, etc. The effectiveness of biochar stabilization of heavy metals can be assigned to the high surface area of the biochar, ability to raise the pH value, small-scale particle, etc. Nevertheless, if biochar is used precisely for its toxicity assessment without soil, a toxic influence is commonly found in living organisms [51]. This negative impact is basically caused by its elevated pH value and potential contaminants, but once biochar is blended with soil in a correct percentage (for example 1% or less), it generally has no noticeable toxic effect and it can improve plant biomass and amount of microorganisms in the soil, which are positive impacts. Studies show that the positive impacts are attributable to the biochar raw material, pyrolysis temperature, biochar percentage and type of soil. The cleaner the biochar raw material is, the less toxic the final biochar product is.

Another biochar application studied is soil remediation and amendment. Biochar has been considered an appropriate matter for this purpose, allowing the absorption and modification of pollutants, through their properties previously mentioned, associated with physical adsorption on the surface and in micropore structures [52].

Biochar has great potential to sequester carbon from materials based on plants, binding CO_2 through long-term storage of carbon in soil. This ability is associated with the yield of biochar, the content of stable carbon in biochar and the biochar stability in several circumstances and timeframes of soils [53].

2.2.2. Wastewater Treatments

Regarding water purification, biochar can be used in wastewater treatments. Biochar is efficient in the removal of several pollutants, as well as organic compounds (dyes, phenolics, pesticides, polynuclear aromatics and antibiotic), nutrients and heavy metals. Heavy metals are toxic, carcinogenic and non-biodegradable components, so their removal is fundamental [54]. This capacity is justified by their absorbent ability in aqueous solutions due their properties, such as porosity, pH, surface area, surface charge and mineral composition [55,56]. Concerning nutrients (nitrogen, phosphorus, sodium, potassium, etc.), if their concentrations exceed the limits, these components become dangerous to the aquatic ecosystem. Physical and chemical properties associated to biochar are of great significance to the removal of these components, through various removal methods, involving electrostatic interaction, ligand exchange, precipitations with Mg^{2+} or Ca^{2+}, complexation with functional hydroxyl, surface sorption, etc. [56–58]. The same is observed in the removal of other organic pollutants, since the efficiency is strongly affected by physical properties, such as specific surface areas and pore-size distribution, surface functional groups and hydrophobic nature [59].

2.2.3. Building Materials

Another application of biochar is as a partial component of cementitious building materials, specifically as a sustainable alterative to concrete cement, sand or another energy-intensive additives used for concrete production [60–63]. Recent studies [61–65] have established that biochar, made from several raw biomass materials under ideal pyrolysis conditions, can lead to an enhancement in strength and biochar-mortar by 15–20% when evaluated to control mixture. The filling of biochar particles can also promote a reduction in capillary water absorption and water infiltration in biochar-mortar mix by 30–40%, thus indicating reduction in water penetration and improved durability of the composite [64]. Heavy metal leaching is a common problem in waste heat treatment products, including ashes and biochar, with a high level of heavy metal content being determined in sources [66]. Heavy metal contained in the biochar can run like leachate when structure builds are exposed to rain and other weathering agents [67].

2.2.4. Activated Carbon

Biochar, with a large surface area and pore formation, can potentially be employed as a low-cost activated carbon [68]. Nevertheless, beyond typical pyrolysis treatment of waste biomass, the resulting biochar frequently shows poorer pore behavior than commercial activated carbon. Therefore, several physical and chemical treatment processes were proposed to convert crude biomass or low-grade coal into activated carbon [69]. Normally, physical activation involves elevated temperature in the presence of steam, air, CO_2, N_2 and inert gases, and chemical activation was carried out utilizing nitric acid, phosphoric acid, sulfuric acid and potassium hydroxide, among others [70–72].

2.2.5. Anaerobic Digestion (AD)

AD is an important expertise for organic waste remediation and bioenergy recovery, thus performing a vital role in development the global circular economy [72]. In fact, biochar has been supported as capable of increasing the AD process through quite a few mechanisms. More precisely, it was found that biochar performs a crucial role in increasing AD through several mechanisms, including promoting direct interspecies electron transfer among different microbial species due to biochar's good conductivity [73]; increasing microbial growth through biochar's immobilization effect [74]; adsorbing inhibitory compounds such as heavy metals, ammonia and volatile fatty acids in anaerobic bioreactor [75] and increasing the buffering capacity of the bioreactor due to the relatively high alkalinity of the biochar [75–77].

3. Life Cycle Assessment (LCA) Definitions

The concern for the environmental impacts generated by the supply of products and services to society has led to the growth of new tools and methods that aim to understand, control and reduce these impacts. Life cycle assessment (LCA) can be characterized as a compilation and assessment of inputs, outputs and potential environmental impacts of a product or system throughout its life cycle. It is the most widely used assessment type with wide international approval to measure environmental impacts [78,79]. LCA includes entire supply chains, representing all the impacts that occur at different steps and locations throughout the life cycle, regardless of particular processes' physical locations [79].

For an LCA study to be validate, it is necessary to follow the steps stipulated by the ISO 14040 standard, which consists of (i) defining an objective and scope; (ii) carrying out an inventory with as much information as possible about inputs and outputs related to the product or service; (iii) calculating environmental impacts; (iv) systematic and interactive review to validate all information.

Several studies report the environmental benefits of using biochar in the most diverse industrial areas. However, the safest way to affirm this is through LCA studies that assess various environmental impacts, such as climate change and ozone layer degradation among others.

According to Matuski et al. (2020), many authors have used the LCA method to assess biochar projects environmental impact, and these articles are systematically revised to discover a general trend or some pattern. The differences in these studies' contexts and characteristics do not allow a direct comparison of results, limiting the spectrum of LCA studies. However, biochar application brings substantial benefits, either by neutralizing the emission of greenhouse gases from agricultural production or as a carbon sequestration approach. There is also a great capacity for energy production using synthesis gas and bio-oil byproducts. The advantages of carbon sequestration in biochar and energy production generally overbalance the greenhouse gas emissions produced through the production and handling of the raw material. On the other hand, the effect on another types of environmental impact needs to be assessed and normalized with the intuition of observing some negative effect to guarantee the project's economic sustainability [80].

3.1. Scope and Objective

The LCA concept's definition includes the full definition and description of the product, process or activity, the choice of the functional unit to be used and establishes the context in which the valuation must be made, identifying the limits, environmental effects and the methodologies considered for the evaluation.

According to Zhu et al. (2022), for the particular case of LCA of biochar, the objectives and scope are, in general, divided into two fields of research, the first one related to the assessment of the impacts of manufacture and use with association of carbon footprint, midpoint impacts, air pollutants, acidification and other parameters. On the other hand, the second field of research is focused on energy consumption efficiency and economic aspects [81].

Table 1 presents some articles that assess the environmental impacts of biochar production and use. They are divided by a functional unit, reference system, software and impact methodologies used and other focuses.

Table 1. LCA case studies for biochar (adapted from [82]).

Region Country	Functional Unit	Reference System	Allocation + System Boundaries	Ref.
Denmark	1 ton of dry seed	Typical Danish rapeseed to production.	Crop cultivation included.	[83]
Belgium, Spain, Italy	1 kg product 1 ha/yr	Compost, compost blend, mineral fertilizer.	System expansion, cut-off (feedstock), construction and pesticide omitted.	[84]
Zambia	Preparation and utilization of 1 kg biochar	x	System expansion—where applicable avoided electricity production (diesel fuel generator wood burning).	[85]
Canada	Production of 1 ton (Mg) biochar	Compare two different temperature scenarios.	System expansion, switchgrass cultivation included, energy production offset.	[86]
Belgium	1 ton of biochar	x	System expansion, energy and fertilizer offset, cut-off (manure) þ all (willow cultivation in marginal soils), pyrolysis plant construction included.	[87]
Vietnam	1 ton of rice straw	Open burning of straw, two seasons (spring and summer) modelled, comparison with enriched biochar.	System expansion, open burning of straw eschewed.	[88]
Finland	1 ton oat flakes	Oat flows used as feed or for energy.	System expansion.	[89]
China	1 ton of odt straw	Three straw utilization scenarios: briquetting gasification, pyrolysis two baseline (reference) scenarios: reincorporation, burning	System expansion, offset from avoided fuel consumption.	[90]

Some authors used LCA study to measure the potential environmental impacts of recovering nutrients from the soil using biochar [84]. Erison et al. (2022), performed an LCA study envisaging the production of biodiesel using biochar as a catalyst [91]. Lefebvre et al. (2021), evaluated the differences between sugarcane biomass and biochar to assess which energy source emitted less CO_2-eq in energy supply [92]. The objectives related to the use of LCA in biochar are diversified, and often adapted to particular needs of the research.

The functional unit used varies within each study, e.g., in the study performed by Field et al. (2013), the functional unit was the conversion of 1 ton of dry biomass into biochar. In Hamedani et al.'s (2019), LCA study of biochar, the production of 1 ton of biochar as functional unit was used. Xu et al. (2019), defined the functional unit of their study as a "hectare of agricultural area used for one year" [87,93,94].

When considering the biochar systems' main objective is the use or management of biomass waste streams, upstream functional units are generally used, such as a dry or wet raw material [90]. Another widely applied approach is related to downstream flows, where functional units are primarily specified as the mass of biochar produced or the mass of a crop produced in the treated field. Additionally, it is also common the combination of the two methodologies, for example, a quantity of raw material that produces a certain amount of biochar [95], or even multiple functional units [96]. In the study of Zhu et al. (2022), the author infers that a commonly used functional unit can be the production of 1 kWh of produced energy, stating that, in terms of comparison, one of the most recommended functional units to be used is 1 ton of feed and 1 ton of biochar. [81]

When referring to the boundaries, in the scope of LCA, they can be called "cradle to gate", "gate to gate", "cradle to grave" and "cradle to cradle". Each type of boundary system is described in the literature in accordance with the detail level of study. In brief, the boundary system "cradle to gate" analyses environmental impacts from the extraction of the raw material to the "entrance" at the factory, while the "gate to gate" system measures the environmental impacts of one or more manufacturing processes. The "cradle to grave" expression is used in the assessment of the impacts that cover the extraction of raw materials, the use phase and the final disposal of the product. On its turn, the "cradle-to-cradle" boundary methodology involves recycling and reuse processes [97], as shown in Figure 4.

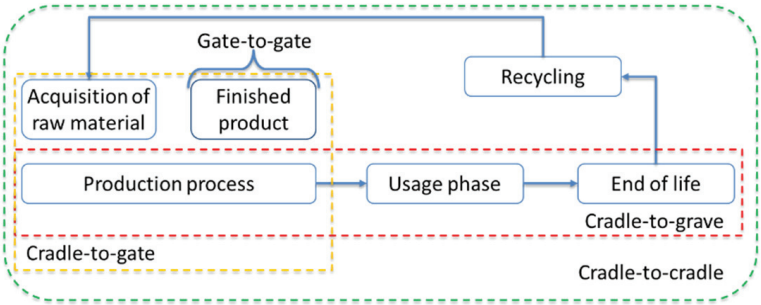

Figure 4. LCA boundary system approach.

In a process of biochar production from agro-wastes obtained through pyrolysis, Tiegam et al. (2021), stated that this system boundary can be classified as cradle-to-grave or cradle-to-gate [98]. On the other hand, in the study carried out by Hamedani et al. (2019), involving pyrolysis of pig manure residues for biochar production, its boundary was characterized as cradle-to-grave [87].

In the study performed by Hammond et al. (2011), the frontier used was gate-to-gate with the aim of calculating the impacts of producing 1 kWh of biochar. In another study conducted by Dutta and Raghavam, (2014), the authors infer in their work that the most-indicated boundary system for LCA studies focused on evaluating greenhouse gas was the cradle-to-grave one [99].

3.2. Life Cycle Inventory

Life cycle inventory (LCI) is the collection and quantification of all natural resources consumed and all substances that are emitted into the environment by the life cycle within life cycle phases expressed in the goal and scope definition of this study. The procedure of collecting inventory data begins on the basis of the data requisite for each life cycle stage, in particular the type of data needed for the stage: foreground or background. Foreground data mean that the data are attributable to the target products precisely, while background data can be obtained from special or temporal averages. LCIs are usually based on average data of material and energy inputs (resources and energy used) and outputs (product, waste and emissions produced) collected at a real site or estimated from the literature or from developing studies performed prior to the LCA study [100]. The LCI has a necessary step where elementary flows are included over time and space and is a demanding activity that requires time and attention [101]. It is essential to understand that LCA and LCI are both supported by concepts and assessment of energy consumption and mass balance, based on the first law of thermodynamics related to the principle of energy conservation, by which energy cannot be created or destroyed, but converted into another form. The second law of thermodynamics is also a fundamental concept for understanding LCA, being related to energy degradation; that is, some losses can be due to heat, radiation and others. In this context, LCA makes an energy balance of materials between inputs and outputs and calculates the environmental impacts through the difference between the loss and energy efficiency [102,103].

Some authors declare that the inventory related to biochar production usually focuses on feedstock, transport, pyrolysis process, use of biochar and end-of-life [104]. Dutta and Raghavam (2014), in their work consider inventory, obtaining feedstock analysis, all transports associated with biochar, pyrolysis process to obtain biochar and use of biochar for energy production [99]. In the study carried out by Llorach-Massana et al. (2017), the inventory was focused on the feedstock, where the feasibility of using tomato plant residues from an urban garden was studied [105]. In other studies, the benefits of producing biochar from rice field residues were analyzed [88].

In the study performed by Matuštík et al. (2020), LCI for biochar must contain information on the raw material, land use, transport, energy used in pyrolysis, pyrolysis gas emissions and, depending on the functional unit and borders, waste must be also accounted for [82].

3.3. Life Cycle Impact Assessment (LCIA)

To understand the potential environmental impact of the use of natural resources and the attempts created by the system, the LCIA stage is essential. In this methodology, flows resulting from a product's life cycle are aggregated into impact categories [82].

The same studies presented in Table 1 were compiled in Table 2 with LCIA methodologies, impact assessment and GWP results.

According to de Vries and de Boer, (2010), the environmental impact types considered during the life cycle of a product are related to the use of resources such as earth or fossil fuels and the emission of the pollutant's ammonia or methane. Ferrão, (2009), and Santero et al. (2011), considered categories of impacts on climate change, eutrophication, acidification, depletion of resources and ecotoxicity, among others, where each type of emission is related to one or more impacts [102,106,107]. The impact assessment uses the inventory results to evaluate the potential of environmental impacts while providing information for interpretation. In this phase, statistical techniques, such as weighting, normalization and aggregation, are essential to comparing impact types and measuring their relevance [100].

Table 2. Study cases with LCIA methodologies, impact categories analyzed and GWP results (adapted from [80]).

Study	LCIA Methodology	Impact Assessment	Results	Ref.
Thers et al. (2019)	IPCC (2013)	GWP 100 yr, 20 yr	171 kg CO_2-eq/Mg dry seed (400 °C) and 111 kg CO_2-eq/Mg dry seed (800 °C) compared to 638 kg CO_2-eq/Mg dry seed for oilseed rape cultivation without biochar amendment = significant GHG reduction.	[83]
Oldfield et al. (2018)	CML	GWP, AP, EP	Net negative—single value not presented.	[84]
Smebye et al. (2017)	ReCiPe 2016 endpoint	GWP, PMF, land occupation, FDP, þ all ReCiPe 1 endpoint categories	Only endpoint GWP value calculated.	[85]
Brassard et al. (2018)	IPCC 2007	GWP	Scenario A (459 °C) −2110 kg CO_2-eq/Mg biochar, Scenario B (591 °C) −2561 kg CO_2-eq/Mg biochar.	[86]
Hamedani et al. (2019)	IMPACT 2002+, CML	All midpoint (IMPACT) and endpoint (CML)	IMPACT 2002+: −2063 kg CO_2-eq/t biochar (willow) and −472 kg CO_2-eq/t biochar (pig manure); CML: −2089.65 kg CO_2-eq/t biochar (willow) and −466 kg CO_2-eq/t biochar (pig manure).	[87]
Uusitalo and Leino, (2019)	IPCC (2013)	GWP	Biochar production from oat side-flows leads to GHG emission reduction of 350 k gCO_2-eq/t oat flake, buffer zone biomass biochar potential of 390 kg CO_2-eq/t oat flake.	[89]
Clare et al. (2015)	IPCC 2007	GWP	−1.35 Mg CO_2 e/odt straw	[90]

There are several methodologies for calculating environmental impacts such as Recipe, CML, Usertox, Carbon Footprint IPCC for parameters and others. According to Zhu et al. (2022), the choice of impact category must converge with the goals. Yang et al. (2018), used the CML methodology; Thers et al. (2019), used the IPCC methodology; Oldefild et al. (2018), applied CML methodology and Smebye et al. (2018), assessed the impact through ReCiPe methodology [82–85,103].

Several authors studying LCA on biochar have used methods such as Eco Indicator 99 and the ReCiPe midpoint approach to evaluate the entire biochar chain [108]. In the study carried out by Hamedani et al. (2019), the use of two methodologies, IMPACT 2002+ and CML, was applied to calculate environmental impacts [87].

When looking at Table 2 and considering all the differences in the limits of the system such as functional units, among other parameters, the LCA results are not comparable. The GWP results presented make a general balance of GHG that varies in value according to the methodology used. According to a study by Brassard et al. (2018), in their work they used biochar for soil correction and observed a GWP impact of up to 2561 mg CO_2-eq/t of biochar [86]; Mohammadi et al. (2016), revealed the carbon footprint of rice production with a change in the biochar of 3.85 kg CO_2-eq/kg. Nevertheless, the results showed similar tendencies. However, when looking closely, the results show a certain tendency. It is remarkable that the biochar–soil correction systems show a clear advantage from the point of view of climate change [88]. Biochar production appraised the neutralization's impact of agricultural production when GHG emissions were positive, such as in the case presented by Thers et al. (2019), and other studies. The processing of raw materials and especially the pyrolysis system are the most important causes of GHG emissions, not including agricultural production's impact. In relation to the impact, it is normally considered residual. The benefit of carbon capture and energy production from biochar,

in addition to the advantages associated with the co-products generated, compensate the GHG emissions caused by the biochar production itself [83].

Biochar application can contribute to carbon sequestration by increasing production, reducing the use of fertilizers and reducing CH_4 or N_2O emissions, among other factors [84].

Other studies have been carried out with the aim of evaluating the influence of biochar production on the impact categories. Concerning acidification and eutrophication potential, agricultural processes, such as the application of fertilizers, are the most important sources of negative impacts [84], as well as with regard to the impact of ecotoxicity categories [87]. Electricity from the network for pyrolysis and agricultural operation was reported as another source of negative impact on acidification and eutrophication potential [109].

4. Life Cycle Cost Assessment (LCCA)

For a process to be viable, in addition to the environmental aspects, it is mandatory to assess their associated costs. Life cycle cost assessment (LCCA) is a method of assessing the total cost of a process. It takes into account all costs of acquiring, owning, operating and disposing. LCCA is especially useful when project alternatives that fulfill the same performance requirements differ with respect to initial costs and operating costs and should be compared in order to select the one that maximizes net savings best.

In this context, conducting a complete LCCA of biochar-based products is an essential step in the breakeven and viability of this technology during the project or industrial application period.

Durairaj et al. (2002), reviewed models for LCCA [110], namely: (i) LCCA model of Fabrycky and Blanchard; (ii) LCCA model of Woodward [111]; (iii) LCCA model of Dahlen and Bolmsjo [112]; (iv) the activity-based costing (ABC) model [113]; (v) the economic input–output LCA model [114]; (vi) the design-to-cost model (DTC) [115]; (vii) the product life cycle costing (PLCC) to manufacturing system [116]; (viii) the total cost assessment (TCA) model.

Fabrycky and Blanchard presented an elaborated LCCA model to approach detailed cost analysis of all the costs related to the entire life cycle of either product.

The major advantage of this model is found in its detailed cost breakdown structure (CBS). First, they split the total cost of a product or a system into four categories, respectively: (1) research and development costs; (2) production and construction costs; (3) operation and maintenance costs; (4) retirement and disposal cost. This model comprises the essential features of a holistic methodology to assess the life cycle and determine the total cost of a product.

Woodward's LCCA model was made to focus on planning and monitoring assets over their entire life cycle—from the development stage through to disposal. The minimum life cycle cost of the asset is given by the optimization of the trade-off among the cost factors. This process requires the estimation of whole-life costs prior to making a purchase choice for an asset from the accessible alternatives. This approach emboldens a long-term perspective on the investment decision-making procedure [111].

Dahlen and Bolmsjö's LCCA model aims to extend the application's field and perform an investment analysis when raising the production factor—labor. It considers all the costs associated with an employee over their employment time. The costs of labor can be graphed like the costs over the life cycle for production equipment [112]. In turn, the ABC Model has the most likely-looking cost-effective evaluation in lifecycle design. Respecting environmental matters, uncertainty must be considered due to the predominant lack of hard data. When there is a lack of information and the existence of unexpected activities, uncertainty conditions must be also used [113]. The economic input–output LCA model is a new tool that can complement the conventional LCA and overcome its limitations. The objective is to augment conventional economic input–output tables with appropriate sectored environmental impacts indices, which are then used to analyze economywide, direct and indirect environmental impacts of changes in the output of selected industries.

This model represents all the supplier relationships in the supply chain for industrial production. Its application was shown to be feasible, rapid and inexpensive [114].

In relation to the DTC model for manufacture systems, it provides a common methodology to merge cost modelling and quality function deployment (QFD) to assess the possible trade-offs among the costs and performance of product alternatives in the initiation of the production system's design. The design-to-cost approach has a plan for choosing a system design [115].

The PLCC model determines the life cycle expenses of capital goods such as machines and manufacturing systems. In this methodology, single processes connected to the product's life cycle are expressed. With an intent to the redesign of present product structures, it is feasible to derive approaches out the cost structures of the life cycle. The early stages of the product life cycle are production, use and disposal or de-production. The design of the product should be directed upon the needs of the use phase to reduce costs in the several phases of the life cycle. A similar dependency comes up in the disposal phase [116].

The TCA model seems to be the most helpful and practical tool for small manufacturers. It supplies a streamlined approach to identifying and quantifying the costs of pollution prevention investments. It expands the scope of capital budgeting to comprise indirect benefits, thereby increasing the magnitude of savings originated from pollution prevention investments. The information requirements of TCA can be readily implemented in the small business scenario.

It is not possible to create a single LCCA model that considers all the requirements, yet it is possible to develop models to answer specific needs, such as the elaboration of an ecological, sustainable and economical product.

Most of the related studies in the literature focus on the economic assessment of biochar systems, such as the studies carried out by Roberts et al. (2010), and Galinato et al. (2011). In these studies, is typical to find that the potential profitability of biochar production systems is highly dependent on the feedstock used. In their study, Yoder et al. (2011), proceed to model the trade-off between product yield and product quality as the conversion temperature increases, exploring the implications of different production techniques and resulting variations in the properties of biochar for overall system performance [117–119].

In another study, Homagain et al. (2016), found that, within the limit of life cycle analysis, the economic viability of the biochar-based bioenergy production system is directly dependent on pyrolysis costs and raw material processing (drying, grinding and pelletizing), in on-site collection, and also in total carbon offset amount provided by the system. Through a sensitivity analysis of the transport distance and the displacement values, it was shown that the system is profitable in the case of high biomass availability within 200 km and when the cost of carbon sequestration exceeds the 60 Canadian dollars-per-ton carbon equivalent (CO_2-eq) [120].

In the study performed by Clare et al. (2015), it was found that straw briquetting for thermal energy is the most economical carbon reduction technology, requiring a subsidized CAD 7 mgCO_2-eq. However, China's current bioelectricity subsidy scheme makes gasification (net present value (NPV) CAD 12.6 million) more financially attractive to investors when compared to briquetting (NPV CAD 7.34 million) and pyrolysis (NPV CAD 1.84 million). The potential for direct carbon reduction from pyrolysis (1.06 mgCO_2-eq per odt straw) is also less than briquetting (1.35 mgCO_2-eq per odt straw) and gasification (1.16 mgCO_2-eq per odt straw). The authors conclude that the indirect carbon reduction processes that results from biochar utilization can significantly improve the pyrolysis scenario and carbon reduction potential, bearing in mind that improving the agronomic benefit of biochar is essential for the pyrolysis scenario to compete as an economically viable and cost-effective mitigation technology [90].

According to the study performed by Cleary, (2018), the added value of pyrolysis for biochar production is more profitable than selling highest quality wood chips for cellulose. The modelled biochar price ranged from CAD 3 to CAD 4/kg, quoted for 10 to 20 kg of biochar packages. The pyrolysis cost was estimated at about CAD 150,000.00, the operating

cost around CAD 78,840.00, including labor and electricity. Thus, it can be concluded that the costs are closely related to the technologies used in biochar production and also to the feedstock used [121].

5. Final Remarks

Two of the most important domains facing specific challenges within the circular economy are biomass and bio-based products. Materials based on biological resources can be used for a wide range of products and energy uses. The bioeconomy offers alternatives to products and energies based on fossil fuels and can contribute to the circular economy. Bio-based materials can also have advantages linked to their renewability, biodegradability, or the possibility of composting. On the other hand, the use of biological resources requires attention to be paid to the environmental impacts of its life cycle and to its sustainable supply. From a circular economy perspective, the cascading use of renewable resources should be promoted, where appropriate, with various cycles of reuse and recycling. Bio-based materials can be used in multiple ways, with the possibility of reusing and recycling them several times, which is consistent with the application of the waste hierarchy and, more generally, with options that lead to the best overall result for the environment.

Biochar is a solid, carbon-rich material generally obtained from thermochemical conversion of biomass and respective carbonization in oxygen-limited environments and has been proposed as a potential solution to climate change, energy security, degradation of natural resources, food security and catastrophic forest fires worldwide. Biochar production implies a complex chemical reaction process where biomass undergoes decomposition, depolymerization and condensation in anoxic high temperature conditions. As was extensively discussed, the many strategies for using biochar facilitate zero waste and the development of the circular economy. In addition, LCA has proven an excellent tool for quantifying the potential of biochar utilization, as well as for fostering and managing its production. Nevertheless, as was shown, multi-purpose applications of biochar make the functional units and system boundaries of different cases variable. Additionally, although these variables can be contextualized, they can barely be eliminated. Therefore, extensive system boundaries and more inclusive inventory considerations must be integrated and comprehensively analyzed in the LCA of biochar production. Although solid international guidelines and frameworks are available to promote consistency, and most of the studies follow the ISO standard for LCA, they still may consider different criteria and assumptions, resulting in different outcomes, so the methodology should be unified allowing to compare the results, at least to some extent. In addition, economic analysis through LCCA should be encouraged to optimize the flows of sustainable biochar production.

Overall, despite all the differences in assumptions and methodologies adopted, LCA proves that biochar is a very promising way of contributing to carbon-efficient resource circulation, mitigation of climate change and economic sustainability.

Author Contributions: Conceptualization J.C. and L.N.; writing—original draft preparation, J.C., L.N., M.S. and N.V.; writing—review and editing, A.R., L.F., A.S. and N.P.; project administration, J.C. and J.A.; funding acquisition, C.V. All authors have read and agreed to the published version of the manuscript.

Funding: This work was co-financed by Compete 2020, Portugal 2020 and the European Union through the European Regional Development Fund—FEDER within the scope of the project WAST'AWARENESS—Technology Transfer in Waste Valorization and Sustainability (POCI-01-0246-FEDER-181304).

Conflicts of Interest: The authors declare no conflict of interest.

Abbreviation

AD	aerobic digestion
EBC	European Biochar Certificate
GHG	greenhouse gas
GWP	global warming potential
IBI	International Biochar Certificate
LCA	life cycle assessment
LCI	life cycle inventory
LCIA	life cycle impact assessment
PAHs	polycycle aromatic hydrocarbons
PCBs	polychlorinated biphenyls

References

1. Korhonen, J.; Honkasalo, A.; Seppälä, J. Circular Economy: The Concept and its Limitations. *Ecol. Econ.* **2018**, *143*, 37–46. [CrossRef]
2. Beaulieu, L.; Durne, G.; Arpin, M. Circular Economy: A Critical Literature Review of Concepts. *CIRAIG-Int. Ref. Cent. Life Cycle Prod. Process. Serv.* **2015**, *91*. [CrossRef]
3. Rashid, A.; Asif, F.M.A.; Krajnik, P.; Nicolescu, C.M. Resource Conservative Manufacturing: An essential change in business and technology paradigm for sustainable manufacturing. *J. Clean. Prod.* **2013**, *57*, 166–177. [CrossRef]
4. Hu, Q.; Jung, J.; Chen, D.; Leong, K.; Song, S.; Li, F.; Mohan, B.C.; Yao, Z.; Prabhakar, A.K.; Lin, X.H.; et al. Biochar industry to circular economy. *Sci. Total Environ.* **2021**, *757*, 143820. [CrossRef]
5. Cha, J.S.; Park, S.H.; Jung, S.C.; Ryu, C.; Jeon, J.K.; Shin, M.C.; Park, Y.K. Production and utilization of biochar: A review. *J. Ind. Eng. Chem.* **2016**, *40*, 1–15. [CrossRef]
6. Biochar Is a Valuable Soil Amendment. WOKA Foundation. Available online: https://biochar-international.org/biochar/ (accessed on 7 September 2022).
7. Xie, Y.; Wang, L.; Li, H.; Westholm, L.J.; Carvalho, L.; Thorin, E.; Yu, Z.; Yu, X.; Skreiberg, Ø. A critical review on production, modification and utilization of biochar. *J. Anal. Appl. Pyrolysis* **2022**, *161*, 105405. [CrossRef]
8. Wang, D.; Jiang, P.; Zhang, H.; Yuan, W. Biochar production and applications in agro and forestry systems: A review. *Sci. Total Environ.* **2020**, *723*, 137775. [CrossRef]
9. Leng, L.; Huang, H. An overview of the effect of pyrolysis process parameters on biochar stability. *Bioresour. Technol.* **2018**, *270*, 627–642. [CrossRef]
10. Zhao, L.; Cao, X.; Mašek, O.; Zimmerman, A. Heterogeneity of biochar properties as a function of feedstock sources and production temperatures. *J. Hazard. Mater.* **2013**, *256–257*, 1–9. [CrossRef]
11. Yao, Z.; You, S.; Ge, T.; Wang, C.-H. Biomass gasification for syngas and biochar co-production: Energy application and economic evaluation. *Appl. Energy* **2018**, *209*, 43–55. [CrossRef]
12. Veses, A.; Aznar, M.; López, J.M.; Callén, M.S.; Murillo, R.; García, T. Production of upgraded bio-oils by biomass catalytic pyrolysis in an auger reactor using low cost materials. *Fuel* **2015**, *141*, 17–22. [CrossRef]
13. Choi, J.H.; Kim, S.-S.; Ly, H.V.; Kim, J.; Woo, H.C. Effects of water-washing Saccharina japonica on fast pyrolysis in a bubbling fluidized-bed reactor. *Biomass Bioenergy* **2017**, *98*, 112–123. [CrossRef]
14. Zhao, B.; O'Connor, D.; Zhang, J.; Peng, T.; Shen, Z.; Tsang, D.C.W.; Hou, D. Effect of pyrolysis temperature, heating rate, and residence time on rapeseed stem derived biochar. *J. Clean. Prod.* **2018**, *174*, 977–987. [CrossRef]
15. Hernández, J.J.; Saffe, A.; Collado, R.; Monedero, E. Recirculation of char from biomass gasification: Effects on gasifier performance and end-char properties. *Renew. Energy* **2020**, *147*, 806–813. [CrossRef]
16. Benedetti, V.; Patuzzi, F.; Baratieri, M. Characterization of char from biomass gasification and its similarities with activated carbon in adsorption applications. *Appl. Energy* **2018**, *227*, 92–99. [CrossRef]
17. Muvhiiwa, R.; Kuvarega, A.; Llana, E.M.; Muleja, A. Study of biochar from pyrolysis and gasification of wood pellets in a nitrogen plasma reactor for design of biomass processes. *J. Environ. Chem. Eng.* **2019**, *7*, 103391. [CrossRef]
18. Krysanova, K.; Krylova, A.; Kulikova, M.; Kulikov, A.; Rusakova, O. Biochar characteristics produced via hydrothermal carbonization and torrefaction of peat and sawdust. *Fuel* **2022**, *328*, 125220. [CrossRef]
19. Krysanova, K.; Krylova, A.; Zaichenko, V. Properties of biochar obtained by hydrothermal carbonization and torrefaction of peat. *Fuel* **2019**, *256*, 115929. [CrossRef]
20. Wang, Z.; Lim, C.J.; Grace, J.R.; Li, H.; Parise, M.R. Effects of temperature and particle size on biomass torrefaction in a slot-rectangular spouted bed reactor. *Bioresour. Technol.* **2017**, *244*, 281–288. [CrossRef] [PubMed]
21. Barskov, S.; Zappi, M.; Buchireddy, P.; Dufreche, S.; Guillory, J.; Gang, D.; Hernandez, R.; Bajpai, R.; Baudier, J.; Cooper, R.; et al. Torrefaction of biomass: A review of production methods for biocoal from cultured and waste lignocellulosic feedstocks. *Renew. Energy* **2019**, *142*, 624–642. [CrossRef]
22. Thengane, S.K.; Bandyopadhyay, S. Biochar mines: Panacea to climate change and energy crisis? *Clean Technol. Environ. Policy* **2020**, *22*, 5–10. [CrossRef]

23. Malmsheimer, R.W.; Bowyer, J.L.; Fried, J.S.; Gee, E.; Izlar, R.L.; Miner, R.A.; Munn, I.A.; Oneil, E.; Stewart, W.C. Managing Forests because Carbon Matters: Integrating Energy, Products, and Land Management Policy. *J. For.* **2011**, *109*, S7–S50.
24. Sanchez, D.L.; Nelson, J.H.; Johnston, J.; Mileva, A.; Kammen, D.M. Biomass enables the transition to a carbon-negative power system across western North America. *Nat. Clim. Chang.* **2015**, *5*, 230–234. [CrossRef]
25. Matrapazi, V.K.; Zabaniotou, A. Experimental and feasibility study of spent coffee grounds upscaling via pyrolysis towards proposing an eco-social innovation circular economy solution. *Sci. Total Environ.* **2020**, *718*, 137316. [CrossRef] [PubMed]
26. Thengane, S.K.; Kung, K.; York, R.; Sokhansanj, S.; Lim, C.J.; Sanchez, D.L. Technoeconomic and emissions evaluation of mobile in-woods biochar production. *Energy Convers. Manag.* **2020**, *223*, 113305. [CrossRef]
27. Yang, X.; Ng, W.; Wong, B.S.E.; Baeg, G.H.; Wang, C.-H.; Ok, Y.S. Characterization and ecotoxicological investigation of biochar produced via slow pyrolysis: Effect of feedstock composition and pyrolysis conditions. *J. Hazard. Mater.* **2019**, *365*, 178–185. [CrossRef]
28. Pecchi, M.; Baratieri, M. Coupling anaerobic digestion with gasification, pyrolysis or hydrothermal carbonization: A review. *Renew. Sustain. Energy Rev.* **2019**, *105*, 462–475. [CrossRef]
29. Woolf, D.; Amonette, J.E.; Street-Perrott, F.A.; Lehmann, J.; Joseph, S. Sustainable biochar to mitigate global climate change. *Nat. Commun.* **2010**, *1*, 56. [CrossRef]
30. Wang, L.; Chen, L.; Tsang, D.C.W.; Kua, H.W.; Yang, J.; Ok, Y.S.; Ding, S.; Hou, D.; Poon, C.S. The roles of biochar as green admixture for sediment-based construction products. *Cem. Concr. Compos.* **2019**, *104*, 103348. [CrossRef]
31. Pan, J.; Ma, J.; Zhai, L.; Luo, T.; Mei, Z.; Liu, H. Achievements of biochar application for enhanced anaerobic digestion: A review. *Bioresour. Technol.* **2019**, *292*, 122058. [CrossRef]
32. Kah, M.; Sigmund, G.; Xiao, F.; Hofmann, T. Sorption of ionizable and ionic organic compounds to biochar, activated carbon and other carbonaceous materials. *Water Res.* **2017**, *124*, 673–692. [CrossRef]
33. Kang, K.; Nanda, S.; Hu, Y. Current trends in biochar application for catalytic conversion of biomass to biofuels. *Catal. Today* **2022**, *404*, 3–18. [CrossRef]
34. Glaser, B.; Lehmann, J.; Zech, W. Ameliorating physical and chemical properties of highly weathered soils in the tropics with charcoal—A review. *Biol. Fertil. Soils* **2002**, *35*, 219–230. [CrossRef]
35. Pandit, N.R.; Mulder, J.; Hale, S.E.; Martinsen, V.; Schmidt, H.P.; Cornelissen, G. Biochar improves maize growth by alleviation of nutrient stress in a moderately acidic low-input Nepalese soil. *Sci. Total Environ.* **2018**, *625*, 1380–1389. [CrossRef]
36. Mohamed, B.A.; Ellis, N.; Kim, C.S.; Bi, X.; Emam, A.E. Engineered biochar from microwave-assisted catalytic pyrolysis of switchgrass for increasing water-holding capacity and fertility of sandy soil. *Sci. Total Environ.* **2016**, *566–567*, 387–397. [CrossRef]
37. Yang, X.; Tsibart, A.; Nam, H.; Hur, J.; El-Naggar, A.; Tack, F.M.G.; Wang, C.-H.; Lee, Y.H.; Tsang, D.C.W.; Ok, Y.S. Effect of gasification biochar application on soil quality: Trace metal behavior, microbial community, and soil dissolved organic matter. *J. Hazard. Mater.* **2019**, *365*, 684–694. [CrossRef]
38. Ruzickova, J.; Koval, S.; Raclavska, H.; Kucbel, M.; Svedova, B.; Raclavsky, K.; Juchelkova, D.; Scala, F. A comprehensive assessment of potential hazard caused by organic compounds in biochar for agricultural use. *J. Hazard. Mater.* **2021**, *403*, 123644. [CrossRef]
39. Purakayastha, T.J.; Bera, T.; Bhaduri, D.; Sarkar, B.; Mandal, S.; Wade, P.; Kumari, S.; Biswas, S.; Menon, M.; Pathak, H.; et al. A review on biochar modulated soil condition improvements and nutrient dynamics concerning crop yields: Pathways to climate change mitigation and global food security. *Chemosphere* **2019**, *227*, 345–365. [CrossRef]
40. Rizwan, M.; Ali, S.; Zia ur Rehman, M.; Rinklebe, J.; Tsang, D.C.W.; Bashir, A.; Maqbool, A.; Tack, F.M.G.; Ok, Y.S. Cadmium phytoremediation potential of Brassica crop species: A review. *Sci. Total Environ.* **2018**, *631–632*, 1175–1191. [CrossRef]
41. Rizwan, M.; Ali, S.; Qayyum, M.F.; Ibrahim, M.; Zia-ur-Rehman, M.; Abbas, T.; Ok, Y.S. Mechanisms of biochar-mediated alleviation of toxicity of trace elements in plants: A critical review. *Environ. Sci. Pollut. Res.* **2016**, *23*, 2230–2248. [CrossRef]
42. Qin, J.; Niu, A.; Liu, Y.; Lin, C. Arsenic in leafy vegetable plants grown on mine water-contaminated soils: Uptake, human health risk and remedial effects of biochar. *J. Hazard. Mater.* **2021**, *402*, 123488. [CrossRef]
43. Kapoor, A.; Sharma, R.; Kumar, A.; Sepehya, S. Biochar as a means to improve soil fertility and crop productivity: A review. *J. Plant Nutr.* **2022**, *45*, 2380–2388. [CrossRef]
44. Ding, Y.; Liu, Y.; Liu, S.; Li, Z.; Tan, X.; Huang, X.; Zeng, G.; Zhou, L.; Zheng, B. Biochar to improve soil fertility. A review. *Agron. Sustain. Dev.* **2016**, *36*, 36. [CrossRef]
45. Tratsch, M.V.M.; Ceretta, C.A.; da Silva, L.S.; Ferreira, P.A.A.; Brunetto, G. Composition and mineralization of organic compost derived from composting of fruit and vegetable waste. *Rev. Ceres* **2019**, *66*, 307–315. [CrossRef]
46. Zhang, L.; Sun, X. Changes in physical, chemical, and microbiological properties during the two-stage co-composting of green waste with spent mushroom compost and biochar. *Bioresour. Technol.* **2014**, *171*, 274–284. [CrossRef]
47. Sanchez-Monedero, M.A.; Cayuela, M.L.; Roig, A.; Jindo, K.; Mondini, C.; Bolan, N. Role of biochar as an additive in organic waste composting. *Bioresour. Technol.* **2018**, *247*, 1155–1164. [CrossRef]
48. Czekała, W.; Malińska, K.; Cáceres, R.; Janczak, D.; Dach, J.; Lewicki, A. Co-composting of poultry manure mixtures amended with biochar—The effect of biochar on temperature and C-CO_2 emission. *Bioresour. Technol.* **2016**, *200*, 921–927. [CrossRef]
49. Sørmo, E.; Silvani, L.; Thune, G.; Gerber, H.; Schmidt, H.P.; Smebye, A.B.; Cornelissen, G. Waste timber pyrolysis in a medium-scale unit: Emission budgets and biochar quality. *Sci. Total Environ.* **2020**, *718*, 137335. [CrossRef]

50. Weng, Z.; Van Zwieten, L.; Singh, B.P.; Tavakkoli, E.; Joseph, S.; Macdonald, L.M.; Rose, T.J.; Rose, M.T.; Kimber, S.W.L.; Morris, S.; et al. Biochar built soil carbon over a decade by stabilizing rhizodeposits. *Nat. Clim. Chang.* **2017**, *7*, 371–376. [CrossRef]
51. Godlewska, P.; Ok, Y.S.; Oleszczuk, P. THE DARK SIDE OF BLACK GOLD: Ecotoxicological aspects of biochar and biochar-amended soils. *J. Hazard. Mater.* **2021**, *403*, 123833. [CrossRef]
52. He, M.; Xiong, X.; Wang, L.; Hou, D.; Bolan, N.S.; Ok, Y.S.; Rinklebe, J.; Tsang, D.C.W. A critical review on performance indicators for evaluating soil biota and soil health of biochar-amended soils. *J. Hazard. Mater.* **2021**, *414*, 125378. [CrossRef]
53. Wang, J.; Wang, S. Preparation, modification and environmental application of biochar: A review. *J. Clean. Prod.* **2019**, *227*, 1002–1022. [CrossRef]
54. Kimbell, L.K.; Tong, Y.; Mayer, B.K.; McNamara, P.J. Biosolids-Derived Biochar for Triclosan Removal from Wastewater. *Environ. Eng. Sci.* **2018**, *35*, 513–524. [CrossRef]
55. Li, H.; Dong, X.; da Silva, E.B.; de Oliveira, L.M.; Chen, Y.; Ma, L.Q. Mechanisms of metal sorption by biochars: Biochar characteristics and modifications. *Chemosphere* **2017**, *178*, 466–478. [CrossRef]
56. Beckinghausen, A.; Reynders, J.; Merckel, R.; Wu, Y.W.; Marais, H.; Schwede, S. Post-pyrolysis treatments of biochars from sewage sludge and A. mearnsii for ammonia (NH4-n) recovery. *Appl. Energy* **2020**, *271*, 115212. [CrossRef]
57. Zhou, J.; Liu, S.; Zhou, N.; Fan, L.; Zhang, Y.; Peng, P.; Anderson, E.; Ding, K.; Wang, Y.; Liu, Y.; et al. Development and application of a continuous fast microwave pyrolysis system for sewage sludge utilization. *Bioresour. Technol.* **2018**, *256*, 295–301. [CrossRef]
58. Nobaharan, K.; Bagheri Novair, S.; Asgari Lajayer, B.; van Hullebusch, E. Phosphorus Removal from Wastewater: The Potential Use of Biochar and the Key Controlling Factors. *Water* **2021**, *13*, 517. [CrossRef]
59. Ambaye, T.G.; Vaccari, M.; van Hullebusch, E.D.; Amrane, A.; Rtimi, S. Mechanisms and adsorption capacities of biochar for the removal of organic and inorganic pollutants from industrial wastewater. *Int. J. Environ. Sci. Technol.* **2021**, *18*, 3273–3294. [CrossRef]
60. Dixit, A.; Gupta, S.; Pang, S.D.; Kua, H.W. Waste Valorisation using biochar for cement replacement and internal curing in ultra-high performance concrete. *J. Clean. Prod.* **2019**, *238*, 117876. [CrossRef]
61. Akhtar, A.; Sarmah, A.K. Novel biochar-concrete composites: Manufacturing, characterization and evaluation of the mechanical properties. *Sci. Total Environ.* **2018**, *616–617*, 408–416. [CrossRef]
62. Gupta, S.; Kua, H.W. Factors Determining the Potential of Biochar As a Carbon Capturing and Sequestering Construction Material: Critical Review. *J. Mater. Civ. Eng.* **2017**, *29*, 04017086. [CrossRef]
63. Gupta, S.; Kua, H.W. Carbonaceous micro-filler for cement: Effect of particle size and dosage of biochar on fresh and hardened properties of cement mortar. *Sci. Total Environ.* **2019**, *662*, 952–962. [CrossRef] [PubMed]
64. Gupta, S.; Kua, H.W.; Koh, H.J. Application of biochar from food and wood waste as green admixture for cement mortar. *Sci. Total Environ.* **2018**, *619–620*, 419–435. [CrossRef] [PubMed]
65. Gupta, S.; Kua, H.W. Effect of water entrainment by pre-soaked biochar particles on strength and permeability of cement mortar. *Constr. Build. Mater.* **2018**, *159*, 107–125. [CrossRef]
66. Kim, J.-Y.; Oh, S.; Park, Y.-K. Overview of biochar production from preservative-treated wood with detailed analysis of biochar characteristics, heavy metals behaviors, and their ecotoxicity. *J. Hazard. Mater.* **2020**, *384*, 121356. [CrossRef]
67. Lee, J. Characterization of urban stormwater runoff. *Water Res.* **2000**, *34*, 1773–1780. [CrossRef]
68. Inyang, M.I.; Gao, B.; Yao, Y.; Xue, Y.; Zimmerman, A.; Mosa, A.; Pullammanappallil, P.; Ok, Y.S.; Cao, X. A review of biochar as a low-cost adsorbent for aqueous heavy metal removal. *Crit. Rev. Environ. Sci. Technol.* **2016**, *46*, 406–433. [CrossRef]
69. Jin, H.; Wang, X.; Gu, Z.; Polin, J. Carbon materials from high ash biochar for supercapacitor and improvement of capacitance with HNO3 surface oxidation. *J. Power Sources* **2013**, *236*, 285–292. [CrossRef]
70. Coetzee, G.H.; Sakurovs, R.; Neomagus, H.W.J.P.; Everson, R.C.; Mathews, J.P.; Bunt, J.R. Particle size influence on the pore development of nanopores in coal gasification chars: From micron to millimeter particles. *Carbon N. Y.* **2017**, *112*, 37–46. [CrossRef]
71. Ge, X.; Wu, Z.; Wu, Z.; Yan, Y.; Cravotto, G.; Ye, B.-C. Microwave-assisted modification of activated carbon with ammonia for efficient pyrene adsorption. *J. Ind. Eng. Chem.* **2016**, *39*, 27–36. [CrossRef]
72. Fagerström, A.; Al Seadi, T.; Rasi, S.; Briseid, T. The role of anaerobic digestion and biogas in the circular economy. *IEA Bioenergy* **2018**, *8*, 1–24.
73. Liu, F.; Rotaru, A.-E.; Shrestha, P.M.; Malvankar, N.S.; Nevin, K.P.; Lovley, D.R. Promoting direct interspecies electron transfer with activated carbon. *Energy Environ. Sci.* **2012**, *5*, 8982. [CrossRef]
74. Fidel, R.B.; Laird, D.A.; Thompson, M.L.; Lawrinenko, M. Characterization and quantification of biochar alkalinity. *Chemosphere* **2017**, *167*, 367–373. [CrossRef]
75. Mumme, J.; Srocke, F.; Heeg, K.; Werner, M. Use of biochars in anaerobic digestion. *Bioresour. Technol.* **2014**, *164*, 189–197. [CrossRef]
76. Sunyoto, N.M.S.; Zhu, M.; Zhang, Z.; Zhang, D. Effect of biochar addition on hydrogen and methane production in two-phase anaerobic digestion of aqueous carbohydrates food waste. *Bioresour. Technol.* **2016**, *219*, 29–36. [CrossRef]
77. Ismaeel, W.S.E. Assessing and Developing the Application of LEED Green Building Rating System as a Sustainable Project Management and Market Tool in the Italian Context. *J. Eng. Proj. Prod. Manag.* **2016**, *6*, 136–152. [CrossRef]
78. Klöpffer, W. *Background and Future Prospects in Life Cycle Assessment*; Springer Science & Business Media: Berlin, Germany, 2014.
79. Souza, D.M.; Teixeira, R.F.M.; Ostermann, O.P. Assessing biodiversity loss due to land use with Life Cycle Assessment: Are we there yet? *Glob. Chang. Biol.* **2015**, *21*, 32–47. [CrossRef]

80. Matuštík, J.; Hnátková, T.; Kočí, V. Life cycle assessment of biochar-to-soil systems: A review. *J. Clean. Prod.* **2020**, *259*, 120998. [CrossRef]
81. Zhu, X.; Labianca, C.; He, M.; Luo, Z.; Wu, C.; You, S.; Tsang, D.C.W. Life-cycle assessment of pyrolysis processes for sustainable production of biochar from agro-residues. *Bioresour. Technol.* **2022**, *360*, 127601. [CrossRef]
82. Miller-Robbie, L.; Ulrich, B.A.; Ramey, D.F.; Spencer, K.S.; Herzog, S.P.; Cath, T.Y.; Higgins, C.P. Life cycle energy and greenhouse gas assessment of the co-production of biosolids and biochar for land application. *J. Clean. Prod.* **2015**, *91*, 118–127. [CrossRef]
83. Thers, H.; Djomo, S.N.; Elsgaard, L.; Knudsen, M.T. Biochar potentially mitigates greenhouse gas emissions from cultivation of oilseed rape for biodiesel. *Sci. Total Environ.* **2019**, *671*, 180–188. [CrossRef] [PubMed]
84. Oldfield, T.L.; Sikirica, N.; Mondini, C.; López, G.; Kuikman, P.J.; Holden, N.M. Biochar, compost and biochar-compost blend as options to recover nutrients and sequester carbon. *J. Environ. Manag.* **2018**, *218*, 465–476. [CrossRef] [PubMed]
85. Smebye, A.B.; Sparrevik, M.; Schmidt, H.P.; Cornelissen, G. Life-cycle assessment of biochar production systems in tropical rural areas: Comparing flame curtain kilns to other production methods. *Biomass Bioenergy* **2017**, *101*, 35–43. [CrossRef]
86. Brassard, P.; Godbout, S.; Pelletier, F.; Raghavan, V.; Palacios, J.H. Pyrolysis of switchgrass in an auger reactor for biochar production: A greenhouse gas and energy impacts assessment. *Biomass Bioenergy* **2018**, *116*, 99–105. [CrossRef]
87. Hamedani, R.; Kuppens, T.; Malina, R. Life cycle assessment and environmental valuation of biochar production: Two case studies in Belgium. *Energies* **2019**, *12*, 2166. [CrossRef]
88. Mohammadi, A.; Cowie, A.; Mai, T.L.A.; de la Rosa, R.A.; Brandao, M.; Kristiansen, P.; Joseph, S. Quantifying the greenhouse gas reduction benefits of utilising straw biochar and enriched biochar. *Energy Procedia* **2016**, *97*, 254–261. [CrossRef]
89. Uusitalo, V.; Leino, M. Neutralizing global warming impacts of crop production using biochar from side flows and buffer zones: A case study of oat production in the boreal climate zone. *J. Clean. Prod.* **2019**, *227*, 48–57. [CrossRef]
90. Clare, A.; Shackley, S.; Joseph, S.; Hammond, J.; Pan, G.; Bloom, A. Competing uses for China's straw: The economic and carbon abatement potential of biochar. *GCB Bioenergy* **2015**, *7*, 1272–1282. [CrossRef]
91. anak Erison, A.E.; Tan, Y.H.; Mubarak, N.M.; Kansedo, J.; Khalid, M.; Abdullah, M.O.; Ghasemi, M. Life cycle assessment of biodiesel production by using impregnated magnetic biochar derived from waste palm kernel shell. *Environ. Res.* **2022**, *214*, 114149. [CrossRef]
92. Lefebvre, D.; Williams, A.; Kirk, G.J.D.; Meersmans, J.; Sohi, S.; Goglio, P.; Smith, P. An anticipatory life cycle assessment of the use of biochar from sugarcane residues as a greenhouse gas removal technology. *J. Clean. Prod.* **2021**, *312*, 127764. [CrossRef]
93. Field, J.L.; Keske, C.M.H.; Birch, G.L.; DeFoort, M.W.; Cotrufo, M.F. Distributed biochar and bioenergy coproduction: A regionally specific case study of environmental benefits and economic impacts. *GCB Bioenergy* **2013**, *5*, 177–191. [CrossRef]
94. Xu, X.; Cheng, K.; Wu, H.; Sun, J.; Yue, Q.; Pan, G. Greenhouse gas mitigation potential in crop production with biochar soil amendment—A carbon footprint assessment for cross-site field experiments from China. *GCB Bioenergy* **2019**, *11*, 592–605. [CrossRef]
95. Barry, D.; Barbiero, C.; Briens, C.; Berruti, F. Pyrolysis as an economical and ecological treatment option for municipal sewage sludge. *Biomass Bioenergy* **2019**, *122*, 472–480. [CrossRef]
96. Hammond, J.; Shackley, S.; Sohi, S.; Brownsort, P. Prospective life cycle carbon abatement for pyrolysis biochar systems in the UK. *Energy Policy* **2011**, *39*, 2646–2655. [CrossRef]
97. Baumann, H.; Tillman, A.-M. The Hitch Hiker´s Guide to LCA—An orientation in LCA methodology and application. *Int. J. Life Cycle Assess.* **2006**, *11*, 142. [CrossRef]
98. Tiegam, R.F.T.; Tchuifon, D.R.T.; Santagata, R.; Nanssou, P.A.K.; Anagho, S.G.; Ionel, I.; Ulgiati, S. Production of activated carbon from cocoa pods: Investigating benefits and environmental impacts through analytical chemistry techniques and life cycle assessment. *J. Clean. Prod.* **2021**, *288*, 125464. [CrossRef]
99. Dutta, B.; Raghavan, V. A life cycle assessment of environmental and economic balance of biochar systems in Quebec. *Int. J. Energy Environ. Eng.* **2014**, *5*, 106. [CrossRef]
100. Ferreira, J.V.R. *Análise de Ciclo de Vida de Produtos*; Instituto Politécnico de Viseu: Viseu Dão Lafões, Portugal, 2004; 80p. [CrossRef]
101. Ismaeel, W.S.E. Midpoint and endpoint impact categories in Green building rating systems. *J. Clean. Prod.* **2018**, *182*, 783–793. [CrossRef]
102. Ferrão, P.C. Ecologia industrial: Princípios e ferramentas. *Eng. Sanit. Ambient.* **2009**, *17*. [CrossRef]
103. Yang, Q.; Zhou, H.; Zhang, X.; Nielsen, C.P.; Li, J.; Lu, X.; Yanga, H.; Chen, H. Hybrid life-cycle assessment for energy consumption and greenhouse gas emissions of a typical biomass gasification power plant in China. *J. Clean. Prod.* **2018**, *205*, 661–671. [CrossRef]
104. Zhang, C.; Liu, L.; Zhao, M.; Rong, H.; Xu, Y. The environmental characteristics and applications of biochar. *Environ. Sci. Pollut. Res.* **2018**, *25*, 21525–21534. [CrossRef] [PubMed]
105. Llorach-Massana, P.; Lopez-Capel, E.; Peña, J.; Rieradevall, J.; Montero, J.I.; Puy, N. Technical feasibility and carbon footprint of biochar co-production with tomato plant residue. *Waste Manag.* **2017**, *67*, 121–130. [CrossRef] [PubMed]
106. Santero, N.J.; Masanet, E.; Horvath, A. Life-cycle assessment of pavements Part II: Filling the research gaps. *Resour. Conserv. Recycl.* **2011**, *55*, 810–818. [CrossRef]
107. De Vries, M.; de Boer, I.J.M. Comparing environmental impacts for livestock products: A review of life cycle assessments. *Livest. Sci.* **2010**, *128*, 1–11. [CrossRef]
108. Muñoz, E.; Curaqueo, G.; Cea, M.; Vera, L.; Navia, R. Environmental hotspots in the life cycle of a biochar-soil system. *J. Clean. Prod.* **2017**, *158*, 1–7. [CrossRef]

109. Ilankoon, I.; Ghorbani, Y.; Chong, M.N.; Herath, G.; Moyo, T.; Petersen, J. E-waste in the international context–A review of trade flows, regulations, hazards, waste management strategies and technologies for value recovery. *Waste Manag.* **2018**, *82*, 258–275. [CrossRef]
110. Durairaj, S. Evaluation of Life Cycle Cost Analysis Methodologies. *Corp. Environ. Strateg.* **2002**, *9*, 30–39. [CrossRef]
111. Woodward, D.G. Life cycle costing—Theory, information acquisition and application. *Int. J. Proj. Manag.* **1997**, *15*, 335–344. [CrossRef]
112. Dahlén, P.; Bolmsjö, G.S. Life-cycle cost analysis of the labor factor. *Int. J. Prod. Econ.* **1996**, *46–47*, 459–467. [CrossRef]
113. Bras, B.; Emblemsvåg, J. Designing for the Life-Cycle: Activity-Based Costing and Uncertainty. In *Design for X*; Springer: Dordrecht, The Netherlands, 1996; pp. 398–423.
114. Cobas-Flores, E.; Hendrickson, C.T.; Lave, L.B.; McMichael, F.C. Life cycle analysis of batteries using economic input-output analysis. In Proceedings of the 1996 IEEE International Symposium on Electronics and the Environment, Dallas, TX, USA, 6–8 May 1996; pp. 130–134.
115. Eversheim, W.; Neuhausen, J.; Sesterhenn, M. Design-to-Cost for Production Systems. *CIRP Ann.* **1998**, *47*, 357–360. [CrossRef]
116. Westkämper, E.; Osten-Sacken, D.v.d. Product Life Cycle Costing Applied to Manufacturing Systems. *CIRP Ann.* **1998**, *47*, 353–356. [CrossRef]
117. Roberts, K.G.; Gloy, B.A.; Joseph, S.; Scott, N.R.; Lehmann, J. Life cycle assessment of biochar systems: Estimating the energetic, economic, and climate change potential. *Environ. Sci. Technol.* **2010**, *44*, 827–833. [CrossRef]
118. Galinato, S.P.; Yoder, J.K.; Granatstein, D. The economic value of biochar in crop production and carbon sequestration. *Energy Policy* **2011**, *39*, 6344–6350. [CrossRef]
119. Yoder, J.; Galinato, S.; Granatstein, D.; Garcia-Pérez, M. Economic tradeoff between biochar and bio-oil production via pyrolysis. *Biomass Bioenergy* **2011**, *35*, 1851–1862. [CrossRef]
120. Homagain, K.; Shahi, C.; Luckai, N.; Sharma, M. Life cycle cost and economic assessment of biochar-based bioenergy production and biochar land application in Northwestern Ontario, Canada. *For. Ecosyst.* **2016**, *3*, 21. [CrossRef]
121. Cleary, J. Life Cycle Impacts and Costs of Biochar Production Using Sawmill Residues. Available online: http//www.biofuelnet.ca/nce/wp-content/uploads/2015/08/Pathways_Clear.pdf (accessed on 7 October 2022).

processes

MDPI

Article

Techno-Economic Assessment of Solar-Driven Steam Gasification of Biomass for Large-Scale Hydrogen Production

Houssame Boujjat [1], Sylvain Rodat [2] and Stéphane Abanades [2,*]

[1] CEA-LITEN Solar and Thermodynamic Systems Laboratory (L2ST), 38054 Grenoble, France; houssame.boujjat@cea.fr
[2] Processes, Materials and Solar Energy Laboratory, PROMES-CNRS, 7 Rue du Four Solaire, 66120 Font-Romeu, France; sylvain.rodat@promes.cnrs.fr
* Correspondence: stephane.abanades@promes.cnrs.fr; Tel.: +33-(0)4-68-30-77-30

Abstract: Solar biomass gasification is an attractive pathway to promote biomass valorization while chemically storing intermittent solar energy into solar fuels. The economic feasibility of a solar gasification process at a large scale for centralized H_2 production was assessed, based on the discounted cash-flow rate of return method to calculate the minimum H_2 production cost. H_2 production costs from solar-only, hybrid and conventional autothermal biomass gasification were evaluated under various economic scenarios. Considering a biomass reference cost of 0.1 €/kg, and a land cost of 12.9 €/m^2, H_2 minimum price was estimated at 2.99 €/kg$_{H2}$ and 2.48 €/kg$_{H2}$ for the allothermal and hybrid processes, respectively, against 2.25 €/kg$_{H2}$ in the conventional process. A sensitivity study showed that a 50% reduction in the heliostats and solar tower costs, combined with a lower land cost of below 0.5 €/m^2, allowed reaching an area of competitiveness where the three processes meet. Furthermore, an increase in the biomass feedstock cost by a factor of 2 to 3 significantly undermined the profitability of the autothermal process, in favor of solar hybrid and solar-only gasification. A comparative study involving other solar and non-solar processes led to conclude on the profitability of fossil-based processes. However, reduced CO_2 emissions from the solar process and the application of carbon credits are definitely in favor of solar gasification economics, which could become more competitive. The massive deployment of concentrated solar energy across the world in the coming years can significantly reduce the cost of the solar materials and components (heliostats), and thus further alleviate the financial cost of solar gasification.

Keywords: solar gasification; hybridization; hydrogen; biomass/waste conversion; syngas; economics

1. Introduction

Today, around 96% of hydrogen is generated from fossil fuels (78% from natural gas and liquid hydrocarbons and 18% from coal) and only a low proportion of 4% is generated from water electrolysis [1]. In industry, hydrogen is mostly generated using carbon-based CO_2-emitting methods, such as steam reforming of light hydrocarbons, partial oxidation (POX) and autothermal reforming (AR) (which is a combination of the two previous processes) followed by coal gasification. Although extremely dependent on the price of natural gas, steam reforming remains the most preferred pathway for H_2 production given that it reached a high state of maturity outlined by lower production costs, usually below 2 $/kg of H_2, including CO_2 capture and sequestration [2,3].

Currently, the largest volumes of hydrogen, produced or commercially available, are consumed in the chemical industry with a share of 63% for the production of ammonia, methanol, polymer and resin industries. Refineries are the second largest hydrogen consumers with a share of more than 30%, mainly for hydrocracking and crude oil hydrotreatment. Metallurgical industry consumes around 6% of the share. It is followed by general industries such as semiconductor, glass production, hydrogenation of vegetable oils and fats, etc., with a minor share of 1% [4].

Hydrogen, used as an intermediate chemical species for the above-mentioned processes, is also seen as a promising zero-carbon footprint energy vector for massive storage of intermittent renewable energies. Clean, i.e., CO_2-neutral hydrogen, can be produced using biomass or/and water as primary feedstocks. The most mature methods for decarbonized H_2 production are water electrolysis and steam biomass gasification [5]. Possibly powered by a renewable energy source such as solar or wind, electrolysis uses an electrical current to split water electrochemically into separate streams of H_2 and O_2. Being commercially available for over a century, current commercial electrolysers reach single-stack/module capacities of several megawatts with conversion efficiencies up to 85% [6]. Biomass gasification has advantages from the extensive accumulated experience of fossil fuels thermochemical gasification, which represents the state-of-the-art for industrial-scale H_2 generation. Biomass steam gasification produces a synthesis gas composed of both H_2 and CO at a high temperature (>900 °C). The syngas, therefore, needs to be upgraded (shifted to hydrogen) and purified in downstream equipment. According to the IEA Bioenergy's report in 2018 [5], hydrogen production from biomass, as a complementary route to increase the share of renewables, cannot be accomplished without the full-process chain validation at a large scale, involving an optimal biomass gasification technology capable of treating and converting a wide range of feedstocks.

Considering the growing demand of biomass in the future, the optimization of the conversion systems to make the best use of biomass is an absolute necessity. A promising way to save the biomass resource while maximizing the yield, quality and purity of the synthesis gas consists of using concentrated sunlight as an external source of energy to drive the endothermal thermochemical reactions instead of continually burning a part of the feedstock. The process goal is to replace feedstock combustion totally (solar-only systems) or partially (hybrid solar/autothermal systems), thanks to external heating using high-temperature concentrating solar technologies.

The solar process viability for coal and biomass gasification has been thoroughly studied at both laboratory [7–13] and pilot scales [14–16]. Accordingly, the extrapolation of these solar technologies to larger scales for semi-central or centralized green solar hydrogen production is auspicious in the future, in view of the increasing decarbonized hydrogen demand. Although more environmentally friendly than the conventional autothermal biomass gasification process (because it avoids the use of part of the biomass source for process heat), the question of the solar process's economic feasibility and competitiveness arises. On the one hand, the solar process allows for the production of a high-quality synthesis gas with a higher gas output per unit of feedstock, and on the other hand, the solar process is highly dependent on an intermittent heat source, which requires an initial substantial investment. The question is, therefore, not simple, and requires detailed investigation to highlight both technical aspects related to the management of the heat source variability [17–20] and economic and financial aspects for accurate cost evaluation [21–23]. In a previous work [19], a dynamic mathematical model of an up-scaled MW steam solar gasifier was developed. The model was used to assess the transient behavior of the reactor for three successive days with and without cloud cover. Different reactants' feeding management strategies were proposed and compared, with the aim of achieving enhanced syngas productivity and optimized use of solar energy. The OPTI mode controlled the supplies (biomass and steam) in order to stabilize the reactor temperature around a set point value (assumed to be 1200 °C) for as long as possible. The HYB production mode used the OPTI mode when the solar irradiation was sufficiently high, to gasify a minimum biomass flow rate (e.g., 1 t/h). Otherwise, the solar heating was assisted by in situ injection of O_2 to counteract the solar power decline and to maintain the reactor temperature constant all day long. Annual data were generated thanks to the dynamic model to estimate the feedstock consumption and syngas productivity under real solar irradiation conditions.

In the present work, a techno-economic study was carried out using the dynamic model predictions regarding the yearly gas production with the two recalled control

strategies (OPTI and HYB). H_2 cost at plant gate for the autothermal (non-solar), hybrid (solar/optimized-combustion) and allothermal (solar-only) processes operating at different design capacities is evaluated using the DOE's H2A tool for hydrogen cost analysis [24]. Furthermore, a sensitivity study is performed to establish the impact of different factors on the cost of hydrogen. Finally, the cost of hydrogen is compared with other solar and non-solar processes for H_2 generation.

2. Solar Hydrogen Cost Model

2.1. General Principle

The DOE's H2A tool used in this study is based on the Discounted Cash Flow (DCF) rate of return method. DCF analysis finds the present value of expected future cash flows using a discount rate. The Internal Rate of Return (IRR) is the discount rate that cancels the Net Present Value (NPV). The *NPV* calculation (Equation (1)) converts all the expected future cash flows of a project into their "present value", i.e., their value at the initial time, at the very beginning of the project. Then, all the present values are added together to characterize the overall value of the company's project, in other words, the profitability of the project. The *NPV* is the cash flow generated at the end of the project

$$NPV = -I + \sum_{p=1}^{p=N} \frac{F_p}{(1+i)^p} \quad (1)$$

with I, the investment, F_p, the cash flow for year p, N, the total duration of the project (years), 'i', the discount rate (it reflects the cost of capital, so it may take the value of the market interest rate for a comparable duration, even though this value is often discussed). In the DOE's tool, 'i' is fixed and the model calculates the minimum hydrogen price so that the *NPV* cancels.

The starting point is a reference conventional (non-solar) biomass gasification process, previously developed by Mann and Steward [25]. The minimum cost of hydrogen was calculated with an indirectly heated steam woody biomass gasifier (based on a dual fluidized bed technology). The process model included biomass treatment and injection units, the reactor, gas compressors and scrubbing units, followed by a steam methane reformer (SMR), water gas shift reactors (WGS), and a Pressure Swing Absorption (PSA) unit to reach a hydrogen purity above 99.9%. Hydrogen was thereafter compressed to 7 MPa prior to shipment through a pipeline. In order to minimize the plant water consumption, the water contained in the syngas was recovered at different points of the cycle. Moreover, part of the electricity needed by the chemical plant was generated by recovering heat from the high-temperature syngas. A heat-recovery system using a steam turbine and a generator was, therefore, coupled to the chemical units. More details about the energy/material inflows and outflows can be found in [25]. The solarization of such a chemical process impacts a number of factors, including the capital investment, the O&M costs, and the plant biomass, water and electricity consumptions. These factors were estimated and integrated with the previously developed cost model using the dynamic simulation results (for yearly productivity estimation), as well as the previously reported Concentrated Solar Tower (CST) plants' operational costs.

2.2. Cost Model Assumptions

2.2.1. Basic Flow Diagram

The solar powered chemical process was modeled using the measured solar data (averaged over a 19-year period: 1991–2010) in Odeillo, in France. This region is characterized by a high duration and quality of sunshine (more than 2.2 MWh/m^2.year) with a great clarity of atmosphere.

The basic process flow diagram is described in Figure 1. It consisted of a solar plant composed of a heliostat field and reflecting towers (beam-down technology), and of a chemical plant for biomass gasification and gas processing/purification. The gasifier

was fed by both steam and air. Air injection was considered only when operating in full autothermal or in hybrid (solar-combustion) modes. In the model, gas cleaning and upgrading chemical units (such as WGS and PSA) were assumed to be able to withstand rapid changes in gas flows and composition. WGS aims to react CO with H_2O to produce H_2 and CO_2, while PSA is used to obtain a pure H_2 stream as a process output. The PSA off-gas thus has no calorific value because CO is first shifted to H_2 in the WGS unit, which means the calorific value of CO contained in the produced syngas is recovered in the form of H_2 after WGS. As the aim was here to yield pure H_2 (for purpose of comparison with other H_2 production methods), the remaining PSA off-gas was not further considered in the study (the remaining PSA off-stream would consist of mainly CO_2 and N_2, but further post-processing was not included).

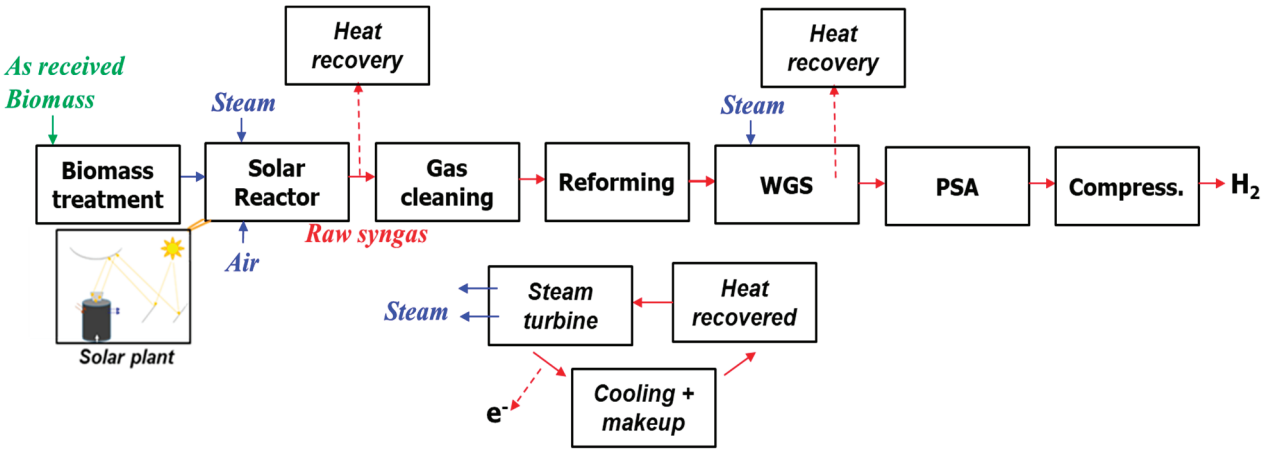

Figure 1. Biomass solar gasification flow diagram.

2.2.2. Capital costs

(i) Direct capital costs:

The major chemical component costs (installed) at the chemical baseline (defined by a design capacity *DC* of 155,236 kg of H_2 per day) are presented in Table 1.

Table 1. Direct capital costs at chemical baseline (installed, to be scaled).

	M€
Feed Handling and Drying	24.57
Gasification, Tar Reforming, and Quench	21.84
Compression and Sulfur Removal	20.28
Steam Methane Reforming, Shift, and PSA	39.39
Steam System and Power Generation	18.72
Cooling Water and Other Utilities	4.42
Buildings and Structures	19.26

These costs were scaled to different design points using Equation (2).

$$Component'i'cost_{at\ DC} = Component_{\ at\ chemical\_baseline}\ cost \cdot \left(\frac{DC}{Chemical\_baseline\ DC}\right)^{n_{chemical}} \quad (2)$$

with $n_{chemical}$ = 0.78 [25] and *DC* in kg of H_2 per day.

The *heliostat field cost* at *DC* was calculated by Equation (3).

$$Heliost\ cost_{at\ DC} = Mirror\ reference\ cost.field\ surface_{\ at\ DC} \quad (3)$$

$$field\ surface_{\ at\ DC} = field\ surface_{\ at\ solar\_baseline} \cdot \frac{DC}{Solar\_baseline_{OPTI,HYB}\ DC} \quad (4)$$

The *mirror reference cost* in €/m^2 was assumed to be equal to 120 €/m^2 based on reference [26]. The solar baseline was defined by a thermal power input on the solar field of 10 MW$_{th}$ (at a Direct Normal Irradiance *DNI* of 1000 W.m^{-2}). Thus, *Solar_baseline* $_{OPTI,\ HYB}$ *DC* was directly deduced from the previously developed dynamic model [19]. It was estimated at 1402.0 kg H_2/day for the OPTI mode and 4196.1 kg H_2/day for the HYB mode. The *field surface* $_{at\ solar\_baseline}$ in m^2 was calculated by Equation (5).

$$field\ surface_{at\ solar\_baseline} = \frac{Q_{sun \to field,max}}{DNI_{max}} \quad (5)$$

with $Q_{sun \to field,max}$ = 10 MW and DNI_{max} = 1000 W.m^{-2}.

Similarly, the *tower cost* $_{at\ DC}$ was calculated by Equation (6).

$$tower\ cost_{at\ DC} = tower\ cost_{at\ solar\_baseline} \cdot \frac{DC}{Solar\_baseline_{OPTI,HYB}\ DC} \quad (6)$$

As tower costs in the literature are often expressed in € per MWe, *tower cost* $_{at\ solar\_baseline}$ was deduced from Equation (7), assuming a solar-to-electric efficiency $\eta_{solar\text{-}to\text{-}electric}$ of 30% [27] including the receiver thermal efficiency and a field efficiency $\eta_{opt,field}$ of 70% [28].

$$tower\ \ cost_{at\ solar\_baseline} = tower\ cost\ in\ /10\ MW_e \cdot (\eta_{opt,field} \cdot \eta_{solar-to-electric}) \quad (7)$$

Tower cost per 10 MW_e was considered equal to 2 M€ based on the data provided by Becker et al. [29] in the Ecostar roadmap;

(ii) Indirect depreciable capital costs:

The site preparation, engineering and design, project contingency and up-front permitting costs were calculated by applying a percentage to the sum of the direct capital costs of the overall plant (solar and chemical). These percentages were, respectively, 2%, 10%, 15%, 15%;

(iii) Non-depreciable capital costs:

The cost of land, which can greatly vary depending on the plant's location, was varied from 0.5 to 50 €/m^2. A typical serviced land in Odeillo costs up to 150 €/m^2 while bare land in rural regions costs only few cents to few euros per m^2. Equation (8) was used to estimate the plant *land cost*.

$$Land\ cost = Chemical\ land\ cost + Solar\ land\ cost \quad (8)$$

The *chemical land cost* was calculated by Equation (9).

$$Chemical\ land\ cost = land\ cost\ per\ m^2 . \left(\frac{DC}{Chemical\_baseline\ DC}\right)^{n_{chemical}} . Chemical.\ land\ required_{at\ Chemical\_\ baseline} \quad (9)$$

where the chemical plant land required at baseline design capacity was assumed equal to 20.2 hectares. The *solar land cost* was calculated by Equation (10).

$$Solar\ land\ cost = land\ cost\ per\ m^2 . solar\ field\ size_{at\ DC} \quad (10)$$

The *solar field size* $_{at\ DC}$ was considered seven times the *field surface* $_{at\ DC}$ (Equation (4)) according to the PS10 plant data in Spain [30].

2.2.3. Fixed Costs

The total *plant staff* was calculated by Equation (11).

$$Plant\ staff\ =\ Chemical\ plant\ staff + Solar\ plant\ staff \quad (11)$$

$$Chemical\ plant\ staff\ =\ chemical\ plant\ staff_{at\ Chemical\_\ baseline} \cdot \frac{DC\ (kg\ H_2/day)}{Chemical\_baseline\ DC\ (kg\ H_2/day)}^{0.25} \quad (12)$$

The *chemical plant staff* $_{at\ chemical\_baseline}$ was considered equal to 54. The CST plant associated one operator for each 6.25 hectares of mirrors, following the equation provided by Sargent and Lundy [31]. The total plant staffing cost was thus deduced, assuming a burdened labor cost of 54 €/person/h. The general and administrative expenses were estimated as 20% of the total plant staffing cost. The property taxes and insurance were assumed to be equal to 2% of the total capital costs, and the material maintenance costs and repairs were assumed to be equal to 0.5% of the project direct capital costs.

2.2.4. Utilities, Feedstock and Variable Costs

(i) Water:

Water was used for different purposes, beyond its main role as a biomass oxidizer. Water was used to clean (by removing impurities such as particulates and tars residuals) and to shift the syngas into hydrogen. An important amount of water was also used for the cooling of syngas at the exit of the gasification unit and after the last stages of compression. It was also substantially used for heat rejection in the condenser and as a makeup for the steam cycle. Design calculations allowed for estimation of the process water consumption at about 3.8 L/kg of H_2. The cooling water consumption was considerably higher, at around 300.0 L/kg of H_2 [25]. Additional washing water was required for the solar-powered chemical plant due to the periodic cleaning of the mirrors. Considering a washing water consumption V_{water} of the heliostat field of 18 L/MWh$_{th,on\ field}$ [32], the amount of required water per kg of H_2 was deduced from Equation (13). The total cost of water per kg of H_2 was hence calculated by Equation (14)

$$Washing\ water\ =\ V_{water} \cdot \frac{Q_{sun \rightarrow field,max}}{Solar\_baseline_{OPTI,HYB}\ DC} \quad (13)$$

$$Cost\ of\ water\ =\ (Washing\ water + Process\ water).\ C2 + Cooling\ water.\ C3 \quad (14)$$

with $C2 = 6.1 \times 10^{-4}$ €/L and $C3 = 3.0 \times 10^{-5}$ €/L;.

(ii) Electricity:

The different chemical plant sections consumed electricity to different extents. The compression of syngas was the most energy-demanding step in the process, representing up to 60% of the total electricity requirement. The heat recovery system generated most of the power. The deficit in electricity was, therefore, directly supplied by the grid. In conventional CST plants, the electrical requirement comprises the Heat Transfer Fluid (HTF) pumping, along with the electricity used for tracking the solar rays, which remains very low. As there is no HTF in the proposed solar gasification concept, and as the energy of the tracking is of minor significance [33], the electricity requirement of the solar plant was neglected. The overall process electricity requirement (supplied by the grid) was estimated in the previous cost model [25] at 0.98 kWh$_e$/kg of H_2, with a cost of electricity of 0.1 €/kWh;

(iii) Biomass:

Biomass consumption varies depending on how the gasifier is heated. In solar gasification, the available solar energy is collected, then concentrated by a field of mirrors and towers to ensure the complete and total conversion of the biomass load. In a purely

autothermal mode, the reactor is heated solely by burning part of the feedstock. In the hybrid mode, the biomass is partially burned, but to a lesser extent than in pure autothermal mode, as it is complemented by solar power when available. The prediction of the biomass consumption (expressed in $kg_{biomass,dry}/kg$ of H_2) for the three modes, OPTI, HYB and autothermal, was done based on the annual simulations. The biomass consumption of the three modes (OPTI, HYB, autothermal) used in the economic analysis are, respectively, 5.8, 8.7, and 9.7 $kg_{biomass,dry}/\ kg_{H2}$;

(iv) Other costs:

Other costs include catalysts and bed materials, environmental surcharges, waste treatment and solid waste disposal. These costs are recalled in Table 2 at the chemical baseline design capacity.

Table 2. Other variable operating costs.

	M€
Other materials	7.00
Waste treatment	1.20
Solid waste disposal	0.73
Environmental surcharges	0.13

The scaling to different design capacities followed Equation (15) [25].

$$Scaled\ variable\ cost\ =\ 1.426.Baseline\ cost\cdot\frac{DC\ (kg\ H_2/day)}{Chemical\_baseline\ DC\ (kg\ H_2/day)} \quad (15)$$

3. Results and Discussion

3.1. Design Parameters

Table 3 shows the calculated design parameters in the three plant configurations.

Table 3. Comparison between the three studied processes at DC = 150,000 kg_{H2}/day.

	Autothermal	**Hybrid**	**Allothermal**
Plant size (hectares)	19.7	250.2	748.9
Solar power on field (MW)	-	357.5	1069.9
Biomass consumption (t_{dry}/day)	1.45×10^3	1.30×10^3	0.87×10^3
Water consumption (m^3/day)	4.58×10^4	4.60×10^4	4.63×10^4
Annual Cold Gas efficiency [19]	0.80	0.93	1.34
CO_2 emissions (t/day) [19]	1.04×10^3	5.78×10^2	29.5

The plant land surface area dramatically increases by 12 times in the hybrid mode and by up to 37 times in the allothermal mode. The solar power is, therefore, 67% lower in the hybrid mode compared to the allothermal mode, at the expense of a greater biomass requirement. In fact, around 0.43×10^3 t/day more biomass is needed to power the reactor during hybrid and full-autothermal phases, which represents about 30% of the total feedstock consumed by the hybrid process. The interest in the allothermal process lies in its high CGE, which by far exceeds those of the hybrid and autothermal processes. The process water requirement, which includes the heat-recovery system for local power generation, is hardly impacted by solarization, as water consumption due to mirror cleaning represents only a small proportion of the total plant water requirement. CO_2 direct emissions due to gasification process (reactor heating and/or gasification reaction) are, on the other hand, 35 times lower in allothermal solar gasification because no combustion is used for process heat supply in this case. The overall carbon balance includes additional greenhouse gas emissions, which are released during the different phases of the solar plant's life-cycle, i.e., during raw material extraction, manufacturing

and assembly, transport, construction, site improvement, maintenance, replacements, dismantling/disposal and/or recycling. The application of credits for CO_2 mitigation and pollution avoidance will further enable the solar thermochemical technologies to compete favorably with fossil-fuel-based processes or autothermal technologies.

3.2. Cost Assessment

3.2.1. Key Parameters

The project was assumed to start in 2030 with a construction period of three years. It was financed through equity contributions and debt. All the financial inputs used in the economic study are recapped in Table 4. Hydrogen cost evaluation was carried out with a fixed operating capacity factor (CF) of 80% (accounting for possible maintenance and outage times). Due to the novelty of the project that may discourage some of the investors, the IRR was varied from 8% to 16%. The impact of equity financing (%) and the IRR on the cost of hydrogen for the three presented configurations is shown in Figure 2 (at a DC of 150,000 kg H_2/day, a biomass reference price of 0.10 €/kg and a land cost of 12.9 €/m^2). Due to the possible variability of the reference values for investment and operational costs estimations (depending on seasonal variations, biomass type, plant location, exploitation period, etc.), several sensitivity studies are proposed in the following discussion.

Table 4. Financial inputs.

Start-up time (years)	1
Analysis period and plant life (years)	30
Length of construction period (years)	3
% of Capital spent in 1st, 2nd and 3rd year of construction	8%, 60%, 32%
Depreciation Schedule Length (years)	20
Depreciation Type	MACRS
% of Fixed Operating Costs During Start-up (%)	100%
% of Revenues During Start-up (%)	50%
% of Variable Operating Costs During Start-up	75%
Decommissioning costs (% of depreciable capital investment)	10%
Salvage value (% of total capital investment)	10%
Inflation rate (%)	1.9%
Interest rate on debt	3.7%
Total Tax Rate (%)	25.7%
Working Capital (%)	15%

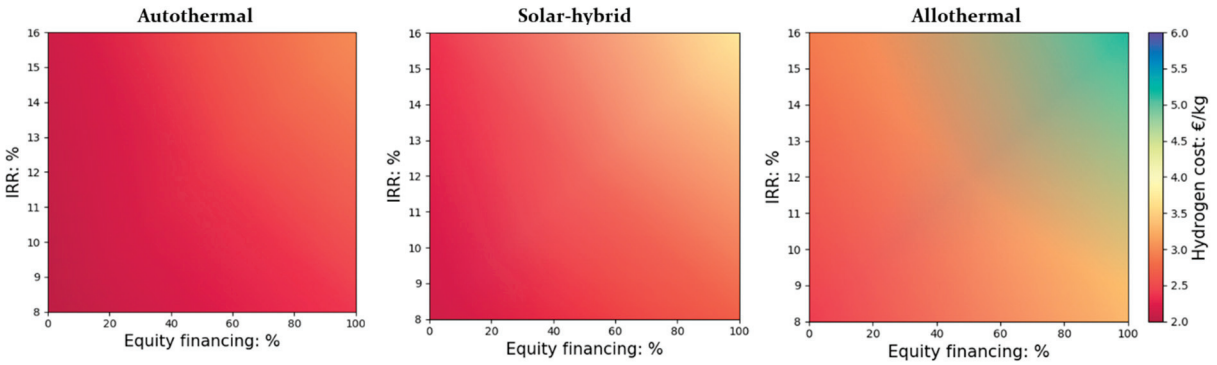

Figure 2. Impact of equity financing (%) and IRR on the cost of H_2 (DC = 150,000 kg H_2/day and a biomass reference price of 0.1 €/kg and land cost of 12.9 €/m^2).

It can be seen that these two purely financial parameters have a considerable impact on the price of hydrogen, which varies from 2.41 to 5.15 €/kg_{H2} for the solar-only heated process, from 2.15 to 3.72 €/kg_{H2} for the hybrid process, and from 2.03 to 3.02 €/kg_{H2} for the autothermal (non-solar) process. The increase in equity financing (at the expense of less incurred debt) drives up the cost of hydrogen markedly; for instance, for an IRR of 8%, an equity increases from 0% to 100% raises the cost of hydrogen by 37%, 25% and 18% (solar-only, hybrid, and autothermal, respectively). The influence of equity percentage on hydrogen price is, therefore, much greater for the allothermal process that required the largest initial capital investment. In such cases, the capital investment of the major pieces of equipment (installed) at *DC* = 150,000 kg H_2/day is 335.7 M€, while it is around 201.0 M€ for the hybrid process and only about 137.01 M€ for the non-solar autothermal process. The new shares issued by the increase in equity contributions hence provide more room to launch the investments, but, on the other hand, imply greater production costs.

In the following, a percentage of equity of 40% with an IRR of 10% is considered. The overall study reference assumptions are recapped in Table 5. The breakdown of the direct capital costs of the studied plants is shown in Figure 3. In the solar-driven processes (solar-only and hybrid solar/autothermal), the heliostat fields hold the largest share of the investment. It contributes to approximately 44% (solar-only) and 24% (hybrid) of the overall direct costs, in agreement with previously reported conventional CST plant values [34,35]. The smallest solar plant size required for the hybrid process leads to a reduced hydrogen price from 2.99 (allothermal) to 2.48 €/kg_{H2} (hybrid). The autothermal process is the cheapest, with a hydrogen price of 2.25 €/kg_{H2}.

Table 5. Reference assumptions.

Biomass cost (€/kg)	0.10
Land cost (€/m^2)	12.9
Mirror cost (€/m^2)	120
Tower cost (M€/MW_{th})	0.42
DC (kg H_2/day)	150,000
Electricity cost (€/kWh)	0.10
Water cost (€/m^3)	0.61 €/m^3 (process), 0.03 €/m^3 (cooling)

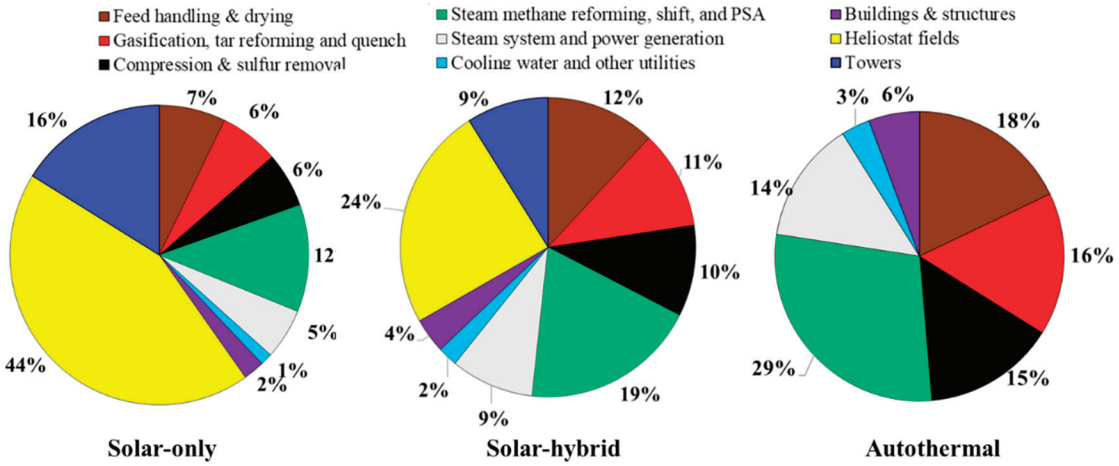

Figure 3. Direct capital investment breakdown (at reference assumptions, Table 5).

Figure 4 shows, in detail, the specific contribution of each item in the plant on the total cost of hydrogen. Solarization respectively increases the capital and the O&M costs

by more than three times and up to 46% (in the allothermal configuration). Moreover, the feedstock cost for the hybrid and the autothermal processes is the most predominant, and contributes to nearly 37% and 39% of the total hydrogen production cost (at plant gate). The allothermal process consumes less biomass, and, therefore, the feedstock cost is lower, representing barely 20%. This is approximately 1.6 times less than for the autothermal process. The impact on the plant variable costs and utilities remains very limited, showing a relative variation of only 2%.

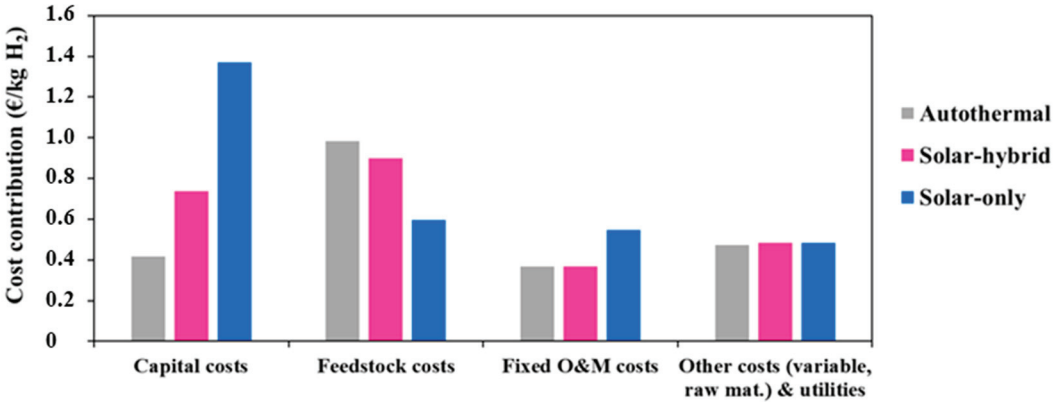

Figure 4. Specific contribution of each project component.

In the following sections, the influence of solar investment and biomass feedstock costs, as major economic factors affecting the minimum hydrogen price, is studied. A sensitivity analysis is carried out on these parameters to examine their impact on the profitability, the competitiveness and the relevance of the projects.

3.2.2. Impact of Solar Investment

The solar investment represents a high proportion of the overall project expenditure, which may be high enough to undermine the economic attractivity and viability of solar processes. In coming years, and in view of the increasing deployment of solar energy worldwide, the solar investment effort is expected to drop appreciably [26]. In fact, innovative designs and new technological solutions are studied intensely at present in many research laboratories with the objective of increasing the concentration efficiency and the durability of the materials. In conjunction with the economy of scale, this should reduce the solar costs to a certain extent, for the benefit of solar and solar hybrid gasification. In this respect, the influence of a possible cost reduction of the main solar compounds (i.e., heliostat field and towers) on the minimum hydrogen price was studied (Figure 5).

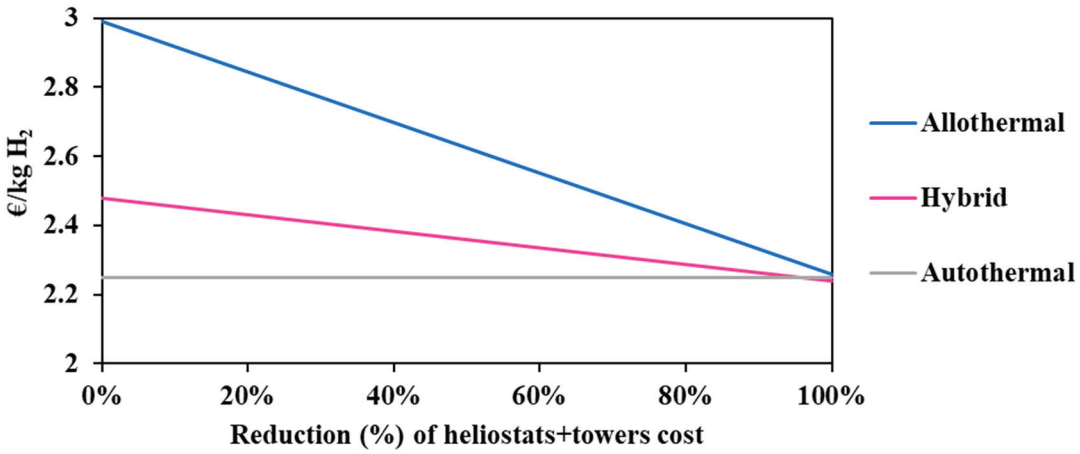

Figure 5. Impact of solar technologies cost reduction on the hydrogen minimum price.

It can be observed in Figure 5 that the solar allothermal process is the most costly. Moreover, the decline in the heliostat and tower costs results in reducing the hydrogen minimum price in a more pronounced fashion in the allothermal configuration. In fact, a 50% cost reduction declines the price of hydrogen by 0.37 €/kg_{H2} for the allothermal process, and by 0.12 €/kg_{H2} for the hybrid process. The intersection between the two curves is achieved only when the cost reduction is beyond 95%, which is practically unattainable. In any case, and whatever the cost reduction, solar and solar hybrid hydrogen generation remains more expensive as compared to the conventional autothermal process, which is due to major additional costs related to the heliostat field and tower, plant land, maintenance and staffing. Design calculations allowed for estimating the total area occupied by the solar plants (allothermal and hybrid): the heliostat field surface at DC = 150,000 kg H_2/day is estimated at 11.5 km^2 for the allothermal process and at 3.9 km^2 for the hybrid process. This represents nearly 57 and 20 times the required chemical plant land surface. Figure 6 shows the impact of the land cost (varied between 0.5 and 50 €/m^2) on the hydrogen minimum price. The graphic shows the importance of the choice of land, which, apart from being highly irradiated and allowing for continuous biomass supply, must be economically profitable. In fact, a quite significant decrease in the cost of hydrogen from 2.99 €/kg_{H2} at reference land cost (12.9 €/m^2) to 2.63 €/kg_{H2} at 0.5 €/m^2 is observed for the allothermal process. As the hybrid plant occupies a smaller area, the hydrogen minimum price decreases less markedly, by 0.16 €/kg_{H2} against 0.36 €/kg_{H2}, in the allothermal process. On the other hand, the autothermal configuration is almost insensitive to land cost, showing a relative H_2 price variation of less than 0.5%. Additionally, a 50% reduction in the heliostats and solar towers costs, combined with a lower land cost below 0.5 €/m^2, allows for reaching an area of competitiveness where the three processes meet. This could also correspond to a more favorable plant site in which the solar resource is greater, e.g., Chilean desert, although the cost of water may be somewhat higher in desert locations.

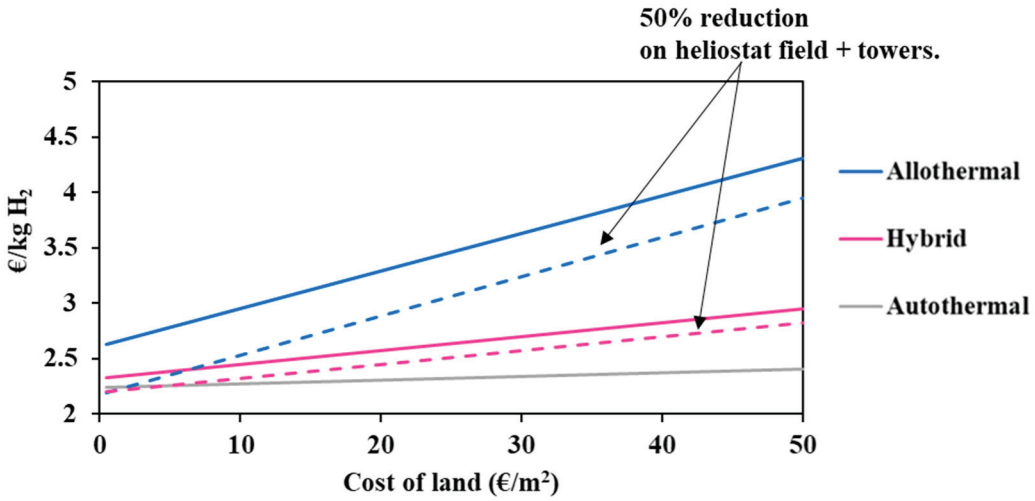

Figure 6. Impact of land cost on the hydrogen minimum price (solid lines: reference assumptions, Table 5; Chain-dotted lines: 50% cost reduction on heliostats and towers).

Another important parameter affecting the level of solar investment is the plant design capacity. This parameter was varied in Figure 7 from 20,000 to 150,000 kg H_2/day to analyze its impact on the solar/chemical direct costs and on the hydrogen minimum price.

It can be observed that the solar direct costs of allothermal process grow at least two times faster than the hybrid process solar direct costs and the chemical facilities costs (reaching a maximum value of 202.3 M€). Conversely, the increase in plant design capacity reduces the hydrogen minimum price by up to 25%, 34%, and 39% for the allothermal, hybrid, and autothermal processes, respectively. Additionally, due to the sharp rise in the

solar facility costs, the relative difference in hydrogen minimum price between the solar processes and the autothermal process goes up from 18% (allothermal) and 6% (hybrid) at 20,000 kg H_2/day to 32% (allothermal) and 10% (hybrid) at 150,000 kg H_2/day. This suggests that, upon scale-up, the competitive gap between the conventional and the solar processes increases. However, this may be due solely to the linearity assumption that was adopted in (Equations (3)–(6)) between the solar costs and the production capacity. As a matter of fact, solar costs prediction is not straightforward and relies on uncertain data. Generally speaking, heliostats field scale-up depends on many factors, such as the design of individual mirrors, their number, their arrangement, their sub-composition and their reflective properties. Larger solar fields impair the quality of concentration and suffer from amplified atmospheric attenuation (due to a greater heliostat-to-receiver slant path) [36]. At the same time, larger solar fields involve higher solar power inputs that allow the use of larger cavity receivers (i.e., gasification reactors), which reduce the energy losses (due to a better absorption of radiation), and thus positively impact the solar costs. A power law with a global scaling exponent factor of 0.7 accounting for these trends was previously used by Kromer et al. [37] for assessing hydrogen cost of several solar thermochemical processes. The impact of this value on the solar costs and on hydrogen minimum price is shown in Figure 7 (scaling exponent factor = 1 in the base case and 0.7 for the dashed lines). The results show that the trends strongly vary with the scaling exponent. The solar costs decline by approximately 72% for the allothermal process and by 60% for the hybrid process at 150,000 kg H_2/day. In the same way, the hydrogen price for the allothermal process sharply drops to 2.09 €/kg_{H2} at 150,000 kg/day, against 2.22 €/kg_{H2} for the hybrid process and 2.25 €/kg_{H2} for the autothermal process. This highlights the necessity of a proper field layout optimization during the scale-up to maximize the energy/materials savings and further reduce the hydrogen cost.

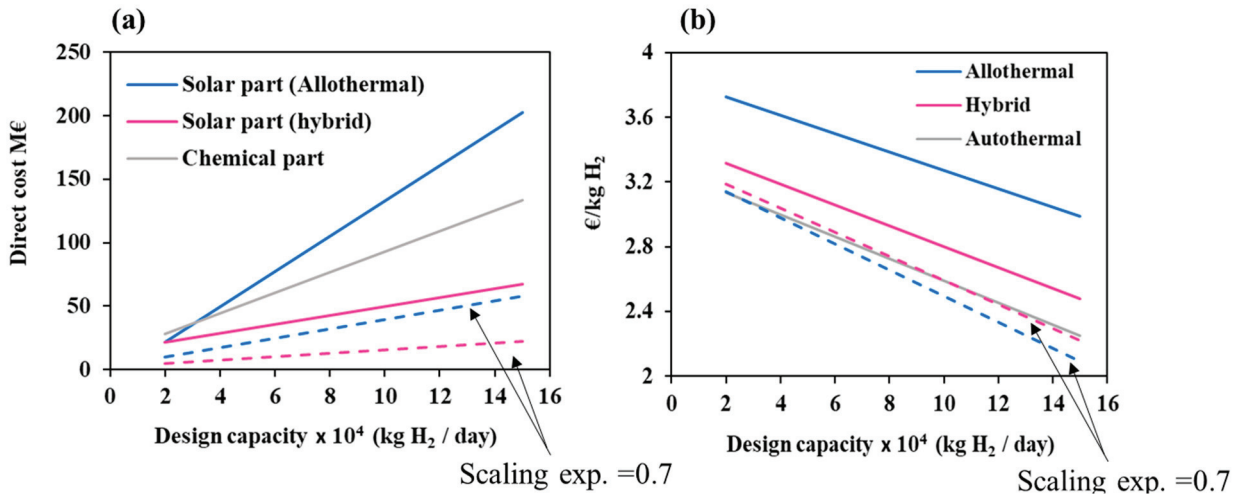

Figure 7. (**a**) Direct costs at different design capacities separated in two parts: solar and chemical and impact of scaling exponent factor; (**b**) Hydrogen minimum price for different design capacities and impact of scaling exponent factor. For the base case (solid lines), the scaling exponent factor is taken equal to 1 for the solar part.

The feedstock cost is another crucial parameter to be studied (Figure 4). Its impact on hydrogen cost is presented in the following section.

3.2.3. Impact of Feedstock Cost

The cost of the feedstock is a key dynamic parameter that evolves with different factors such as local supply chains, resource availability, sustainability criteria, political choices or competing uses of biomass. In this part of the study, the biomass price was varied in the 0–1 €/kg interval to cover a large range of woody and non-woody biomasses

(such as food waste, agricultural and crop waste, and Solid Recovered Fuels) and also a potential increase in the resource price (due, for instance, to the increasing pressure on the resource in the incoming years or to extra-cost associated with additional required feedstock pre-treatment). Figure 8 shows the hydrogen cost as a function of the biomass price for the three studied processes (at reference conditions represented by solid lines). Two additional scenarios are considered: the first one assumes a 50% cost reduction of the heliostat field and towers (at reference land cost) and the second one assumes (in addition) a land cost of 0.5 €/m^2. Two zones on these graphs can be observed for each of the considered solar scenarios: one zone when the biomass price is below a critical value and one zone when the resource price is above. In the first zone, the autothermal mode prevails and imposes lower production costs. In the second zone, a significant reversal trend occurs in favor of the solar processes. Table 6 shows the critical biomass prices at the intersection between the autothermal and solar processes curves. It can be seen that the trend turnaround occurs faster in the allothermal process than in the hybrid one at reference assumptions. In fact, it takes place at a biomass critical price of 0.29 €/kg (for the allothermal mode, which represents three times the reference biomass price), against 0.37 €/kg for the hybrid configuration. By reducing the solar equipment cost by 50%, the turnaround biomass price decreases by about 31% for the allothermal mode and by 38% for the hybrid mode (at reference land cost). It decreases even more, by a total of 69% (allothermal) and 84% (hybrid), when the land cost is set to 0.5 €/m^2. In the latter scenario, the turnaround occurs earlier in the hybrid process.

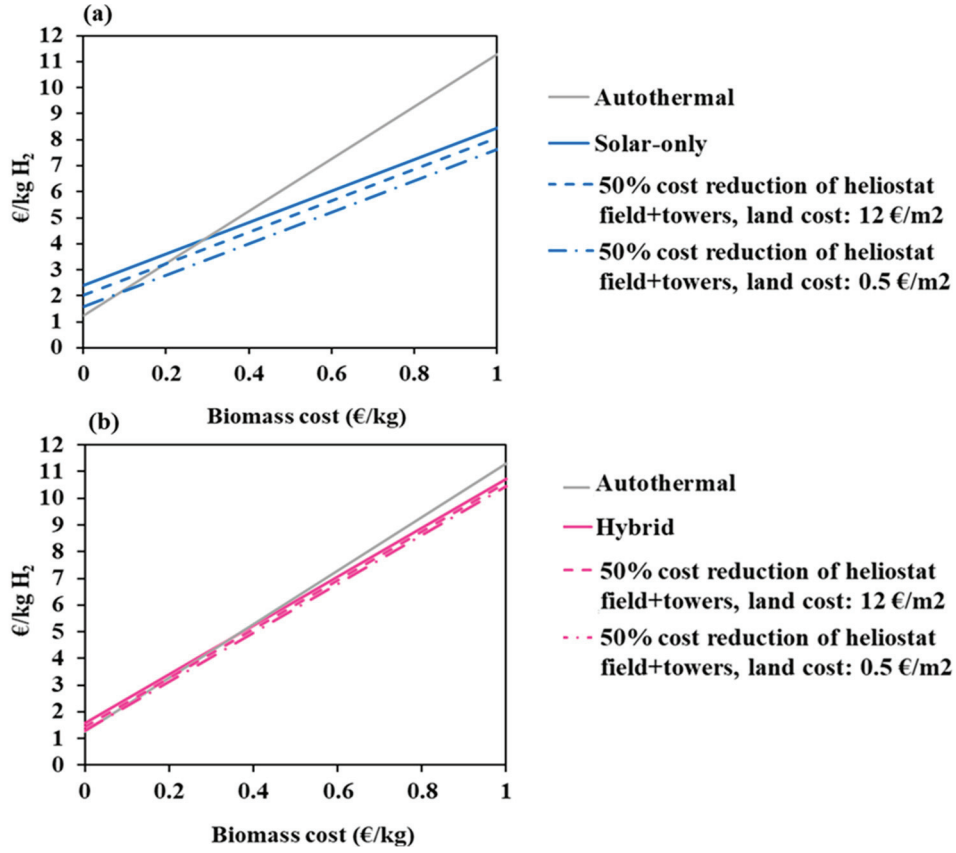

Figure 8. Impact of biomass cost on hydrogen minimum price; (**a**)-solar-only, (**b**)-hybrid.

Table 6. Turnaround biomass price (€/kg): autothermal/solar, DC = 150,000 kg H_2/day.

	Autothermal/Allothermal	Autothermal/Hybrid
Reference assumptions	0.29	0.35
+50% reduction on (heliostats + towers), land cost = 12.9 €/m^2	0.20	0.23
+50% reduction on (heliostats + towers), land cost = 0.50 €/m^2	0.09	0.06

In summary, the analysis shows that a slight increase in the price of the feedstock undermines the autothermal process. The better use of biomass provided by the solar processes clearly limits the increase in hydrogen cost, especially when combined with lower solar plant and land costs. Zero or even negative-priced feedstocks remain more profitable using the conventional autothermal process. However, in the case of waste gasification, CO_2 emissions and environmental impact should be considered if carbon is not renewable (e.g., plastic waste). Direct CO_2 emissions released by the solar processes are negligible or significantly lower than those from the current autothermal processes. Solar gasification processes thus have favorable long-term prospects because they avoid or reduce costs for CO_2 mitigation and pollution abatement. Moreover, due to the more heterogeneous nature of waste, its conversion implies additional costs, to deal with syngas impurities, especially the H_2S content that is a major corrosive constituent. More costly reactor materials and gas cleaning units are thus required for waste feedstock.

3.2.4. Impact of Environmental Subsidies

As shown in Table 3, solar gasification avoids, respectively, 3.08 and 6.73 kg of CO_2 (due to reaction) per kilogram of H_2 in hybrid and allothermal processes, which is significant. Although a detailed analysis has not yet been published comparing the three processes based on environmental criteria, important and achievable CO_2 emission mitigation is greatly expected thanks to solar heating. In fact, a conventional CSP tower plant generates barely 38 g of CO_2/kWh_e [38], which is far (more than 10 times) lower than the 750–900 g of CO_2/kWh_e generated by conventional Integrated Gasification Combined Cycles (IGCC) power plants when no CO_2 capture is considered. The capture/sequestration of 80% of CO_2 during operation decreases the net emissions to about 200 g of CO_2/kWh_e, resulting in a total saving of more than 550 g of CO_2/kWh_e [39]. In this sense, solar-driven processes can drastically reduce the Greenhouse gas (GHG) emissions, which allows them to take advantage of carbon pricing and environmental subsidies to improve their economic balance and their competitiveness. Indeed, the application of credits for CO_2 mitigation and pollution avoidance will further enable the solar thermochemical technologies to compete favorably with conventional processes. Carbon price varies from country to country [40], and, in France, it is estimated to be 100 €/t CO_2 in 2030 according to Quinet report [41]. In Europe, carbon prices are expected to double by 2021, and even quadruple to reach up to 55 €/t CO_2, as stipulated in the Paris climate agreement [42]. In this section, the impact of possible capital subsidies due to CO_2 emission reduction is studied. The total subventions were calculated on the basis of the amount of CO_2 that would have been emitted by the conventional process. For allothermal gasification, the subvention was estimated at 14.74 M€ (6.73 × 150,000 × 80% × 365 × 50/1000) and at about 6.74 M€ for the hybrid process (3.08 × 150,000 × 80% × 365 × 50/1000) for DC = 150 000 kg H_2/day, a capacity factor of 80% and a capital subsidy of 50 €/tCO_2. Figure 9 shows the impact of CO_2 subsidies on hydrogen cost.

At reference conditions, the intersection between the curves (autothermal and solar processes) takes place at CO_2 subventions of 82 €/tCO_2 (allothermal) and 55 €/tCO_2 (hybrid). Considering a cost reduction for heliostats and towers of 50% and a fixed environmental subsidy of 30 €/tCO_2, the biomass turnaround price goes down to 0.14 €/kg and 0.09 €/kg (lower than reference cost ~0.1 €/kg) for the allothermal and hybrid processes, respectively. This confirms that subsidies can play a key role in the reduction in solar hydrogen costs.

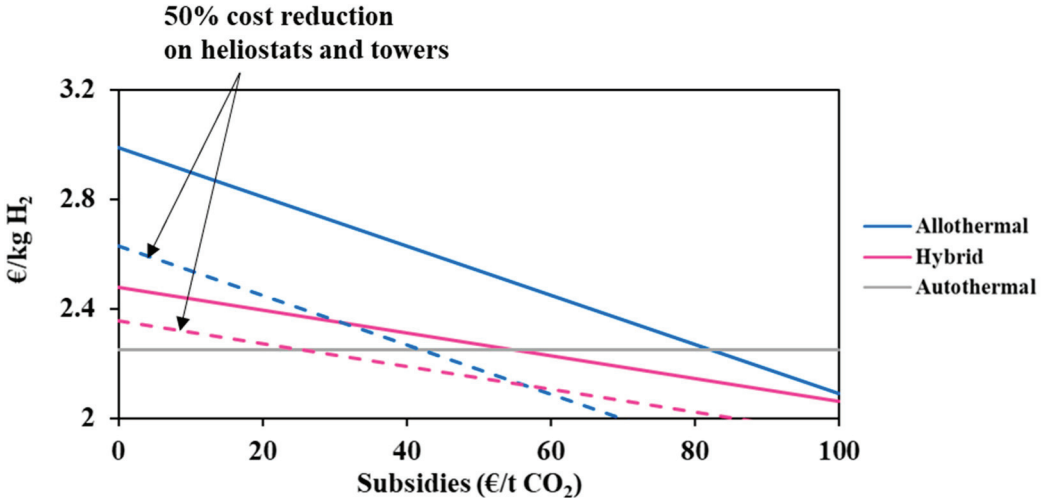

Figure 9. Impact of CO_2 subsidies on hydrogen cost

3.3. Comparison with Other Hydrogen Production Methods

This part of the study gives insights into hydrogen production costs with different technologies, such as biomass gasification, coal gasification, natural gas reforming and water electrolysis (based on a solid oxide technology). Previously developed NREL cost models were used for this purpose [43]. The financial inputs of all the technologies are the same as those presented in Table 4, and the operating capacity factor is fixed to 80%. To focus on the comparison with low-carbon technologies, the considered coal gasification and natural gas-reforming models integrate carbon capture and sequestration units that remove CO_2 from syngas before storing it in underground reservoirs. The reference primary resources costs used in this section are: biomass cost = 0.1 €/kg, coal cost = 0.04 €/kg, NG cost = 0.01 €/kWh, electricity cost for electrolysis = 0.10 €/kWh. Figure 10 shows the hydrogen minimum price of the different technologies. The grey bars show the sensitivity to the primary resource price (electricity price for electrolysis; process water was fixed to 0.61 €/m^3) when it increases from zero to twice the reference cost.

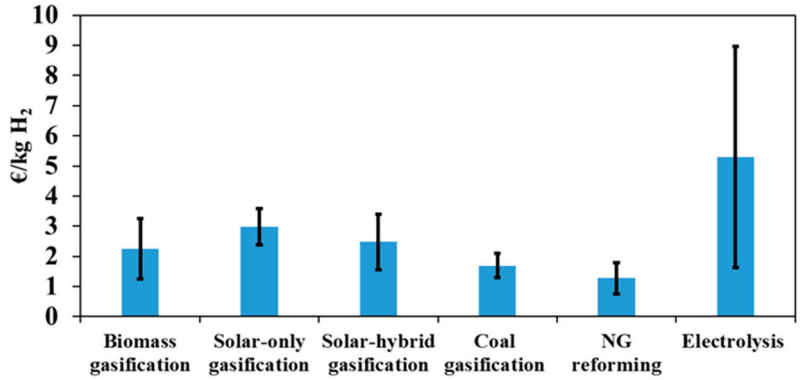

Figure 10. Hydrogen production cost and sensitivity on the primary resource cost (electricity for electrolysis) when ranging from zero to twice the reference cost (Table 4).

It can be seen that natural gas reforming is the most profitable process so far, with a hydrogen production cost of only 1.28 €/kg. This process is followed by coal (1.69 €/kg) and biomass gasification. The difference between these three processes is mainly due to two factors: the cost of the primary resource and the capacity of the plant. Clearly, due to the low fossil fuel cost, fossil-based processes are the most competitive on the market.

Moreover, very large plants can be envisaged, which lowers the price of hydrogen even further thanks to the economy of scale. The cost of hydrogen produced by electrolysis is much higher than that of the other processes (5.48 €/kg), and shows a greater sensitivity to primary resource cost. It can be seen that, for a zero-resource cost, the price of hydrogen produced by electrolysis decreases drastically to 1.68 €/kg, making this technology potentially more competitive when recovering and valorizing unusable electricity (due, for example, to lack of demand and storage). Although coal gasification plant capacity is seven times larger than that of biomass gasification (and, therefore, benefits from the economy of scale), it appears that, for low feedstock costs, hydrogen price is almost the same in both configurations. This is due to the extra costs entailed by CO_2 capture and sequestration operations (which are not considered in biomass gasification). Finally, NG reforming with CO_2 capture and sequestration is the cheapest process with a hydrogen cost below than that of coal and biomass gasification (solar and non-solar), making this technology the most economically attractive option at present for decarbonized hydrogen generation.

It is essential to recall that other solar thermochemical processes are prospected for the generation of solar fuels. In view of the increasingly stringent environmental regulations, and noting the urgency of climate change, the sustainable paths have undergone extensive research and development to increase efficiency and cost-effectiveness. The number of publications in this field considerably increased, by more than five times since 2000 [44]. This brought significant insights regarding the technical feasibility and the possibilities of scale up. A number of economic studies were carried out to estimate the cost of hydrogen using different solar thermochemical technologies. Although initial assumptions differ from one study to another regarding plant site, solar material cost, operating hours, installation costs and optical/thermal efficiencies, the calculated values estimate the prices and their sensitivity to the input parameters. Möller et al. [45] analyzed the solar steam reforming of natural gas for the production of 103.8 Million Nm^3/year (i.e., ~25,594 kg/day) of hydrogen. The study showed that the solar process allows 40% of the fuel to be saved compared to the conventional process, with a hydrogen cost of less than 0.05 €/kWh LHV of H_2 (~1.67 €/kg of H_2). Similarly, Rodat et al. [46] studied solar thermal decomposition of natural gas at a plant design capacity of 436 kg of H_2/day. Hydrogen cost was about 1.42 $/kg and showed great sensitivity to carbon blacks' (which are the process byproducts) selling price. The study determined carbon blacks' minimum cost, making solar thermal decomposition of natural gas competitive with solar and conventional reforming processes. Baykara and Bilgen [47] compared commercial, hybrid and solar coal gasification processes for the production of hydrogen. The plants were designed to produce 10^7 GJ of H_2 per year (~228,310 kg/day). The study showed that the commercial process (based on partial feedstock combustion) is the most cost-effective, with a hydrogen price of 0.94 $/kg, which is 5.2% and 6.3% lower than the hybrid and solar (only) process and is, in some respects, consistent with the present study outcomes. This means that solarization is still economically challenging and requires incentive environmental policies. Other researchers took a keen interest in the thermochemical splitting of water using high-temperature solar heat. Given that single-step direct thermolysis, at temperatures beyond 2500 °C, was hardly feasible, thermochemical cycles technologies were rather considered. This process involves several reactional intermediates, which are regenerated during the cycles to lower the water dissociation temperature. Over 280 cycles were developed and screened to select the most suitable ones for coupling with concentrated solar thermal energy [48]. Among the most promising cycles studied from an economic perspective, zinc, ferrite, and sulphur cycles were proposed. Charvin et al. [49,50] studied two-step (ZnO/Zn and Fe_3O_4/FeO) and three-step (Fe_2O_3/Fe_3O_4) thermochemical cycles driven by concentrated solar energy. The economic study was performed with a design capacity ranging from 50 to 250 kg/h of H_2. The analysis gave a hydrogen production cost between 7.98 and 14.75 $/kg of H_2 depending on process intensification and on the targeted hydrogen productivity. In a similar study, Steinfeld [51]

analyzed hydrogen production cost via two-step water-splitting ZnO/Zn redox system, and the hydrogen price was around 4–5 €/kg at a design capacity of 61 Million-kWh/year (~5014 kg/day), which is somewhat larger than Charvin et al. [49] design capacity and therefore lowers hydrogen prices. Solar hydrogen production costs from the hybrid-sulfur cycle and a metal oxide-based cycle were studied and compared to that of commercial electrolysis (powered by a CSP plant with a thermal storage capacity of 4.5 h) by Graf et al. [52]. The metal-oxide-based cycle hydrogen cost ranged between 3.5 and 12.8 €/kg, and thus covered the ranges calculated Charvin et al. [49] and Steinfeld [51]. It showed the greatest cost variability due to the high demand of the metal oxide and its cost dependence. Hydrogen costs for hybrid sulfur cycle were the lowest and ranged between 3.9 and 5.6 €/kg. Water electrolysis was highly influenced by the cost of electricity, with a hydrogen price between 2.1 and 6.8 €/kg.

Overall, it appears from these results that, to date, solar thermochemical processes are far from being competitive with conventional processes based on fossil fuels (coal and natural gas). Major challenges remain to improve the efficiency of the processes. They concern the cost of the solar concentrators, which represents a significant part of the investment, and the cost of the receiver, which, in many cases, must withstand high temperatures in the presence of highly corrosive chemical species. Another challenge concerns the solar reactor design, which should minimize the heat losses and maximize the chemical conversion for a better use of the solar resource. The recycling of chemicals in thermochemical cycles that impose a high degree of purity and a precise control of phases and constituent separation is another issue that needs to be properly managed and solved. Carbon-based solar thermochemical technologies generally show lower hydrogen production costs. These processes, which, by definition, are less harmful to the environment, offer the possibility to extend the lifespan of fossil resources on earth and can play a role in the transition towards a zero-carbon economy.

4. Conclusions

A techno-economic study of solar and solar hybrid gasification was carried out. The study was based on the discounted cash-flow rate of return method to calculate the minimum hydrogen production cost. At first, the most important solar parameters were identified, and they were then integrated to a previously developed autothermal gasification cost model. The new solarized cost model was thereafter used to examine the profitability and the cost-effectiveness of each of the studied heating configurations (i.e., allothermal, hybrid and autothermal). A sensitivity analysis of the main cost-influencing factors was carried out. The analysis showed that at the current biomass reference cost (considered equal to 0.1 €/kg), the most competitive scenario (in which solar hydrogen cost is lower than conventional hydrogen), assumes a cost reduction of 50% of the heliostats and towers costs, with a land cost of 0.5 €/m^2, which is clearly challenging at present and requires an important economic effort. However, the analysis also showed that an increase in the biomass cost by a factor of 2 to 3 significantly undermines the profitability of the autothermal process, in favor of solar gasification, which becomes more competitive without any substantial economic and financial efforts. A comparative analysis with other solar and non-solar clean technologies was carried out. This confirmed that the two most economically favorable processes for hydrogen generation are those based on fossil fuels with CO_2 capture and sequestration. These processes will, therefore, make the greatest contribution to the hydrogen market in the near future. Nonetheless, fossil fuels are neither universally available nor inexhaustible, and depend on a large number of strategic and geopolitical parameters that remain uncertain, sensitive and hardly predictable. Moreover, carbon sequestration is not without risk for the environment and human health. Leakage during transport and storage is possible, and the long-term process performance is uncertain, especially in cases of large-scale development. These represent major constraints to circumvent in order to ensure security and sustainability. Renewable technologies are hardly competitive with fossil-based technologies at present,

and require more effort to gain in efficiency, durability and cost-effectiveness. Government policy incentives have also a major role to play through the use of mechanisms like carbon credits, renewable energy credits, capital subsidies, and reverse auctions. This way, the financial viability of the sustainable path can be improved.

Author Contributions: Conceptualization, H.B., S.R. and S.A.; methodology, H.B., S.R. and S.A.; validation, H.B., S.R. and S.A.; formal analysis, H.B., S.R. and S.A.; investigation, H.B., S.R. and S.A.; writing—original draft preparation, H.B., S.R. and S.A.; writing—review and editing, S.R. and S.A.; visualization, H.B.; supervision, S.R. and S.A.; project administration, S.R. and S.A. All authors have read and agreed to the published version of the manuscript.

Funding: This research received no external funding.

Institutional Review Board Statement: Not applicable.

Informed Consent Statement: Not applicable.

Data Availability Statement: The data presented in this study are available on request from the corresponding author.

Acknowledgments: The support of ADEME (French Environment and Energy Management Agency) is gratefully acknowledged.

Conflicts of Interest: The authors declare no conflict of interest.

References

1. Hydrogen—Chemical Economics Handbook (CEH) | IHS Markit. Available online: https://ihsmarkit.com/products/hydrogen-chemical-economics-handbook.html (accessed on 14 July 2020).
2. Safari, F.; Dincer, I. A review and comparative evaluation of thermochemical water splitting cycles for hydrogen production. *Energy Convers. Manag.* **2020**, *205*, 112182. [CrossRef]
3. Ursua, A.; Gandia, L.M.; Sanchis, P. Hydrogen Production from Water Electrolysis: Current Status and Future Trends. *Proc. IEEE* **2011**, *100*, 410–426. [CrossRef]
4. Fraile, D.; Lanoix, J.C.; Maio, P.; Rangel, A.; Torres, A. Overview of the Market Segmentation for Hydrogen across Potential Customer Groups, Based on Key Application Areas. 2015. Available online: https://www.certifhy.eu/images/D1_2_Overview_of_the_market_segmentation_Final_22_June_low-res.pdf (accessed on 1 January 2021).
5. Binder, M.; Kraussler, M.; Kuba, M.; Luisser, M. *IEA Bioenergy Hydrogen from Biomass Gasification*; Reinhard Rauch, Ed.; IEA Bioenergy, December 2018; ISBN 978-1-910154-59-5. Available online: https://www.ieabioenergy.com/blog/publications/hydrogen-from-biomass-gasification/ (accessed on 26 February 2020).
6. Schmidt, O.; Gambhir, A.; Staffell, I.; Hawkes, A.; Nelson, J.; Few, S. Future cost and performance of water electrolysis: An expert elicitation study. *Int. J. Hydrogen Energy* **2017**, *42*, 30470–30492. [CrossRef]
7. Boujjat, H.; Rodat, S.; Chuayboon, S.; Abanades, S. Numerical simulation of reactive gas-particle flow in a solar jet spouted bed reactor for continuous biomass gasification. *Int. J. Heat Mass Transf.* **2019**, *144*, 118572. [CrossRef]
8. Chuayboon, S.; Abanades, S.; Rodat, S. Experimental analysis of continuous steam gasification of wood biomass for syngas production in a high-temperature particle-fed solar reactor. *Chem. Eng. Process. Process. Intensif.* **2018**, *125*, 253–265. [CrossRef]
9. Gokon, N.; Ono, R.; Hatamachi, T.; Liuyun, L.; Kim, H.-J.; Kodama, T. CO_2 gasification of coal cokes using internally circulating fluidized bed reactor by concentrated Xe-light irradiation for solar gasification. *Int. J. Hydrogen Energy* **2012**, *37*, 12128–12137. [CrossRef]
10. Kodama, T.; Kondoh, Y.; Tamagawa, T.; Funatoh, A.; Shimizu, K.-I.; Kitayama, Y. Fluidized Bed Coal Gasification with CO_2 under Direct Irradiation with Concentrated Visible Light. *Energy Fuels* **2002**, *16*, 1264–1270. [CrossRef]
11. Kruesi, M.; Jovanovic, Z.R.; Dos Santos, E.C.; Yoon, H.C.; Steinfeld, A. Solar-driven steam-based gasification of sugarcane bagasse in a combined drop-tube and fixed-bed reactor—Thermodynamic, kinetic, and experimental analyses. *Biomass Bioenergy* **2013**, *52*, 173–183. [CrossRef]
12. Muroyama, A.P.; Guscetti, I.; Schieber, G.L.; Haussener, S.; Loutzenhiser, P.G. Design and demonstration of a prototype 1.5 kWth hybrid solar/autothermal steam gasifier. *Fuel* **2018**, *211*, 331–340. [CrossRef]
13. Taylor, R.; Berjoan, R.; Coutures, J. Solar gasification of carbonaceous materials. *Sol. Energy* **1983**, *30*, 513–525. [CrossRef]
14. Gregg, D.; Taylor, R.; Campbell, J.; Taylor, J.; Cotton, A. Solar gasification of coal, activated carbon, coke and coal and biomass mixtures. *Sol. Energy* **1980**, *25*, 353–364. [CrossRef]
15. Piatkowski, N.; Wieckert, C.; Steinfeld, A. Experimental investigation of a packed-bed solar reactor for the steam-gasification of carbonaceous feedstocks. *Fuel Process. Technol.* **2009**, *90*, 360–366. [CrossRef]
16. Vidal, A.; Denk, T.; Steinfeld, L.; Zacarías, L.; Almería, T. Upscaling of a 500 kW Solar Gasification Plant. *Proc. WHEC* **2010**, *78*, 177–181.

17. Rodat, S.; Abanades, S.; Boujjat, H.; Chuayboon, S. On the path toward day and night continuous solar high temperature thermochemical processes: A review. *Renew. Sustain. Energy Rev.* **2020**, *132*, 110061. [CrossRef]
18. Boujjat, H.; Rodat, S.; Chuayboon, S.; Abanades, S. Experimental and numerical study of a directly irradiated hybrid solar/combustion spouted bed reactor for continuous steam gasification of biomass. *Energy* **2019**, *189*, 116118. [CrossRef]
19. Boujjat, H.; Junior, G.M.Y.; Rodat, S.; Abanades, S. Dynamic simulation and control of solar biomass gasification for hydrogen-rich syngas production during allothermal and hybrid solar/autothermal operation. *Int. J. Hydrogen Energy* **2020**, *45*, 25827–25837. [CrossRef]
20. Saw, W.L.; Guo, P.; Van Eyk, P.J.; Nathan, G.J. Approaches to accommodate resource variability in the modelling of solar driven gasification processes for liquid fuels synthesis. *Sol. Energy* **2017**, *156*, 101–112. [CrossRef]
21. Nickerson, T.A.; Hathaway, B.J.; Smith, T.M.; Davidson, J.H. Economic assessment of solar and conventional biomass gasification technologies: Financial and policy implications under feedstock and product gas price uncertainty. *Biomass Bioenergy* **2015**, *74*, 47–57. [CrossRef]
22. Rahbari, A.; Shirazi, A.; Venkataraman, M.B.; Pye, J. A solar fuel plant via supercritical water gasification integrated with Fischer–Tropsch synthesis: Steady-state modelling and techno-economic assessment. *Energy Convers. Manag.* **2019**, *184*, 636–648. [CrossRef]
23. Saw, W.; Kaniyal, A.; Van Eyk, P.; Nathan, G.; Ashman, P. Solar Hybridized Coal-to-liquids via Gasification in Australia: Techno-economic Assessment. *Energy Procedia* **2015**, *69*, 1819–1827. [CrossRef]
24. NREL H2A. H2A: Hydrogen Analysis Production Models | Hydrogen and Fuel Cells | NREL. Available online: https://www.nrel.gov/hydrogen/h2a-production-models.html (accessed on 7 July 2020).
25. Spath, P.; Aden, A.; Eggeman, T.; Ringer, M.; Wallace, B.; Jechura, J. *Biomass to Hydrogen Production Detailed Design and Economics Utilizing the Battelle Columbus Laboratory Indirectly Heated Gasifier*; NREL Technical Report; NREL: Golden, CO, USA, 2005. Available online: https://www.nrel.gov/docs/fy05osti/37408.pdf (accessed on 1 January 2021).
26. Kolb, G.J.; Jones, S.A.; Donnelly, M.W.; Gorman, D.; Thomas, R.; Davenport, R.; Lumia, R. *Heliostat Cost Reduction Study*; Sandia Report; Sandia National Laboratories: Albuquerque, NM, USA, June 2007. Available online: https://prod.sandia.gov/techlib-noauth/access-control.cgi/2007/073293.pdf (accessed on 1 January 2021).
27. Mendelsohn, M.; Lowder, T.; Canavan, B. *Utility-Scale Concentrating Solar Power and Photovoltaics Projects: A Technology and Market Overview*; NREL Technical Report; NREL: Golden, CO, USA, April 2012. Available online: https://www.nrel.gov/docs/fy12osti/51137.pdf (accessed on 1 January 2021).
28. Sudiro, M.; Bertucco, A. Synthetic Fuels by a Limited CO_2 Emission Process Which Uses Both Fossil and Solar Energy. *Energy Fuels* **2007**, *21*, 3668–3675. [CrossRef]
29. Becker, M.; Klimas, P.; Chavez, J.; Kolb, G.; Meinecke, W. *Second Generation Central Receiver Technologies*; Germany; p. 1993, ISBN 3-7880-7482-5. Available online: https://www.osti.gov/etdeweb/biblio/5295357 (accessed on 26 February 2021).
30. SOLARPACES PS10. Available online: https://solarpaces.nrel.gov/planta-solar-10 (accessed on 2 August 2020).
31. Sargent & Lundy LLC Consulting Group Chicago, Illinois. *Executive Summary: Assessment of Parabolic Trough and Power Tower Solar Technology Cost and Performance Forecasts*; NREL: Golden, CO, USA, October 2003. Available online: https://www.nrel.gov/docs/fy04osti/35060.pdf (accessed on 1 January 2021).
32. Bracken, N.; Macknick, J.; Tovar-Hastings, A.; Komor, P.; Gerritsen, M.; Mehta, S. Concentrating Solar Power and Water Issues in the U.S. Southwest. *Conc. Sol. Power Water Issues U.S. Southwest* **2015**. [CrossRef]
33. Hinkley, J.T.; Hayward, J.A.; Curtin, B.; Wonhas, A.; Boyd, R.; Grima, C.; Tadros, A.; Hall, R.; Naicker, K. An analysis of the costs and opportunities for concentrating solar power in Australia. *Renew. Energy* **2013**, *57*, 653–661. [CrossRef]
34. Pfahl, A. Survey of Heliostat Concepts for Cost Reduction. *J. Sol. Energy Eng.* **2013**, *136*, 014501. [CrossRef]
35. Pidaparthi, A.; Hoffmann, J. Effect of heliostat size on the levelized cost of electricity for power towers. *AIP Conf. Proc.* **2017**, *1850*, 030038.
36. Lovegrove, K.; Stein, W. *Concentrating Solar Power Technology*; Woodhead Publishing, October 2012; Available online: https://www.sciencedirect.com/book/9781845697693/concentrating-solar-power-technology (accessed on 14 July 2020).
37. Kromer, M.; Roth, K.; Takata, R.; Chin, P. *Support for Cost Analyses on Solar-Driven High Temperature Thermo-Chemical Water-Splitting Cycles*; TIAX LLC: Lexington, MA, USA, 2011.
38. Burkhardt, J.J.; Heath, G.; Cohen, E. Life Cycle Greenhouse Gas Emissions of Trough and Tower Concentrating Solar Power Electricity Generation. *J. Ind. Ecol.* **2012**, *16*, 93. [CrossRef]
39. Ordorica-Garcia, G.; Douglas, P.; Croiset, E.; Zheng, L. Technoeconomic evaluation of IGCC power plants for CO_2 avoidance. *Energy Convers. Manag.* **2006**, *47*, 2250–2259. [CrossRef]
40. Carbon Pricing Dash Board. Available online: https://carbonpricingdashboard.worldbank.org/map_data (accessed on 2 August 2020).
41. Quinet, A. Report of the Commission Chaired by A. Quinet, State-imposed Value of Carbon, Center for Strategic Analysis. 2009. Available online: https://www.vie-publique.fr/sites/default/files/rapport/pdf/094000195.pdf (accessed on 1 January 2021).
42. Carbon Tracker REPORT Carbon Countdown: Prices and Politics in the EU-ETS. Available online: https://carbontracker.org/reports/carbon-countdown/ (accessed on 20 July 2020).

43. Penev, M.; Saur, G.; Hunter, C.; Zuboy, J. NREL, Hydrogen & Fuel Cells, H2A Hydrogen Production Model: Version 3.2018 User Guide. Available online: https://www.nrel.gov/hydrogen/assets/pdfs/h2a-production-model-version-3-2018-user-guide-draft.pdf (accessed on 1 January 2021).
44. Yadav, D.; Banerjee, R. A review of solar thermochemical processes. *Renew. Sustain. Energy Rev.* **2016**, *54*, 497–532. [CrossRef]
45. Möller, S.; Kaucic, D.; Sattler, C. Hydrogen Production by Solar Reforming of Natural Gas: A Comparison Study of Two Possible Process Configurations. *J. Sol. Energy Eng.* **2006**, *128*, 16–23. [CrossRef]
46. Rodat, S.; Abanades, S.; Flamant, G. Methane Decarbonization in Indirect Heating Solar Reactors of 20 and 50 kW for a CO_2-Free Production of Hydrogen and Carbon Black. *J. Sol. Energy Eng.* **2011**, *133*, 031001. [CrossRef]
47. Baykara, S.; Bilgen, E. Synthesis gas and H_2 production from solar gasification of albertan coal. *Energy Convers. Manag.* **1985**, *25*, 391–398. [CrossRef]
48. Abanades, S.; Charvin, P.; Flamant, G.; Neveu, P. Screening of water-splitting thermochemical cycles potentially attractive for hydrogen production by concentrated solar energy. *Energy* **2006**, *31*, 2805–2822. [CrossRef]
49. Charvin, P.; Abanades, S.; Lemort, F.; Flamant, G. Analysis of solar chemical processes for hydrogen production from water splitting thermochemical cycles. *Energy Convers. Manag.* **2008**, *49*, 1547–1556. [CrossRef]
50. Charvin, P.; Abanades, S.; Lemort, F.; Flamant, G. Hydrogen Production by Three-Step Solar Thermochemical Cycles Using Hydroxides and Metal Oxide Systems. *Energy Fuels* **2007**, *21*, 2919–2928. [CrossRef]
51. Steinfeld, A. Solar hydrogen production via a two-step water-splitting thermochemical cycle based on Zn/ZnO redox reactions. *Int. J. Hydrogen Energy* **2002**, *27*, 611–619. [CrossRef]
52. Graf, D.; Monnerie, N.; Roeb, M.; Schmitz, M.; Sattler, C. Economic comparison of solar hydrogen generation by means of thermochemical cycles and electrolysis. *Int. J. Hydrogen Energy* **2008**, *33*, 4511–4519. [CrossRef]

processes

MDPI

Article

Extraction of Added-Value Triterpenoids from *Acacia dealbata* Leaves Using Supercritical Fluid Extraction

Vítor H. Rodrigues, Marcelo M. R. de Melo, Inês Portugal and Carlos M. Silva *

CICECO—Aveiro Institute of Materials, Department of Chemistry, University of Aveiro, Campus Universitário de Santiago, 3810-193 Aveiro, Portugal; vitorhrodrigues@ua.pt (V.H.R.); marcelo.melo@ua.pt (M.M.R.d.M.); inesport@ua.pt (I.P.)

* Correspondence: carlos.manuel@ua.pt

Abstract: Forestry biomass is a by-product which commonly ends up being burnt for energy generation, despite comprising valuable bioactive compounds with valorisation potential. Leaves of *Acacia dealbata* were extracted for the first time by supercritical fluid extraction (SFE) using different conditions of pressure, temperature and cosolvents. Total extraction yield, individual triterpenoids extraction yields and concentrations were assessed and contrasted with Soxhlet extractions using solvents of distinct polarity. The extracts were characterized by gas chromatography coupled to mass spectrometry (GC-MS) and target triterpenoids were quantified. The total extraction yields ranged from 1.76 to 11.58 wt.% and the major compounds identified were fatty acids, polyols, and, from the triterpenoids family, lupenone, α-amyrin and β-amyrin. SFE was selective to lupenone, with higher individual yields (2139–3512 mg kg_{leaves}^{-1}) and concentrations (10.1–12.4 wt.%) in comparison to Soxhlet extractions, which in turn obtained higher yields and concentrations of the remaining triterpenoids.

Keywords: *Acacia dealbata*; GC-MS; leaves; lupenone; supercritical fluid extraction; Soxhlet extraction; triterpenoids

1. Introduction

The genus *Acacia* is widespread through the Portuguese landscape, consisting of three main species: *Acacia dealbata*, *Acacia longifolia* and *Acacia melanoxylon* [1]. *A. dealbata* was introduced for dune erosion protection as well as ornamental and wood supply purposes during the 19th and 20th century [2]. Currently, it is considered a plague due to its fast growth and dominance over the natural flora [1,3]. From 2005 to 2015, the occupied area of *Acacia* species increased 4000 ha in Portugal, corresponding to an estimated total arboreal biomass growth of 2 Mt [4]. The removal of these trees generates forest biomass that, under the Renewable Energy Directive II of the European Union Commission [5], can be utilized for the production of liquid and gaseous biofuels. However, it is a common practice to leave these residues in the forest for soil remediation.

The research towards *A. dealbata* biomass extraction has focused on several morphological parts, namely wood [6–10], bark [6–8,10–14], flowers [11,15–20] and leaves [6,8,11,17,21,22]. The explored extraction methods so far consist of solid-liquid extraction with organic solvents, such as dichloromethane, ethanol, methanol, hexane, acetone and some hydroalcoholic mixtures. Extraction of essential oils by steam distillation has been applied only to flowers [16]. Besides these conventional methods, there are few works on greener and more innovative extraction procedures, such as the work of Borges et al. [22], who applied microwave and ultrasound-assisted extraction to the leaves, and Lopez-Hortas et al. [16], using microwave hydrodiffusion to obtain the flower essential oil. One alternative technique for the extraction of vegetable biomass is supercritical fluid extraction (SFE) [23]. It is mainly employed with carbon dioxide (CO_2) as solvent due to its low cost, safety,

availability and low critical point conditions, which allows extraction at near room temperatures [24]. The manipulation of temperature and pressure allows the tuning of CO_2 properties (density, viscosity and diffusivity) that maximize the desired responses, such as total extraction yield or the selective uptake of target chemical families or compounds. For example, triterpenic acids in the case of *Eucalyptus globulus* leaves [25,26] and bark [27–29], triterpenes from *Vitis vinifera* leaves [30], friedelin from *Quercus cerris* cork [31] and sterols from *Eichhornia crassipes* [32].

The phytochemistry of *A. dealbata* biomass (bark, leaves, wood, flowers and seeds) includes several families of compounds, such as alkaloids [8], amines [33], phenolics [8,10,13, 15], polysaccharides [9], chalcone glycosides [18], steryl glucosides [7], tannins [10,11,13], caffeic acid esters [12], sterols [6] and triterpenes [6,17]. SFE is a proven technology for the selective removal of triterpenes and sterols from many vegetable matrices [23,30–32,34,35]. For instance, compounds such as lupenone, lupeol, lupenyl palmitate, lupenyl cinnamate, squalene, β-amyrone, α-amyrin, β-amyrin and 22,23-dihydrospinasterol have already been identified and quantified [6,17]. These have been reported for several potential bioactive properties, namely anti-inflammatory, anti-virus, anti-diabetes, anti-cancer and antiproliferative, among others [36–45] which may explain the association of *Acacia* species with traditional medicine practices [46,47]. The wide range of biological activities potentiates the interest for multiple applications of the extracts, for example, to obtain active pharmaceutical ingredients or for incorporation in nutraceuticals, food, animal feed and cosmetic products.

This work focuses on the SFE of triterpenoids from *Acacia dealbata* leaves under different experimental conditions of pressure, temperature and cosolvents content, and its comparison with conventional Soxhlet extraction using organic solvents of distinct polarity. The extracts were characterized by gas chromatography coupled to mass spectrometry (GC-MS) and triterpenoids contents were determined. To the best of our knowledge, this is the first time SFE is applied to *Acacia dealbata* leaves aiming for the extraction of potential bioactive compounds.

2. Materials and Methods

2.1. Chemicals

Carbon dioxide (CO_2, purity 99%) was supplied by Air Liquide (Algés, Portugal). Dichloromethane (purity 99.98%), *n*-hexane (purity 99%) and ethanol (purity 99.5%) were supplied by Fisher Scientific (Leicestershire, UK). Ethyl acetate (purity 99%) was supplied by VWR International (Fontenay-sous-Bois, France). Pyridine (purity 99.5%), tetracosane (purity 99%) N,O-Bis(trimethylsilyl)trifluoroacetamide (BSTFA, purity 98%) and chlorotrimethylsilane (TMSCl, purity 99%) were supplied by Sigma Aldrich (Madrid, Spain). Betulinic, oleanolic and ursolic acids (purity 98%) were supplied by AK Scientific (Union City, CA, USA).

2.2. Acacia Dealbata Biomass

The *A. dealbata* leaves were supplied by RAIZ—Forest and Paper Research Institute (Eixo, Portugal). The leaves were collected from 8-year-old *Acacia dealbata* trees located in Porto/Valongo (Portugal) region during the winter season. The leaves (see Figure 1) were manually separated from the branches and dried at 35 °C for 72 h in a forced convection oven, reducing their moisture content from 65.6 to 4.5 wt.%.

Figure 1. Oven-dried *Acacia dealbata* leaves.

2.3. Soxhlet Extraction

The leaves of *A. dealbata* were extracted with *n*-hexane, dichloromethane, ethyl acetate and ethanol (Table 1). In each assay, extraction of the leaves (ca. 3 g) was performed with 180 mL of each solvent for 6 h. The produced extracts were evaporated to dryness in a rotary evaporator, weighed for the determination of total extraction yield (η_{Total}, wt.%) and analyzed by GC-MS to evaluate triterpenoids individual yields (η_{i}, mg kg_{leaves}^{-1}) and concentrations (C_{i}, wt.%), as follows:

$$\eta_{\text{Total}} = \frac{m_{\text{extract}}}{m_{\text{dry leaves}}} \times 100 \quad (1)$$

$$\eta_{\text{i}} = \frac{m_{\text{i}}}{m_{\text{dry leaves}}} \times 10^6 \quad (2)$$

$$C_{\text{i}} = \frac{m_{\text{i}}}{m_{\text{extract}}} \times 100 \quad (3)$$

where $m_{\text{dry leaves}}$ is the mass of dry leaves, m_{extract} corresponds to extract mass free of solvent and m_{i} is the mass of triterpenoids measured by GC-MS.

Table 1. List of Soxhlet and SFE assays with the respective operating conditions.

Run	Method	Solvent	T (°C)	P (bar)	ρ_{f} (kg m^{-3})
SX1	Soxhlet	*n*-Hexane	68.5 *	1	-
SX2		Dichloromethane	39.6 *	1	-
SX3		Ethyl acetate	77.1 *	1	-
SX4		Ethanol	78.4 *	1	-
SFE1	SFE	CO_2	40	200	840.6 [48]
SFE2		CO_2	80	200	594.9 [48]
SFE3		CO_2	60	300	830.4 [48]
SFE4		CO_2:Ethanol (95:5 wt.%)	80	300	764.6 [49]
SFE5		CO_2:Ethyl acetate (95:5 wt.%)	80	300	761.4 [50]

* boiling point of the pure solvents.

2.4. Supercritical Fluid Extraction

The SFE assays were performed in a lab scale Spe-ed SFE unit, a model of Helix SFE System-Applied Separations, Inc., (Allentown, PA, USA) schematically presented in Figure 2. In each run, ca. 25 g of leaves were loaded into the extractor while the supercritical fluid flowed upwards at constant flow rate (Q_{CO_2}) of 12 g min^{-1} for 6 h. The experimental conditions of pressure, temperature and cosolvent content are presented in Table 1 (runs SFE1 to SFE3). The detailed procedure is described elsewhere [25]. The total extraction yield, the individual compound concentrations and respective yields were determined according to Equations (1)–(3), respectively.

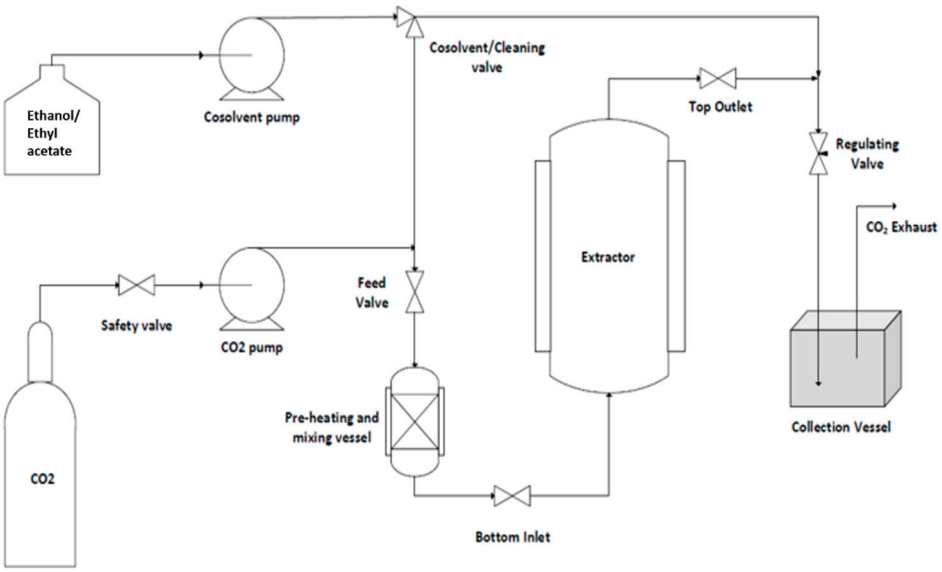

Figure 2. Simplified scheme of the SFE installation. Reprinted with permission from [25]. Copyright 2021, Elsevier.

For the runs, SFE4 and SFE5 ethanol and ethyl acetate were added as cosolvent to modify the supercritical fluid polarity and the solubility of solutes. In these runs, the cosolvent was fed to the pre-heating vessel using a HPLC pump, as presented in Figure 2.

The densities of the supercritical fluids (ρ_f), both pure and modified supercritical carbon dioxide (SC-CO_2), at each experimental condition are presented in Table 1. They were obtained using the equation of state of Pitzer and Schreiber for pure SC-CO_2 [48], Falco and Kiran for SC-CO_2 modified with ethyl acetate [50] and Pöhler and Kiran for SC-CO_2 modified with ethanol [49].

2.5. Gas Chromatography Coupled to Mass Spectrometry

The extracts were analyzed by GC–MS using a Trace Gas Chromatograph Ultra equipped with a DB-1 J&W capillary column (30 m × 0.32 mm i.d., 0.25 μm film thickness) and coupled with a Thermo DSQ mass spectrometer. The extracts were prepared and analyzed following a procedure previously published [28,29]. For the quantification of individual triterpenoids in the extracts, tetracosane and pure betulinic, oleanolic and ursolic acids were selected as internal and external standards, respectively. The identification of the compounds was performed with the aid of reverse match factors (RSI) from Wiley 9 library, which defines thresholds of mass spectral match: 900 and above is considered excellent; 800–900 is considered good, 700–800 is considered fair, and below 700 is considered a poor match [51].

3. Results and Discussion

3.1. Total Extraction Yield

The total extraction yield (η_{Total}, Equation (1)) measures the total extract amount produced independently of its composition. The results obtained with Soxhlet and SFE can be visualized in Figure 3. Concerning Soxhlet extraction, the η_{Total} values increased with the polarity of the solvent and ranged from 3.60 to 11.58 wt.% for dichloromethane and ethanol, respectively. The second highest value (7.97 wt.%) was obtained by ethyl acetate, and *n*-hexane achieved an equivalent value to dichloromethane (3.64 wt.%). Literature results on Soxhlet extractions of *A. dealbata* leaves present unequal yield scores. For instance, Oliveira et al. [6] obtained a η_{Total} of 6.2 wt.% with dichloromethane, almost double of the value obtained in this work, which may be due to the particle size reduction performed. On the other hand, Luís et al. [8] obtained a η_{Total} of 6.75 wt.% with ethanol, which is considerably lower than the value obtained in this work, and may be due to a different time of extraction, as it was stopped as soon as the extraction solvent became colorless. Borges et al. [22] obtained a η_{Total} of 13 wt.% using water and 16 h of Soxhlet extraction, which can compare with the value obtained with ethanol (11.58 wt.%), the closest solvent in terms of polarity. However, it is noteworthy that extraction with ethanol (6 h at 78.4 °C) would be more energy efficient than with water (16 h at 100 °C).

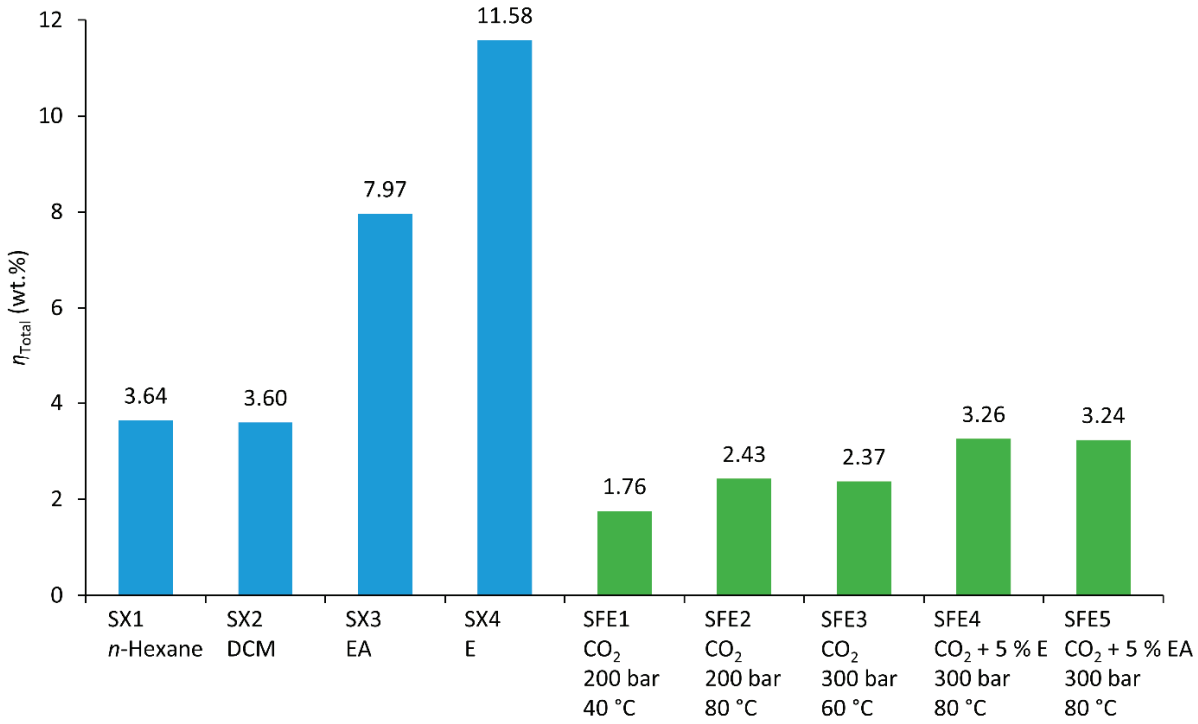

Figure 3. Total extraction yields (η_{Total}) obtained by Soxhlet using *n*-hexane, dichloromethane (DCM), ethyl acetate (EA), ethanol (E) and SFE at different conditions.

Regarding SFE assays, the η_{Total} results varied from 1.76 to 3.26 wt.% for SFE1 (200 bar, 40 °C, no cosolvent) and SFE5 (300 bar, 80 °C, 5 wt.% ethanol), respectively. Three experimental parameters were tested in these runs: pressure, temperature and cosolvent addition. Setting SFE1 (200 bar, 40 °C, no cosolvent) as the reference run, the effect of temperature on η_{Total} can be assessed by comparison with run SFE2 (200 bar, 80 °C, no cosolvent), where an increase of 38% was observed. Even though higher temperatures lower the solvent power due to SC-CO_2 density decrease (840.6 kg m^{-3} for SFE1 and 594.6 kg m^{-3} for SFE2), they increase the vapour pressure of solutes (i.e., their solubility in the supercritical solvent). These opposing effects can lead to different results from system to system, and in this case, the solubility enhancement effect was

prevalent. Moving to Run SFE3 (300 bar, 60 °C, no cosolvent), this assay was performed at more 100 bar and less 20 °C of SFE2, but yielded an identical η_{Total} (2.37 wt.%). This occurs possibly because the higher SC-CO_2 density in Run 3 (830.4 kg m^{-3}, i.e., 40% more than in SFE2) compensated the thermal penalization on the vapor pressure side of solutes. Furthermore, the addition of cosolvents was tested at 300 bar and 80 °C in runs SFE4 (5 wt.% of ethanol) and SFE5 (5 wt.% of ethyl acetate). The results were identical for both runs (3.24–3.26 wt.%), almost doubling the η_{Total} value of SFE1. The different cosolvents did not significantly affect the fluid densities between each other (764.6 kg m^{-3} for SFE4 and 761.4 kg m^{-3} for SFE5) and imposed an increase of only 2.4% in relation to pure SC-CO_2 under the same $P - T$ conditions (746.2 kg m^{-3}) [48]. Hence, the yield gain in runs SFE4 and SFE5 was attributed to a greater affinity of the solute to solvent mixtures of higher polarity.

Overall, it is clear that Soxhlet extraction produces higher η_{Total}, especially when employing high polarity solvents (i.e., ethanol or ethyl acetate). When employing low polarity solvents (i.e., dichloromethane or *n*-hexane), the η_{Total} values are analogous to those of modified SC-CO_2 and higher than those of SFE without entrainers.

3.2. Volatile Extractives

The extracts were analyzed by GC-MS, and the chromatograms of runs SX2 (A), SX4 (B) and SFE1 (C) are presented in Figure 4A–C. These are representative of the Soxhlet extractions with low and higher polarity solvents, and SFE runs, respectively. It is possible to observe that the chromatograms of runs SX2 and SFE1 (Figure 4A,C) are considerably similar, as the same peaks appear in both, which in turn confirms the affinity of dichloromethane and SC-CO_2 to similar solutes. On the contrary, SX4 (Figure 4B) stands out due to the proliferation of peaks in the region on the left of the internal standard—i.e., at retention time (Rt) lower than 38.76 min—and also due to the very sharp peak at Rt = 27.55 min, identified as *myo*-inositol (whose structure is disclosed in Figure 5). The latter forced a rescaling of the relative absorbance axis to a comparable range (from 100% in SX2 and SFE1 to 6% in SX4). All but one of the identified compounds in these peaks encompassed RSI scores comprehended between 700 and 942, which correspond to a matching quality from fair to excellent. In fact, the only exception to this was α-amyrin, whose RSI score was 691.

The full list of identified compounds for all Soxhlet extractions and SFE runs is reported in Table 2, altogether with the respective retention times and maximum RSI scores within the analyzed extracts. As previously observed in Figure 4B, run SX4 shows more peaks in the left half of the chromatogram, and that observation can be confirmed in Table 2, also for runs SX3 (ethyl acetate) and SX4 (ethanol), specifically amid retention times of 10.77 to 44.37 min. The said peaks consist mainly of polyols (P) and monosaccharides (M). After these come the fatty acids (FA), long-chain aliphatic alcohols (LCAA) and triterpenoids (TT), although these were also found in every extract. Furthermore, SX1 (*n*-hexane) and SX2 (dichloromethane) present a very similar pattern of detected compounds, as well as the runs SFE1-SFE5. This corroborates what was observed in the analysis of Figure 4A,C. Such similarities show that the polarity of the solvent strongly influences the compounds extracted, and that, in the case of SFE, the modification of SC-CO_2 with 5 wt.% of ethanol or ethyl acetate was not enough to lead to the extraction of volatile compounds with higher affinity to polar organic solvents.

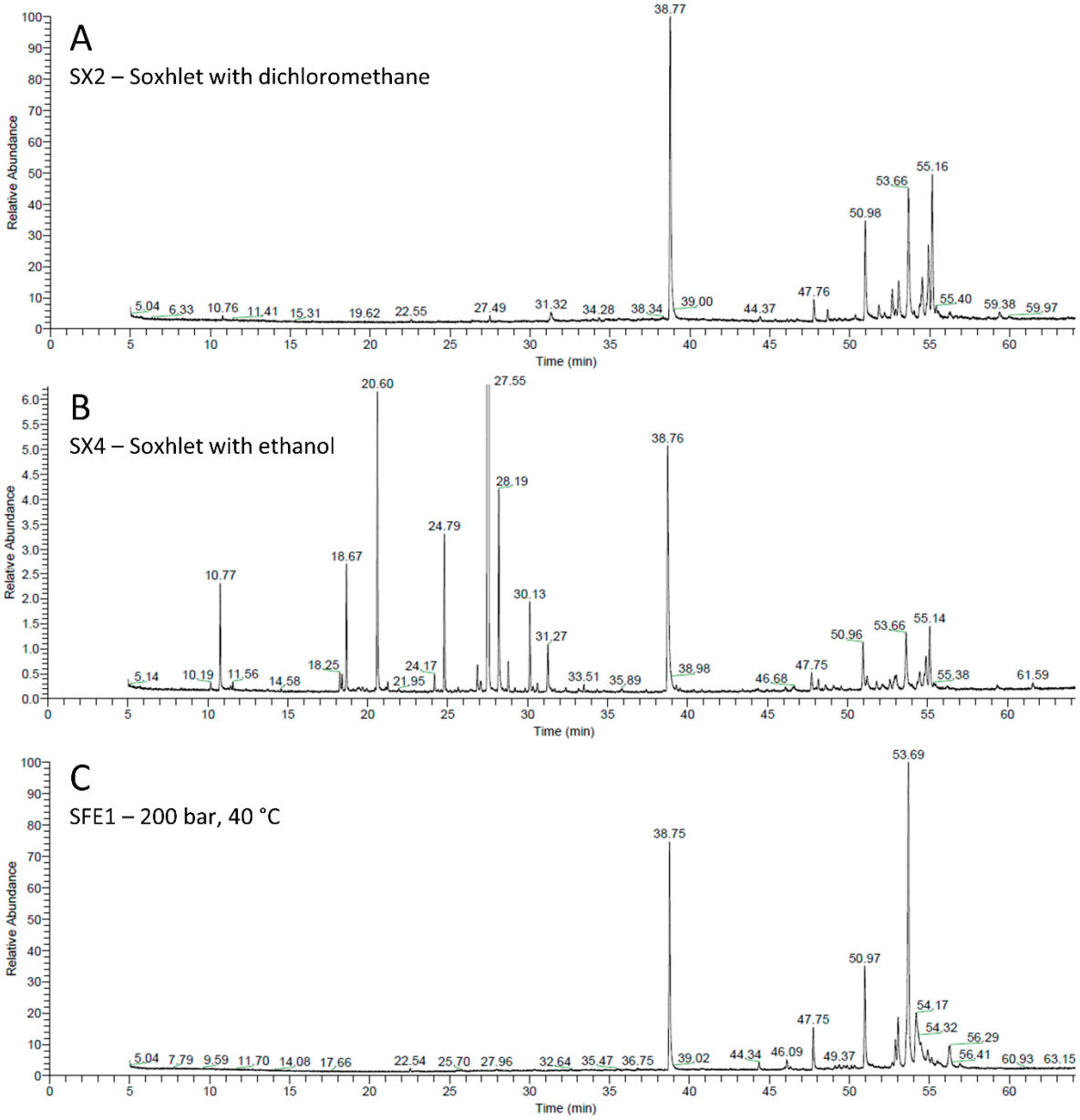

Figure 4. Chromatograms of the extracts from runs (**A**) SX2 (dichloromethane), (**B**) SX4 (ethanol) and (**C**) SFE1 (200, bar 40 °C). Internal standard (tetracosane) appears at 38.7 min.

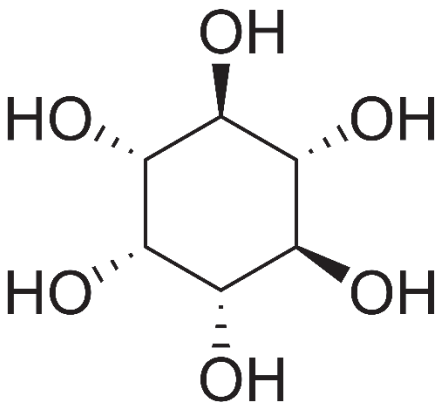

Figure 5. Structural formula of *myo*-inositol.

Table 2. List of identified compounds and respective retention times and reverse match factors (RSI) for all Soxhlet and SFE runs.

Rt (min)	Compound	Family	RSI	SX1	SX2	SX3	SX4	SFE1	SFE2	SFE3	SFE4	SFE5
10.77	Glycerol	P	909	-	+	+	+	-	-	-	-	-
18.67	Erythritol	P	942	-	-	+	+	-	-	-	-	-
20.6	5-Hydroxypipecolic acid	CA	770	-	-	-	+	-	-	-	-	-
24.17	Xylitol	P	800	-	-	+	+	-	-	-	-	-
24.79	Ribitol	P	887	-	-	+	+	-	-	-	-	-
27.55	*myo*-Inositol	P	803	-	-	+	+	-	-	-	-	-
28.19	Tyramine	A	890	-	-	-	+	-	-	-	-	-
28.79	D-Mannose	M	803	-	-	+	+	-	-	-	-	-
30.13	Mannitol	P	851	-	-	+	+	-	-	-	-	-
31.27	Glucose	M	827	-	-	+	+	-	-	-	-	-
44.37	Docosanoic acid	FA	729	+	+	-	-	+	+	+	+	+
46.09	Squalene	TT	833	-	-	-	-	+	+	+	+	+
47.76	Pentacosanoic acid	FA	829	+	+	+	+	+	+	+	+	+
48.61	Hexadecanoic acid	FA	705	+	+	+	-	-	-	-	-	-
50.98	Octacosanoic acid	FA	849	+	+	+	+	+	+	+	+	+
51.82	Octacosan-1-ol	LCAA	811	+	-	+	-	-	-	-	-	-
52.66	4'-OH,5-OH,7-Di-O-Glucoside	F	688	+	+	+	+	+	+	+	+	+
52.86	α-Amyrone	TT	786	+	+	-	-	+	+	+	+	+
53.06	β-Amyrone	TT	738	+	+	+	+	+	+	+	+	+
53.66	Lupenone	TT	843	+	+	+	+	+	+	+	+	+
54.92	β-Amyrin	TT	755	+	+	+	+	+	+	+	+	+
55.16	α-Amyrin	TT	691	+	+	+	+	+	+	+	+	+
56.28	Lupenyl acetate	TT	742	+	+	-	-	+	+	+	+	+

P—polyol; CA—carboxylic acid; A—amine; M—monosaccharide; FA—fatty acid; TT—triterpenoid; LCAA—long-chain aliphatic alcohol; F—flavonoid.

As observed in Figure 4B, *myo*-inositol (see Figure 5) peak has an area of different magnitude from the targeted triterpenoids, thirteen times higher (run SX4) than the internal standard. Even though it is a known constituent of plant and animal cells, the results obtained demonstrate the potential of ethanol and ethyl acetate, and potentially other polar organic solvents, for the production of *myo*-inositol-rich extracts. According to the literature, this compound and its derivatives have been identified and quantified in several plant species [52–56], including *Acacia* trees, such as in *Acacia pennata* and *Acacia farnesiana* leaves [57], and *Acacia mangium* and *Acacia maidenii* seeds [58]. Moreover, *myo*-inositol plays an important role in several cell functions, such as growth, development and reproduction, among others [59]. As a dietary supplement, it can be beneficial for human disorders associated with insulin resistance, such as polycystic ovary syndrome, gestational diabetes mellitus or metabolic syndrome, and the prevention or treatment of some diabetic complications, namely, neuropathy, nephropathy and cataract [59]. Even though this represents a promising result for the valorisation of *Acacia dealbata* biomass, the main focus of this work is the triterpenoid fraction attainable by SFE, which leaves *myo*-inositol out of the work scope. Nevertheless, it might open the way to sequential extraction strategies.

The main triterpenoids (TT) identified in the produced extracts were squalene, α-amyrone, β-amyrone, lupenone, β-amyrin, α-amyrin and lupenyl acetate. These contain 30 carbon atoms, except for lupenyl acetate which has 32, and all of these compounds are interrelated by known biosynthesis pathways, as summarized in Figure 6. Here, it can be seen that squalene is the prime precursor, having been originated by successive condensation reactions of the isomers of isopentenyl diphosphate and dimethylallyl diphosphate [60–62]. Eventually, squalene can be oxidized to 2,3-oxidosqualene, which in turn is the direct precursor of tricyclic, tetracyclic or pentacyclic triterpenoids. When under the chair-chair-chair conformation, 2,3-oxidosqualene can undergo cyclization reactions forming the tetracyclic dammarenyl cation, which, after ring expansions, originates

diverse skeletons of pentacyclic triterpenoids, such as the lupane, oleanane and ursane types (see Figure 6). The latter three types are the precursors of lupeol, β-amyrin and α-amyrin, respectively [60–63]. Upon undergoing further rearrangements, and/or oxidation, substitution or glycosylation reactions, other triterpenoids are generated, namely lupenone, β-amyrone and α-amyrone (as the ketone versions of lupeol, β-amyrin and α-amyrin, respectively), and lupenyl acetate (as the acetylated version of lupeol). To conclude, the majority of these compounds were also identified in previous extraction works of *A. dealbata* biomass [6,17], especially in the leaves, bark and other external parts, since they are thought to provide protection against insects and microbes [63].

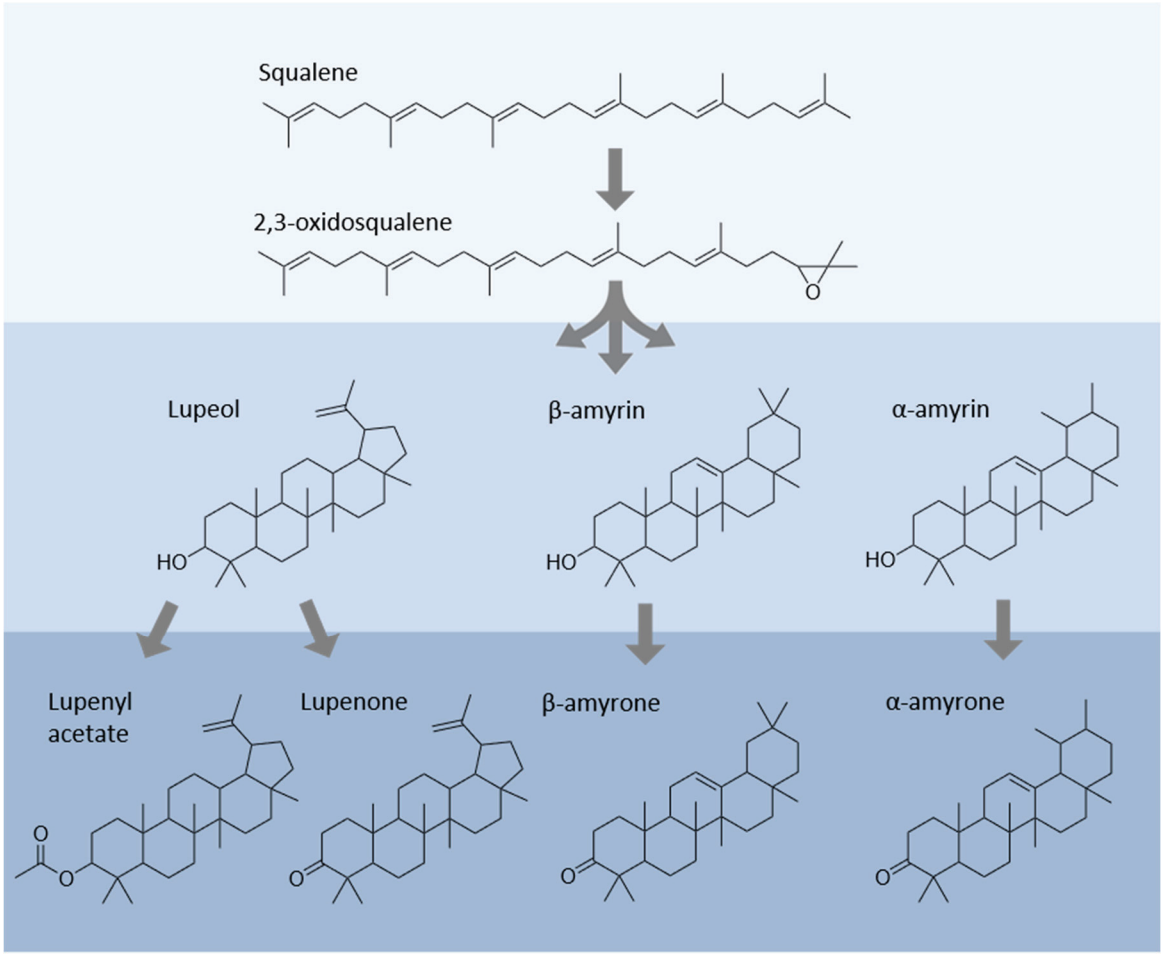

Figure 6. Scheme representative of synthesis pathways of triterpenoids from squalene, namely the lupane, oleanane and ursane series.

3.3. Triterpenoid Extraction Yields

The individual (η_i) and total triterpenoid ($\eta_{\text{Total TT}}$) extraction yields of Soxhlet and SFE assays are presented in Figure 7A,B, respectively. Regarding Soxhlet extractions (Figure 7A), lupenone was the most extracted compound of the four organic solvents tested, with η_{lupenone} values ranging from 2114 to 2994 mg kg_{leaves}^{-1} for *n*-hexane and ethyl acetate extraction, respectively. It was followed by α-amyrin, with yields from 1249 to 2851 mg kg_{leaves}^{-1} for dichloromethane and ethyl acetate, respectively. Although $\eta_{\beta-\text{amyrin}}$ was generally lower than $\eta_{\alpha-\text{amyrin}}$, this difference is especially evident in the dichloromethane Soxhlet extract, where the latter yielded circa 2.7 times more. In turn, ethyl acetate attenuated the two amyrin yields, with their ratio falling to ca. 1.6. For extracts produced with more polar solvents, the two amyrin yields approached the values of η_{lupenone}. This was translated to the magnitude of $\eta_{\text{Total TT}}$, which incremented from the minimum of 4908 mg kg_{leaves}^{-1} for *n*-hexane to 8201 mg kg_{leaves}^{-1} for ethyl acetate and

to 6259 mg kg^{-1}_{leaves} for ethanol. The remaining triterpenoids did not differ significantly between organic solvents, and their individual yields were markedly low.

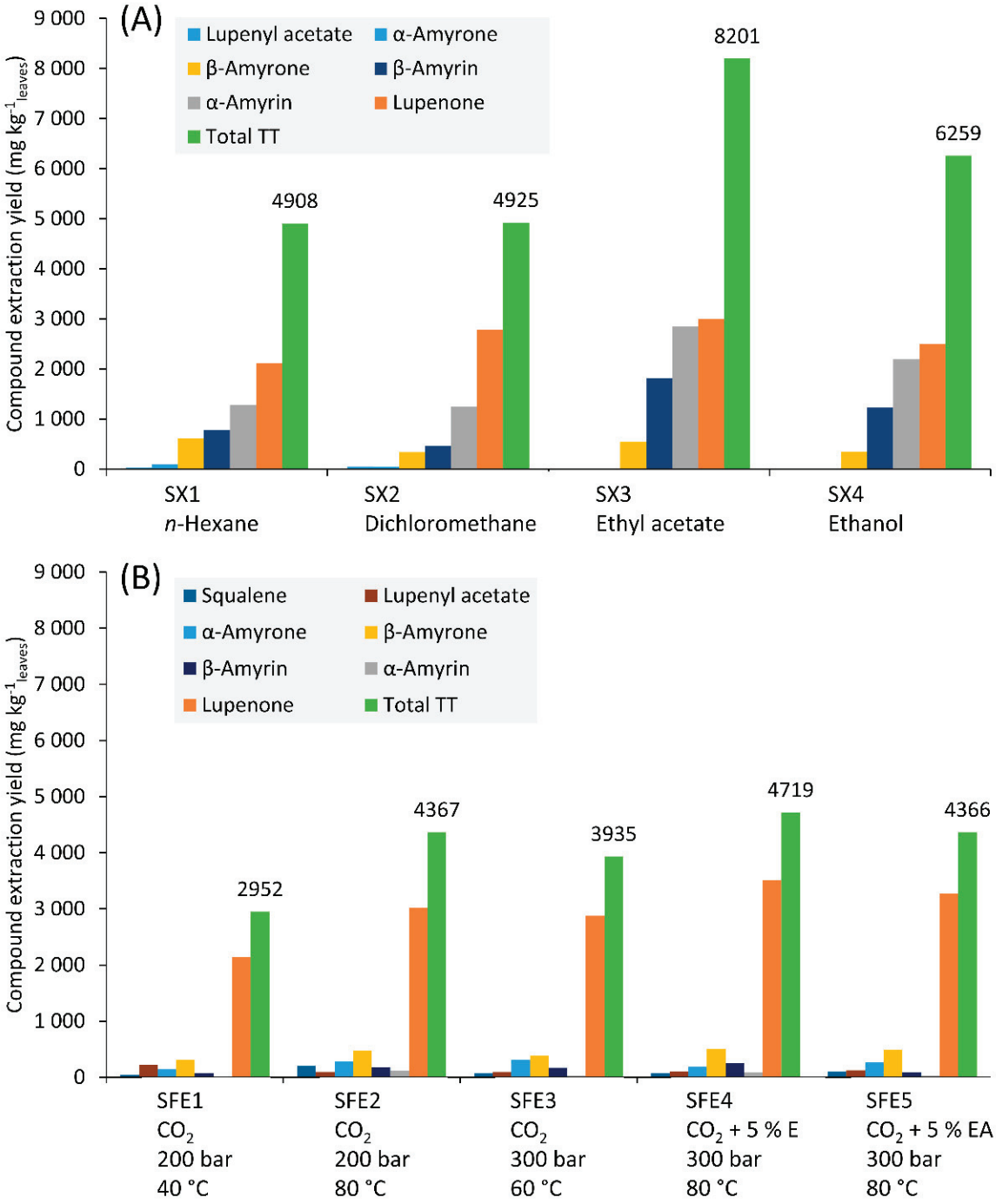

Figure 7. Individual and total triterpenoid (Total TT) extraction yields in: (**A**) Soxhlet extracts using different organic solvents, and (**B**) SFE at different conditions of temperature, pressure, and ethanol (E) or ethyl acetate (EA) content as modifiers.

Concerning uptake of triterpenoids by SFE (see Figure 7B), lupenone confirmed its leading individual yield also in this separation method, which varied from 2139 to 3512 mg kg^{-1}_{leaves} for SFE1 (200 bar, 40 °C, no cosolvent) and SFE4 (300 bar, 80 °C, 5 wt.% of ethanol), respectively. None of the remaining triterpenoids surpassed 500 mg kg^{-1}_{leaves} threshold. The increase of temperature from 40 °C to 80 °C of runs SFE1 and SFE2,

respectively, improved the η_{lupenone} by 41% and, if contrasted with the 38% increase verified in the η_{Total} (recall Figure 3), represents a proportional increase. Furthermore, run SFE3 (300 bar, 60 °C, no cosolvent) shows that even though it produced a similar η_{Total} of SFE2, the joint $P - T$ change decreased the lupenone uptake to 2879 mg kg_{leaves}^{-1}. This confirms that the favorable effect of temperature on solubility prevailed over the loss of SC-CO_2 density. With the employment of ethanol and ethyl acetate at 300 bar and 80 °C (runs SFE4 and SFE5), higher lupenone yields were obtained, namely 3512 mg kg_{leaves}^{-1} and 3273 mg kg_{leaves}^{-1}, respectively. This suggests that the joint optimization of P, T and cosolvent content can be determinant to potentiate the removal of this compound by SFE.

The low yields for the other triterpenoids explain the lower $\eta_{\text{Total TT}}$ obtained by SFE. These were only slightly inferior to the Soxhlet extractions with *n*-hexane and dichloromethane, but substantially lower in relation to ethyl acetate and ethanol, whose $\eta_{\text{Total TT}}$ values scored, respectively, 74% and 33% higher than of SFE4 (the richest in $\eta_{\text{Total TT}}$ with 4719 mg kg_{leaves}^{-1}).

3.4. Triterpenoid Concentration in Extracts

To assess the effect of distinct extraction methods and operating conditions on the selectivity of the identified triterpenoids, their individual concentrations were determined and are presented in Figure 8A,B for Soxhlet and SFE assays, respectively.

Regarding the Soxhlet extracts (Figure 8A), the concentration trend does not follow those of total or individual triterpenoid yields. The highest extract concentration of lupenone amounted 7.7 wt.% and occurred for dichloromethane assay (SX2), followed by *n*-hexane (SX1) with 5.8 wt.%, ethyl acetate (SX3) with 3.8 wt.%, and finally, ethanol (SX4) with 2.2 wt.%. Even though $\eta_{\text{Total TT}}$ and η_{lupenone} of dichloromethane and *n*-hexane Soxhlet extraction were lower than those of ethyl acetate and ethanol, they resulted in higher C_{lupenone}. This is due to the fact that, as discussed previously (see Table 2), the more polar solvents are able to coextract other families of compounds, thus diluting the content of triterpenoids and fading the selectivity towards them, namely to lupenone. The same can be observed for the remaining triterpenoids. Another interesting result is the levelled scores of $C_{\alpha-\text{amyrin}}$ among the four organic solvents studied, ranging from 1.89 to 3.57 wt.%, which were far from expected given the significantly higher $\eta_{\alpha-\text{amyrin}}$ obtained with ethyl acetate and ethanol (see Figure 7A). The observed yield/concentration nuances are ultimately reflected in the $C_{\text{Total TT}}$ response, which was as low as 10.3% and 5.4 wt.% for ethyl acetate and ethanol, respectively, against 13.4 and 14.4 wt.% for dichloromethane and *n*-hexane, respectively. As a result, the use of the two non-polar solvents are better choices than ethanol or ethyl acetate when seeking a higher selectivity to lupenone, despite having lower yields of this compound as counterpart.

The SFE results (see Figure 8B) show higher C_{lupenone} than any of the Soxhlet extracts, ranging from 10.1 to 12.4 wt.%, for runs SFE5 (300 bar, 80 °C, 5 wt.% of ethyl acetate) and SFE2 (200 bar, 80 °C, no cosolvent), respectively. Once again, one can observe that the discussed trends on $\eta_{\text{Total TT}}$ and η_{lupenone} are not verified for the concentration values. Accordingly, even though run SFE2 showed the highest selectivity towards lupenone, it only attained the third highest η_{lupenone} (see Figure 7B), and the same applies to run SFE1 (200 bar, 40 °C, no cosolvent). In turn, the inclusion of polar modifiers in runs SFE4 (300 bar, 80 °C, 5 wt.% of ethanol) and SFE5 (300 bar, 80 °C, 5 wt.% of ethyl acetate) created the same penalization observed in Soxhlet: lower C_{lupenone} was attained despite the higher $\eta_{\text{Total TT}}$ and η_{lupenone} scores (see Figures 3 and 7B). As a result, the SFE results show that pure SC-CO_2 was the most selective to lupenone, but the method was not able to selectively coextract other triterpenoids. In terms of $C_{\text{Total TT}}$, similarly to what was observed for the triterpenoid yield (see Figure 7B), the values follow the lupenone trend since the remaining triterpenoids were extracted in significantly lower amounts. Accordingly, the maximum was attained by run SFE2 (200 bar, 80 °C, no cosolvent), where $C_{\text{Total TT}}$ is worth 18.0 wt.%. The individual contribution of other triterpenoids in the extract for this score did not surpass 2 wt.%.

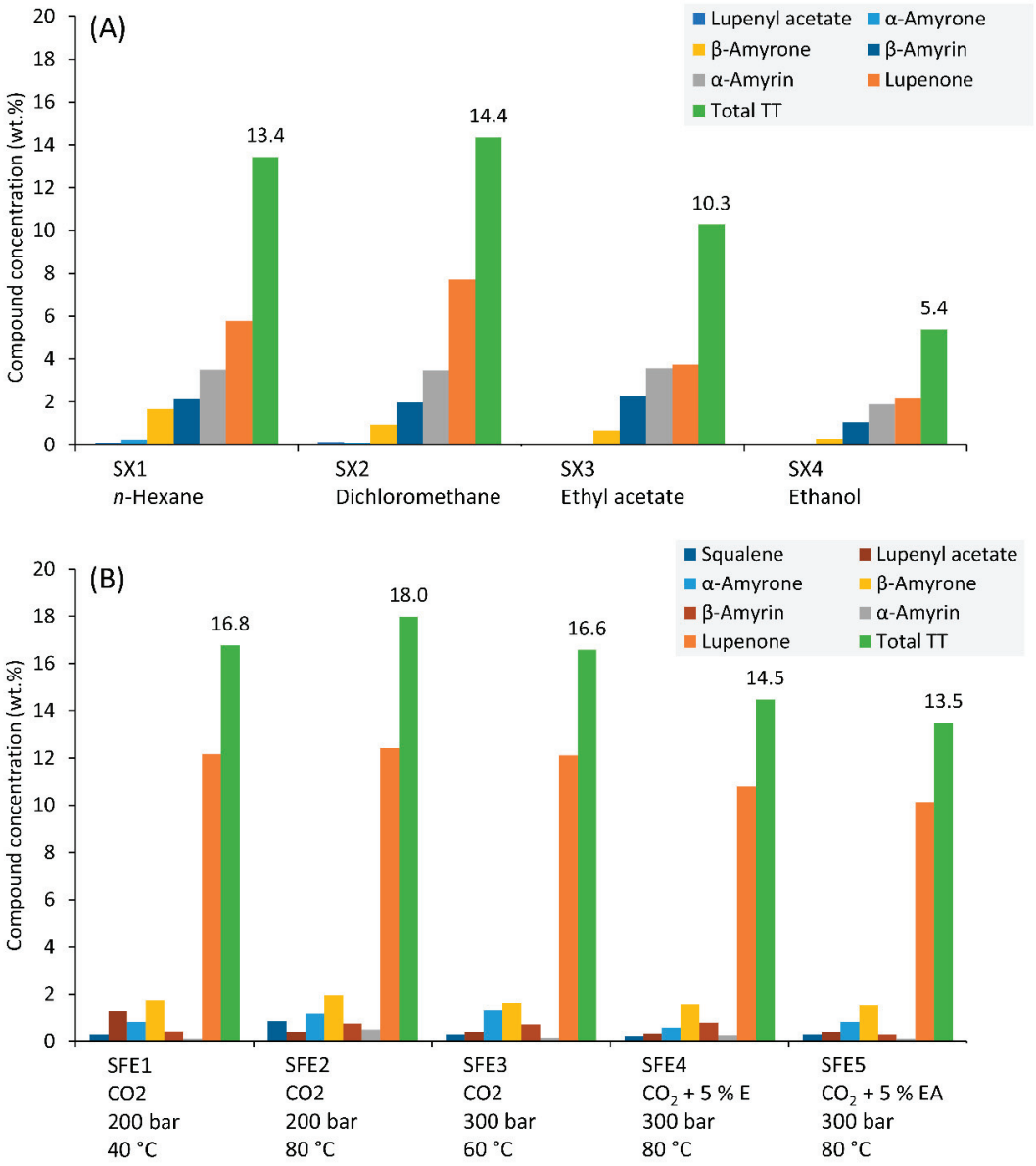

Figure 8. Plots of the concentrations of individual triterpenoids identified in (**A**) Soxhlet extracts and respective solvents, and (**B**) SFE at different conditions of temperature, pressure, and addition of ethanol (E) and ethyl acetate (EA) as modifiers.

Overall, the attained SFE results show that the method can selectively extract lupenone from the leaves of *A. dealbata*, even though similar triterpenoids are only coextracted on a negligible basis. Furthermore, lupenone therapeutic potential for inflammation, virus, infection, diabetes, cancer, and treatment of Chagas disease [36] justifies its valorisation in an industrial process for pharmaceutical and food applications.

4. Conclusions

Soxhlet extraction of *Acacia dealbata* leaves provided higher total extraction yields than SFE, and the yield increased with the polarity of the organic solvent. In turn, SFE yields were favored by increasing temperature and pressure, and by the addition of polar cosolvents. In both cases the main triterpenoids extracted were squalene, β-amyrone, α-amyrone, β-amyrin, α-amyrin, lupenyl acetate and lupenone, with the latter exhibiting the highest content. Overall, Soxhlet extracts exhibited higher amounts of total triterpenoids in comparison to SFE extracts. Interestingly SFE selectively extracted lupenone, reaching higher contents than those obtained with Soxhlet.

Even though the increase of pressure and temperature combined with the addition of cosolvents favored the SFE total yield, the same effect was not so evident for lupenone yield. In fact, pure CO_2 attained a lupenone yield comparable to the maximum value achieved at high pressure with SC-CO_2 modified with ethanol. Furthermore, the highest lupenone concentration was also obtained for pure CO_2 extracts.

Considering the anti-inflammatory, anti-virus, anti-diabetes, and anti-cancer properties of lupenone, as well as its potential for the treatment of Chagas disease, one may state that SFE contributes to the valorisation of *A. dealbata* leaves in the production of lupenone-enriched extracts for the pharmaceutical, nutraceutical or food industries.

Globally, this work envisions SFE technology as a tool to address the current challenges associated to the management of *A. dealbata* spread, namely by pointing to biorefinery opportunities for its leaves. Even though the present study indicates that high selectivity to lupenone may be achieved by SFE, optimization of the extraction conditions and a preliminary economic evaluation of the process are highly recommended.

Author Contributions: Conceptualization, C.M.S.; writing—original draft preparation, V.H.R. and M.M.R.d.M.; methodology, V.H.R. and M.M.R.d.M.; investigation, V.H.R.; formal analysis, M.M.R.d.M., I.P. and C.M.S.; writing—review and editing, I.P. and C.M.S.; supervision, I.P. and C.M.S.; funding acquisition, C.M.S.; resources, C.M.S. All authors have read and agreed to the published version of the manuscript.

Funding: This work was developed within the scope of the project CICECO-Aveiro Institute of Materials, UIDB/50011/2020 & UIDP/50011/2020, financed by national funds through the FCT/MEC and, when appropriate, co-financed by FEDER under the PT2020 Partnership Agreement. Authors want to thank Project inpactus—innovative products and technologies from eucalyptus, Project N° 21874 funded by Portugal 2020 through European Regional Development Fund (ERDF) in the frame of COMPETE 2020 n°246/AXIS II/2017. Authors want to thank the funding from Project AgroForWealth (CENTRO-01-0145-FEDER-000001), funded by Centro2020, through FEDER and PT2020.

Conflicts of Interest: The authors declare no conflict of interest.

References

1. Lorenzo, P.; Gonzalez, L.O.; Reigosa, M.J. The genus Acacia as invader: The characteristic case of *Acacia dealbata* Link in Europe. *Ann. For. Sci.* **2010**, *67*, 101. [CrossRef]
2. Kull, C.A.; Shackleton, C.M.; Cunningham, P.J.; Ducatillon, C.; Dufour-Dror, J.-M.; Esler, K.J.; Friday, J.B.; Gouveia, A.C.; Griffin, A.R.; Marchante, E.; et al. Adoption, use and perception of Australian acacias around the world. *Divers. Distrib.* **2011**, *17*, 822–836. [CrossRef]
3. Le Maitre, D.C.; Gaertner, M.; Marchante, E.; Ens, E.-J.; Holmes, P.M.; Pauchard, A.; O'Farrell, P.J.; Rogers, A.M.; Blanchard, R.; Blignaut, J.; et al. Impacts of invasive Australian acacias: Implications for management and restoration. *Divers. Distrib.* **2011**, *17*, 1015–1029. [CrossRef]
4. Instituto da Conservação da Natureza e das Florestas. *Inventário Florestal Nacional (IFN6)–Principais Resultados*; 2019.
5. European Commission Directive (EU) 2018/2002 of the European Parliament and of the Council of 11 December 2018 amending Directive 2012/27/EU on energy efficiency. *Off. J. Eur. Union* **2018**, *61*, 1–230.
6. Oliveira, C.S.D.; Moreira, P.; Resende, J.; Cruz, M.T.; Pereira, C.M.F.; Silva, A.M.S.; Santos, S.A.O.; Silvestre, A.J.D. Characterization and Cytotoxicity Assessment of the Lipophilic Fractions of Different Morphological Parts of *Acacia dealbata*. *Int. J. Mol. Sci.* **2020**, *21*, 1814. [CrossRef]
7. Freire, C.; Coelho, D.S.C.; Santos, N.M.; Silvestre, A.J.D.; Neto, C. Identification of Δ7 phytosterols and phytosteryl glucosides in the wood and bark of several *Acacia* species. *Lipids* **2005**, *40*, 317–322. [CrossRef]
8. Luís, A.; Gil, N.; Amaral, M.E.; Duarte, A.P. Antioxidant activities of extracts from *Acacia melanoxylon*, *Acacia dealbata* and *Olea europaea* and alkaloids estimation. *Int. J. Pharm. Pharm. Sci.* **2012**, *4*, 225–231.
9. Yáñez, R.; Gómez, B.; Martínez, M.; Gullón, B.; Alonso, J.L.; Estévez, B.G. Valorization of an invasive woody species, *Acacia dealbata*, by means of Ionic liquid pretreatment and enzymatic hydrolysis. *J. Chem. Technol. Biotechnol.* **2014**, *89*, 1337–1343. [CrossRef]
10. Yildiz, S.; Gürgen, A.; Can, Z.; Tabbouche, S.A.; Kiliç, A.O. Some bioactive properties of Acacia dealbata extracts and their potential utilization in wood protection. *Drewno* **2018**, *61*, 81–97. [CrossRef]
11. Devi, S.R.; Prasad, M.N.V. Tannins and related polyphenols from ten common *Acacia* species of India. *Bioresour. Technol.* **1991**, *36*, 189–192. [CrossRef]

12. Freire, C.S.R.; Silvestre, A.J.D.; Neto, C.P. Demonstration of long-chain n-alkyl caffeates and Δ7-steryl glucosides in the bark of *Acacia* species by gas chromatography-mass spectrometry. *Phytochem. Anal.* **2007**, *18*, 151–156. [CrossRef]
13. Lisperguer, J.; Saraiva, Y.; Vergara, E. Structure and thermal behavior of tannins from *Acacia dealbata* bark and their reactivity toward formaldehyde. *J. Chil. Chem. Soc.* **2016**, *61*, 3188–3190. [CrossRef]
14. Neiva, D.M.; Luís, Â.; Gominho, J.; Domingues, F.; Duarte, A.P.; Pereira, H. Bark residues valorization potential regarding antioxidant and antimicrobial extracts. *Wood Sci. Technol.* **2020**, *54*, 559–585. [CrossRef]
15. Casas, M.P.; Conde, E.; Ribeiro, D.; Fernandes, E.; Domínguez, H.; Torres, M.D. Bioactive properties of *Acacia dealbata* flowers extracts. *Waste Biomass Valoriz.* **2020**, *11*, 2549–2557. [CrossRef]
16. López-Hortas, L.; Falqué, E.; Domínguez, H.; Torres, M.D. Microwave hydrodiffusion and gravity versus conventional distillation for *Acacia dealbata* flowers. Recovery of bioactive extracts for cosmetic purposes. *J. Clean. Prod.* **2020**, *274*. [CrossRef]
17. Pereira, F.B.M.; Domingues, F.M.J.; Silva, A.M.S. Triterpenes from *Acacia dealbata*. *Nat. Prod. Lett.* **1996**, *8*, 97–103. [CrossRef]
18. Imperato, F. A chalcone glycoside from *Acacia dealbata*. *Phytochemistry* **1982**, *21*, 480–481. [CrossRef]
19. Rodolphe, P.; Katharina, B.; Meierhenrich, U.J.; Elise, C.; Georges, F.; Nicolas, B. Chemical composition of french mimosa absolute oil. *J. Agric. Food Chem.* **2010**, *58*, 1844–1849. [CrossRef]
20. Soto, M.L.; Parada, M.; Falqué, E.; Domínguez, H. Personal-care products formulated with natural antioxidant extracts. *Cosmetics* **2018**, *5*, 13. [CrossRef]
21. Silva, E.; Fernandes, S.; Bacelar, E.; Sampaio, A. Antimicrobial activity of aqueous, ethanolic and methanolic leaf extracts from *Acacia* spp. and *Eucalyptus nicholii*. *Afr. J. Tradit. Complement. Altern. Med.* **2016**, *13*, 130–134. [CrossRef]
22. Borges, A.; José, H.; Homem, V.; Simões, M. Comparison of Techniques and Solvents on the Antimicrobial and Antioxidant Potential of Extracts from *Acacia dealbata* and *Olea europaea*. *Antibiotics* **2020**, *9*, 48. [CrossRef]
23. de Melo, M.M.R.; Oliveira, E.L.G.; Silvestre, A.J.D.; Silva, C.M. Supercritical fluid extraction of vegetable matrices: Applications, trends and future perspectives of a convincing green technology. *J. Supercrit. Fluids* **2014**, *92*, 115–176. [CrossRef]
24. Reverchon, E.; Marco, I. De Supercritical fluid extraction and fractionation of natural matter. *J. Supercrit. Fluids* **2006**, *38*, 146–166. [CrossRef]
25. Rodrigues, V.H.; de Melo, M.M.R.; Portugal, I.; Silva, C.M. Extraction of *Eucalyptus* leaves using solvents of distinct polarity. Cluster analysis and extracts characterization. *J. Supercrit. Fluids* **2018**, *135*, 263–274. [CrossRef]
26. Rodrigues, V.H.; de Melo, M.M.R.; Portugal, I.; Silva, C.M. Supercritical fluid extraction of *Eucalyptus globulus* leaves. Experimental and modelling studies of the influence of operating conditions and biomass pretreatment upon yields and kinetics. *Sep. Purif. Technol.* **2018**, *191*, 173–181. [CrossRef]
27. Domingues, R.M.A.; de Melo, M.M.R.; Oliveira, E.L.G.; Neto, C.P.; Silvestre, A.J.D.; Silva, C.M. Optimization of the supercritical fluid extraction of triterpenic acids from *Eucalyptus globulus* bark using experimental design. *J. Supercrit. Fluids* **2013**, *74*, 105–114. [CrossRef]
28. de Melo, M.M.R.; Oliveira, E.L.G.; Silvestre, A.J.D.; Silva, C.M. Supercritical fluid extraction of triterpenic acids from *Eucalyptus globulus* bark. *J. Supercrit. Fluids* **2012**, *70*, 137–145. [CrossRef]
29. Domingues, R.M.A.; Oliveira, E.L.G.; Freire, C.S.R.; Couto, R.M.; Simões, P.C.; Neto, C.P.; Silvestre, A.J.D.; Silva, C.M. Supercritical fluid extraction of *Eucalyptus globulus* bark-A promising approach for triterpenoid production. *Int. J. Mol. Sci.* **2012**, *13*, 7648–7662. [CrossRef]
30. de Melo, M.M.R.; Carius, B.; Simões, M.M.Q.; Portugal, I.; Saraiva, J.; Silva, C.M. Supercritical CO2 extraction of *V. vinifera* leaves: Influence of cosolvents and particle size on removal kinetics and selectivity to target compounds. *J. Supercrit. Fluids* **2020**, *165*, 104959. [CrossRef]
31. de Melo, M.M.R.; Vieira, P.G.; Şen, A.; Pereira, H.; Portugal, I.; Silva, C.M. Optimization of the supercritical fluid extraction of *Quercus cerris* cork towards extraction yield and selectivity to friedelin. *Sep. Purif. Technol.* **2020**, *238*, 116395. [CrossRef]
32. Martins, P.F.; de Melo, M.M.R.; Sarmento, P.; Silva, C.M. Supercritical fluid extraction of sterols from *Eichhornia crassipes* biomass using pure and modified carbon dioxide. Enhancement of stigmasterol yield and extract concentration. *J. Supercrit. Fluids* **2016**, *107*, 441–449. [CrossRef]
33. Evans, C.S.; Qureshi, M.Y.; Bell, E.A. Free amino acids in the seeds of *Acacia* species. *Phytochemistry* **1977**, *16*, 565–570. [CrossRef]
34. Domingues, R.; Guerra, A.; Duarte, M.; Freire, C.; Neto, C.; Silva, C.; Silvestre, A. Bioactive Triterpenic Acids: From Agroforestry Biomass Residues to Promising Therapeutic Tools. *Mini Rev. Org. Chem.* **2014**, *11*, 382–399. [CrossRef]
35. de Melo, M.M.R.; Domingues, R.M.A.; Silvestre, A.J.D.; Silva, C.M. Extraction and purification of triterpenoids using supercritical fluids: From lab to exploitation. *Mini Rev. Org. Chem.* **2014**, 362–381. [CrossRef]
36. Xu, F.; Huang, X.; Wu, H.; Wang, X. Beneficial health effects of lupenone triterpene: A review. *Biomed. Pharmacother.* **2018**, *103*, 198–203. [CrossRef]
37. Saleem, M. Lupeol, a novel anti-inflammatory and anti-cancer dietary triterpene. *Cancer Lett.* **2009**, *285*, 109–115. [CrossRef]
38. Meneses-Sagrero, S.E.; Navarro-Navarro, M.; Ruiz-Bustos, E.; Del-Toro-Sánchez, C.L.; Jiménez-Estrada, M.; Robles-Zepeda, R.E. Antiproliferative activity of spinasterol isolated of *Stegnosperma halimifolium* (Benth, 1844). *Saudi Pharm. J.* **2017**, *25*, 1137–1143. [CrossRef]
39. Lou-Bonafonte, J.M.; Martínez-Beamonte, R.; Sanclemente, T.; Surra, J.C.; Herrera-Marcos, L.V.; Sanchez-Marco, J.; Arnal, C.; Osada, J. Current Insights into the Biological Action of Squalene. *Mol. Nutr. Food Res.* **2018**, *62*, 1–16. [CrossRef]

40. Aragão, G.F.; Carneiro, L.M.V.; Junior, A.P.F.; Vieira, L.C.; Bandeira, P.N.; Lemos, T.L.G.; de B. Viana, G.S. A possible mechanism for anxiolytic and antidepressant effects of alpha- and beta-amyrin from Protium heptaphyllum (Aubl.) March. *Pharmacol. Biochem. Behav.* **2006**, *85*, 827–834. [CrossRef]
41. Aragão, G.F.; Cunha Pinheiro, M.C.; Nogueira Bandeira, P.; Gomes Lemos, T.L.; de Barros Viana, G.S. Analgesic and anti-inflammatory activities of the isomeric mixture of alpha- and beta-amyrin from protium heptaphyllum (Aubl.) March. *J. Herb. Pharmacother.* **2007**, *7*, 31–47. [CrossRef] [PubMed]
42. da Silva Júnior, W.F.; Lima Bezerra de Menezes, D.; Calvarho de Oliveira, L.; Scherer Koester, L.; Olveira de Almeida, P.D.; Lima, E.S.; Pereira de Azevedo, E.; da Veiga Júnior, V.F.; Neves de Lima, Á.A. Inclusion complexes of β and HPβ-cyclodextrin with α, β amyrin and in vitro anti-inflammatory activity. *Biomolecules* **2019**, *9*, 241. [CrossRef]
43. Holanda Pinto, S.A.; Pinto, L.M.S.; Cunha, G.M.A.; Chaves, M.H.; Santos, F.A.; Rao, V.S. Anti-inflammatory effect of α, β-Amyrin, a pentacyclic triterpene from Protium heptaphyllum in rat model of acute periodontitis. *Inflammopharmacology* **2008**, *16*, 48–52. [CrossRef]
44. Oliveira, F.A.; Vieira-Júnior, G.M.; Chaves, M.H.; Almeida, F.R.C.; Florêncio, M.G.; Lima, R.C.P., Jr.; Silva, R.M.; Santos, F.A.; Rao, V.S.N. Gastroprotective and anti-inflammatory effects of resin from Protium heptaphyllum in mice and rats. *Pharmacol. Res.* **2004**, *49*, 105–111. [CrossRef]
45. Okoye, N.N.; Ajaghaku, D.L.; Okeke, H.N.; Ilodigwe, E.E.; Nworu, C.S.; Okoye, F.B.C. Beta-Amyrin and alpha-Amyrin acetate isolated from the stem bark of Alstonia boonei display profound anti-inflammatory activity. *Pharm. Biol.* **2014**, *52*, 1478–1486. [CrossRef] [PubMed]
46. Jæger, D.; O'Leary, M.C.; Weinstein, P.; Møller, B.L.; Semple, S.J. Phytochemistry and bioactivity of *Acacia sensu stricto* (Fabaceae: Mimosoideae). *Phytochem. Rev.* **2019**, *18*, 129–172. [CrossRef]
47. Subhan, N.; Burrows, G.E.; Kerr, P.G.; Obied, H.K. Phytochemistry, Ethnomedicine, and Pharmacology of *Acacia*. *Stud. Nat. Prod. Chem.* **2018**, *57*, 247–326. [CrossRef]
48. Pitzer, K.S.; Schreiber, D.R. Improving equation-of-state accuracy in the critical region; equations for carbon dioxide and neopentane as examples. *Fluid Phase Equilib.* **1988**, *41*, 1–17. [CrossRef]
49. Pöhler, H.; Kiran, E. Volumetric properties of carbon dioxide + ethanol at high pressures. *J. Chem. Eng. Data* **1997**, *42*, 384–388. [CrossRef]
50. Falco, N.; Kiran, E. Volumetric properties of ethyl acetate + carbon dioxide binary fluid mixtures at high pressures. *J. Supercrit. Fluids* **2012**, *61*, 9–24. [CrossRef]
51. Gujar, A.; Anderson, T.; Cavagnino, D.; Patel, A. Comparative analysis of mass spectral matching for confident compound identification using the Advanced Electron Ionization source for GC-MS. *Thermoscientific* **2018**, *10598*, 1–7.
52. Zuluaga, A.M.; Mena-García, A.; Soria Monzón, A.C.; Rada-Mendoza, M.; Chito, D.M.; Ruiz-Matute, A.I.; Sanz, M.L. Microwave assisted extraction of inositols for the valorization of legume by-products. *LWT* **2020**, *133*, 109971. [CrossRef]
53. Zuluaga, A.M.; Mena-García, A.; Chito-Trujillo, D.; Rada-Mendoza, M.; Sanz, M.L.; Ruiz-Matute, A.I. Development of a microwave-assisted extraction method for the recovery of bioactive inositols from lettuce (*Lactuca sativa)* byproducts. *Electrophoresis* **2020**, *41*, 1804–1811. [CrossRef] [PubMed]
54. Mena-García, A.; Rodríguez-Sánchez, S.; Ruiz-Matute, A.I.; Sanz, M.L. Exploitation of artichoke byproducts to obtain bioactive extracts enriched in inositols and caffeoylquinic acids by Microwave Assisted Extraction. *J. Chromatogr. A* **2020**, *1613*, 460703. [CrossRef]
55. Ruiz-Aceituno, L.; García-Sarrió, M.J.; Alonso-Rodriguez, B.; Ramos, L.; Sanz, M.L. Extraction of bioactive carbohydrates from artichoke (*Cynara scolymus* L.) external bracts using microwave assisted extraction and pressurized liquid extraction. *Food Chem.* **2016**, *196*, 1156–1162. [CrossRef] [PubMed]
56. Chóez-Guaranda, I.; Ruíz-Barzola, O.; Ruales, J.; Manzano, P. Antioxidant activity optimization and GC-MS profile of aqueous extracts of *Vernonanthura patens* (Kunth) H. Rob. leaves. *Nat. Prod. Res.* **2020**, *34*, 2505–2509. [CrossRef]
57. Somsub, W.; Kongkachuichai, R.; Sungpuag, P.; Charoensiri, R. Effects of three conventional cooking methods on vitamin C, tannin, myo-inositol phosphates contents in selected Thai vegetables. *J. Food Compos. Anal.* **2008**, *21*, 187–197. [CrossRef]
58. Warren, C.R.; Aranda, I.; Cano, F.J. Responses to water stress of gas exchange and metabolites in *Eucalyptus* and *Acacia* spp. *Plant Cell Environ.* **2011**, *34*, 1609–1629. [CrossRef]
59. Croze, M.L.; Soulage, C.O. Potential role and therapeutic interests of myo-inositol in metabolic diseases. *Biochimie* **2013**, *95*, 1811–1827. [CrossRef] [PubMed]
60. Pütter, K.M.; van Deenen, N.; Müller, B.; Fuchs, L.; Vorwerk, K.; Unland, K.; Bröker, J.N.; Scherer, E.; Huber, C.; Eisenreich, W.; et al. The enzymes OSC1 and CYP716A263 produce a high variety of triterpenoids in the latex of *Taraxacum koksaghyz*. *Sci. Rep.* **2019**, *9*, 5942. [CrossRef] [PubMed]
61. Yendo, A.C.A.; De Costa, F.; Gosmann, G.; Fett-Neto, A.G. Production of plant bioactive Triterpenoid saponins: Elicitation strategies and target genes to improve yields. *Mol. Biotechnol.* **2010**, *46*, 94–104. [CrossRef]
62. Fukushima, E.O.; Seki, H.; Ohyama, K.; Ono, E.; Umemoto, N.; Mizutani, M.; Saito, K.; Muranaka, T. CYP716A Subfamily Members are Multifunctional Oxidases in Triterpenoid Biosynthesis. *Plant Cell Physiol.* **2011**, *52*, 2050–2061. [CrossRef] [PubMed]
63. Brendolise, C.; Yauk, Y.K.; Eberhard, E.D.; Wang, M.; Chagne, D.; Andre, C.; Greenwood, D.R.; Beuning, L.L. An unusual plant triterpene synthase with predominant α-amyrin—Producing activity identified by characterizing oxidosqualene cyclases from *Malus* × *domestica*. *FEBS J.* **2011**, *278*, 2485–2499. [CrossRef] [PubMed]

processes

MDPI

Article

Improvement of Enzymatic Saccharification of Cellulose-Containing Raw Materials Using *Aspergillus niger*

Ekaterina Budenkova [1], Stanislav Sukhikh [1], Svetlana Ivanova [2,3,*], Olga Babich [1], Vyacheslav Dolganyuk [1,4], Philippe Michaud [5] and Olga Kriger [1]

[1] Institute of Living Systems, Immanuel Kant Baltic Federal University, A. Nevskogo Street 14, 236016 Kaliningrad, Russia; abudenkova@kantiana.ru (E.B.); stas-asp@mail.ru (S.S.); olich.43@mail.ru (O.B.); dolganuk_vf@mail.ru (V.D.); olgakriger58@mail.ru (O.K.)
[2] Natural Nutraceutical Biotesting Laboratory, Kemerovo State University, Krasnaya Street 6, 650043 Kemerovo, Russia
[3] Department of General Mathematics and Informatics, Kemerovo State University, Krasnaya Street 6, 650043 Kemerovo, Russia
[4] Department of Bionanotechnology, Kemerovo State University, Krasnaya Street 6, 650043 Kemerovo, Russia
[5] CNRS, SIGMA Clermont, Institut Pascal, Université Clermont Auvergne, F-63000 Clermont-Ferrand, France; philippe.michaud@uca.fr
* Correspondence: pavvm2000@mail.ru; Tel.: +7-384-239-6832

Abstract: Enzymatic hydrolysis of cellulose-containing raw materials, using *Aspergillus niger*, were studied. Filter paper, secondary cellulose-containing or starch-containing raw materials, miscanthus cellulose after alkaline or acid pretreatment, and wood chip cellulose, were used as substrates. The study focused on a wild *A. niger* strain, treated, or not (control), by ultraviolet (UV) irradiations for 45, 60, or 120 min (UV45, UV60, or UV120), or by UV irradiation for 120 min followed by a chemical treatment with NaN_3 + ItBr for 30 min or 80 min (UV120 + CH30 or UV120 + CH80). A mixture of all the *A. niger* strains (MIX) was also tested. A citrate buffer, at 50 mM, wasthe most suitable for enzymatic hydrolysis. As the UV exposure time increased to 2 h, the cellulase activity of the surviving culturewas increased ($r = 0.706$; $p < 0.05$). The enzymatic activities of the obtained strains, towards miscanthus cellulose, wood chips, and filter paper, were inferior to those obtained with commercial enzymes (8.6 versus 9.1 IU), in some cases. Under stationary hydrolysis at 37 °C, pH = 4.7, the enzymatic activity of *A. niger* UV120 + CH30 was 24.9 IU. The enzymatic hydrolysis of secondary raw materials, using treated *A. niger* strains, was themost effective at 37 °C. Similarly, the most effective treatment of miscanthus cellulose and wood chips occurred at 50 °C. The maximum conversion of cellulose to glucose was observed using miscanthus cellulose (with alkaline pretreatment), and the minimum conversion was observed when using wood chips. The greatest value of cellulase activity was evidenced in the starch-containing raw materials, indicating that *A. niger* can ferment not only through cellulase activity, but also via an amylolytic one.

Keywords: cellulose-containing raw materials; enzymatic hydrolysis; *Aspergillus niger*; bioethanol; cellulase activity; ultraviolet treatment

1. Introduction

The development of efficient methods for the production of biofuels is becoming increasingly important, due to the depletion of fossil fuels and the environmental conditions that are associated with their extraction. Possessing environmental and economic advantages, bioethanol is able to compete in the global fuel market. It can be used alone or as an additive to gasoline [1].

Bioenergy production has significantly increased in the recent decades, as part of the transition to a carbon-neutral energy system, and its growth is expected to continue, particularly in the form of biofuels such as bioethanol. The global market is forecasted to increase the share of bioethanol production from the current 2% to 27% by 2050 [2].

Bioethanol production has been strongly supported by the United States and Brazil, which are the leading producing countries [3]. Several patents that are devoted to methods of converting cellulosic material into ethanol by fermentation (RU 2432368, RU 2456394, RU 2529371, and RU 2593724) and GOST R 33872-2016 [4–6], are registered in Russia. However, Russian biofuel production is only inthe pilot stage [7].

Cellulosic biomass is attractive as a source of raw materials, due to its availability and renewability [3,8–11]. The study [12] showed that microorganisms with visual differences in the morphology and growth of colonies (including bacteria, yeast, and filamentous fungi), were found in mangroves in Brazil.Metagenomic sequencing data showed the predominance of the following bacterial types: *Proteobacteria* (57.8%), *Firmicutes* (12.3%), and *Actinobacteria* (8.4%). It was found that these microorganisms produce a large number of enzymes that are involved in the degradation of polycyclic aromatic compounds. Specific sequences that are involved in cellulolytic degradation, belonging to cellulases, hemicellulases, carbohydrate-binding domains, dockerins, and cohesins, were identified. It became possible to isolate cultivated fungi and bacteria that are associated with biomass decomposition and the potential for use in biofuel production. These results showed that cellulosolytic microorganisms that are present in mangroves possess all the basic molecular tools for building the cellulosome, which is necessary for the efficient degradation of cellulosic material and the release of sugar.

To provide an economically viable process for its bioconversion into bioethanol, it is necessary to achieve effective splitting of polymeric lignocellulosic raw materials into monomeric sugars, which are further fermented by microorganisms (yeast or bacteria). The composition and concentration of sugars in the lignocellulose hydrolysate vary depending on the composition of the raw material and the processing method. Other important factors of alcoholic fermentation include the selection and preparation of the substrate, the selection and adaptation of the microorganisms, and the process conditions [1].

Enzymatic hydrolysis is conducted using the cellulase enzyme complex. Endoglucanases rapidly and randomly break down the internal cellulose sites. The products of this reaction serve as a substrate for the action of exoglucanases, which mainly release cellobiose by breaking down oligosaccharides. Enzymatic hydrolysis occurs under the synergistic action of the following three main classes of cellulases: endoglucanase, exoglucanase, and β-glucosidase [13]. The main advantages of enzymatic hydrolysis include technological accessibility, the high specificity of enzymes, and reduced generation of by-products and inhibitory products. The disadvantages include the high cost of enzyme preparations and the duration of the hydrolysis process (48–72 h). It is important to consider the concentration and structure of the substrate (reaction rate) and enzyme concentration (price/reaction rate ratio) in enzymatic hydrolysis [14].

The main constraints of the lignocellulosic biomass fermentation are the crystalline structure of cellulose and the formation of a lignin–cellulose complex. High pressure and temperature lead to the destruction of glucose and the formation of reaction by-products [3].

Fungal amylases are used to hydrolyze carbohydrates, proteins, and other components of soybeans and wheat, into peptides, amino acids, sugars, and other low-molecular-weight compounds [13,15]. The study [13] was carried out to assess the amylase activity of the amylolytic fungi *Aspergillus niger*, using cassava waste as a fodder substrate. Fungi were isolated from soil samples and identified as *Aspergillus niger*, based on lactophenol cotton blue staining and plating on an appropriate fungal growth medium. The production of *Aspergillus niger* amylase was detected by the disappearance of the blue color in the agar medium, with starch around the microbial colonies after incubation. Cassava was used as a substrate for amylase production. Solid-phase fermentation was performed using *Aspergillus niger* to obtain amylase. Amylase activity was determined by the following four methods: the DNSA method, dextrinization method, reduction in starch–iodine color intensity, and assay on plates.

Solid-phase fermentation has great potential for the amylase enzyme production by *Aspergillus niger* [16].Hard substrates that are rich in starch, such as rice bran, wheat bran, rye bran, coconut oil cake, ginger cake, and peanut cake, are used.These agro-industrial residues are cheap raw materials for amylase production.It was found that *Aspergillus niger* is the best amylase producer.The addition of carbohydrates and nitrogen increased the yield of amylase [16].

Membrane enzymatic hydrolysis, in comparison with chemical hydrolysis, has significant application potential [17,18], due to the higher yield of a low-toxic product, environmental friendliness, complete decomposition of lignocellulosic biomass [16], high degree of conversion of carbohydrates, absence of toxic waste, greater yield of the target product, and the ability to modify and cultivate microorganisms to obtain significant quantities of high-quality biofuel. Nonetheless, this method requires modernization and adaptation.

Using membranes to extract and reuse cellulase saves energy, reduces the cost of purchasing an enzyme preparation, and shortens the time that is required by the stages of enzymatic hydrolysis [14]. Membrane filtration is widely used in this process. In this case, the enzyme, while maintaining its relative catalytic activity, recirculates up to 75% of the enzyme and is reused in the process of hydrolysis [11]. The membranes are made from hollow fibers of cellulose acetate, polysulfone, nylon, and polyethersulfone.

The rigid structure of lignocellulosic biomass prevents the enzymatic hydrolysis of polysaccharides, which prevents the conversion of biomass into bioethanol [3]. The combined use of several methods in pretreatment (chemical, physical, electrical, and biological) promotes the degradation of lignocellulose, reduces the impermeability of the biomass, and facilitates the access of enzymes to their substrates; however, the processes of the pretreatment of lignocellulosic materials cause an increased formation of undesirable by-products, originating from lignin, which can inhibit the growth of microbes and, consequently, reduce the fermentation yield [19,20]. The use of microorganisms helps to avoid many of these difficulties and, in combination with the membrane methods of enzymatic purification, helps to intensify this process.

It is known [21] that *Aspergillus niger* secretes endoglucanase, exoglucanase, and β-glucosidases (EC 3.2.1.21, EC 3.2.1.4, EC 3.2.1.74), which have many biotechnological and industrial applications. It was found that the purified enzyme with a molecular weight of 116 kDa, forms monomers in the solution, according to the data of native gel electrophoresis, and has a pI value of 4.55, as found for most fungal β-glucosidases. Small-angle X-ray experiments showed that these β-glucosidases have a tadpole-like structure, with an N-terminal catalytic domain and a C-terminal fibronect in III-like domain (FnIII) linked by a long linker peptide (~100 amino acid residues) in an extended conformation. This molecular organization resembles the organization of other cellulases (such as, for example, cellobiohydrolases), which often contain a catalytic domain that is associated with a cellulose-binding module, which mediates their binding to insoluble and polymeric cellulose. The reasons why β-glucosidases from *Aspergillus niger* act on small soluble substrates and have the form of a tadpole molecule, are not entirely clear. However, assays with reduced enzymes with various polymeric substrates suggest that these β-glucosidases have little or no ability to bind and adsorb cellulose, xylan, and starch, but have a high lignin affinity. Molecular dynamics simulations have shown that clusters of residues that are located in the C-terminal domain of FnIII, strongly interact with lignin fragments. Modeling has shown that numerous arginine residues, scattered over the surface of FnIII, play an essential role in the interaction with lignin through the π-stacking of cations with lignin aromatic rings. These results indicate that the C-terminal domain of FnIII can act to immobilize the enzyme on the cell wall and prevent the unproductive binding of cellulase to lignin [21].

Aspergillus niger fungus produces a significant amount of cellulase and protease activity in its extracellular environment. The maturation rate of fungi during the takeover of large territories is unique (within three days, intensive sporulation occurs). This study

is aimed at experimentally selecting the optimal process for the enzymatic hydrolysis of cellulose-containing raw materials, using *Aspergillus niger* exposed to ultraviolet (UV) radiation and chemical treatments.

2. Materials and Methods

2.1. Microorganisms

Aspergillus niger F-1270 was acquired from the collection of microorganisms of the Federal Institution "State Research Institute of Genetics and Selection of Industrial Microorganisms of the National Research Center" Kurchatov Institute (Moscow, Russia). The recommended cultivation conditions were as follows: temperature of 26 °C, and a malt-peptone agar medium (malt extract 30 g/L, peptone 1 g/L, agar 20 g/L). The culture medium was sterilized at 121 °C for 20 min. The cultivation was carried out by the quadrant or the thinning streak methods on Petri dishes, in test tubes with a cotton and gauze plug. The passage of microscopic fungi was carried out with a bacteriological loop. In addition to the recommended medium, we used the Czapek–Dox and the Mandels–Weber mineral nutrient media to stimulate cellulolytic activity [18].

Potato agar medium (potato extract/dried and milled potato waste 4 g/L, agar–agar 15 g/L, pH 5) was used to stimulate starch-degrading activity. The media were used for modifications with/without added cellulose and with/without added glucose. Malt-peptone agar was used to disperse microorganisms.

At the stage of the exposure to mutagenic factors, these media were used with the addition of glucose at a concentration of 1 g/L. The media were sterilized by autoclaving at 121 °C for 20 min. A KH_2PO_4 solution and solution of trace elements ($FeSO_4 \cdot 7H_2O$ 5.0 mg/L, $MnSO_4 \cdot 7H_2O$ 1.6 mg/L, $ZnSO_4 \cdot 7H_2O$ 1.4 mg/L, $CoCl_2 \cdot 6H_2O$ 20 mg/L) were prepared and sterilized separately, and the combination with the stock solution was carried out after cooling solutions to room temperature.

The medium used for preparing a spore suspension and enzymatic hydrolysis contained the following (g/L): 0.3 urea, 1.4 $(NH_4)_2SO_4$, 2.0 KH_2PO_4, 0.4 $CaCl_2 \cdot 2H_2O$, 0.3 $MgSO_4 \cdot 7H_2O$, 1.0 peptone, 0.2 Tween 80, 0.005 $FeSO_4 \cdot 7H_2O$, 0.0016 $MnSO_4 \cdot 7H_2O$, 0.0014 $ZnSO_4 \cdot 7H_2O$, 0.02 $CoCl_2 \cdot 6H_2O$, 10.0 cellulose; pH 5.

As a control of cellulolytic activity, we used the "Cellulase Ultra" enzyme preparation from *Trichoderma reeseii* (Sibbiopharm, Berdsk, Russia), a widespread cellulase-producing culture [22], which can be used as a reference for studying the cellulase production of *Aspergillus niger*. This preparation hydrolyzes β-1,4-glycosidic bonds with an activity of 2500 U per 1 g of enzyme at working ranges of temperatures and pH between 30 to 65 °C and pH 2–7, respectively (optimum at 50–60 °C and pH 4.0–5.5).To prepare the stock solution of the enzyme preparation (control 3), 10 mL (with an accuracy of 0.2 μL) of the preparation was suspended in a small amount of distilled water (up to 50 cm^3) on a magnetic stirrer for 15 min. The suspension was quantitatively transferred into a volumetric flask with a capacity of 200 cm^3 and the volume was brought up to the mark with distilled water. The resulting suspension was centrifuged at 7000 rpm for 15 min. The supernatant was used for analysis.

2.2. Characterization and Pretreatment of Raw Materials

The cellulose of miscanthus (*Miscanthus sinensis Andersson*) was used as a substrate for enzymatic hydrolysis. The cellulose of alder chips was used as the primary raw material, and starch and cellulose-containing household waste (potato and bread) were used as secondary raw materials. Miscanthus cellulose is a natural polysaccharide built from anhydro-D-glucopyranose units interconnected with a β-glycosidic bond, with a degree of polymerization (the number of elementary units in a cellulose macromolecule) of 15–20 thousand. The chemical composition of cellulose obtained from miscanthus included α-cellulose 89.4%, ash content 0.34%, acid-insoluble lignin 1.45%, pentosans 9.4%; the crystallinity index was 0.6. Alder chip cellulose is a natural cellulose, high-molecular-weight linear polysaccharide, poly-1.4-β-D-glucopyranosyl-D-glucopyranose with a degree of

polymerization from 2000 to 26,000. The average degree of polymerization of alder chip cellulose is 5000–10,000. The chemical composition of cellulose obtained from miscanthus included α-cellulose 88.4%, ash content 0.04%, lignin 0.44%, pentosans 6.0%; the crystallinity index was 0.66. Cellobiose disaccharide is the main structural element that is repeated in the polysaccharide macromolecule. Cellulose-containing waste includes the following: α-cellulose 73.7–77.0%, ash content 0.03%, residual amount of lignin 3.7%, pentosans 9–16%, resins and fats 0.04%; the viscosity of cellulose solutions is 31.0 mPa·s, the crystallinity index is 0.56% [23,24].

The secondary raw materials were not additionally pretreated. Starch-containing raw materials were used to advance knowledge of the *Aspergillus niger* activity against potato starch. Filter paper (blue ribbon filter) was used to determine the cellulolytic activity of microorganisms.

The primary raw material underwent alkaline and acid delignifications. Delignification was performed under hydrolysis conditions with sodium hydroxide solution, namely, 10 g of dry biomass of miscanthus was placed in a two-neck round-bottom flask with a magnetic stirrer, reflux condenser, and thermometer. Water was added to the biomass in a ratio of 10:1, and 4 g of NaOH was added with stirring. The mixture was stirred for 4 h at 75 °C. In the case of acid hydrolysis, trifluoroacetic acid (30 mL) and a 30% hydrogen peroxide solution (20 mL) were used per 10 g of dry biomass supplemented with 50 mL of water. In addition, 2 mL of sulfuric acid (H_2SO_4) was added to the reaction mixture as a catalyst. The mixture was heated at 60 °C for an hour with constant stirring. As a result, fibers were obtained, which were separated by filtration and washed with distilled water.

2.3. MALDI-TOFMethod

The process of optimizing the delignification conditions, and the procedure for the physicochemical analysis of the reaction products, was carried out according to the technique described in [22]. For this, the MALDI-TOF method was used. The MALDI-TOF method is based on the procedure of soft ionization of the test material (analyte), which allows, in the presence of a special substance, the so-called matrix, under the influence of a laser to ionize biological macromolecules (peptides, proteins, DNA, oligonucleotides, lipopolysaccharides, and sugars) without their fragmentation and destruction. The most widely used matrix is α-cyano-4-hydroxycinnamic acid (CHCA), sinapinic acid (SA), ferulic acid (FA), and 2,5-dihydroxybenzoic acid (DHB). After the laser beam ionization, the system scans for microbial proteins, which generally fall in the range of 4000 to 20,000 Da (60 to 70% of the dry weight of the bacterial cell). After desorption, predominantly single-charged ionized molecules are accelerated in an electric field, enter the separating part of the device (a tube in the cavity of which a vacuum is maintained), after passing through which the ions reach the detector. The speed of movement and, accordingly, the time it takes to travel from the point of ionization to the detector, is inversely proportional to the mass of the ions. Knowing the path length of ion movement from the ionizer to the detector, as well as the time of this movement, it is possible to calculate the speed of ion movement and, based on its value, calculate the mass of particles present in the analyte, as well as generate a spectrum characterizing the qualitative composition of the object under study [25].

2.4. Induced Mutagenesis of Microorganisms

The studied microorganisms were consistently subjected to physical and chemical mutagenic effects to enhance their cellulolytic properties. The technique used to induce mutagenesis is described hereafter and was created based on those presented in [20,26–30] and adapted to the existing conditions.

Physical mutagenesis was carried out in the microbiological safety cabinet BMB-II-Laminar-S-1.2 (221.120) Class II (Type A2) using a Philips TUV 30W G13 ultraviolet lamp (LAMSYSTEMS, Mias, Russia) with maximum radiation at253.7 nm. A suspension based on sodium phosphate buffer (pH 7.0) at a concentration of 10^8 spores/mL was

prepared from a 5-day culture of microorganisms. A quantity of 2 mL of the resulting suspension was placed on a Petri dish with a nutrient medium. The medium contained the following (g/L): 0.3 urea, 1.4 $(NH_4)_2SO_4$, 2.0 KH_2PO_4, 0.4 $CaCl_2 \cdot 2H_2O$, 0.3 $MgSO_4 \cdot 7H_2O$, 1.0 peptone, 0.2 Tween 80, 0.005 $FeSO_4 \cdot 7H_2O$, 0.0016 $MnSO_4 \cdot 7H_2O$, 0.0014 $ZnSO_4 \cdot 7H_2O$, 0.02 $CoCl_2 \cdot 6H_2O$, 10.0 cellulose; pH 5.

Then, the cups were positioned at a distance of 10–13 cm from the UV lamp. The exposure time varied from 45 to 120 min, after which the dishes were incubated in the dark at 30 °C for three days. The spore solution was prepared as follows: A suspension was prepared from a 3-day culture of microorganisms based on sodium phosphate buffer (pH 7.0) and a concentration of 10^8 spores/mL. The resulting suspension was mixed with a solution of sodium azide/ethidium bromide in ratios of 9:1 and 1:1. The concentration of sodium azide in the solution was 5 and 400 mg/mL, ethidium bromide 5 and 150 mg/mL, respectively. After exposure for 30 and 80 min at room temperature, the spores were washed three times with sterile deionized water. The supernatant was removed after 15 min of centrifugation at 6000× *g*. Spores were resuspended in sodium phosphate buffer and transferred to plates with a nutrient medium. They were incubated for 5 days, after which the cellulolytic activity was checked and the most effective colonies were selected for subsequent studies. A spore suspension was washed with 0.05 M citrate buffer (pH = 4.8) from a plate with a 5-day culture.

Spore concentration was determined using a Hirst volumetric impaction sampler (General Electric Company plc, Borehamwood, UK). The spores fixed on the strip were examined using a light microscope. Ten fields of view were selected and the number of spores was counted on the strip segment corresponding to a 3-h log.

Chemical mutagenesis was performed as described above using the sole sodium azide and ethidium bromide treatment. Spores were resuspended in sodium phosphate buffer and transferred onto plates with a nutrient medium. Spores were incubated for 5 days, followed by a verification of cellulolytic activity and the selection of the most effective colonies for subsequent studies.

2.5. CellulolyticActivities Measurement

Cellulase activity was determined using an enzymatic assay.

The Bradford method [31] was used to obtain the protein concentration. This method is based on the shift of the absorption maximum of the optical density of the acid blue 90 (Coomassie Brilliant Blue R-250) dye from 470 to 595 nm, observed due to the binding of the protein to the dye.

The enzymatic activity of the preparation was determined in comparison with a standard sample (SS) of this enzyme under the same experimental conditions. The enzymatic activity (EA) in the appropriate units (IU or U) was calculated by the following formula [32]:

$$EA = P \cdot C \cdot A0/P0, \quad (1)$$

where *A*0—SS enzymatic activity is in units (IU or U) per 1 g of protein or preparation; *P*0—value of the measured parameter for SS; *p*—value of the measured parameter for the test preparation; *C*—coefficient equalizing the concentrations of solutions of the test preparation and SS.

Enzyme activity is expressed in international units IU (or U) and is equal to the amount of enzyme that catalyzes the conversion of 1 μM of reducing sugars (glucose equivalent) in 1 min at 50 °C.

2.6. Aspergillus Niger Growth Parameters and Determination of the Concentration of Spores in Suspension

The protocol used for the enzymatic hydrolysis is an adaptation of the hydrolysis techniques described in the literature [32,33]. Enzymatic hydrolysis was carried out in 1 and 0.25 L conical flasks with cotton and gauze plugs with a working volume of 200 and 50 mL, respectively. The flasks were closed with plastic stoppers and periodically

stirred in an IKA KS4000I control incubator shaker (DV-Ekspert, Moscow, Russia). Stirring trajectory was orbital. Torque range was from 10 to 500 rpm. The reaction was carried out under static conditions at a temperature of 30–37 °C for 3–7 days. The substrate concentration in all samples was 60 g/L. The inoculum concentration varied from 10^6 to 10^8 spores/mL. The growth curve of *A. niger* during cultivation is shown in Figure 1. The strains were grown at a temperature of 27–30 °C.

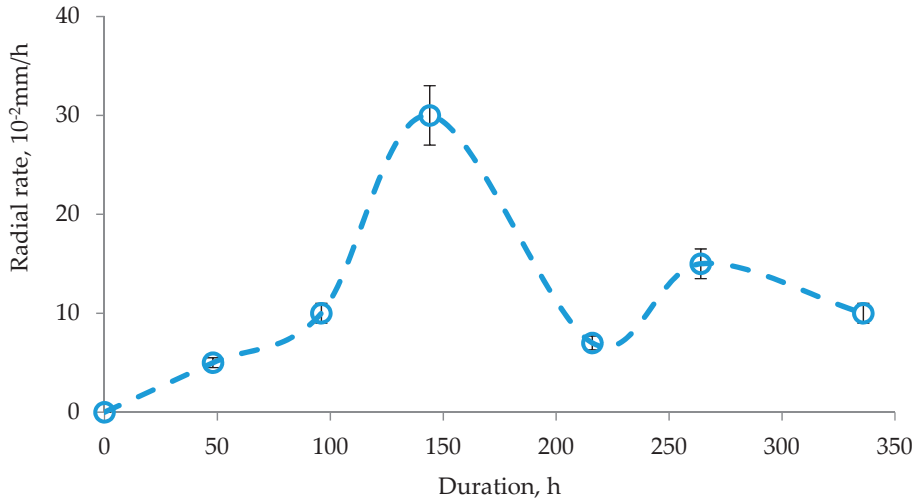

Figure 1. *A. niger* growth curve.

The concentration of the spore suspension was obtained measuring A_{600} Smart Spec Plus spectrophotometer (BioRad Laboratories Inc., Hercules, CA, USA) (r = 0.63). Enzymatic activity was interrupted by heating in an autoclave to 121 °C without standing.

2.7. Optimization of Conditions for Enzymatic Hydrolysis

Original and treated strains were cultivated under the same conditions. To optimize the parameters of enzymatic hydrolysis, the cellulase activity of treated and original strains of *Aspergillus niger* were studied at temperatures of 30, 37, and 50 °C. The enzymatic activity of original and treated microorganisms was compared at these temperatures. The influence of the composition of the nutrient medium, on which the microorganism culture (UV microorganism) was incubated, on the cellulolytic activity during hydrolysis was assessed. For this purpose, microorganisms were inoculated in malt-peptone agar, Czapek–Dox medium, Mandels–Weber saline medium, and potato agar [18]. These media were used because they are standard nutrient media for the cultivation of microorganisms (in particular, fungi), contain all the necessary nutrient components (sources of sodium, potassium, magnesium, iron, agar, peptone, sucrose, and other nutrient components), have optimal pH for the development of microorganisms. They are easy to prepare and convenient to use.

The hydrolysis duration was 1 h and 48 h. To optimize the enzymatic hydrolysis parameters, the total cellulolytic activity level of all studied strains was determined relative to the following different compositions of raw materials: filter paper, recycled cellulose-containing raw materials, secondary starch-containing raw materials (fruit waste, potato starch), miscanthus cellulose after alkaline pretreatment, miscanthus cellulose after acid pretreatment and cellulose. Small substandard fruit products affected by pests (a mixture of apricots and prunes 1:1) were used as substrates (fruit waste) for enzymatic hydrolysis. Fruits were ground using a KT-1321 laboratory grinder (Profit, Moscow, Russia). Potato starch was obtained by processing substandard, non-standard small potatoes, as described in [34].

2.8. Method for the Analysis of Hydrolysis Products

The content of reducing substance in the sample was determined using the reagent 3,5-dinitrosalicylic acid (DNS) according to the method described in GOST R 54905-2012 (Enzyme preparation. Methods of beta-glucanase enzyme activity determination), which allows determining the total amount of reducing sugars (in our studies it was glucose) [35,36]. Glucose is the most important reducing substance in hydrolyzed cellulose samples.

A solution of 1% DNS per 1 L was prepared by dissolving 10 g of DNS in a small amount of water at room temperature and the subsequent gradual addition of 16.05 g of sodium hydroxide and 300 g of potassium–sodium tartrate (in a water bath at 47 ± 1 °C, "soft" cooling that does not destroy the molecules of substances). The reagents were purchased from Pushchinskie Laboratorii (Moscow, Russia). The resulting solution had a bright yellow color. To construct a calibration graph, a stock solution of D-glucose (1 μmol/mL) and a series of its dilutions (0.3–0.6 μmol/mL) were prepared based on citrate or acetate buffer, depending on the medium in which the hydrolysis was carried out. Before analysis, the DNS solution was measured on a spectrophotometer to clarify the absorption maximum. The obtained value (530 nm) was slightly lower than that indicated in GOST (540 nm). To assess the content of the reducing substance, and to build a calibration curve, a 2 mL solution of DNS was thoroughly mixed with 1 mL of the sample and heated in a water bath for 5 min with an accuracy of a few seconds. After cooling, the sample volume was brought to 25 mL with buffer and analyzed on a Shimadzu UV-1800 spectrophotometer (Shimadzu, Kyoto, Japan) at a wavelength of 530 nm in cuvettes with a 10 mm light-absorbing layer.

2.9. Statistical Analysis Methods

Statistical processing was performed using Excel (2019, Microsoft, Redmond, Washington, USA) and IBM SPSS Statistics 22 (2013, SPSS: An IBM Company, Chicago, IL, USA). All experiments were carried out in triplicate. Data are presented as the median ± standard deviation. The Kruskal–Wallis test was used to compare the medians of the samples (significance of differences at $p < 0.05$). For intergroup comparisons, the Mann–Whitney U-test was used with the Bonferroni correction (significance of differences at $p < 0.01$). To check for the presence of a correlation between the UV exposure time and quantitative indicators of cellulolytic activity, the Spearman's rank correlation coefficient was used (significance of differences at $p < 0.05$).

3. Results

3.1. Evaluation of the Original Strain Cellulolytic Activity

The effect of the buffer on the cellulolytic activity of *A. niger* (37 °C, pH = 4.7) is shown in Table 1.

Table 1. Effect of buffer on *A. niger* cellulolytic activity (concentration of reducing substance, mg/mL).

Buffer	C_M	Control 1		Control 2	
		1 h	48 h	1 h	48 h
citrate	1	0.22 ± 0.01	0.23 ± 0.01	0.21 ± 0.03	0.78 ± 0.03
	0.1	0.22 ± 0.01	0.23 ± 0.01	0.19 ± 0.06	0.61 ± 0.09
	0.05	0.23 ± 0.01	0.23 ± 0.02	0.24 ± 0.04	0.45 ± 0.03
acetate	1	0.35 ± 0.01	0.34 ± 0.01	0.38 ± 0.02	0.37 ± 0.03
	0.1	0.35 ± 0.01	0.34 ± 0.02	0.36 ± 0.01	0.42 ± 0.02
	0.05	0.37 ± 0.03	0.47 ± 0.03	0.24 ± 0.04	0.40 ± 0.01

C_M—molar concentration; control 1—without microorganisms; control 2—with the original *A. niger* strain (the concentration of the reducing substance has been reduced). Hydrolysis substrate–filter paper (50 mg/L, according to the commercial enzyme dosage). Data are presented as median ± standard deviation ($n = 3$).

The cellulolytic activity of the original *A. niger* strain was evaluated, compared to the control without microorganisms (Table 1). The 50 mM citrate buffer was found to be more suitable for enzymatic hydrolysis with *A. niger*, and this advantage was noticeable after 48 h of hydrolysis.

The cellulolytic activity of *A. niger* (37 °C, pH = 4.7) in various substrates is shown in Table 2. In addition to reducing sugars, a protein complex was found.

Table 2. *A. niger* cellulolytic activity (concentration of the reducing substance, mg/mL) in different substrates.

Samples	Substrates					
	1	**2**	**3**	**4**	**5**	**6**
Control 1	0.24 ± 0.04	0.35 ± 0.01	0.34 ± 0.01	0.39 ± 0.01	0.34 ± 0.01	0.36 ± 0.01
Control 2	0.37 ± 0.03	0.41 ± 0.01	0.52 ± 0.01	0.75 ± 0.01	0.67 ± 0.01	0.38 ± 0.01

Control 1—without microorganisms; control 2—with the original *A. niger* strain. Hydrolysis substrates: 1—filter paper (50 mg/L, according to the commercial enzyme dosage), 2—secondary cellulose-containing raw materials, 3—secondary starch-containing raw materials, 4—miscanthus cellulose after alkaline pretreatment, 5—miscanthus cellulose after acid pretreatment, 6—wood chip cellulose. Data are presented as median ± standard deviation (n = 3).

When comparing the cellulase activity of *A. niger* with non-model substrates, it was found that the maximum conversion of cellulose into reducing sugars was observed when using miscanthus cellulose, and the minimum when using alder chips (Table 2). Reducing substances were found in insignificant amounts in control 1 (without microorganisms), since reducing sugars were included in the culture media of *A. niger*.

The MALDI-TOF method was used to study the residues of oligosaccharides and lignin in the filtrate. The cellulose yield was 87% with alkaline treatment and 95% with the acid one. The resulting substrate was sterilized by autoclaving for 20 min at 121 °C. The results of studying oligosaccharides and lignin that were extracted in the process of producing cellulose (pulp) from the miscanthus biomass, are shown in Figure 2.

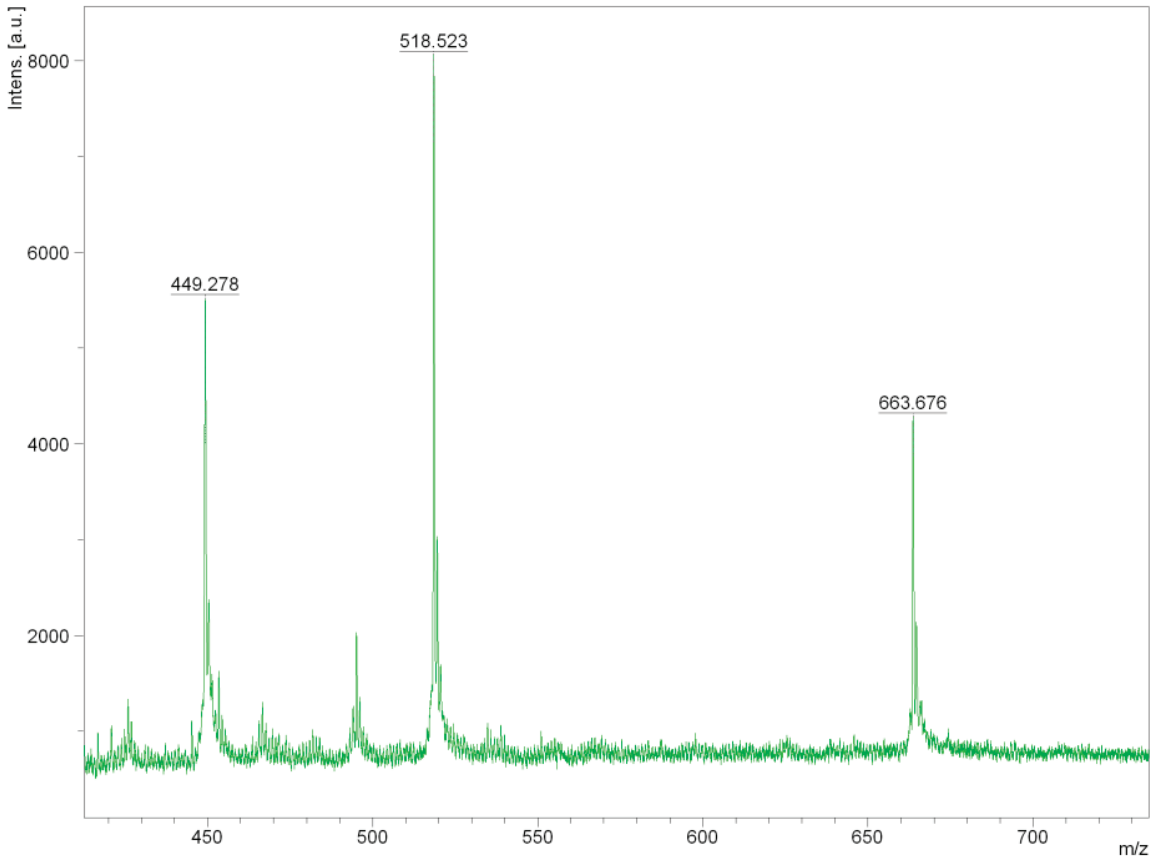

Figure 2. The study of the reaction mixture aqueous phase after delignification by MALDI-TOF spectrometry.

Next, we studied the aqueous phase of the reaction mixture after delignification by MALDI-TOF spectrometry. The analysis of the obtained MALDI-TOF mass spectrometry data resulted in a conclusion on the structure of lignin fragments extracted into an alkaline solution (Figure 3).

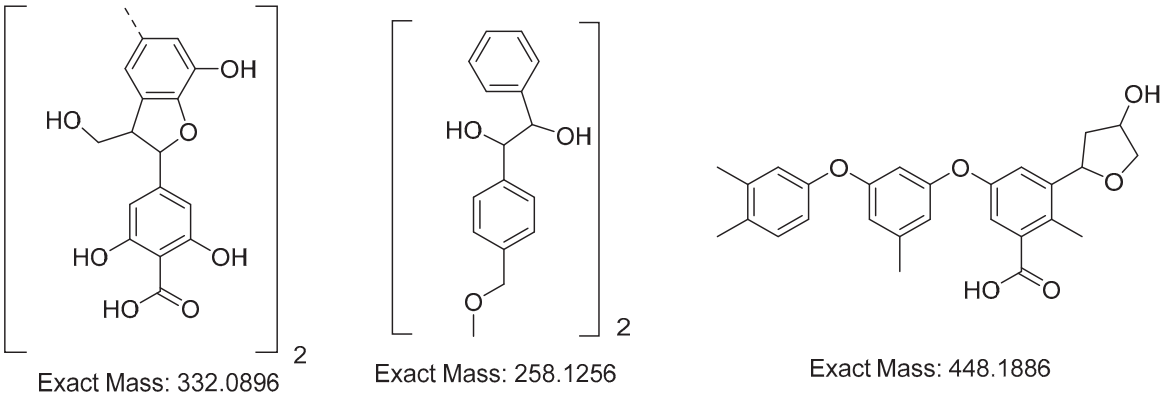

Figure 3. Structure of lignin fragments extracted during the cellulose (pulp) production from miscanthus biomass by hydrotropic delignification in the presence of sodium hydroxide.

The results of the studied oligosaccharides and lignin from the miscanthus biomass, by the method of hydrotropic delignification, presented in Figure 1, show that the signal with a mass of 663.676 *m/z* corresponds to dimeruphenylcumaronic acid, the signal with a mass of 518.523 *m/z* corresponds to the dimer 1-(4-methoxyphenyl)phenyl)-2-phenylethane-1,2-diol, and the signal with a mass of 449.278 *m/z* corresponds to a phenoxy-phenylcumaronic acid fragment.

3.2. Analysis of the Enzyme Preparation Cellulolytic Activity

In the second stage of the study, the cellulase activity of a commercial enzyme preparation was studied, in the concentration range of 0.1–10 mg/1.5 mL of citrate buffer, relative to a model cellulose substrate, i.e., filter paper (50 mg/L, according to the commercial enzyme dosage). The results are shown in Table 3. The obtained data are consistent with the dosages and units of the commercial enzyme for all types of cellulose-containing raw materials.

The enzyme preparation with a concentration of 10 mg/mL on the miscanthus cellulose substrate after alkaline pretreatment (Table 3) had the highest cellulase activity.

3.3. Cellulolytic Activity of A. niger Mutant Strains

UV radiation damages the overall microbial structure. Numerous kinds of mutations are caused by UV irradiation, as follows: base substitution (transitions and transversions) and reading frame shifts (deletions and insertions). Complex mutations also occurin DNA, when one of its sections is replaced by one of a different length and a different nucleotide composition. Mutations are formed unevenly along the DNA; therefore, chemical mutagenesis is additionally used. As a result of the induced mutagenesis of *A. niger* spores by UV irradiation and/or chemical mutagenesis, mutated strains were obtained, as shown in Figure 4.

A qualitative assessment of the cellulolytic activity of the UV-treated *A. niger* strain is shown in Figure 5.

A qualitative reaction using a Congo red solution (Figure 4) showed an increase in the cellulolytic activity of the treated *A. niger* samples, by increasing the light spot radius around the colony.

Table 3. Characterization of the cellulase activity (concentration of the reducing substance, mg/mL) of the enzyme preparation.

Enzyme Preparation Concentration, mg/mL	Substrates					
	1	**2**	**3**	**4**	**5**	**6**
			30 °C			
Control 2	0.24 ± 0.04 ^{a}	0.35 ± 0.01 ^{a}	0.34 ± 0.01 ^{a}	0.39 ± 0.01 ^{ab}	0.34 ± 0.01 ^{a}	0.38 ± 0.01 ^{a}
0.1	0.37 ± 0.01 ^{ab}	0.46 ± 0.01 ^{b}	0.61 ± 0.01 ^{b}	0.37 ± 0.01 ^{ab}	0.50 ± 0.01 ^{b}	0.39 ± 0.01 ^{a}
1	0.50 ± 0.01 ^{b}	0.52 ± 0.01 ^{b}	0.67 ± 0.01 ^{b}	0.50 ± 0.01 ^{b}	1.22 ± 0.01 ^{c}	0.73 ± 0.01 ^{b}
10	0.71 ± 0.01 ^{c}	0.70 ± 0.01 ^{c}	0.90 ± 0.01 ^{c}	0.71 ± 0.01 ^{c}	2.40 ± 0.01 ^{d}	1.27 ± 0.02 ^{c}
			37 °C			
Control 2	0.24 ± 0.04 ^{a}	0.35 ± 0.01 ^{a}	0.34 ± 0.01 ^{a}	0.39 ± 0.01 ^{a}	0.34 ± 0.01 ^{a}	0.38 ±0.01 ^{a}
0.1	0.39 ± 0.01 ^{b}	0.55 ± 0.01 ^{b}	1.00 ± 0.01 ^{b}	0.54 ± 0.01 ^{b}	0.90 ± 0.01 ^{b}	0.43 ± 0.01 ^{a}
1	1.80 ± 0.01 ^{c}	1.11 ± 0.01 ^{c}	2.13 ± 0.01 ^{c}	2.09 ± 0.01 ^{c}	2.01 ± 0.01 ^{c}	0.75 ± 0.01 ^{b}
10	1.84 ± 0.01 ^{c}	2.34 ± 0.01 ^{d}	3.06 ± 0.01 ^{d}	7.42 ± 0.03 ^{d}	3.00 ± 0.01 ^{d}	3.42 ± 0.02 ^{c}
			50 °C			
Control 2	0.24 ± 0.04 ^{a}	0.35 ± 0.01 ^{a}	0.34 ± 0.01 ^{a}	0.39 ± 0.01 ^{a}	0.34 ±0.03 ^{a}	0.38 ±0.01 ^{a}
0.1	0.48 ± 0.01 ^{b}	0.88 ± 0.01 ^{b}	0.49 ± 0.01 ^{b}	0.83 ± 0.01 ^{b}	1.03 ± 0.01 ^{b}	0.47 ± 0.01 ^{a}
1	1.71 ± 0.01 ^{c}	2.31 ± 0.01 ^{c}	2.06 ± 0.01 ^{c}	3.15 ± 0.01 ^{c}	2.08 ± 0.01 ^{c}	1.32 ± 0.01 ^{b}
10	2.19 ± 0.01 ^{d}	4.59 ± 0.02 ^{d}	2.53 ± 0.01 ^{c}	5.14 ± 0.03 ^{d}	4.23 ± 0.02 ^{d}	3.76 ± 0.01 ^{c}

Control 2—with the original *A. niger* strain. Hydrolysis substrates: 1—filter paper, 2—secondary cellulose-containing raw materials, 3—secondary starch-containing raw materials, 4—miscanthus cellulose after alkaline pretreatment, 5—miscanthus cellulose after acid pretreatment, 6—wood chip cellulose. Data are presented as median ± standard deviation ($n = 3$). Values in a column followed by the same letter a, b, c and d do not differ significantly ($p > 0.05$) as assessed by the Kruskal–Wallis test.

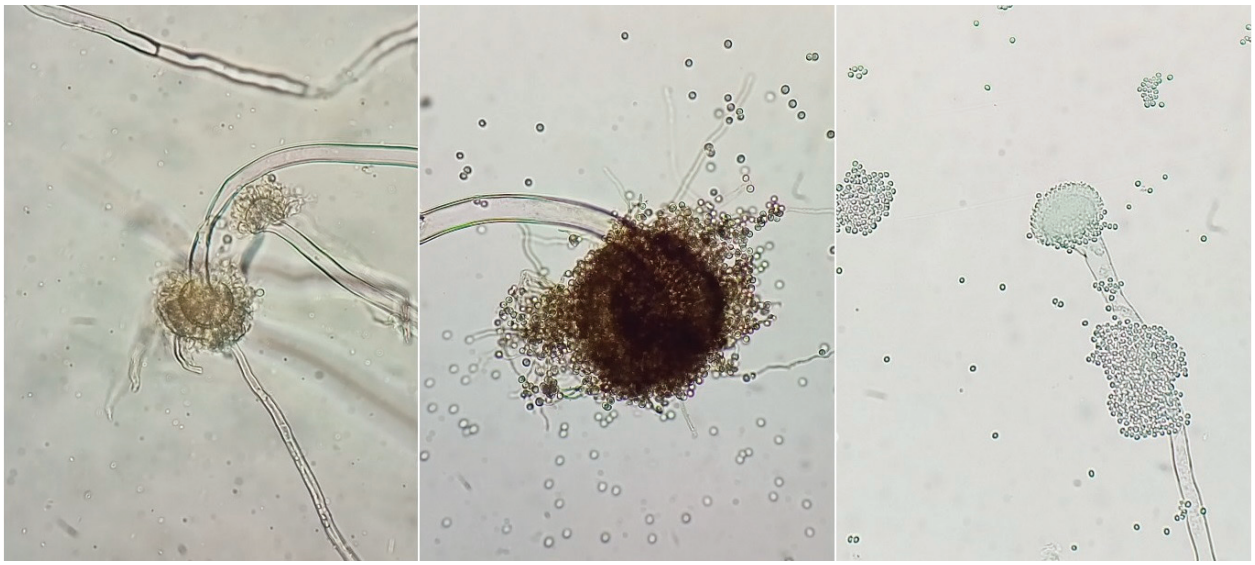

(**a**) (**b**) (**c**)

Figure 4. Morphology of *A. niger* conidiophores: (**a**)—original; (**b**)—UV-treated (2ч); (**c**)—chemically treated, (magnification 400×).

Quantitative assessment of the enzymatic activity of cellulase that was obtained using treated *A. niger*, on Mandels–Weber medium (M-W) and potato agar (PA) media, is shown in Table 4. These media were chosen because they contain the main nutrient components for the microbiological production of cellulases, which are as follows: $(NH_4)_2SO_4$, KH_2PO_4, $CaCl_2 \cdot 2H_2O$, $MgSO_4 \cdot 7H_2O$, $FeSO_4 \cdot 7H_2O$, $MnSO_4 \cdot H_2O$, $ZnSO_4 \cdot 7H_2O$, $CoC_{l2} \cdot 6H_2O$, peptone, carbohydrates, and other nutrients. When cultivated on these media, *A. niger* and reference *T. reesei* show the greatest growth [37].

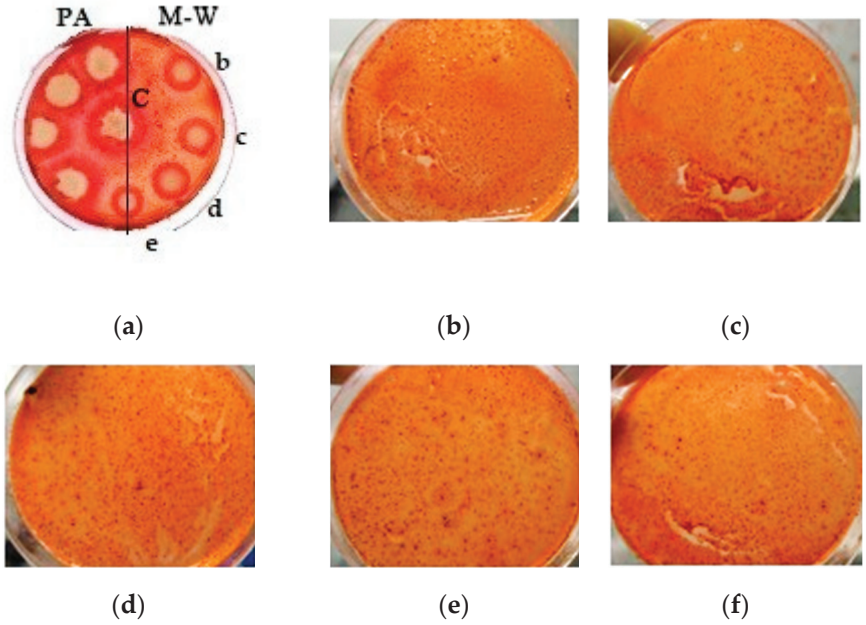

Figure 5. Qualitative assessment of the cellulolytic activity of the UV-treated *A. niger* strain: (**a**) all strains on one plate (left—mutants grown on potato agar (PA); right—grown on Mandels–Weber (M-W) medium; in the center control (C)—original strain; from top to bottom there are strains with different modes of exposure); (**b**) strain obtained by UV irradiation for 45 min; (**c**) strain obtained by UV irradiation for 1 h; (**d**) strain obtained by intermittent UV irradiation for 1 h, (**e**) a strain obtained by UV irradiation for 2 h; (**f**) strain obtained by UV irradiation for 2 h with additional exposure (NaN3 + ItBr).

Table 4. Quantitative assessment (concentration of the reducing substance, mg/mL) of the enzymatic activity cellulase obtained using treated *A. niger*.

Samples	Substrates			
	M-W		PA	
	1	2	1	3
Control 1	0.04 ±0.03 ^{a}	0.10 ±0.03 ^{a}	0.04 ± 0.01 ^{a}	0.06 ± 0.02 ^{a}
Control 2	0.23 ± 0.01 ^{b}	0.38 ± 0.03 ^{b}	0.23 ± 0.01 ^{b}	0.36 ± 0.08 ^{b}
UV45	0.64 ± 0.01 ^{c}	1.45 ± 0.05 ^{c}	0.70 ± 0.02 ^{c}	1.61 ± 0.03 ^{c}
UV60	0.69 ± 0.02 ^{c}	1.84 ± 0.01 ^{cd}	0.68 ± 0.06 ^{c}	15.63 ± 4.41 ^{d}
UV60-I	0.82 ± 0.09 ^{c}	1.46 ± 0.01 ^{c}	0.73 ± 0.02 ^{c}	1.68 ± 0.21 ^{c}
UV120	0.36 ± 0.02 ^{b}	2.41 ± 0.81 ^{d}	0.36 ± 0.02 ^{b}	16.99 ± 3.86 ^{d}
UV120 + CH30	1.78 ± 0.14 ^{d}	2.41 ± 0.01 ^{d}	1.10 ± 0.01 ^{d}	3.76 ± 0.01 ^{e}
UV120 + CH80	0.68 ± 0.01 ^{c}	2.10 ± 0.01 ^{d}	0.69 ± 0.01 ^{c}	2.05 ± 0.01 ^{be}
MIX	1.24 ± 0.01 ^{d}	6.44 ± 0.01 ^{e}	0.76 ± 0.04 ^{c}	16.04 ± 0.02 ^{d}

Control 1—without microorganisms, control 2—original *A. niger* strain, UV45—mutant *A. niger* strain obtained by UV irradiation for 45 min; UV60—mutant *A. niger* strain obtained by UV irradiation for 60 min; UV60-I—mutant *A. niger* strain obtained by interval UV irradiation for 60 min; UV120—mutant *A. niger* strain obtained by UV irradiation for 120 min; UV120 + CH30—mutant *A. niger* strain obtained by UV irradiation for 120 min followed by chemical treatment with NaN_3 + ItBr for 30 min; UV120 + CH80—mutant *A. niger* strain obtained by UV irradiation for 120 min followed by chemical treatment with NaN_3 + ItBr for 80 min; MIX—a mixture of all *A. niger* strains (original, UV, UV + CH). Hydrolysis substrates: 1—filter paper, 2—secondary cellulose-containing raw materials, 3—secondary starch-containing raw materials; M-W—Mandels–Weber medium, PA—potato agar. Data are presented as median ± standard deviation (n = 3). Values in a column followed by the same letter a, b, c, d and e do not differ significantly ($p > 0.05$) as assessed by the Kruskal–Wallis test.

Quantification of the enzymatic activity of the treated strains also showed a positive result (Table 4). The highest enzymatic activity was observed for the MIX sample on PA medium, and it was 16.04 ± 0.02 mg/mL.

3.4. Optimization of Conditions for Enzymatic Hydrolysis

The numerical values of the optimization of the temperature of enzymatic hydrolysis are shown in Table 5. The optimal growth range for *A. niger* was 27–30 °C.

Table 5. Optimization of the temperature factor during enzymatic hydrolysis.

Substrates	T, °C	Reducing Substance, mg/mL			
		Control 1	Control 2	UV120	UV120 + CH30
1	30	$0.24 \pm 0.04^{a/a}$	$0.36 \pm 0.01^{a/a}$	$0.39 \pm 0.01^{a/a}$	$0.57 \pm 0.01^{a/b}$
	37	$0.24 \pm 0.04^{a/a}$	$0.37 \pm 0.03^{a/a}$	$0.36 \pm 0.02^{a/a}$	$1.78 \pm 0.14^{b/b}$
	50	$0.24 \pm 0.05^{a/a}$	$0.36 \pm 0.06^{a/a}$	$0.55 \pm 0.07^{b/b}$	$1.16 \pm 0.05^{c/c}$
2	30	$0.35 \pm 0.01^{a/a}$	$0.41 \pm 0.01^{a/a}$	$1.56 \pm 0.01^{a/b}$	$1.92 \pm 0.01^{a/c}$
	37	$0.39 \pm 0.03^{a/a}$	$0.41 \pm 0.01^{a/a}$	$2.41 \pm 0.01^{b/b}$	$2.41 \pm 0.01^{b/b}$
	50	$0.39 \pm 0.04^{a/a}$	$0.43 \pm 0.02^{a/a}$	$2.06 \pm 0.52^{b/b}$	$2.50 \pm 0.86^{b/c}$
3	30	$0.34 \pm 0.01^{a/a}$	$0.37 \pm 0.01^{a/a}$	$10.94 \pm 0.11^{a/b}$	$2.05 \pm 0.01^{a/c}$
	37	$0.37 \pm 0.09^{a/a}$	$0.52 \pm 0.01^{a/b}$	$16.99 \pm 3.86^{b/c}$	$3.76 \pm 1.01^{b/d}$
	50	$0.63 \pm 0.02^{b/a}$	$0.66 \pm 0.01^{b/a}$	$12.34 \pm 1.37^{c/b}$	$2.78 \pm 0.52^{a/c}$
4	30	$0.39 \pm 0.01^{a/a}$	$0.39 \pm 0.01^{a/a}$	$0.87 \pm 0.01^{a/b}$	$1.05 \pm 0.01^{a/b}$
	37	$0.37 \pm 0.01^{a/a}$	$0.75 \pm 0.01^{b/b}$	$1.68 \pm 0.41^{b/c}$	$1.07 \pm 0.01^{a/b}$
	50	$0.36 \pm 0.02^{a/a}$	$1.05 \pm 0.09^{c/b}$	$4.27 \pm 0.56^{c/c}$	$1.08 \pm 0.35^{a/b}$
5	30	$0.34 \pm 0.01^{a/a}$	$0.39 \pm 0.01^{a/ab}$	$0.54 \pm 0.01^{a/b}$	$2.15 \pm 0.01^{a/c}$
	37	$0.34 \pm 0.01^{a/a}$	$0.67 \pm 0.01^{b/b}$	$0.61 \pm 0.01^{a/b}$	$4.83 \pm 0.01^{b/c}$
	50	$0.85 \pm 0.03^{b/a}$	$0.77 \pm 0.05^{b/b}$	$2.64 \pm 0.34^{b/c}$	$1.72 \pm 0.88^{c/d}$
6	30	$0.34 \pm 0.01^{a/a}$	$0.39 \pm 0.01^{a/a}$	$0.36 \pm 0.01^{a/a}$	$1.01 \pm 0.01^{a/b}$
	37	$0.36 \pm 0.01^{a/a}$	$0.38 \pm 0.01^{a/a}$	$0.38 \pm 0.01^{a/a}$	$1.31 \pm 0.01^{a/b}$
	50	$0.36 \pm 0.01^{a/a}$	$0.36 \pm 0.03^{a/a}$	$1.06 \pm 0.02^{b/b}$	$1.09 \pm 0.21^{a/b}$

Control 1—without microorganisms, control 2—original *A. niger* strain, UV120—mutant *A. niger* strain obtained by UV irradiation for 120 min; UV120 + CH30—mutant *A. niger* strain obtained by UV irradiation for 120 min followed by chemical treatment with NaN3 + ItBr for 30 min. Hydrolysis substrates: 1—filter paper, 2—secondary cellulose-containing raw materials, 3—secondary starch-containing raw materials, 4—miscanthus cellulose after alkaline pretreatment, 5—miscanthus cellulose after acid pretreatment, 6—wood chip cellulose. Data are presented as median ± standard deviation ($n = 3$). Values in a column/row followed by the same letter a, b, c and d do not differ significantly ($p > 0.05$) as assessed by the Kruskal–Wallis test.

The recommended temperature for enzymatic hydrolysis with UV120 + CH30, using filter paper, secondary starch-containing raw materials, miscanthus cellulose after acid pretreatment, and wood chip cellulose, was 37 °C (Table 5).

The amount of protein produced by *A. niger*, determined by the Bradford method, is shown in Table 6.

Table 6. The amount of protein produced by *A. niger* according to the Bradford method.

Substrates	Protein Amount, mg/mL			
	Control 2	Control 3	UV120	UV120 + CH30
1	1008 ± 20^{a}	1152 ± 30^{b}	1075 ± 20^{a}	1196 ± 30^{b}
2	1004 ± 20^{a}	1049 ± 20^{ab}	1063 ± 20^{b}	1064 ± 20^{b}
3	1022 ± 20^{a}	1109 ± 30^{a}	1250 ± 30^{b}	1150 ± 30^{ac}
4	1060 ± 20^{a}	1200 ± 30^{b}	1180 ± 30^{b}	1185 ± 30^{b}
5	1039 ± 20^{a}	1104 ± 20^{ab}	1004 ± 20^{a}	1199 ± 30^{b}
6	1007 ± 20^{a}	1109 ± 20^{b}	1004 ± 20^{a}	1083 ± 20^{ab}

Control 2—original *A. niger* strain, control 3—enzyme preparation, UV120—mutant *A. niger* strain obtained by UV irradiation for 120 min; UV120 + CH30—mutant *A. niger* strain obtained by UV irradiation for 120 min followed by chemical treatment with NaN_3 + ItBr for 30 min. Hydrolysis substrates: 1—filter paper, 2—secondary cellulose-containing raw materials, 3—secondary starch-containing raw materials, 4—miscanthus cellulose after alkaline pretreatment, 5—miscanthus cellulose after acid pretreatment, 6—wood chip cellulose. Data are presented as median ($n = 3$). Values in a row followed by the same letter a, b and c do not differ significantly ($p > 0.05$) as assessed by the Kruskal–Wallis test.

The greatest amount of proteins (Table 5) is produced by strain UV120, on a substrate containing secondary starch-containing raw materials.

According to Formula (1), the activity of the cellulolytic enzymes of *A. niger*, original and subjected to undirected mutagenesis (in addition to a commercial preparation for comparison), during hydrolysis of the considered substrates, was calculated (Table 7).

Table 7. Comparison of the enzymatic activity of microorganisms.

Substrates	T, °C	Activitiesper Unit Time, IU			
		Control 2	Control 3	UV120	UV120 + CH30
1	30	0.7 ^{a}	2.7 ^{b}	0.8 ^{a}	1.8 ^{d}
	37	0.7 ^{a}	9.1 ^{b}	0.7 ^{a}	8.6 ^{b}
	50	0.7 ^{a}	10.8 ^{b}	1.7 ^{a}	5.1 ^{d}
2	30	0.1 ^{a}	2.3 ^{b}	6.7 ^{c}	8.7 ^{cd}
	37	0.1 ^{a}	11.1 ^{b}	11.2 ^{b}	11.2 ^{b}
	50	0.2 ^{a}	24.2 ^{b}	9.3 ^{c}	11.7 ^{d}
3	30	0.2 ^{a}	2.8 ^{b}	58.9 ^{c}	9.5 ^{d}
	37	0.8 ^{a}	15.2 ^{b}	92.3 ^{c}	18.8 ^{b}
	50	0.2 ^{a}	12.1 ^{b}	65.1 ^{c}	11.9 ^{b}
4	30	0.1 ^{a}	2.3 ^{b}	2.7 ^{b}	3.7 ^{d}
	37	2.1 ^{a}	38.8 ^{b}	7.3 ^{c}	3.9 ^{d}
	50	3.8 ^{a}	26.2 ^{b}	21.7 ^{b}	4.0 ^{a}
5	30	0.3 ^{a}	11.1 ^{b}	1.1 ^{c}	10.1 ^{b}
	37	1.8 ^{a}	15.3 ^{b}	1.5 ^{a}	24.9 ^{d}
	50	0.0 ^{a}	18.7 ^{b}	9.9 ^{c}	4.8 ^{d}
6	30	0.3 ^{a}	5.2 ^{b}	0.1 ^{a}	3.7 ^{d}
	37	0.1 ^{a}	17.1 ^{b}	0.1 ^{a}	5.3 ^{d}
	50	0.0 ^{a}	24.2 ^{b}	3.9 ^{c}	4.1 ^{cd}

Control 2—original *A. niger* strain, control 3—enzyme preparation, UV120—mutant *A. niger* strain obtained by UV irradiation for 120 min; UV120 + CH30—mutant *A. niger* strain obtained by UV irradiation for 120 min followed by chemical treatment with NaN_3 + ItBr for 30 min. Hydrolysis substrates: 1—filter paper, 2—secondary cellulose-containing raw materials, 3—secondary starch-containing raw materials, 4—miscanthus cellulose after alkaline pretreatment, 5—miscanthus cellulose after acid pretreatment, 6—wood chip cellulose. Data are presented as median (n = 3). Values in a row followed by the same letter a, b, c and d do not differ significantly ($p > 0.05$) as assessed by the Kruskal–Wallis test.

The most active strain was UV120 when secondary starch-containing raw materials were used as a substrate (Table 7).

The Kruskal–Wallis test showed statistically significant differences ($p < 0.05$) when comparing the cellulolytic activity of four groups (control 2, control 3, UV120, strain UV120 + CH30), relative to the substrates 1, 2, 3, 4, and 5, under all three temperatures (30, 37, and 50 °C). When using the substrate six, significant differences between the groups were found at temperatures of 30 and 37 °C. In all the cases, differences were found with a 1 h hydrolysis. The influence of the composition of the nutrient medium on which the culture of the microorganism (UV) was incubated, on the cellulolytic activity during hydrolysis, was assessed (Figure 6a). To assess the contribution of the pH level during the hydrolysis process, a substrate was used that showed the highest sensitivity to the action of cellulases of the studied microorganism. The UV-treated strain (UV120) was used as an enzyme source, as the most effective one (Figure 6b).

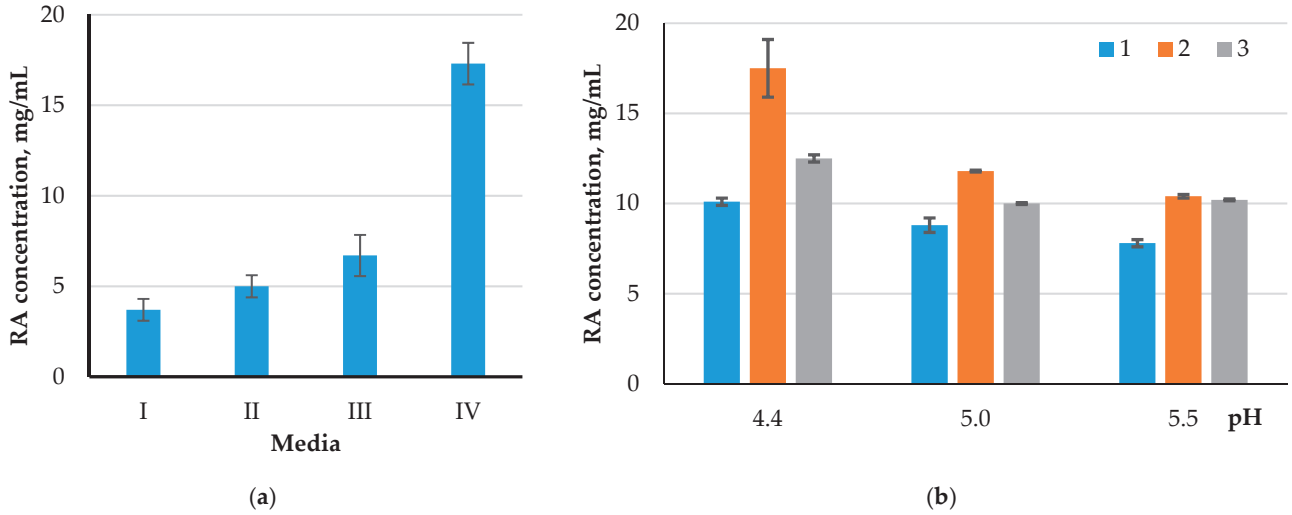

Figure 6. Comparison of the enzymatic activity of UV120 strain when cultivated on different nutrient media (**a**) and different pH values of the medium during hydrolysis (**b**): I—MPA, II—C-D, III—M-W, IV—PA; 1—30 °C, 2—37 °C, 3—50 °C.

To summarize the data, a comparative histogram is presented, which clearly shows the level of total cellulolytic activity of all the studied strains relative to different types of substrate (Figure 7).

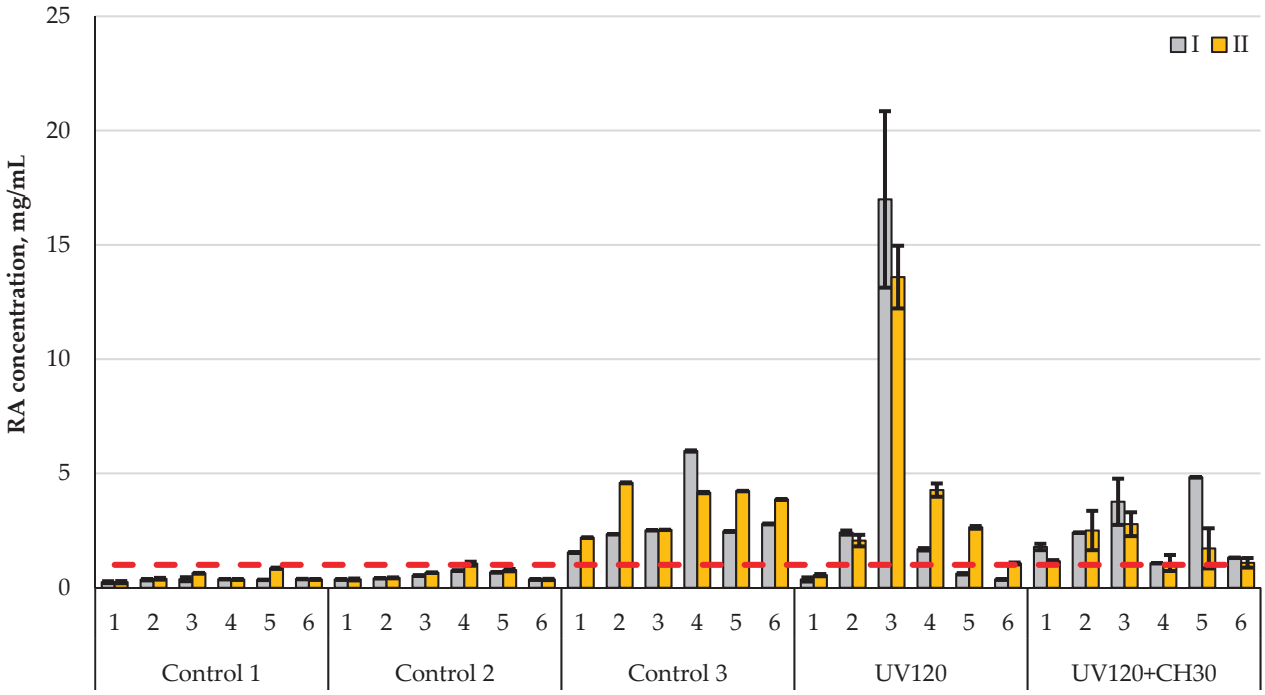

Figure 7. Comparison of cellulolytic activity of original (control 2) and treated *A. niger* (UV120 and UV120 + CH30) with a commercial enzyme preparation (control 3) at the following different process temperatures: I—37 °C; II—50 °C. Control 1—without microorganisms, control 2—original *A. niger* strain, control 3—enzyme preparation, UV120—mutant *A. niger* strain obtained by UV irradiation for 120 min; UV120 + CH30—mutant *A. niger* strain obtained by UV irradiation for 120 min followed by chemical treatment with NaN_3 + ItBr for 30 min. Hydrolysis substrates: 1—filter paper, 2—secondary cellulose-containing raw materials, 3—secondary starch-containing raw materials, 4—miscanthus cellulose after alkaline pretreatment, 5—miscanthus cellulose after acid pretreatment, 6—wood chip cellulose. The red dotted line is the maximum level of enzymatic activity of the original *A. niger* strain. Data are presented as median ± standard deviation (n = 3).

The greatest reducing substanceis evidenced in starch-containing raw materials, which indicates that *A. niger* can ferment not only through cellulase activity, but also via amylolytic activity [16].

4. Discussion

In the first stage of this study, the cellulolytic activity of the original *A. niger* strain was assessed in relation to six insoluble substrates, one of which being the model (filter paper). It was found that citrate buffer, with a concentration of 50 mM, was more suitable for enzymatic hydrolysis, and the advantage was noticeable after 48 h of hydrolysis (Table 1). The hydrolysis conditions were as follows: stationary, 30 °C, and pH = 4.7. The recommended substrate (filter paper) concentration for hydrolysis is 50 mg/L. With a further increase in the concentration of the substrate, the formation of the reducing substance decreased. The relatively low degree of hydrolysis (Table 1) is explained by the endothermicity of this process. The degree of hydrolysis increased concomitantly with the increasein temperature, and the equilibrium shiftedtowards the hydrolysis products formation, as confirmed by the data in Table 3.

When using acetate buffer as a medium for the hydrolysis process, the yield of the reducing substance was slightly higher in comparison with that of the citrate buffer. However, when a suspension of microorganisms was added to the acetate buffer, the yield of the reducing substance dropped. It is likely that the acetate buffer inhibited the functioning of the microorganisms. In addition, it was noted [32] that the acetate buffer is able to suppress the enzymatic activity of microorganisms, which can adversely affect further use of the hydrolysate under alcoholic fermentation.

When comparing the cellulase activity of *A. niger* with non-model substrates (Table 2), it was found that the maximum conversion of cellulose into reducing sugars was observed when using miscanthus cellulose (with alkaline pretreatment), and the minimum one was observed using wood chips. The hydrolysis conditions were as follows: stationary, 37 °C, and pH = 4.7.

As a result of the first stage, it was revealed that the studied original strain exhibited stable, but low, cellulase activity. Our results agree with the data that are available in the literature. Thus, in foreign studies in this area, it is customary to use either directed genetically treated microorganisms or commercial enzyme preparations. In Russian studies, it is customary to use commercial enzyme preparations. Within the framework of this study, a decision was made to activate cellulase activity by physicochemical action, and also to optimize the enzymatic hydrolysis. The expected results were obtained, which confirms the adequacy of the functioning of a commercial enzyme preparation; an increase in cellulolytic activity, with an increase in the dose of the preparation, and with an increase in the temperature of the hydrolysis. Our results allow for the correlation of the level of enzymatic activity in the studied microorganisms, with cultivation conditions. The hydrolysis conditions were as follows: stationary, 37 °C, and pH = 4.7. The filter paper was hydrolyzed according to a commercial enzyme dosage of 50 mg/L. The obtained data are consistent with the dosages and units of the commercial enzyme for all types of cellulose-containing raw materials.

A qualitative reaction, using a Congo red solution (Figure 3), showed an increase in the cellulolytic activity of the treated *A. niger* samples, by increasing the radius of the light spot around the colony (the dye reacts with glucose obtained from the cleavage of cellulose contained in the medium). A variant of the medium without the addition of simple carbohydrates was used for verification purposes.

A quantitative assessment of the enzymatic activity of the mutant strains also showed a positive result (Table 4). The obtained data are consistent with the dosages and units of the commercial enzyme for all types of cellulose-containing raw materials.

After mutagenic action, the spore suspension was separated and partly cultivated on a nutrient medium containing cellulose, and partly on a medium containing potato waste. The total cellulase activity of the first passage was maximal in the cultures that

were exposed to UV treatment for two hours; as the UV exposure time increased to two hours, the cellulase activity of the surviving part of the culture increased ($r = 0.706$; $p < 0.05$).

The studied temperature range was limited from 30 to 50 °C. With respect to secondary raw materials, enzymatic hydrolysis using treated strains was more efficient at 37 °C, whereas miscanthus cellulose and wood chips were more efficiently hydrolyzed at 50 °C. The obtained data are consistent with the literature [26,34,38–44]. In these studies, the highest enzymatic activity of the relative secondary raw materials was found in the UV strain (92.3 IU/h or 1.5 IU/min).

Comparatively, similar data were obtained in [26], in which the cellulase activity of *A. niger* during the hydrolysis of fruit wastes was 64.5 IU. Zao et al. [43] showed an increase in enzymatic activity with the combined use of recombinant *A. niger* and *T. reesei,* up to 12 IU. In a study by Abdullah et al. [44], the cellulase activity of UV-treated *Bacillus* sp. increased to 11 IU compared to the control (7.5 IU).

The enzymatic activity of the strains that were obtained in this work, relative to the primary raw material (miscanthus cellulose and wood chips), and filter paper in some cases, was inferior to that of the commercial enzyme preparation (8.6 versus 9.1 IU in the hydrolysis of filter paper, for example). However, it was possible to increase the total cellulase activity in the case of joint use.

During the fermentation of miscanthus cellulose (Table 8) in an acidic medium, *A. niger* UV120 + CH30, obtained by us, exhibited a greater enzymatic activity than the microorganisms that have been presented in other studies [43,44]. However, during the hydrolysis of fruit waste and wood chips, it was possible to achieve a greater enzymatic activity of *A. niger*.

Table 8. Cellulose fermentation indicators.

Hydrolysis Temperature, °C	Hydrolysis pH	Microorganisms	Secondary Raw Materials	Enzymatic Activities, IU	Sources
37	4.7	*A. niger* UV120 + CH30	Miscanthus cellulose	24.9	Our results
40	4.0	*A. niger*	Fruit waste	64.5	[26]
40	5.1	*A. niger* and *T. reesei*	Miscanthus cellulose	12.0	[43]
35	4.8	*Bacillus* sp.	Miscanthus cellulose	11.0	[44]
50	4.7	*A. niger*	Wood chips	92.3	[34,38–44]

The results of the enzymatic activity of the samples vary significantly (Table 8). However, they prove the possibility of obtaining an enzyme that breaks down cellulose of various origins, and the very fact of this enzymatic cleavage. The variation in the parameters is explained by the difference in the microorganisms producing the enzyme, and the conditions of enzymatic hydrolysis (different temperature, time, pH of the process) [26,34,38–44].

The results of the study favor the use of the PA and M-W media, in addition to a more acidic medium (pH = 4.4). A higher enzymatic activity of cellulases inthe mutated *A. niger*, compared to the original strain, was shown. When using the *A. niger* UV strain, the highest yield of the reducing substance was observed when using secondary starch-containing raw materials, at both 37 and 50 °C. It is more expedient to carry out enzymatic hydrolysis of the wood chips and cellulose of miscanthus using a UV strain at a temperature of 50 °C.

In this case, miscanthus cellulose after alkaline pretreatment was more exposed to degradation. The CH strain exhibited a cellulolytic activity with less deviation from the mean relative to the type of substrate used. The activity of this strain was not statistically significant relative to the hydrolysis temperature, except for the case in which the substrate was miscanthus cellulose after acid pretreatment.

The model substrate (filter paper) and wood chips were the least susceptible to enzymatic degradation under the influence of the cellulolytic complex, by both UV and CH strains of *A. niger*.

5. Conclusions

A number of stages were undertaken in this research, as follows: the pretreatment of various cellulose-containing raw materials was carried out, the cellulolytic activity of microorganisms was studied, physicochemical undirected mutagenesis of microorganisms was conducted to intensify the enzymatic activity, and the optimal conditions for the enzymatic hydrolysis of filter paper, secondary cellulose-containing raw materials, secondary starch-containing raw materials, miscanthus cellulose after alkaline pretreatment, miscanthus cellulose after acid pretreatment, and wood chip cellulose, were selected. As a result, the treated strains of *Aspergillus niger*, with an increased ability to break down cellulose and starch, were obtained. The analysis of the hydrolysis parameters was carried out to identify the recommended conditions, as follows: hydromodule 1:20, temperature 37 °C. To obtain a higher yield of RA for the cultivation of microorganisms, a Mandels–Weber salt medium should be used for the further hydrolysis of the cellulose-containing substrate, and a PA medium for the hydrolysis of starch-containing raw materials. A quantity of 0.05 M citrate buffer with pH 4.4 is more suitable as a medium for enzymatic hydrolysis.

Our future research will focus on the intensification of the process of enzymatic hydrolysate production for subsequent alcoholic fermentation. However, there are numerous potential applications of fermented cellulose. Some studies [45,46] showed that fermented celluloses are a vivid example of natural sources of innovative technologies for use in materials science and biotechnology. A variation in the applications exists for nanocellulose (from mass-produced industrial goods to high-quality medical products).

Research teams are actively working to globally expand the range of nanocellulose products, and find entirely new areas of application [8,46–48]. It has been established that microbial cellulose is an extremely versatile biomaterial that can be used in a wide variety of applied scientific purposes, such as paper products, electronics, acoustics, and biomedical devices. Biomedical devices have recently received a large amount of attention due to an increased interest in tissue products for wound care, and the regeneration of damaged or diseased organs. Due to its unique nanostructure and properties, microbial cellulose is a natural candidate for numerous applications in medicine and tissue engineering. The microbial cellulose membrane can be successfully used as a wound-healing device for severely damaged skin, and for replacing small-diameter blood vessels. Microbial cellulose microfibril nonwoven ribbons strongly resemble the structure of native extracellular matrices, suggesting that they can function as a scaffold for the production of many tissue-engineered structures. In addition, microbial cellulose membranes with a unique nanostructure have many other uses in wound healing and regenerative medicine, for example, in guided tissue regeneration, the treatment of periodontitis, or as a replacement for the dura mater (the membrane that surrounds brain tissue). Microbial cellulose can function as a scaffold for the regeneration of a wide variety of tissues, showing that it could ultimately become an excellent technological platform for medicine.

Author Contributions: Conceiving and designing the research—O.B. and O.K.; analyzing and interpreting the data—S.S., S.I. and V.D.; contributing reagents, materials, analysis tools or data—E.B. and V.D.; writing review and editing—V.D., S.I., P.M., O.B. and O.K. All authors have read and agreed to the published version of the manuscript.

Funding: This research was funded by the RUSSIAN FOUNDATION FOR BASIC RESEARCH, grant number 19-416-390001.

Institutional Review Board Statement: Not applicable.

Informed Consent Statement: Not applicable.

Data Availability Statement: Data are contained within the article.

Conflicts of Interest: The authors declare no conflict of interest.

References

1. Djelal, H.; Chniti, S. Identification of strain isolated from dates (*Phœnix dactylifera* L.) for enhancing very high gravity ethanol production. *ESPR* **2017**, *24*, 9886–9894. [CrossRef] [PubMed]
2. Neelakandan, T.; Usharani, G. Optimisation and production of bioethanol from Cashew apple juice using yeast cells by Saccharomyces cerevisiae. *AEJSR* **2009**, *4*, 85–88.
3. Verardi, A.; Lopresto, C.G. Bioconversion of lignocellulosic biomass to bioethanol and biobutanol. In *Lignocellulosic Biomass to Liquid Biofuels*; Yousuf, A., Sannino, F., Eds.; Academic Press, Elsevier Ltd.: Cambridge, UK, 2020; pp. 67–125.
4. Pavlov, I.N.; Denisova, M.N.; Makarova, E.I.; Budaeva, V.V.; Sakovich, G.V. Versatile thermobaric setup and production of hydrotropic cellulose therein. *Cellul. Chem. Technol.* **2015**, *49*, 847–852.
5. Siqueira, J.G.W.; Rodrigues, C. Current advances in on-site cellulase production and application on lignocellulosic biomass conversion to biofuels: A review. *Biomass Bioenergy* **2020**, *132*, 105419. [CrossRef]
6. Zucaro, A.; Fiorentino, G. Constraints, impacts and benefits of lignocellulose conversion pathways to liquid biofuels and biochemical. In *Lignocellulosic Biomass to Liquid Biofuels*; Yousuf, A., Sannino, F., Eds.; Academic Press, Elsevier Ltd.: Cambridge, UK, 2020; pp. 249–282.
7. Santos, F.; Eichler, P. Production of second-generation ethanol from sugarcane. In *Sugarcane Biorefinery, Technology and Perspectives*, 1st ed.; Santos, F., Rabelo, S.C., Eds.; Academic Press, Elsevier Ltd.: Cambridge, UK, 2020; pp. 195–228.
8. Klemm, D.; Heublein, B.; Fink, H.-P.; Bohn, A. Cellulose: Fascinating biopolymer and sustainable raw material. *J. Ger. Chem. Soc.* **2005**, *44*, 3358–3393.
9. Sanchez, O.J.; Cardona, C.A. Trends in biotechnological production of fuel ethanol from different feedstocks. *Bioresour. Technol.* **2008**, *99*, 5270–5295. [CrossRef] [PubMed]
10. Sharma, P.R.; Joshi, R.; Sharma, S.K.; Hsiao, B.S. A simple approach to prepare carboxycellulose nanofibers from untreated biomass. *Biomacromolecules* **2017**, *18*, 2333–2342. [CrossRef]
11. Hafid, H.S.; Rahman, N.A.A. Feasibility of using kitchen waste as future substrate for bioethanol production: A review. *Renew. Sustain. Energy Rev.* **2017**, *74*, 671–686. [CrossRef]
12. Thompson, C.E.; Beys-da-Silva, W.O.; Santi, L.; Berger, M.; Vainstein, M.H.; Guimarães, J.A.; Vasconcelos, A.T.R. A potential source for cellulolytic enzyme discovery and environmental aspects revealed through metagenomics of Brazilian mangroves. *AMB Expr.* **2013**, *3*, 65. [CrossRef]
13. Sakthi, S.S.; Kanchana, D.; Saranraj, P.; Usharani, G. Evaluation of amylase activity of the amylolytic fungi Aspergillus niger using Cassava as substrate. *Int. J. Appl. Microbiol. Sci.* **2012**, *1*, 24–34.
14. Soares, J.F.; Confortin, T.C. Dark fermentative biohydrogen production from lignocellulosic biomass: Technological challenges and future prospects. *Renew. Sustain Energy Rev.* **2020**, *117*, 109484. [CrossRef]
15. Bellaouchi, R.; Abouloifa, H.; Rokni, Y.; Hasnaoui, A.; Ghabbour, N.; Hakkou, A.; Bechchari, A.; Asehraou, A. Characterization and optimization of extracellular enzymes production by Aspergillus niger strains isolated from date by-products. *JGEB* **2021**, *19*, 50. [CrossRef]
16. Ramasamy, S.; Benazir, J.F.; Ramalingam, S.; Kumar, R.; Hari, A.; Raman, N.; Nidhiya, K.A.; Kavitha, G.; Lakshmi, R. Amylase production by Aspergillus Niger under solid state fermentation using agroindustrial wastes. *IJEST* **2011**, *3*, 1756–1763.
17. Kriger, O.; Budenkova, E. The process of producing bioethanol from delignified cellulose isolated from plants of the Miscanthus genus. *Bioengineering* **2020**, *7*, 61. [CrossRef] [PubMed]
18. Cyrus, E.T.; Juwon, A.D. effects of radiation and chemical mutagenesis on expression of aflatoxigenic traits in Aspergillus parasiticus SMS08-C. *Res. J. Microbiol.* **2015**, *10*, 205. [CrossRef]
19. Janusz, G.; Pawlik, A.; Sulej, J.; Burek, U.Ś.; Wilkołazka, A.J.; Paszczyński, A. Lignin degradation: Microorganisms, enzymes involved, genomes analysis and evolution. *FEMS Microbiol. Rev.* **2017**, *41*, 941–962. [CrossRef]
20. Javed, U.; Aman, A. Utilization of corncob xylan as a sole carbon source for the biosynthesis of endo-1, 4-β xylanase from Aspergillus niger KIBGE-IB36. *Bioresour. Bioprocess.* **2017**, *4*, 1–7. [CrossRef]
21. Lima, M.A.; Oliveira-Neto, M.; Kadowaki, M.A.; Rosseto, F.R.; Prates, E.T.; Squina, F.M.; Leme, A.F.; Skaf, M.S.; Polikarpov, I. Aspergillus niger β-glucosidase has a cellulase-like tadpole molecular shape: Insights into glycoside hydrolase family 3 (GH3) β-glucosidase structure and function. *J. Biol. Chem.* **2013**, *288*, 32991–33005.
22. Reddy, G.P.K.; Narasimha, G. Cellulase production by Aspergillus niger on different natural lignocellulosic substrates. *Int. J. Curr. Microbiol. Appl. Sci.* **2015**, *4*, 835–845.
23. Bušić, A.; Marđetko, N.; Kundas, S.; Morzak, G.; Belskaya, H.; Ivančić Šantek, M.; Komes, D.; Novak, S.; Šantek, B. Bioethanol production from renewable raw materials and its separation and purification: A review. *Food Technol. Biotechnol.* **2018**, *56*, 289–311. [CrossRef] [PubMed]
24. Choudhury, A.R.K. Easy-care finishing. In *Textiles, Principles of Textile Finishing*; Choudhury, A.K.R., Ed.; Woodhead Publishing, Elsevier Ltd.: Cambridge, UK, 2017; pp. 245–284. [CrossRef]

25. Il'ina, A.; Kulikova, O.; Maltsev, D.; Krasnov, M.; Rybakova, E.; Skripnikova, V.; Kuznetsova, E.; Buriak, A.; Iamskova, V.; Iamskov, I. MALDI-TOF mass spectrometric identification of novel intercellular space peptides. *Appl. Biochem. Microbiol.* **2011**, *47*, 118–122. [CrossRef]
26. Kumar, A.K.; Parikh, B.S. Use of combined UV and chemical mutagenesis treatment of Aspergillus terreus D34 for hyper-production of cellulose-degrading enzymes and enzymatic hydrolysis of mild-alkali pretreated rice straw. *Bioresour. Bioprocess.* **2015**, *2*, 35. [CrossRef]
27. Meena, S.S.; Vinay, S. In vitro optimisation of fungal cellulase production from fruit waste for handmade paper industries. *Biotechnology* **2018**, *17*, 35–43. [CrossRef]
28. Chandra, M.S.; Viswanath, B. Cellulolytic enzymes on lignocellulosic substrates in solid-state fermentation by *Aspergillus niger*. *Indian J. Microbiol.* **2007**, *47*, 323–328. [CrossRef]
29. Edor, S.P.; Edogbanya, O.P. Cellulase activity of Aspergillus niger in the biodegradation of rice husk. *MOJBM* **2018**, *3*, 49–51. [CrossRef]
30. Zapata, Y.; Galviz-Quezada, A. Cellulases production on paper and sawdust using native Trichoderma asperellum. *Univ. Sci.* **2018**, *23*, 419–436. [CrossRef]
31. Mæhre, H.K.; Dalheim, L.; Edvinsen, G.; Elvevoll, E.O.; Jensen, I.-J. Protein determination—method matters. *Foods* **2018**, *7*, 5. [CrossRef] [PubMed]
32. Brummer, V.; Jurena, T. Enzymatic hydrolysis of pretreated waste paper–Source of raw material for production of liquid biofuels. *Bioresour. Technol.* **2014**, *152*, 543–547. [CrossRef]
33. Zhao, C.; Deng, L. Mixed culture of recombinant Trichoderma reesei and Aspergillus niger for cellulase production to increase the cellulose degrading capability. *Biomass Bioenergy* **2018**, *112*, 93–98. [CrossRef]
34. Omojasola, F.P.; Jilani, O.P. Cellulase production by Trichoderma longi, Aspergillus niger and Saccharomyces cerevisae cultured on waste materials from orange. *Pak. J. Biol. Sci.* **2008**, *11*, 2382–2388. [CrossRef]
35. Eleazu, C.H.; Eleazu, K.; Amarachi, I. In vitro starch digestibility, α-amylase and α-glucosidase inhibitory capacities of raw and processed forms of three varieties of Livingstone potato (Plectranthus esculentus). *Innov. Food Sci. Emerg. Technol.* **2016**, *37*, 37–43. [CrossRef]
36. Hernández-López, A.; Félix, D.A.S.; Sierra, Z.Z.; Bravo, I.G.; Dinkova, T.D.; Avila-Alejandre, A.X. Quantification of reducing sugars based on the qualitative technique of Benedict. *ACS Omega* **2020**, *5*, 32403–32410. [CrossRef] [PubMed]
37. Oberoi, H.; Dhillon, G.; Bansal, S. production of cellulases through solid state fermentation using kinnow pulp as a major substrate. *Food Bioproc. Tech.* **2010**, *3*, 528–536. [CrossRef]
38. Chandra, R.; Raj, A.; Purohit, H.J.; Kapley, A. Characterisation and optimisation of three potential aerobic bacterial strains for kraft lignin degradation from pulp paper waste. *Chemosphere* **2007**, *67*, 839–846. [CrossRef] [PubMed]
39. Sudhakar Reddy, C.; Alekhya, V.V.L.; Saranya, K.; Kakkara, A.; Jha, C.; Diwakar, P.; Dadhwal, V. Monitoring of fire incidences in vegetation types and Protected Areas of India: Implications on carbon emissions. *J. Earth Syst. Sci.* **2017**, *126*, 11. [CrossRef]
40. Kumar, V.; Hart, A.J.; Wimalasena, T.T.; Tucker, G.A.; Greetham, D. Expression of RCK2 MAPKAP (MAPK-activated protein kinase) rescues yeast cells sensitivity to osmotic stress. *Microb. Cell Fact.* **2015**, *14*, 85. [CrossRef] [PubMed]
41. Zapata, L.; Pich, O.; Serrano, L.; Kondrashov, F.A.; Ossowski, S.; Schaefer, M.H. Negative selection in tumor genome evolution acts on essential cellular functions and the immunopeptidome. *Genome Biol.* **2018**, *19*, 67. [CrossRef] [PubMed]
42. Abdullah, A.; Hamid, H.; Christwardana, M.; Hadiyanto, H. Optimization of cellulase production by Aspergillus niger ITBCC L74 with Bagasse as Substrate using Response Surface Methodology. *J. Biosci.* **2018**, *25*, 115–125.
43. Zhao, X.; Wei, C.-M.; Yang, L.; Chou, M. Reply. Physical review letters. *Phys. Rev. Lett.* **2005**, *94*, 219702. [CrossRef]
44. Abdullah, N.H.; Shamsuddin, A.; Wahab, E.; Aziati, A. The relationship between organizational culture and product innovativeness. *Procedia-Soc. Behav. Sci.* **2014**, *129*, 140–147. [CrossRef]
45. Klemm, D.; Cranston, E.D.; Fischer, D.; Gama, M.; Kedzior, S.A.; Kralisch, D.; Kramer, F.; Kondo, T.; Lindström, T.; Nietzsche, S.; et al. Nanocellulose as a natural source for groundbreaking applications in materials science: Today's state (Review). *Mater. Today* **2018**, *21*, 720–748. [CrossRef]
46. Sharma, P.R.; Sharma, S.K.; Antoine, R.; Hsiao, B.S. Efficient removal of arsenic using zinc oxide nanocrystal-decorated regenerated microfibrillated cellulose scaffolds. *ACS Sustain. Chem. Eng.* **2019**, *7*, 6140–6151. [CrossRef]
47. Velusamy, S.; Sakthivel, S.; Sangwai, J.S. Effect of imidazolium-based ionic liquids on the interfacial tension of the alkane–water system and its influence on the wettability alteration of quartz under saline conditions through contact angle measurements. *Ind. Eng. Chem. Res.* **2017**, *56*, 13521–13534. [CrossRef]
48. Geng, L.; Peng, X.; Zhan, C.; Naderi, A.; Sharma, P.R.; Mao, Y.; Hsiao, B.S. Structure characterization of cellulose nanofiber hydrogel as functions of concentration and ionic strength. *Cellulose* **2017**, *24*, 5417–5429. [CrossRef]

processes

MDPI

Article

The Influence of Solvent and Extraction Time on Yield and Chemical Selectivity of Cuticular Waxes from *Quercus suber* Leaves

Rita Simões, Isabel Miranda * and Helena Pereira

Centro de Estudos Florestais (CEF), Associate Laboratory TERRA, Instituto Superior de Agronomia, Universidade de Lisboa, Tapada da Ajuda, 1349-017 Lisbon, Portugal
* Correspondence: imiranda@isa.ulisboa.pt

Abstract: The cuticular lipid compounds, usually named cuticular waxes, present in the cuticular layering of *Quercus suber* adult leaves were extracted with solvents of different polarities (n-hexane, dichloromethane and acetone) and analysed by GC–MS. *Q. suber* leaves have a substantial cuticular wax layer (2.8% of leaf mass and 239 μg/cm^2), composed predominantly by terpenes (43–63% of all compounds), followed by aliphatic long chain molecules, mainly fatty acids, and by smaller amounts of aliphatic alcohols and n-alkanes. The major identified compound was lupeol (1.2% of leaves in n-hexane extract). The recovery and composition of cuticular lipids depended on the solvent and extraction time. The non-polar or weak polar solvents n-hexane and dichloromethane extracted similar lipid yields (77% and 86% of the total extract, respectively) while acetone solubilised other cellular compounds, namely sugars, with the lipid compounds representing 43% of the total extract. For cuticular lipids extraction, solvents with a low polarity such as n-hexane are the more suitable with an adequate extraction duration, e.g., n-hexane with a minimum extraction of 3 h.

Keywords: cork oak; cuticular wax; solvents; terpenes; lupeol

1. Introduction

The extracellular surfaces of plant leaves are covered by a layer consisting of cutin, an insoluble polyester glyceride and of a complex mixture of lipids soluble in organic solvents, commonly called cuticular waxes, which are located within and above the cutin structural matrix and named, respectively, intracuticular and epicuticular waxes [1,2]. This hydrophobic interface confers a resistance to a wide range of biotic and abiotic stresses and is involved in the regulation of non-stomatal water loss and gas exchange [2–4]. The functional barrier against water diffusion through the cuticle is preferentially established by intracuticular lipids [5–7] which consist of long-chain aliphatic molecules and alicyclic waxes, including triterpenoids, while the epicuticular lipids, comprising long-chain aliphatic molecules (e.g., alkanes, primary alcohols, fatty acids), are important for interactions between leaf surface and environment [5–7].

The cuticle, as a boundary between the plant and environment, has an enhanced role under adverse environmental conditions. This is the case for most species growing in the Mediterranean region under high solar irradiances, air temperatures, and vapor pressure deficits with a limited water availability, thereby showing a high sclerophyll character. Under drought stress, plants react namely by an ABA-induced stomatal closure, the accumulation of cuticular lipids, and the formation of a deep root system which improves their drought tolerance. Cork oak (*Quercus suber* L.), an evergreen sclerophyllous tree species distributed in the western Mediterranean basin, is an example of a species with great economic importance due to its production of cork, a material with a very interesting set of properties that feeds a dedicated industrial chain [8].

In leaves of *Q. suber* sampled in spring and summer, Martins et al. [9] described a layer of cuticular wax composed mainly of n-alkyl esters (25–45% of the wax extract)

and alkanols (18–50%) with a significant content variability. A more comprehensive study by our group on the cork oak leaves of trees from six seed provenance sources observed that a substantial wax layer (154–235 μg/cm^2) covered the leaves, with the majority of compounds being pentacyclic triterpenoids and long chain aliphatic compounds, and related the cork oak cuticular characteristics to the species since the trees of different seed origins did not differ [10]. The triterpene fraction contained a large amount of lupeol, a compound that has shown beneficial effects on human health [11–15].

Given the important role of the cuticular waxes in establishing the tree adaptation to adverse environmental conditions, it is of a high interest to clarify the influence of extraction conditions in their content and compositional determinations. In this study, we provide a characterization of the lipophilic compounds present in the leaf cuticle of *Q. suber* extracted with solvents of different polarities and with different extraction times. The results presented here will contribute to the knowledge of the lipophilic compounds in *Q. suber* cuticular leaves and their extraction specificity, allowing to direct the solubilisation process to obtain potential highly valuable phytochemicals of diverse industrial interest.

2. Materials and Methods

2.1. Plant Material

Mature leaves were collected from two mature *Q. suber* L. trees that were never submitted to cork removal, grown on the campus of the School of Agriculture, in the region of Lisbon, Portugal. The leaves were collected randomly from different branches on the south exposed crown side, in the lower part of the canopy up to a height of approximately 2 m, making up a total sample per tree of about 200 leaves. A composite sample was prepared by combining the leaves of the two trees.

The area of 80 leaves randomly selected from the composite sample was measured by digitalizing and it was calculated with Leica Qwin vs. 3.0 Image Analysis Software.

2.2. Cuticular Wax Extraction

The influence of the solvent polarity and extraction time on the yields of solubilized cuticular waxes and on their chemical profile was studied. Conventional Soxhlet extractions were used for the extraction of the cuticular waxes from the whole and intact cork oak leaves taken randomly from the leaf composite sample. Three replicates of leaf samples (without petiole) with a dry mass of around 1.5 g (corresponding to about 10 leaves) were placed in the Soxhlet apparatus and the lipophilic fractions were extracted using organic solvents n-hexane (dielectric constant 2.02), dichloromethane (dielectric constant 9.1), and acetone (dielectric constant 20.7), with different extraction times (5 min, 1, 2, 3, and 6 h with each solvent). The amount of the soluble compounds removed with each solvent and extraction time was determined from the mass difference in the extracted leaves after drying at 105 °C. The results were expressed as a mass percent of the leaf dry mass (g per 100 g leaves) and on a leaf surface area basis (μg per cm^2 leaf area) as the ratio between the extract and the two-sided leaf surface area, obtained by digitalization.

The lipid fraction in the crude extracts was determined from the mass of lipidic compounds estimated by GC–MS (alkanes, alkanols, fatty acids, terpenes, and sterols) and expressed as a percent of the extract mass and as a percent of the leaf dry mass. The estimated quantification of the compounds in the GC–MS chromatograms was done by the calculation of each compound peak area and expressed as a percent of the total chromatogram peak area.

2.3. Cuticular Wax Composition

The extracts were analysed using gas chromatography–mass spectrometry (GC–MS) after trimethylsilylation according to Simões et al. [10]. The extract was treated with BSTFA (N,O–bis(trimethylsilyl)trifluoroacetamide) in pyridine (30 min at 70 °C) and analysed in a gas chromatograph coupled to a mass spectrometer (EMIS, Agilent 5973 MSD, Palo Alto, CA, USA) using a Zebron 7HG-G015-02 column (30 m, 0.25 mm; ID, 0.1 μm film

thickness) with an electron ionization at 70 eV, and helium as a carrier gas at 1.0 mL min^{-1} flux. The column temperature was initially held at 50 °C for 1 min, raised to 150 °C at a rate of 10 °C min^{-1}, then to 300 °C at 4 °C min^{-1}, to 370 °C at 5 °C min^{-1}, and at 8 °C min^{-1} until it reached 380 °C, and followed by an isothermal 5 min period. The compounds were identified and quantified as TMS derivatives by comparing their mass spectra with a GC–MS spectral library (Wiley, NIST) and by comparing their fragmentation profiles with the published data, reference compounds, ion fragmentation patterns, or retention times [10]. The results are given as a percent of each compound peak area to the total chromatogram peak areas. The results are to be considered as only semiquantitative since no internal standards were added nor were the response factors of the different compounds calculated.

The proportion of specific chemical classes in the extracts (e.g., lipids, terpenes, aromatics, sugars), expressed as a % of the extract or in mg per g of leaf dry mass, was calculated using the extract amount per dry leaf mass and the compound area proportion in the total GC–MS chromatogram.

3. Results and Discussion

In the present work, the effect of the solvent and extraction time on the yield and composition of the cuticular wax removed from the *Q. suber* leaves surface was studied using three solvents with a different polarity index (by increasing polarity: n-hexane, dichloromethane and acetone) and different extraction times. In the procedure used here, the solubilisation of the compounds refers to both the adaxial and abaxial leaf surfaces. With the relatively long extraction time by Soxhlet (from 1 h to 6 h), the cuticular lipids that are released correspond to a mixture of both the epicuticular and intracuticular lipids [5,16]. Therefore, the resulting extracts reflect the total lipid composition, averaging over the entire depth of the cuticle, rather than assessing only the surface. The potential exception is the 5 min extraction which may target mostly the epicuticular waxes, as discussed later.

Although some techniques have been applied in other works to study separately the chemical composition of epicuticular and intracuticular lipids, e.g., by physically stripping the epicuticular lipids from the leaf surfaces or by using very short dipping times [5,7,17], this was not the objective of the present work. Therefore, the results presented below on the cuticular lipids comprise both epicuticular and intracuticular compounds.

A specific observation should be made on the term cuticular waxes used throughout this work. Although wax is chemically defined as very long-chain esters, the compounds solubilised from the leaf cuticle by the organic solvents have a complex composition comprising long chain fatty acids, primary and secondary alcohols, aldehydes, wax esters, ketones and linear hydrocarbons, that are derived from fatty acid precursors [18]. A more accurate designation should therefore be "extracellular surface lipids" [19]. However, most literature dealing with leaf cuticles uses the term cuticular waxes, and this was maintained here.

3.1. Extraction Yields

Table 1 shows the average extract yields (in g per 1000 g of dry leaves) and leaf surface coverage (in μg per cm^2 leaf surface) obtained with the different solvents and extraction times. A previous study from our group on the cuticular waxes of cork oak leaves from different tree provenances showed that a 6 h Soxhlet extraction with dichloromethane solubilised on average 2.2% of the dry leaf mass, corresponding to a surface coverage of 189 $\mu g/cm^2$ [10]. The results obtained here with dichloromethane after 6 h (2.8% of leaf mass and 239 $\mu g/cm^2$) are similar to those previously reported.

There was a clear difference between the solvents in their extracting ability: the yields were higher for acetone and hexane (3.6% and 3.4% of the leaf mass, respectively, after 6 h of extraction) in comparison to dichloromethane. The extraction time also had an effect on the extract yield (Table 1). Increasing the extraction time resulted in a higher removal, although the relative extraction power of the three solvents was maintained, i.e., lower

for dichloromethane. It should be noted that the extraction yields are related to the solubilization power and selectivity of the solvent to both lipid and non-lipid compounds, as given namely by their polarity, and discussed in detail in the following sections.

Table 1. Yields of material solubilized from the surface of whole *Q. suber* leaves by different solvents and extraction times, in g per 100 g dry leaves, and μg per cm^2 of leaf surface.

	5 min	1 h	2 h	3 h	6 h
n-Hexane					
g/100 g leaves	0.33 ± 0.04	1.92 ± 0.72	1.98 ± 0.25	3.11 ± 0.11	3.39 ± 0.19
μg/cm^2	28.13 ± 3.09	165.67 ± 62.33	170.58 ± 21.52	286.02 ± 9.27	287.15 ± 23.18
Dichloromethane					
g/100 g leaves	0.51 ± 0.03	1.17 ± 0.09	1.23 ± 0.13	1.79 ± 0.33	2.77 ± 0.17
μg/cm^2	43.83 ± 2.88	101.36 ± 7.66	108.30 ± 11.17	154.10 ± 28.52	239.00 ± 14.25
Acetone					
g/100 g leaves	0.35 ± 0.07	1.27 ± 0.25	2.70 ± 0.15	3.16 ± 0.02	3.57 ± 0.49
μg/cm^2	30.29 ± 5.84	109.42 ± 21.81	232.86 ± 12.81	272.24 ± 2.12	308.33 ± 42.32

The short 5 min extraction time led to a very partial removal of the soluble compounds, e.g., hexane, dichloromethane, and acetone solubilised only, respectively, 10%, 18%, and 10% of the extracts obtained with a 6 h extraction.

These results point out that a full, or at least a major, solubilisation of the leaf cuticular compounds is only possible if sufficient extraction time is given. Therefore, protocols that use a short or very short contact between the solvent and the leaf surface will only solubilise a small fraction of the cuticular lipids, namely only the epicuticular waxes, as previously discussed [10]. This is the reason for the difference in the extraction yield found between the present results and a previous study on young cork oak leaves using a quick dipping and shaking in the chloroform [9].

3.2. Effect of Solvent on Lipid Extraction

The extraction yield, i.e., the compounds solubilized by the solvent in relation to the leaf mass, is a quantitative but undifferentiating indicator of the molecules removed from the surface of the leaves, meaning that other non-lipid compounds may be solubilized, and more so with solvents with an increased polarity. Previous reports on the composition of the solubilized compounds from *Q. suber* leaves using dichloromethane showed that 80% of the extract was of a lipid nature, with about 2% corresponding to aromatics and a small proportion of sugars, as calculated from the corresponding peak areas in relation to the total chromatogram peak area [10].

The composition of the extracts is therefore an important aspect when analysing the solvent efficiency to solubilize the cuticular lipids. Considering the total amount of lipidic compounds present in the cuticular extracts, as determined from their GC–MS analysis (which will be reported in detail in the next section), by grouping alkanes, alkanols, fatty acids and glycerides, terpenes, and sterols, a new insight is obtained on the solvent role to attain higher lipid yields. Figure 1 represents the lipid yields obtained with the three solvents and five extraction times. The proportion of the lipid extractives was consistent with the order of the polarity of the solvent.

The 6 h acetone extraction shows the lowest proportion of extracted lipid compounds as estimated by their peak area proportion in the total chromatogram (15.3 mg/g of dry leaves, corresponding to 43% of the total extract), while the non-polar or weak polar solvents n-hexane and dichloromethane extracted a similar lipid proportion estimated as 26.1 and 24.1 mg/g of dry leaves, corresponding to 77% and 86% of the total extract, respectively (Figure 1). The lipid proportion in the extracts increased with the extraction time, e.g., from 1.7% to 2.6% with n-hexane, and from 0.5% to 1.5% with acetone for 1 h and 6 h extractions, respectively.

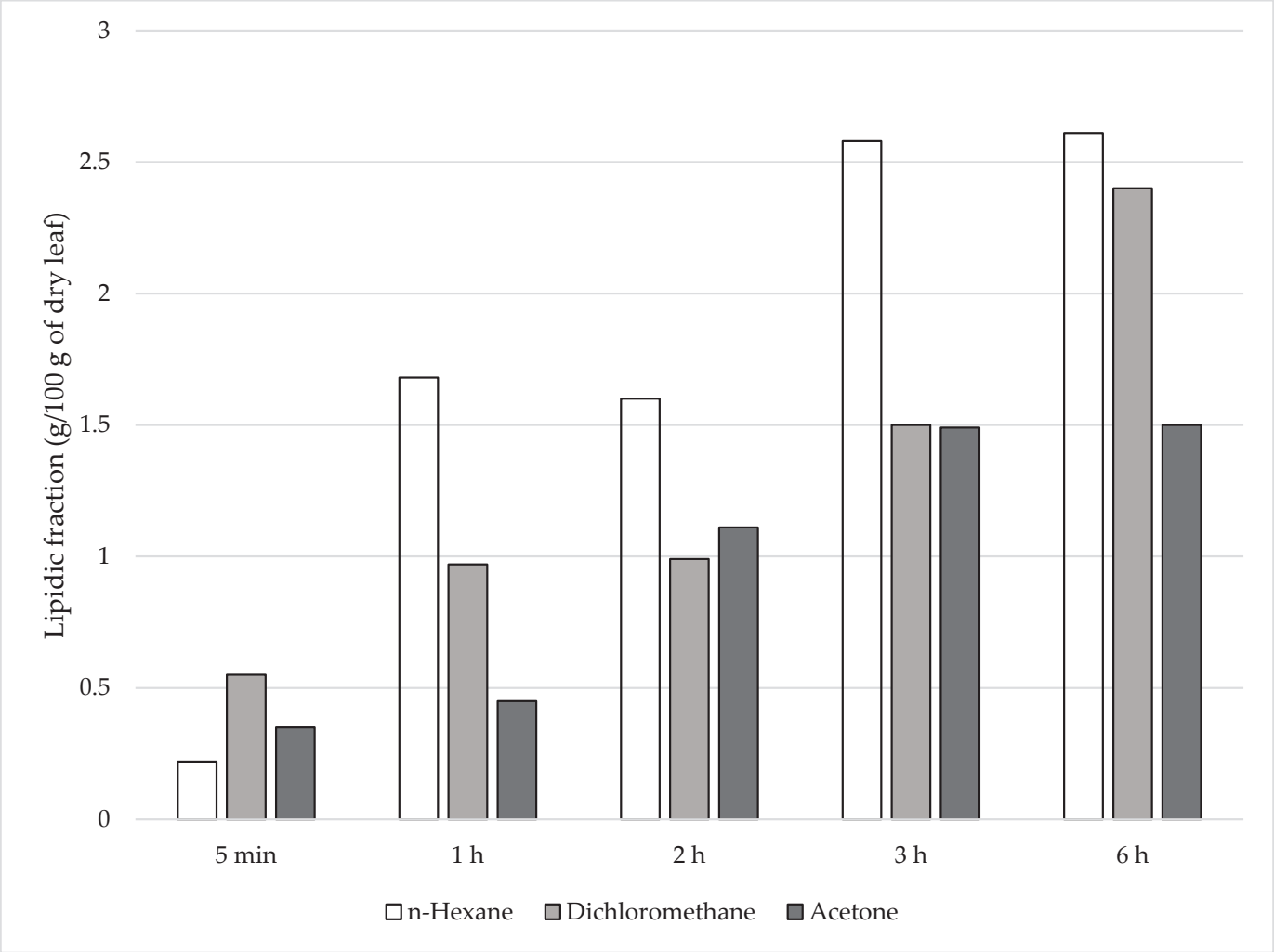

Figure 1. Lipidic fraction obtained from extraction of *Q. suber* leaves with solvents with different polarity indices with different extraction times.

For solubilisation of the cuticular lipids from *Q. suber* leaves (Figure 1), n-hexane was the most effective solvent in providing the highest recovery, which was attained with a 3 h extraction in the experimental conditions used. Dichloromethane, as used in the previous *Q. suber* cuticular studies, also provided a similar lipid recovery with a 6 h extraction [10].

3.3. Compositional Analysis of Extracts by Chemical Family

The composition by the chemical family of the cuticular waxes of cork oak leaves solubilised by different solvents with different extraction times, as a percentage of the total peak area in the GC–MS chromatograms, are presented in Table 2, and detailed for the three solvents in Tables 3–5. The results are a semiquantitative approximation of compound proportion since no internal standards were added or response factors were calculated.

The composition of n-hexane and dichloromethane extracts is quite similar. With the exception of the 5 min extracts, that will be discussed subsequently, the extracts are mainly made up of terpenes (43–63% of all compounds), followed by aliphatic long chain molecules, mainly fatty acids (11–26% of all compounds), and by smaller amounts of aliphatic alcohols, n-alkanes, and with some phenolics. This is in accordance with the reported composition of the cuticular wax from *Q. suber* leaves where triterpenes and aliphatic compounds predominate (61–72% and 17–23% of the total compounds, respectively) [10]. For the short extraction time of 5 min, the compounds solubilised were aliphatic alcohols that represented

98% and 96% of all compounds, respectively, in the n-hexane and dichloromethane extracts. This suggests that the more easily accessible external layer of the cuticle predominantly contains alkanols [20].

Table 2. Composition of the cuticular extracts of leaves from *Q. suber* solubilised by different solvents and extraction times by chemical class as a percentage of total peak area in the GC–MS chromatograms.

	Proportion of Total Compounds, %														
	n-Hexane					Dichloromethane					Acetone				
Family	**5 min**	**1 h**	**2 h**	**3 h**	**6 h**	**5 min**	**1 h**	**2 h**	**3 h**	**6 h**	**5 min**	**1 h**	**2 h**	**3 h**	**6 h**
Alkanes	0.3	6.9	3.5	6.9	6.6	0.4	3.4	3.1	2.2	3.6	-	0.5	1.8	0.4	0.2
Alkanols	98.4	5.5	4.0	3.7	7.0	95.5	5.1	7.3	5.5	7.3	2.1	3.8	3.7	4.2	2.0
Fatty acids	0.2	11.8	11.0	16.3	16.1	0.9	12.6	25.0	25.3	20.0	39.6	5.4	11.6	11.7	9.0
Glycerides	-	0.1	0.2	0.5	0.3	-	1.0	2.5	0.9	0.2	-	1.1	1.9	1.8	1.2
Sterols	-	0.01	3.2	4.2	2.7	-	2.0	3.0	2.7	3.4	-	1.1	1.5	1.6	1.2
Terpenes	0.1	59.7	63.4	52.0	44.6	2.0	59.9	42.7	48.4	44.8	-	19.5	20.3	20.5	22.2
Aromatics	-	1.7	4.5	5.6	4.1	-	4.7	5.6	5.7	4.5	13.5	2.9	3.2	2.6	2.7
Sugars	-	0.0	0.0	0.0	0.0	-	0.1	0.5	1.4	0.6	39.7	56.8	50.0	41.3	46.8
Others	-	1.6	0.9	0.6	0.3	-	1.1	0.5	1.4	1.4	5.0	6.2	1.7	9.9	8.4
Total Identified	99.0	87.3	90.7	89.8	81.7	99.5	90.0	90.7	93.7	85.5	99.8	93.4	92.0	89.7	91.6

Table 3. Composition of the cuticular waxes of cork oak leaves solubilised by n-hexane with different extraction times, as determined by GC–MS, in % of total peak area (only compounds with over 1% are shown; complete composition in Supplementary Table S1).

	Extraction Time				
Wax Constituent (% Total Peak Area)	**5 min**	**1 h**	**2 h**	**3 h**	**6 h**
Alkanes					
Heptacosane (C_{27})	-	-	-	1.12	1.02
Triacontane (C_{30})	-	5.10	2.47	4.89	4.66
Alkanols					
Hexadecan-1-ol ($C_{16}OH$)	-	1.15	-	-	-
Docosan-1-ol ($C_{22}OH$)	1.24	-	-	-	-
Tretracosan-1-ol ($C_{24}OH$)	96.64	2.91	3.11	3.05	4.34
Fatty acids					
Saturated					
Hexadecanoic acid ($C_{16:0}$)	-	7.57	5.35	5.57	5.32
Hexacosanoic acid ($C_{26:0}$)	-	-	-	1.00	1.05
Octacosanoic acid ($C_{28:0}$)	-	-	-	2.61	3.39
Triacontanoic acid ($C_{30:0}$)	-	-	-	1.08	1.37
Unsaturated					
9,12-Octadecadienoic acid ($C_{18:2}$)	-	-	-	1.12	0.81
9,12,15-Octadecatrienoic acid ($C_{18:3}$)	-	-	2.28	3.43	2.11
Sterols					
β-Systosterol	-	-	2.82	3.50	2.50
Terpenes					
pentacyclic triterpenes					
β-Amyrin	-	3.02	2.83	3.11	2.47
Germanicol	-	11.19	17.31	7.49	6.00
Lupeol	-	43.93	40.43	37.76	33.04
Betulin	-	-	-	1.12	0.97
Aromatics					
Hexadecyl-(E)-p-coumarate	-	-	4.21	5.32	3.66

Table 4. Composition of the cuticular waxes of cork oak leaves solubilised in dichloromethane with different extraction times, as determined by GC–MS in % of total peak area (only compounds with over 1% are shown; complete composition in Supplementary Table S2).

	Extraction Time				
Wax Constituent (% Total Peak Area)	**5 min**	**1 h**	**2 h**	**3 h**	**6 h**
Alkanes					
Nonacosane (C_{29})	-	2.53	2.18	1.47	2.56
Alkanols					
Hexadecan-1-ol ($C_{16}OH$)	0.90	-	-	-	-
Docosan-1-ol ($C_{22}OH$)	2.38	0.77	1.12	1.10	1.85
Tretracosan-1-ol ($C_{24}OH$)	92.12	3.47	4.59	3.31	4.62
Fatty acids					
Saturated					
Hexadecanoic acid ($C_{16:0}$)	-	7.60	9.84	9.71	9.68
Octacosanoic acid ($C_{28:0}$)	-	1.60	2.31	1.14	2.49
Unsaturated					
9,12-Octadecadienoic acid ($C_{18:2}$)	-	0.14	1.73	2.38	0.75
9,12,15-Octadecatrienoic acid ($C_{18:3}$)	-	0.39	6.43	8.04	2.69
Glycerides					
Glycerol	-	0.95	2.14	0.51	-
Sterols					
β-Systosterol	-	1.59	2.55	2.33	3.24
Terpenes					
Pentacyclic triterpenes					
β-Amyrin	-	2.75	2.29	2.56	2.11
Germanicol	-	9.15	5.46	6.46	4.77
Lupeol	1.61	45.44	31.56	35.28	35.37
Aromatics					
Hexadecyl-(E)-p-coumarate	-	4.27	5.31	5.19	4.09
Sugars					
Fructofuranose	-	0.09	0.54	1.43	0.18

Table 5. Composition of the cuticular waxes of cork oak leaves solubilised in acetone with different extraction times, as determined by GC–MS, in % of total peak area (only compounds with over 1% are shown; complete composition in Supplementary Table S3).

	Extraction Time				
Wax Constituent (% Total Peak Area)	**5 min**	**1 h**	**2 h**	**3 h**	**6 h**
Alkanols					
1,4-Butanediol	1.85	-	-	-	-
Tretracosan-1-ol ($C_{24}OH$)	-	3.22	3.21	2.74	1.28
Fatty acids					
Saturated					
Hexadecanoic acid ($C_{16:0}$)	-	2.51	5.54	5.92	4.35
Unsaturated					
9,12-Octadecadienoic acid ($C_{18:2}$)	-	0.03	0.66	1.23	0.48
9,12,15-Octadecatrienoic acid ($C_{18:3}$)	-	0.07	0.61	0.07	1.26
Diacids					
Butanedioic acid ($C_{4:0}$)	-	0.95	0.99	2.45	1.69
Glycerides					
Glycerol	-	1.04	1.72	1.36	0.95
Sterols					
β-Systosterol	-	0.32	0.99	1.43	1.15

Table 5. *Cont.*

	Extraction Time				
Wax Constituent (% Total Peak Area)	**5 min**	**1 h**	**2 h**	**3 h**	**6 h**
Terpenes					
pentacyclic triterpenes					
β-Amyrin	-	0.72	-	1.18	1.19
Germanicol	-	2.89	2.05	2.71	2.86
Lupeol	-	14.53	16.25	14.71	16.15
Aromatics					
Catechine	13.18	-	-	-	-
Hexadecyl-(E)-p-coumarate		1.67	1.62	2.35	2.42
Sugars					
Myo Inositol	19.98	-	15.34	-	−0.11
Scyllo Inositol	-	15.44	14.27	12.39	14.88
Deoxinositol	-	6.28	1.81	5.24	6.3
D-Fructose	-	15.47	11.27	10.68	8.61
(α/β) D-Glucopyranose (isomer)	-	17.11	6.28	11.18	15.01
Sucrose	18.62	0.48	0.21	0.47	0.4
Others compounds					
Quininic acid	38.18	4.6	0.94	7.2	7.15
Shikimic acid, 4TMS derivative	5.03	-	-	-	-

The compositional profile of the acetone extract clearly differs, with sugars being the main chemical class (57–47% of all compounds), followed by triterpenes (19–23%), and fatty acids (5–12%) with lower proportions of the other chemical families. The presence of other non-lipid compounds, mainly of sugars, indicates that, in contrast to the other solvents used, acetone penetrates into the leaf interior and solubilises the more polar sugar molecules. The degradation of the cellular membranes by solvents such as chloroform and acetone have been reported, leading to the solubilisation of cellular compounds not related to the cuticular matrix, for instance of indole alkaloids [21], and chlorophyll and cytoplasmic sterols. The effect of acetone on the leaf cells was noticed already for the short 5 min extraction with the solubilisation of fatty acids, sugars, and aromatics. This is in agreement with reports of an instant destruction of cell integrity when using chloroform [21].

The recovery (in g/100 g leaves) of the extracted cuticular lipids by the chemical family under the different conditions is shown in Figure 2. The difference in the acetone extract in comparison with the hexane and dichloromethane extracts is clear with the major extract fraction being sugars representing 1.67 g/100 g leaves (6 h extraction). Hexane and dichloromethane permit the recovery of cuticular terpenes (1.51 and 1.24 g/100 g leaves, respectively) and fatty acids (0.55 and 0.55 g/100 g leaves, respectively).

The extraction time had only a moderate impact on the recovery of the extracellular cuticular lipids with the differences given more by the extraction yield (Table 1) than by the compositional profile, which remains independent of the extraction time (Table 2). For instance, the recovery of terpenes with n-hexane increased from 11.5 mg/g of leaves with 1 h to 15.1 mg/g of leaves with 6 h of contact, while the extraction with dichloromethane was the one most impacted by duration, e.g., terpenes recovery increased from 7.0 mg/g of leaves with 1 h to 12.4 mg/g of leaf with 6 h of contact (Figure 2).

These results should be taken with caution and restricted to the experimental procedure used here (Soxhlet extraction). Martins et al. [9] studied the extraction of extracellular surface lipids in the leaves of young *Q. suber* by immersion for a few seconds in chloroform, thus extracting only the epicuticular layer, and this explains the compositional differences in relation to our results, for example, the extract contained only small amounts of triterpenoids. Loneman et al. [19] applied a quick surface extraction method by dipping maize seedling leaves with chloroform and hexane:diethyl ether for 1 to 10 min, and observed that the recovery and composition depended on the solvent and duration of the extraction.

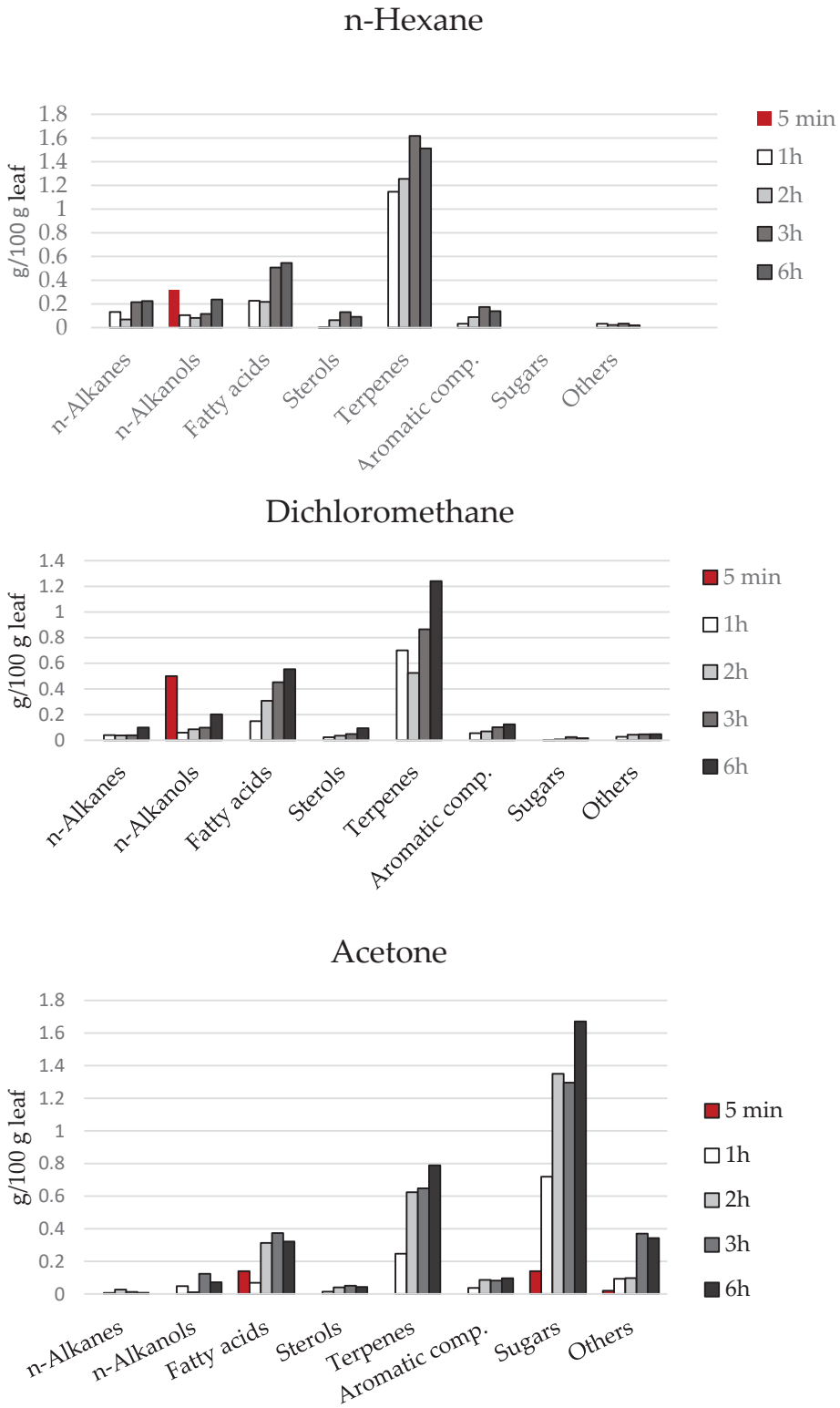

Figure 2. Composition (g/100 g leaves) by chemical family of the cuticular lipids extracted from *Q. suber* leaves with different solvents and extraction time.

3.4. Chemical Composition of Extracts

The composition of n-hexane, dichloromethane, and acetone extracts is summarised in Tables 3–5 that include only the compounds with at least 1.0% of the chromatogram peak area. The complete compositional profile and the GC–MS chromatogram of the derivatised extracts at 5 min and 3 h is given as the supplementary data (Supplementary Tables S1–S3, respectively,

for n-hexane, dichloromethane, and acetone extracts) and Supplementary Figures S1–S3, respectively, for n-hexane, dichloromethane, and acetone extracts at 5 min and 3 h, respectively, exemplify the quality of the chromatograms that were obtained for all the cases.

In the terpenic family, the triterpenoid lupeol was among the most prominent individual compound, followed by germanicol and α- and β-amyrin, e.g., lupeol with 33–43% of all compounds (about 75% of the terpenic fraction) and germanicol with 6–17% of all compounds (about 15% of terpenic fraction). Smaller amounts of other triterpenoids such as betulin, betulinic, oleanolic, and ursonic acids were also identified (Supplementary Tables S1–S3). All of the identified triterpenes were previously reported as cuticular wax components of *Q. suber* leaves [10].

Triterpenoids are one of the largest and structurally diverse classes of natural specialized metabolites with various ecological and biological properties, with a broad spectrum of relevant clinical activities, such as antihypertensive, antidiabetic, anti-inflammatory, anticancer, and antimicrobial properties leaves [11–15]. The high proportion of lupeol in the cuticular extracts may lead to considering *Q. suber* leaves as a source of this compound, e.g., a lupeol recovery of 1.18 g/100 g of leaves may be obtained with a 3 h n-hexane extraction.

Four sterols were identified in the extracts (β-systosterol, δ-tocopherol; stigmasterol and 25-hydroxycholesterol, Supplementary Tables S1–S3) with β-systosterol showing the highest abundance with 2.5–3.5% of all compounds.

The hydrocarbon fraction includes fatty acids, n-alkanols, and n-alkanes. With 6 h of contact, fatty acids are mostly saturated fatty acids, accounting to 79% and 59% of the total fatty acids in the n-hexane and dichloromethane extracts, and 59% of the total fatty acids content in the acetone extract. Fatty acids were identified in the homologous series from heptanoic acid (C7:0) to triacontanoic acid (C30:0), with a strong even-over-odd carbon atom predominance. Hexadecanoic acid (palmitic acid, C16:0) was the most abundant saturated fatty acid in the three extracts (5.3% of all compounds in n-hexane extract, 9.7% in dichloromethane extract, and 4.4% in acetone extract). Smaller amounts of octacosanoic acid (C28:0), hexacosanoic acid (C26:0), and triacontanoic acid (C30:0) were also found. Three unsaturated acids were identified in the extracts: 9,12,15-octadecatrienoic (linoleic acid), 9,12-octadecadienoic (linolenic acid), and 9-cis-hexadecenoic (palmitoleic acid) acids.

Fatty alcohols represented only a small fraction of the total amount of lipophilic extractives. A series of n-fatty alcohols ranging from C4 to C28 were present in cork oak wax leaves extracts, with tetracosanol (C24OH) as the most abundant (4.3% of all compounds in the n-hexane wax extract, 4.6% in the dichloromethane extract, and 1.4% in the acetone wax extract)

A series of n-alkanes ranging from nonadecane (C19) to hentriacontane (C31) occurred in the extracts, with a strong odd-over-even carbon atom number predominance. Nonacosane (C29) was the most abundant in the dichloromethane extract (72% of alkanes) and triacontane (C30 in the n-hexane extract (74% of alkanes)).

The composition of the identified aliphatic compounds is similar to that obtained for the cuticular wax of *Q. suber* leaves from different sources extracted with dichloromethane with 6 h of contact, that included fatty acids with a chain length C30, C28, and C16, n-alkanes with chain lengths ranging between C15 and C31 [10].

Low amounts of acylglycerols including mono-glycerides such as monopalmitin, 2-monostearin, 1-linolenoylglycerol, and 3-hydroxypropyl hexadecanoate were identified in all the extracts, together representing 0.45%, 0.57%, and 0.19% of the n-hexane, dichloromethane, and acetone extracts, respectively.

Aromatic compounds were also detected in all the extracts such as benzoic acid and p-coumarates. P-coumarates were the dominant aromatic compound corresponding to 5.3%, 4.1%, and 2.4% of the n-hexane, dichloromethane, and acetone extracts, respectively.

High amounts of sugars were found in the acetone extracts (56% of all compounds) including fructose, glucose, sucrose, the free cyclitols myo-inositol, scyllo-inositol, and deoxinositol. Scyllo-inositol has been considered as a potential therapeutic agent for Aβ amyloid disorders such as Alzheimer's disease, Down's syndrome, and cerebrovascular dementia [22,23].

4. Conclusions

This study confirmed that the extent and selectivity of the solubilisation of non-polar and amphipathic molecules that are part of the cuticular layering of plant leaves, as exemplified for the case of *Q. suber* adult leaves, depends on the solvent and on the extraction duration. Less polar solvents such as n-hexane or dichloromethane solubilize the lipid components and a small number of aromatics, while more polar solvents, such as acetone, remove a large proportion of sugars arising from the solubilisation of cellular material. For the purpose of cuticular lipids extraction, solvents with a low polarity, such as n-hexane, are the more suitable and an adequate extraction duration should be considered for an extensive removal, including both the epicuticular and intracuticular lipids. In the present case, n-hexane with a minimum 3 h extraction is proposed. Although not specifically studied here, the procedural method for the extraction should also play a role in the extent of solubilization. The cuticular lipid compounds, usually named cuticular waxes, include as major components terpenes and a large fraction of long-chain fatty acids and other long-chain aliphatics, with a low proportion of sterols, aromatics, and other compounds. It is therefore probable that the terpenes will establish the transpiration barrier in association with the long chain aliphatic compounds.

Supplementary Materials: The following supporting information can be downloaded at: https://www.mdpi.com/article/10.3390/pr10112270/s1, Table S1: Composition of the cuticular waxes of cork oak leaves solubilised in n-hexane with different extraction times as determined by GC–MS, in % of total peak área; Table S2: Composition of the cuticular waxes of cork oak leaves solubilised in dichloromethane with different extraction times as determined by GC–MS, in % of total peak area; Table S3: Composition of the cuticular waxes of cork oak leaves solubilised in acetone with different extraction times as determined by GC–MS, in % of total peak area. Figure S1: GC–MS chromatogram of the derivatised n-hexane extract from the cuticular waxes of cork oak leaves. Figure S2: GC–MS chromatogram of the derivatised dichloromethane extract from the cuticular waxes of cork oak leaves; Figure S3: GC–MS chromatogram of the derivatised acetone extract from the cuticular waxes of cork oak leaves

Author Contributions: Conceptualization, H.P. and I.M.; methodology, I.M. and R.S.; validation, H.P., I.M. and R.S.; formal analysis, R.S.; investigation, R.S.; data curation, R.S., H.P. and I.M.; writing—original draft preparation, I.M. and R.S.; writing—review and editing, H.P., I.M. and R.S. All authors have read and agreed to the published version of the manuscript.

Funding: This research was funded by Fundação para a Ciência e a Tecnologia (FCT) through funding of the Forest Research Centre (UIDB/00239/2020). Funding for this work was also provided by a doctoral scholarship from FCT SUSFOR Doctoral Programme (PD/BD/128259/2016).

Data Availability Statement: Not applicable.

Acknowledgments: Rita Simões acknowledges a doctoral scholarship from FCT with the SUSFOR Doctoral Programme (PD/BD/128259/2016). We thank Ana Rodrigues for her technical assistance in field sampling.

Conflicts of Interest: The authors declare no conflict of interest.

References

1. Pollard, M.; Beisson, F.; Li, Y.; Ohlrogge, J.B. Building lipid barriers: Biosynthesis of cutin and suberin. *Trends Plant Sci.* **2008**, *13*, 236–246. [CrossRef] [PubMed]
2. Buschhaus, C.; Jetter, R. Composition differences between epicuticular and intracuticular wax substructures: How do plants seal their epidermal surfaces? *J. Exp. Bot.* **2011**, *62*, 841–853. [CrossRef] [PubMed]
3. Jeffree, C.E. The fine structure of the plant cuticle. In *Biology of the Plant Cuticle*; Riederer, M., Müller, C., Eds.; Annual Plant Review; Blackwell: Oxford, UK, 2006; Volume 23, pp. 11–125.
4. Schreiber, L.; Schönherr, J. *Water and Solute Permeability of Plant Cuticles: Measurement and Data Analysis*; Springer: Berlin/Heidelberg, Germany, 2009.
5. Jetter, R.; Riederer, M. Localization of the transpiration barrier in the epi- and intracuticular waxes of eight plant species: Water transport resistances are associated with fatty acyl rather than alicyclic components. *Plant Physiol.* **2016**, *170*, 921–993. [CrossRef] [PubMed]

6. Zeisler-Diehl, V.; Müller, Y.; Schreiber, L. Epicuticular wax on leaf cuticles does not establish the transpiration barrier, which is essentially formed by intracuticular wax. *J. Plant Physiol.* **2018**, *227*, 66–74. [CrossRef] [PubMed]
7. Bourgault, R.; Matschi, S.; Vasquez, M.; Qiao, P.; Sonntag, A.; Charlebois, C.; Mohammadi, M.; Scanlon, M.J.; Smith, L.G.; Molina, I. Constructing functional cuticles: Analysis of relationships between cuticle lipid composition, ultrastructure and water barrier function in developing adult maize leaves. *Ann. Bot.* **2020**, *125*, 79–91. [CrossRef] [PubMed]
8. Pereira, H. *Cork: Biology, Production and Uses*; Elsevier Science: Amsterdam, The Netherlands, 2007.
9. Martins, C.M.C.; Mesquita, S.M.M.; Vaz, W.L.C. Cuticular waxes of the holm (*Quercus ilex* L. subsp. ballota (Desf.) Samp.) and cork (*Q. suber* L.) oaks. *Phytochem. Anal.* **1999**, *10*, 1–5. [CrossRef]
10. Simões, R.; Rodrigues, A.; Ferreira-Dias, S.; Miranda, I.; Perreira, H. Chemical composition of cuticular waxes and pigments and morphology of leaves of *Quercus suber* trees of different provenance. *Plants* **2020**, *9*, 1165. [CrossRef] [PubMed]
11. Fernández, M.A.; Heras, B.; García, M.D.; Sáenz, M.T.; Villar, A. New insights into the mechanism of action of the anti-inflammatory triterpene lupeol. *J. Pharm. Pharmacol.* **2001**, *53*, 1533–1539. [CrossRef] [PubMed]
12. Yamashita, K.; Lu, H.; Lu, J.; Chen, G.; Yokoyama, T.; Sagara, Y.; Manabe, M.; Kodama, H. Effect of three triterpenoids, lupeol, betulin, and betulinic acid on the stimulus-induced superoxide generation and tyrosyl phosphorylation of proteins in human neutrophils. *Clin. Chim. Acta* **2002**, *325*, 91–96. [CrossRef]
13. Prasad, S.; Kumar, Y.V.; Srivastava, S.; Shukla, Y. Protective effects of lupeol against benzo[a]pyrene induced clastogenicity in mouse bone marrow cells. *Mol. Nutr. Food Res.* **2008**, *52*, 1117–1120. [CrossRef] [PubMed]
14. Siddique, H.R.; Saleem, M. Beneficial health effects of lupeol triterpene: A review of preclinical studies. *Life Sci.* **2011**, *88*, 285–293. [CrossRef] [PubMed]
15. Ahmad, R.; Khan, A.; Lee, H.J.; Rehman, I.U.; Khan, I.; Alam, S.I.; Kim, M.O. Lupeol, a plant-derived triterpenoid, protects mice brains against Aβ-induced oxidative stress and neurodegeneration. *Biomedicines* **2020**, *8*, 380. [CrossRef] [PubMed]
16. Jetter, R.; Schäffer, S.; Riederer, M. Leaf cuticular waxes are arranged in chemically and mechanically distinct layers: Evidence from *Prunus laurocerasus* L. *Plant Cell Environ.* **2000**, *23*, 619–628. [CrossRef]
17. Sharma, P.; Kothari, S.L.; Rathore, M.; Gour, V. Properties, variations, roles, and potential applications of cuticular wax: A review. *Turk. J. Bot.* **2018**, *42*, 135–149. [CrossRef]
18. Yeats, T.H.; Rose, J.K. The formation and function of plant cuticles. *Plant Physiol.* **2013**, *163*, 5–20. [CrossRef] [PubMed]
19. Loneman, D.M.; Peddicord, L.; Al-Rashid, A.; Nikolau, B.J.; Lauter, N.; Yandeau-Nelson, M.D. A robust and efficient method for the extraction of plant extra cellular surface lipids as applied to the analysis of silks and seedling leaves of maize. *PLoS ONE* **2017**, *12*, e0180850. [CrossRef] [PubMed]
20. Fernández, V.; Guzmán-Delgado, P.; Graça, J.; Santos, S.; Gil, L. Cuticle structure in relation to chemical composition: Re-assessing the prevailing m7odel. *Front. Plant Sci.* **2016**, *7*, 427. [CrossRef] [PubMed]
21. Abouzeid, S.; Beutling, U.; Selmar, D. Stress-induced modification of indole alkaloids: Phytomodificines as a new category of specialized metabolites. *Phytochemistry* **2019**, *159*, 102–107. [CrossRef] [PubMed]
22. Fenili, D.; Brown, M.; Rappaport, R.; McLaurin, J. Properties of *scyllo*-inositol as a therapeutic treatment of AD-like pathology. *J. Mol. Med.* **2007**, *85*, 603–611. [CrossRef] [PubMed]
23. Lee, D.; Lee, W.S.; Lim, S.; Kim, Y.K.; Jung, H.-Y.; Das, S.; Lee, J.; Luo, W.; Kim, K.-T.; Chung, S.-K. A guanidine-appended *scyllo*-inositol derivative AAD-66 enhances brain delivery and ameliorates Alzheimer's phenotypes. *Sci. Rep.* **2017**, *7*, 14125. [CrossRef] [PubMed]

processes

MDPI

Article

Evaluation of the Gas Emissions during the Thermochemical Conversion of Eucalyptus Woodchips

João Silva [1,2,*], Carlos Castro [1], Senhorinha Teixeira [2] and José Teixeira [1]

[1] MEtRICs Research Centre, University of Minho, 4800-058 Guimarães, Portugal
[2] ALGORITMI Research Centre/LASI, University of Minho, 4800-058 Guimarães, Portugal
* Correspondence: js@dem.uminho.pt

Abstract: The combustion of solid biomass in industrial boilers involves a sequence of processes that include heating, drying, devolatilization, and char conversion. To maintain a repeatable and fully controlled environment, and to monitor all the dynamics involved in the phenomena at a real scale, field-scale experiments become necessary to perform investigations. In this way, to evaluate different thermochemical conversion conditions of biomass particles under an oxidative atmosphere, and to quantify the emission of the main gas compounds continuously, a small-scale reactor was developed and presented in this paper. Hence, in this work, larger particles of eucalyptus are burned at 400 and 800 °C under different stoichiometric conditions to understand the differences between different biomass conversion regimes (gasification and combustion). The analysis of the mass loss at the different temperatures was characterized by only two different and consecutive stages for both thermochemical conditions. The first region does not present the influence on the air flow rate; however, there is a significant difference in the second region. This fact highlighted the importance of the diffusion of oxygen during the char conversion. Regarding the quantification of the gas compounds, an increase of around 3 times in the CO and CO_2 emissions when gasification occurs was observed at 400 °C. However, at 800 °C, the same trend was verified, also verifying a considerable amount of CH_4.

Keywords: biomass; combustion; gas emissions; macro thermogravimetric analysis; pyrolysis; woodchips

1. Introduction

Solid biomass fuels, unlike fossil fuels such as coal, do not take millions of years to develop and, every year, a vast amount of biomass grows through the photosynthesis process by absorbing CO_2 from the atmosphere. Solid biomass is thus considered a renewable energy source and an interesting route to diversify energy production and reduce the dependence on fossil fuels [1]. Eucalyptus is the most representative solid biomass species in Portugal [2]. It was reported in 2015 that this species occupied 882,000 ha of the total forest area. It is still growing and is a major resource for paper production as well as fuel for heat production (both in households and in industry) [3]. Although the major source of solid biomass comes from the trunk, the literature emphasizes other streams of solid biomass with high potential. As an example, Roman et al. [4] have studied the potential of forest waste biomass for briquette production. Such works are a major contribution to the area as they present alternatives for the current solid biomass streams.

Regarding the main technological pathways for the production of heat and power, or combined heat and power, through the utilization of solid biomass, combustion and gasification are the main options [5]. Combustion represents one of the oldest technologies of biomass thermochemical conversion and utilization. The combustion process is an exothermic reaction between oxygen and biomass-volatile compounds that produce heat. The heat released is the main source of energy used in this process [6]. In a typical biomass combustion process, three main stages can be observed: drying, devolatilization, and char

burning. The drying stage is associated with the water evaporation present in the biomass. During the devolatilization stage, volatile compounds are released and burned with the oxygen present in the atmosphere. For the char combustion stage, the remaining carbon reacts with the oxygen, leaving ashes at the end of the combustion [7,8]. In the operation of biomass boilers, the design of the air supply system, including primary and secondary air, plays an important role in the combustion efficiency of biomass [9,10]. Yin et al. [11] reported that for grate-firing, one of the main technologies in biomass combustion, the overall excess air is usually set to 25% or above.

In its turn, gasification consists of burning biomass with insufficient oxygen under sub-stoichiometric conditions to produce combustible gases, which are collectively referred to as syngas. This is an attractive method of efficient energy extraction, mainly because a considerable amount of CO and CH_4 are obtained in comparison with combustion. Hence, in solid biomass gasification, an air-to-fuel ratio around 1.5:1 to1.8:1 is necessary, while a combustion ratio is around 3.8:1 [12].

Since, in both technologies, the main stages of biomass thermochemical conversion remain the same, the study and comprehension of the gas-release evolution in a practical way can provide knowledge to develop computer models or to design equipment, such as furnaces, stoves, boilers, and gasifiers [13]. Among the three stages, devolatilization is considered one of the most important for heat and power generation. Hence, it is related to the oxidation, under different stoichiometric conditions depending on the conversion technology, of the volatile compounds and has a significant impact on the exothermic reaction. For that reason, it is also important to study and understand the composition of the gas released during the devolatilization stage. Usually, complete combustion yields only CO_2 and H_2O as reaction products. However, other compounds can be formed, such as CH_4, CO, and H_2, increasing pollutant emissions and contaminating the environment [14].

To study the thermochemical conversion behavior of solid biomass, TGA (Thermo Gravimetric Analysis), a well-known thermal analysis technique and one of the most used, is applied [15,16]. Several authors have applied TGA to characterize the conversion of samples with a reduced size and mass in a kinetic way. However, TGA experiments are limited to assess the gas phase, and the lack of information in the literature relative to the gas emissions in this type of work persists [17–20]. Nevertheless, the gaseous release process analysis can be evaluated using the same technique but on a larger scale, commonly known as macro TGA [21]. In this way, the experiments are closer to the real thermochemical conversion processes, either in industrial or domestic equipment. Hence, macro TGA experiments take into account heat and mass transfer effects.

Regarding the literature concerning macro TGA experiments, Becidan et al. [22] presented the application of chromatography and spectrophotometry to study the gases released during the combustion of biomass residues. A fraction of the exhaust gases is collected and analyzed by a Fourier-Transform Infrared Spectroscopy (FTIR) analyzer and a micro-gas chromatograph. The FTIR was used to quantify CO_2, CO, CH_4, C_2H_2, and C_2H_4. The gas samples were also quantified online using a micro-gas chromatograph equipped with two thermal conductivity detectors and a double injector connected to two columns to separate and quantify CO_2, hydrocarbons (CH_4, C_2H_2, C_2H_4, and C_2H_6), and the remaining gases (H_2, O_2, CH_4, CO, and N_2) in another column. Brunner et al. [23] and Gauthier et al. [24] also applied both techniques to analyze the NOx emissions, ash release, and the main gaseous species and tar, respectively. Additionally, Weissinger et al. [25] described the release of nitrogen compounds using FTIR spectroscopy. Both works refer to the importance of the determination of nitrogen gaseous compounds that may serve as input profiles for Computational Fluid Dynamics (CFD) simulations. Bennadji et al. [26] and Nikku et al. [27] measured the fractions of light species from pyrolysis at low temperatures and compared the reactivity of municipal solid wastes with biomass and coal samples through the FTIR technique, respectively. Hu et al. [28] analyzed the influence of different atmospheres in the gaseous conversion using the mass spectrometer.

Although the quantification of the gaseous compounds released during the thermal conversion of biomass is not addressed, there are works in the literature where the conversion of biomass was analyzed separately through the macro TGA technique. Baumgarten et al. [29] and Samuelson et al. [30] analyzed the combustion behavior under typical isothermal conditions in the start-up of furnaces. Orang et al. [31] observed the effect of moisture content on combustion behavior. The author highlighted the higher drying and the ignition times due to the increase of the moisture content.

Thus, macro TGA experiments provide the possibility to control and maintain external heat fluxes in order to better represent, at a small-scale, the conditions expected in industrial boilers.

Gauthier et al. [24] used a purpose-built horizontal lamp tube reactor to perform pyrolysis of centimeter-scale wood particles, for temperatures ranging between 450 and 1050 °C. Yang et al. [32] studied the effect of the particle size (pinewood cubes ranging from 5 to 35 mm) on pinewood combustion in a batch reactor by measuring the mass loss rate and the temperature profile at different bed locations and gas composition in the out-of-bed flue gases. Ryu et al. [33] studied the combustion of four biomass materials with different fuel properties under fuel-rich conditions, measuring temperature, mass loss, and gas composition. Mahmoudi et al. [34] focused on developing a numerical model using the Euler-Lagrange model in which the fluid phase is a continuous phase and each particle is tracked with the Lagrangian approach to understand the combustion phase. This work was performed along with an experimental study, with temperature and mass loss monitoring, to validate the numerical model. Wurzenberger et al. [35] created a combined transient single particle and fuel-bed model of a furnace in order to optimize its efficiency and emissions by acquiring information about all the physical and chemical effects on the process. Markovic et al. [36] studied the combustion of wood waste with pre-heated primary air up to 350 °C and the secondary air distributed via nozzles above the waste layer. The authors measured temperature, gas composition, mass loss, and the influence of primary air speed, fuel moisture, and inert content on the combustion characteristics. Eric et al. [37] focused the study on the kinetics of loose biomass in a vertical tube reactor measuring the fuel mass loss rate, with two biomass combustion models (piston and batch model). Most of the testing conditions resemble the traditional (micro) TGA operation where the sample follows a pre-defined heating curve. Usually, this leads to heating rates well below those expected inside a furnace. Long et al. [38] reported an alternative approach in which the sample was introduced into a reactor set at a predefined temperature. The authors only reported mass loss rates. Lelis et al. [39] measured the mass loss and variation of the elemental composition of pine wood pellets. The authors used a macro TGA to investigate the influence of temperature and time on devolatilization of C, H, and N. The experiments were carried out at a constant temperature, and it was found that the rate of release of N is higher than other compounds. However, no information on the actual species formed was provided.

This work presents an experimental facility developed to study how biomass fuels may behave in industrial power plants. Thus, the mass loss profiles at different thermo-chemical conditions of eucalyptus woodchips are presented together with the composition of the gases released over time. Furthermore, it is important to point out that the motivation for this work is related to the need to understand the composition of the gas compounds released during the conversion of solid biomass particles. It is necessary to know the composition, the amount of pyrolysis products in different reactor thermal conditions, and the reaction rate of the particles. A recent investigation mentioned that numerical prediction inside a grate-fired boiler depends on the devolatilization kinetics mechanism, which can significantly affect the outputs from the bed model [40]. Most of the CFD models usually employed biomass elemental composition and enthalpy conservation equations or models, like that proposed by Thunman et al. [41] and Neves et al. [42], to determine the composition of pyrolysis products (e.g., [43]). However, the results of this type of approach can produce unrealistic results. Therefore, there is a clear need to develop macro TGA

experiments to obtain experimental information that may be used to develop mathematical models to describe the devolatilization of biomass. These models can be used as an input to CFD models for grate-type combustors.

2. Materials and Methods

2.1. Samples

The woodchips necessary for the macro TGA experiments were prepared from large eucalyptus trunks by means of a knife chipper. Hence, larger particles were obtained, with dimensions similar to the ones used in biomass power plants, ranging from a few millimeters up to hundreds of millimeters. The particles were then spread in a room to be air-dried and to reduce the moisture content. After this, the particles were then sieved, and the particle size distribution was assessed by horizontal screening according to the standard EN 15149-1:2010 Part 2 using sieves with square hole apertures of 3.15, 8, 16, and 50 mm. The most representative particle class size was between 8 to 16 mm, which is in agreement with the analysis carried out on a biomass power plant [44]. In this way, the particles within this class size were collected and used for the experimental program. At that time, and after being air-dried for approximately one month, the moisture content of the particles was observed to be between 10 to 15% (dry basis). The elemental and proximate composition of the particles was also evaluated considering the standards for solid fuel characterization (CEN/TS 15414:2006 and CEN/TS 15104:2005, respectively), and the results are presented in Table 1.

Table 1. Composition of the eucalyptus woodchips.

Proximate Analysis (wt.%, Dry Basis)		Ultimate Analysis (wt.%, Dry Ash Free)	
Volatile matter	88.90	Carbon	48.68
Ash	1.00	Hydrogen	6.91
Fixed carbon	10.10	Nitrogen	0.23
		Oxygen	44.18

2.2. Experimental Apparatus and Procedure

A lab-scale reactor to represent the different thermochemical conversion conditions of solid biomass particles was designed. During the design stage, some important constraints were addressed. The first issue was related to the possible amount of biomass in each experiment and the ease of access to the interior of the reactor in order to introduce the sample. This was particularly important in order to consider secondary reactions in the fuel bed appropriately and also to consider high heating rates of the fuel comparable to real-scale grate-fired boilers. Secondly, high flexibility regarding analytical equipment connected with the reactor, and easy handling during the experiment without any interference with the sample, was also important. Moreover, online recording of relevant operation data was paramount.

Hence, the reactor can replicate the behavior of a fuel sample used in different combustion or gasification devices and, thereby, evolve through the different reaction stages (drying, devolatilization, and char combustion). The reactor had a cylindrical shape, 200 mm in diameter and 350 mm in height. In the surrounding walls, there was a 2 kW electrical heater and refractory material to avoid heat losses. At the upper part of the reactor, there was a rotating lid with a rip of 10 mm to allow the connection of a small basket with the biomass particles to a digital scale. Furthermore, two type K thermocouples were connected to a digital temperature controller, Eurotherm brand, that controlled its operation. The desired temperature in the equipment can be defined in the set-point temperature, but there is no possibility to monitor and acquire their variation over time. There are other external devices necessary to develop the experiment. An external flowmeter and scale were used to control the gas flow rate supplied to the reactor and to measure the mass loss variation of the sample, respectively.

The weight measurement of the sample was carried out by using a perforated cylindrical basket of 60 mm in diameter and 50 mm in height inside the reactor, suspended from the digital scale by a stainless-steel wire of 2 mm in diameter. Consequently, as there were three different devices, a data acquisition and monitoring program was developed using LabVIEW software to centralize the information of the different parameters and to be able to record the data throughout the experiments. Consequently, the LabVIEW program continuously recorded the weight, air flow rate, and temperature. In addition to these devices, a portable gas analyzer, Rapidox 5100 model, was used to measure the main gas compounds (CO_2, CO, H_2, and CH_4) released during the experiment. All the gases have a ±1% full scale accuracy and a 0.1% resolution. The collection and analysis of the gas samples were only possible through the utilization of a vacuum pump and a particle and moisture filter.

Thus, the mass loss and the gas emissions during each experiment are measured over time. Figure 1 presents a schematic diagram of the apparatus involved in the macro TGA experiments.

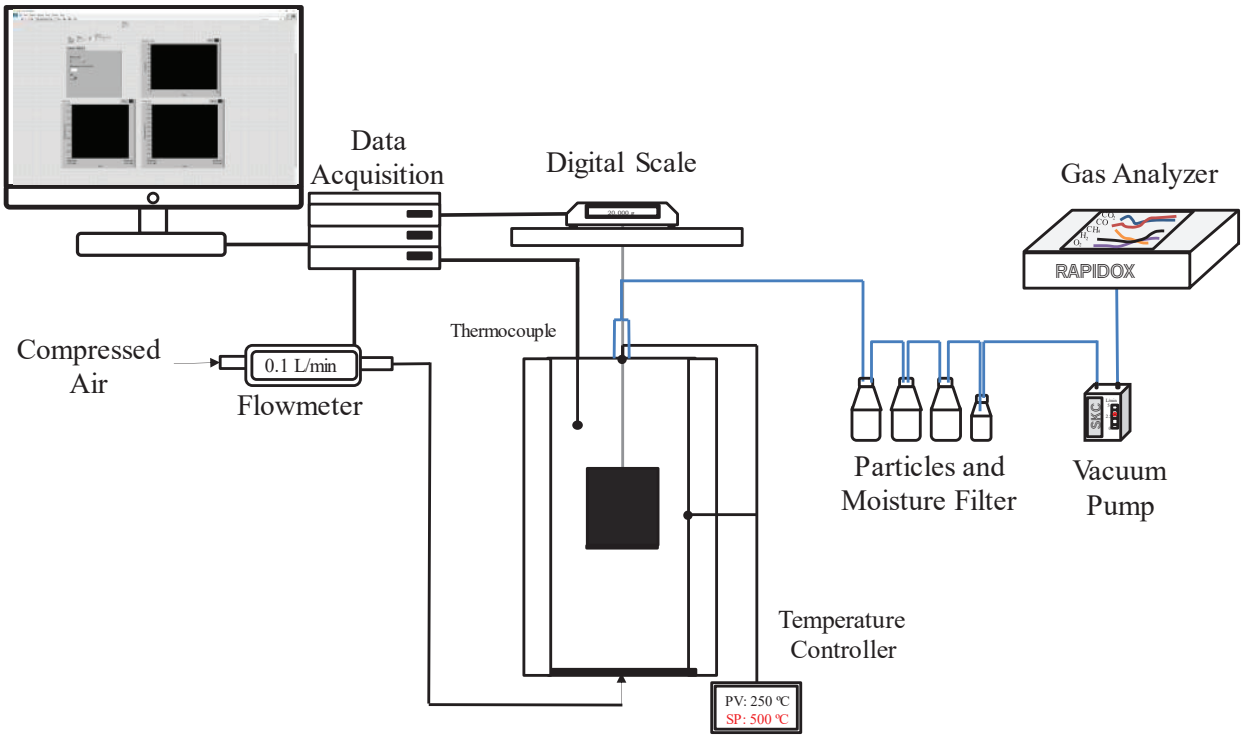

Figure 1. Experimental apparatus.

Regarding the experimental procedure, the small-scale reactor was turned on and preheated to the desired temperature before each experiment. The temperatures considered in this work were 400 and 800 °C in order to present a comprehensive view of biomass conversion over a wide temperature range. Inside the reactor, the walls radiated heat to the surface of the basket, which was in the middle of the reactor. The perforated basket allowed for an air flow to enter and react with the woodchip particles. After reaching a constant temperature in the reactor, the basket was removed, the sample with approximately 20 g was quickly loaded, and the basket was then introduced back into the reactor.

During each experiment, the air flow was controlled at different air flow rates in order to reproduce gasification and combustion regimes at any desired temperature. The air flow necessary for each conversion regime was determined by using Equations (1) and (2), which represent a stoichiometric combustion reaction and the air-to-fuel ratio (λ).

$$C_xH_yO_z + a(O_2 + 3.76\,N_2) \rightarrow b\,CO_2 + cH_2O + d\,N_2 \quad (1)$$

$$\lambda = \frac{\frac{m_{air,real}}{m_{fuel}}}{\frac{a \cdot \mathrm{M}_{air}}{x \cdot \mathrm{C} + y \cdot \mathrm{H} + z \cdot \mathrm{O}}} \quad (2)$$

Hence, taking into account the elemental composition of the eucalyptus woodchips presented in Table 1 and the reference value of the air-to-fuel ratio for gasification (0.1 to 0.3) and combustion (1.4), the air flow rate used for gasification experiments was 0.1 L/min, 15.5 for combustion experiments, and 50 L/min for experiments using 400 and 800 °C, respectively. The different air flow rates used for experiments at the highest temperature were necessary because the reaction is considerably faster than at 400 °C. The experiments were run in duplicate for 15 and 10 min for experiments at 400 and 800 °C, respectively. The average values were computed and are reported in the following section. The standard deviation during all experiments was not higher than 0.09%.

3. Results and Discussion

3.1. Thermochemical Conversion: Mass Loss

The mass loss of the samples of eucalyptus woodchips for gasification and combustion regime is presented in Figure 2. Two distinct zones can be identified, each one with a nearly linear variation with time.

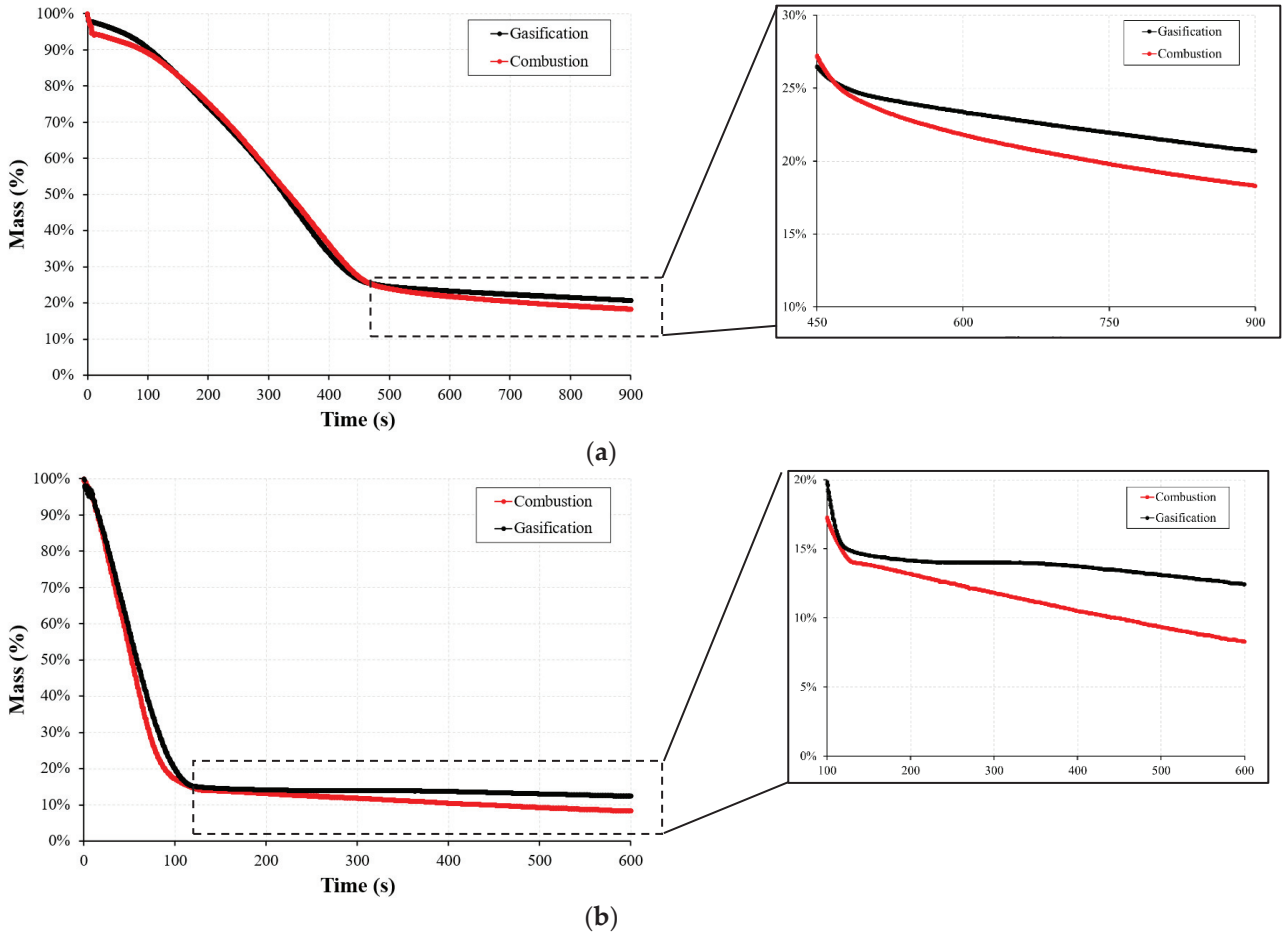

Figure 2. Mass loss curves considering the gasification and combustion regime at: (**a**) 400 °C and (**b**) 800 °C.

In the first region, which includes both the drying and devolatilization stages, there is no significant difference between gasification and combustion conversion regimes. At 400 °C the average mass loss was 75%, while at 800 °C the mass loss was approximately

85%. This suggests that temperature has a small impact on the sample's mass loss. However, temperature has a major impact on the devolatilization rate. The average mass loss rate detected was 0.16 and 0.72%/s in gasification conditions at 400 and 800 °C, respectively. However, in combustion conditions, the devolatilization rate increases from 0.16 to 0.70%/s at 400 and 800 °C, respectively. This means there is an increase of nearly four times the devolatilization rate by increasing the process temperature from 400 to 800 °C.

However, after the first region, the mass loss decreases over time but at a much slower rate. Hence, when the moisture and volatile matter are completely released, char oxidation starts and the mass loss starts to decrease more slowly. Mau et al. [45] showed this phenomena in his work by performing TGA on several char samples.

Hence, in the second region, it is possible to observe that there are differences between the mass loss curves at different thermochemical conditions and at both temperatures. For this stage, the average mass loss rate was 0.016 and 0.006%/s in gasification conditions at 400 and 800 °C, and 0.024 and 0.012%/s in combustion conditions at 400 and 800 °C, respectively. There are two main characteristics that can be noticed. In the first one, the mass loss rate was higher in combustion conditions, indicating that the presence of air enhances thermal loss due to the higher diffusion of oxygen into the solid biomass particles when compared with reduced oxygen in gasification. Simultaneously, at 400 °C the mass loss rate was higher compared with the tests performed at 800 °C for both conditions. This suggests that the remaining volatile matter that could not be devolatilized in the first stage is used to improve the char oxidation. This is in agreement to the review by Li [46] in which the author demonstrated the importance of the volatile-char interactions during the gasification process.

Furthermore, another important issue that can be observed by analyzing the mass loss curves is that the drying and devolatilization stages happen at the same time. One of the reasons might be because the moisture content of the samples was not so significant. However, higher moisture content can introduce some variance on the mass loss on a TGA experiment [47]. As it can be observed, there are no variations of the mass loss in the early stages, which states clearly that the gasification and combustion processes of larger particles do not have the sequence of distinct conversion stages when large particles are burned. In smaller samples, these two steps can be clearly identified as separate events, as the thermal gradients inside the particles are negligible [48]. Table 2 presents some characteristic parameters of the mass loss curves, which corroborate the abovementioned findings. Additionally, the results of the final mass suggest that char conversion also depends on the environment temperature. This fact is highlighted by the difference observed in the result between the experiments at low and high temperatures. Hence, mass transfer (diffusion of oxygen) and kinetics control the second mass region.

Table 2. Characteristic parameters of the mass loss curves at different regimes of thermochemical conversion in the same period of the experiment (600 s).

Temperature	Mass Loss—1st Stage (%)	Devolatilization Time (s)	Final Mass (%)
Gasification			
400 °C	74.49	466	23.35
800 °C	84.60	117	12.44
Combustion			
400 °C	75.19	477	21.80
800 °C	85.80	126	8.30

3.2. Gas Release: Product Distribution

The gases released during all conversion periods were collected. Figure 3 presents the average results from these experiments and shows, in particular, that gaseous emissions are strongly dependent on the operating temperature and the thermochemical conversion

regime. The standard deviation during all experiments was not higher than 0.5%. The remaining volume percentage corresponds to the nitrogen and oxygen content.

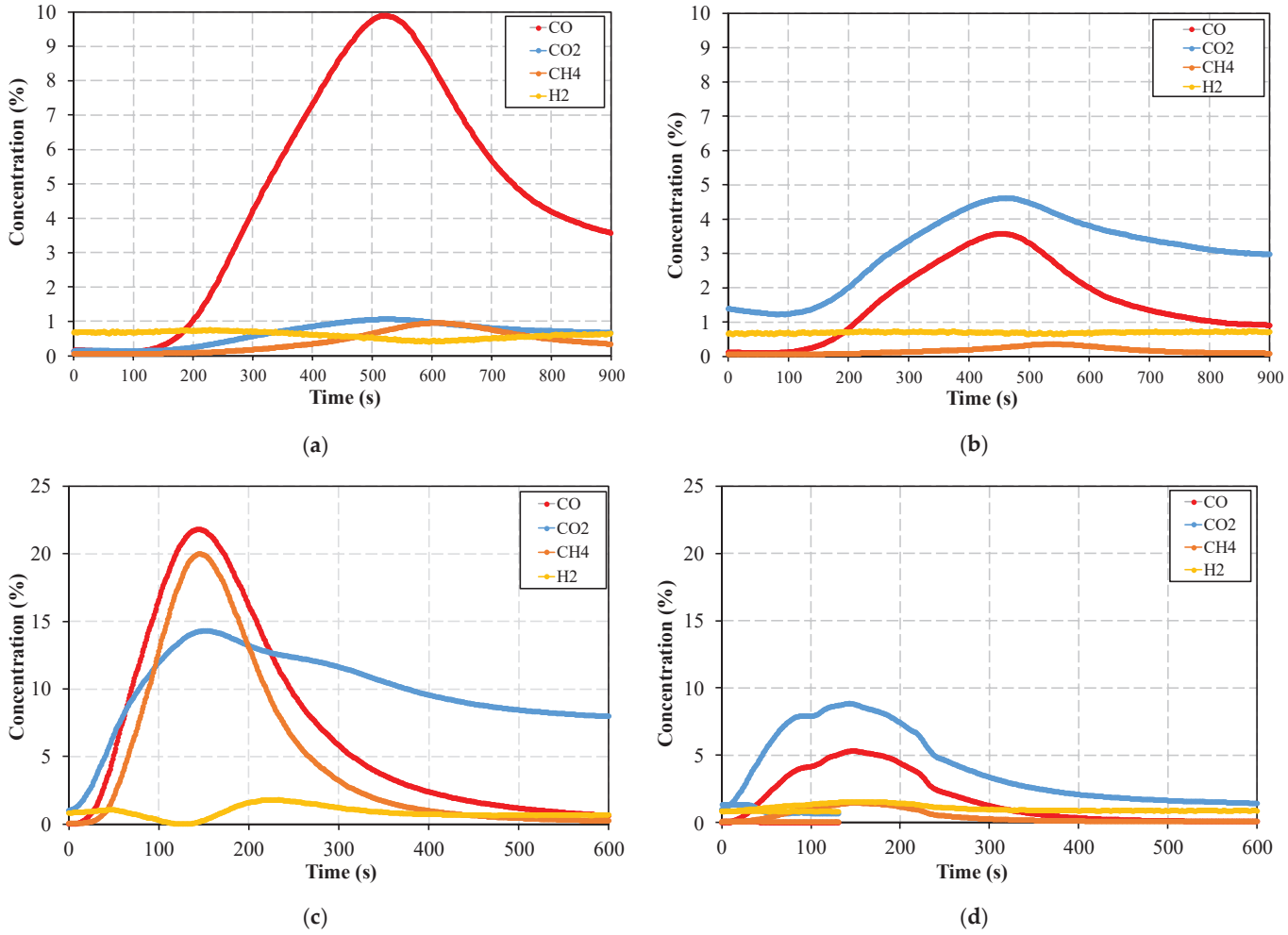

Figure 3. Gas emissions at different reactor temperatures and conversion conditions: (**a**) gasification at 400 °C, (**b**) combustion at 400 °C, (**c**) gasification at 800 °C, (**d**) combustion at 800 °C.

A similar trend was reported by Neves et al. [42], where it was found that at temperatures above 500 °C, the gaseous products strongly become temperature-dependent, leading to a substantial increase in the CO mass fractions. This was considered a result of secondary reactions, which resulted in the decrease in the tar mass fraction, also due to the conversion to CH_4. The same behavior was described by Mehrabian et al. [43] based on dedicated experiments and data collected from the literature. Secondary reactions of the volatiles are negligible at low temperatures, and most of the permanent gases result directly from biomass thermal degradation. Within the low temperature range, gases like CO and CO_2 are the main permanent gas compounds with low quantities of CH_4. As the temperature increases, secondary reactions occur, and an increase in CO and CH_4 are attributed to the decrease of tar. Here, due to higher temperatures, the yields of the volatiles have a strong correlation with the temperature and CO is considered responsible for the conversion of two-thirds of the tar.

Although the tar was not measured during the experiments, the results are in accordance with the theory. As depicted in Figure 3, there is a considerable increment of the CO from 10 to 21%, CH_4 from 1 to 20%, and CO_2 from 1 to almost 15% (peak) in gasification conditions, when increasing the temperature. In combustion conditions, the increase in temperature also enhanced the concentration of CO and CO_2 from 3.5 to 5% and 4.5 to 9%, respectively. Regarding the influence of the air in the process, at 400 °C, increasing

the air flow rate enhanced the combustion process by converting the CO into CO_2. At 800 °C, once again, the air revealed a major influence on gas conversion, specifically for the CO and CH_4 that decreased their concentration from 21 to 5% and 20 to 1%, respectively. This fact is in line with the previously mentioned findings reported in the literature. To quantify the differences between both conversion regimes and the influence of the reactor temperature, the volume of each gas compound, as well as their average value, was computed during the experiment. Table 3 presents these values and it is possible to observe that all gas compounds, except H_2, increased when the experiment was developed at 800 °C, particularly in sub-stoichiometric conditions.

Table 3. Normalized gas emissions considering the different regimes of thermochemical conversion, temperatures, and the duration of the experiment (600 s). The numbers in brackets refer to the average percentage during the experiment.

	Gasification		Combustion	
	400 °C	**800 °C**	**400 °C**	**800 °C**
Value (L/g Biomass)				
CO_2	0.32 (0.57)	3.96 (9.99)	1.43 (3.01)	1.28 (4.05)
CO	2.58 (4.50)	2.79 (7.07)	0.86 (1.82)	0.53 (1.73)
CH_4	0.18 (0.30)	2.02 (5.13)	0.08 (0.17)	0.13 (0.44)
H_2	0.32 (0.63)	0.34 (0.87)	0.32 (0.69)	0.36 (1.06)

4. Conclusions

This work presented a purpose-built facility developed to study how solid biomass fuels behave in conditions similar to those found in industrial power plants. This work stands out from the major of macro TGA in literature as it employs a single work temperature in contrast to the usual increase of the temperature on a fixed heating rate [38,49]. From a practical point of view, this information may be valuable for developing mathematical models. Hence, the mass loss profiles at different thermochemical conditions of eucalyptus woodchips are presented together with the composition of the gases released over time at two different temperatures.

The reactor proved to be a very useful equipment to analyze the combustion behavior, study the phenomena, which are relevant in an industrial furnace on a small scale, and demonstrated good reproducibility. Furthermore, the weight loss and the release quantification of the different gas compounds were particularly important to expose the differences between the different thermochemical conversion regimes. The main results and findings led to the following conclusions:

- Mainly due to the low moisture content, only two different stages can characterize the mass loss of eucalyptus woodchips at low and high temperatures with different kinetics for both thermochemical regimes.
- The first region, which corresponds to a mass loss of 75 to 85% (gasification and combustion, respectively), does not present the influence of the air flow rate, which defines the thermochemical conversion condition; however, there is a significant difference between gasification and combustion conversion at different temperatures. Therefore, the kinetics of the reaction in the devolatilization stage is mainly dependent on the temperature.
- The second conversion stage, in its turn, is dependent on the air flow rate and, therefore, dependent on the diffusion of the oxygen supplied to the solid biomass particles. However, it was verified that at the lowest reactor temperature this reaction presented a contribution of the temperature. This might be related to the remaining volatile matter that was not consumed in the devolatilization stage and was used to react with the remaining carbon.
- Regarding the gases released during all conversion periods, a strong dependency on the reactor temperature and the thermochemical conversion regime was observed.

- All gas compounds, except H_2, increased substantially with reactor temperature and, mainly, when gasification occurred. This suggests that the success of obtaining a better combustible gas during the gasification process depends substantially on process temperature [50].
- The yield of the lowest temperature, comparing both thermochemical conversion conditions, the CO and CO_2 emissions are approximately 3 times higher when gasification occurs. However, at 800 °C, the same trend was verified, while a considerable amount of CH_4 was also verified.
- The gas emissions also showed the impact of the air injection in the conversion of combustible gases and in non-combustible gases. By increasing the CO_2, CO, and CH_4, concentrations for both temperatures were reduced.
- The measurement of the gas emissions in the purpose-built facility also demonstrated a useful strategy to further define the correct boundary conditions for CFD simulations.

For future work, data concerning reaction kinetics and gas emissions will be incorporated into a numerical model to describe the thermochemical conversion behavior inside an industrial grate-fired boiler. This type of information is one of the main drawbacks of commercial simulation software. Additionally, this approach extends to other types of fuels whose behavior is less understood.

Author Contributions: Conceptualization, J.S., C.C. and J.T.; Methodology, J.S., C.C. and J.T.; Investigation, J.S.; Writing—original draft preparation, J.S., C.C., J.T. and S.T.; Writing—review and editing, J.S., C.C., J.T. and S.T.; Supervision, J.T. and S.T. All authors have read and agreed to the published version of the manuscript.

Funding: This work was supported by the Portuguese Foundation for Science and Technology (FCT) within the R&D Units Project Scope UIDB/00319/2020 (ALGORITMI), and R&D Units Project Scope UIDP/04077/2020 (MEtRICs).

Institutional Review Board Statement: Not applicable.

Informed Consent Statement: Not applicable.

Acknowledgments: The first author would like to express his gratitude for the support given by FCT through the Ph.D. Grant SFRH/BD/130588/2017.

Conflicts of Interest: The authors declare no conflict of interest.

References

1. Demirbas, A. Potential applications of renewable energy sources, biomass combustion problems in boiler power systems and combustion related environmental issues. *Prog. Energy Combust. Sci.* **2005**, *31*, 171–192. [CrossRef]
2. Ferreira, S.; Monteiro, E.; Brito, P.; Vilarinho, C. Biomass resources in Portugal: Current status and prospects. *Renew. Sustain. Energy Rev.* **2017**, *78*, 1221–1235. [CrossRef]
3. GPP—Gabinete de Planeamento Políticas e Administração Geral. Caderno de Análise e Prospetiva Cultivar. 2018. Available online: https://doi.org/2183-5624 (accessed on 11 September 2022).
4. Roman, K.; Barwicki, J.; Rzodkiewicz, W.; Dawidowski, M. Evaluation of Mechanical and Energetic Properties of the Forest Residues Shredded Chips during Briquetting Process. *Energies* **2021**, *14*, 3270. [CrossRef]
5. Anca-Couce, A.; Hochenauer, C.; Scharler, R. Bioenergy technologies, uses, market and future trends with Austria as a case study. *Renew. Sustain. Energy Rev.* **2020**, *135*, 110237. [CrossRef]
6. Basu, P. *Biomass Gasification, Pyrolysis and Torrefaction: Practical Design and Theory*, 2nd ed.; Elsevier Inc.: Amsterdam, The Netherlands, 2013; p. 530. [CrossRef]
7. Vainio, E. Fate of Fuel-Bound Nitrogen and Sulfur in Biomass-Fired Industrial Boilers. Ph.D. Thesis, Åbo Akademi University, Turku, Finland, 2014.
8. Sadaka, S.; Johnson, D. Biomass Combustion. Agriculture and Natural Resources. 2010. Available online: https://www.researchgate.net/publication/268207461_Biomass_Combustion (accessed on 11 September 2022).
9. Kirch, T.; Birzer, C.; van Eyk, P.; Medwell, P.R. Influence of Primary and Secondary Air Supply on Gaseous Emissions from a Small-Scale Staged Solid Biomass Fuel Combustor. *Energy Fuels* **2017**, *32*, 4212–4220. [CrossRef]
10. Sun, J.; Shen, Z.; Zhang, L.; Zhang, Q.; Lei, Y.; Cao, J.; Huang, Y.; Liu, S.; Zheng, C.; Xu, H.; et al. Impact of primary and secondary air supply intensity in stove on emissions of size-segregated particulate matter and carbonaceous aerosols from apple tree wood burning. *Atmos. Res.* **2017**, *202*, 33–39. [CrossRef]

11. Yin, C.; Rosendahl, L.A.; Kær, S.K. Grate-firing of biomass for heat and power production. *Prog. Energy Combust. Sci.* **2008**, *34*, 725–754. [CrossRef]
12. Perera, S.M.; Wickramasinghe, C.; Samarasiri, B.; Narayana, M. Modeling of thermochemical conversion of waste biomass—A comprehensive review. *Biofuel Res. J.* **2021**, *8*, 1481–1528. [CrossRef]
13. Ragland, K.; Aerts, D.; Baker, A. Properties of wood for combustion analysis. *Bioresour. Technol.* **1991**, *37*, 161–168. [CrossRef]
14. Hellén, H.; Hakola, H.; Haaparanta, S.; Pietarila, H.; Kauhaniemi, M. Influence of residential wood combustion on local air quality. *Sci. Total Environ.* **2008**, *393*, 283–290. [CrossRef]
15. Jia, Y.; Li, Z.; Wang, Y.; Wang, X.; Lou, C.; Xiao, B.; Lim, M. Visualization of Combustion Phases of Biomass Particles: Effects of Fuel Properties. *ACS Omega* **2021**, *6*, 27702–27710. [CrossRef] [PubMed]
16. Grønli, M.G.; Varhegyi, G.; Di Blasi, C. Thermogravimetric Analysis and Devolatilization Kinetics of Wood. *Ind. Eng. Chem. Res.* **2002**, *41*, 4201–4208. [CrossRef]
17. Chen, Z.; Hu, M.; Zhu, X.; Guo, D.; Liu, S.; Hu, Z.; Xiao, B.; Wang, J.; Laghari, M. Characteristics and kinetic study on pyrolysis of five lignocellulosic biomass via thermogravimetric analysis. *Bioresour. Technol.* **2015**, *192*, 441–450. [CrossRef]
18. Mishra, R.K.; Mohanty, K. Pyrolysis kinetics and thermal behavior of waste sawdust biomass using thermogravimetric analysis. *Bioresour. Technol.* **2018**, *251*, 63–74. [CrossRef] [PubMed]
19. Xiao, R.; Yang, W.; Cong, X.; Dong, K.; Xu, J.; Wang, D.; Yang, X. Thermogravimetric analysis and reaction kinetics of lignocellulosic biomass pyrolysis. *Energy* **2020**, *201*, 117537. [CrossRef]
20. Gaitán-Álvarez, J.; Moya, R.; Puente-Urbina, A.; Rodriguez-Zúñiga, A. Thermogravimetric, Devolatilization Rate, and Differential Scanning Calorimetry Analyses of Biomass of Tropical Plantation Species of Costa Rica Torrefied at Different Temperatures and Times. *Energies* **2018**, *11*, 696. [CrossRef]
21. Fernandez, A.; Soria, J.; Rodriguez, R.; Baeyens, J.; Mazza, G. Macro-TGA steam-assisted gasification of lignocellulosic wastes. *J. Environ. Manag.* **2018**, *233*, 626–635. [CrossRef]
22. Becidan, M.; Skreiberg, Ø.; Hustad, J.E. Products distribution and gas release in pyrolysis of thermally thick biomass residues samples. *J. Anal. Appl. Pyrolysis* **2007**, *78*, 207–213. [CrossRef]
23. Brunner, T.; Biedermann, F.; Kanzian, W.; Evic, N.; Obernberger, I. Advanced Biomass Fuel Characterization Based on Tests with a Specially Designed Lab-Scale Reactor. *Energy Fuels* **2013**, *27*, 5691–5698. [CrossRef]
24. Gauthier, G.; Melkior, T.; Grateau, M.; Thiery, S.; Salvador, S. Pyrolysis of centimetre-scale wood particles: New experimental developments and results. *J. Anal. Appl. Pyrolysis* **2013**, *104*, 521–530. [CrossRef]
25. Weissinger, A. In situ FT-IR spectroscopic investigations of species from biomass fuels in a laboratory-scale combustor: The release of nitrogenous species. *Combust. Flame* **2004**, *137*, 403–417. [CrossRef]
26. Bennadji, H.; Smith, K.; Shabangu, S.; Fisher, E. Low-Temperature Pyrolysis of Woody Biomass in the Thermally Thick Regime. *Energy Fuels* **2013**, *27*, 1453–1459. [CrossRef]
27. Nikku, M.; Deb, A.; Sermyagina, E.; Puro, L. Reactivity characterization of municipal solid waste and biomass. *Fuel* **2019**, *254*, 115690. [CrossRef]
28. Hu, Q.; He, X.; Yao, Z.; Dai, Y.; Wang, C.-H. Gaseous production kinetics and solid structure analysis during isothermal conversion of biomass pellet under different atmospheres. *J. Energy Inst.* **2021**, *98*, 53–62. [CrossRef]
29. Baumgarten, B.; Reinhardt, J.; Lepski, C.; Risio, B.; Thorwarth, H. Kinetics of Wood Devolatilization during Start-up. *Energy Fuels* **2019**, *33*, 11285–11291. [CrossRef]
30. Samuelsson, L.N.; Umeki, K.; Babler, M.U. Mass loss rates for wood chips at isothermal pyrolysis conditions: A comparison with low heating rate powder data. *Fuel Process. Technol.* **2017**, *158*, 26–34. [CrossRef]
31. Orang, N.; Tran, H. Effect of feedstock moisture content on biomass boiler operation. *TAPPI J.* **2015**, *14*, 629–637. [CrossRef]
32. Bin Yang, Y.; Ryu, C.; Khor, A.; Sharifi, V.N.; Swithenbank, J. Fuel size effect on pinewood combustion in a packed bed. *Fuel* **2005**, *84*, 2026–2038. [CrossRef]
33. Ryu, C.; Yang, Y.B.; Khor, A.; Yates, N.E.; Sharifi, V.N.; Swithenbank, J. Effect of fuel properties on biomass combustion: Part I. Experiments—Fuel type, equivalence ratio and particle size. *Fuel* **2006**, *85*, 1039–1046. [CrossRef]
34. Mahmoudi, A.H.; Markovic, M.; Peters, B.; Brem, G. An experimental and numerical study of wood combustion in a fixed bed using Euler–Lagrange approach (XDEM). *Fuel* **2015**, *150*, 573–582. [CrossRef]
35. Wurzenberger, J.C.; Wallner, S.; Raupenstrauch, H.; Khinast, J. Thermal conversion of biomass: Comprehensive reactor and particle modeling. *AIChE J.* **2002**, *48*, 2398–2411. [CrossRef]
36. Markovic, M.; Bramer, E.A.; Brem, G. Experimental investigation of wood combustion in a fixed bed with hot air. *Waste Manag.* **2014**, *34*, 49–62. [CrossRef] [PubMed]
37. Erić, A.; Nemoda, S.; Komatina, M.; Dakić, D.; Repić, B. Experimental investigation on the kinetics of biomass combustion in vertical tube reactor. *J. Energy Inst.* **2019**, *92*, 1077–1090. [CrossRef]
38. Long, Y.; Zhou, H.; Meng, A.; Li, Q.; Zhang, Y. Interactions among biomass components during co-pyrolysis in (macro)thermogravimetric analyzers. *Korean J. Chem. Eng.* **2016**, *33*, 2638–2643. [CrossRef]
39. Fraga, L.G.; Silva, J.; Teixeira, J.C.; Ferreira, M.E.C.; Teixeira, S.F.; Vilarinho, C.; Gonçalves, M.M. Study of Mass Loss and Elemental Analysis of Pine Wood Pellets in a Small-Scale Reactor. *Energies* **2022**, *15*, 5253. [CrossRef]
40. Jiang, M.; Lai, A.; Law, A. Solid Waste Incineration Modelling for Advanced Moving Grate Incinerators. *Sustainability* **2020**, *12*, 8007. [CrossRef]

41. Thunman, H.; Niklasson, F.; Johnsson, F.; Leckner, B. Composition of Volatile Gases and Thermochemical Properties of Wood for Modeling of Fixed or Fluidized Beds. *Energy Fuels* **2001**, *15*, 1488–1497. [CrossRef]
42. Neves, D.; Thunman, H.; Matos, A.; Tarelho, L.; Gómez-Barea, A. Characterization and prediction of biomass pyrolysis products. *Prog. Energy Combust. Sci.* **2011**, *37*, 611–630. [CrossRef]
43. Mehrabian, R.; Shiehnejadhesar, A.; Scharler, R.; Obernberger, I. Multi-physics modelling of packed bed biomass combustion. *Fuel* **2014**, *122*, 164–178. [CrossRef]
44. Silva, J.P.; Teixeira, S.; Grilo, É.; Peters, B.; Teixeira, J.C. Analysis and monitoring of the combustion performance in a biomass power plant. *Clean. Eng. Technol.* **2021**, *5*, 100334. [CrossRef]
45. Mau, V.; Gross, A. Energy conversion and gas emissions from production and combustion of poultry-litter-derived hydrochar and biochar. *Appl. Energy* **2018**, *213*, 510–519. [CrossRef]
46. Li, C.-Z. Importance of volatile–char interactions during the pyrolysis and gasification of low-rank fuels—A review. *Fuel* **2013**, *112*, 609–623. [CrossRef]
47. Magdziarz, A.; Werle, S. Analysis of the combustion and pyrolysis of dried sewage sludge by TGA and MS. *Waste Manag.* **2014**, *34*, 174–179. [CrossRef]
48. Fraga, L.G.; Silva, J.; Teixeira, S.; Soares, D.; Ferreira, M.; Teixeira, J. Influence of Operating Conditions on the Thermal Behavior and Kinetics of Pine Wood Particles Using Thermogravimetric Analysis. *Energies* **2020**, *13*, 2756. [CrossRef]
49. Skreiberg, A.; Sandquist, J.; Sørum, L. TGA and macro-TGA characterisation of biomass fuels and fuel mixtures. *Fuel* **2011**, *90*, 2182–2197. [CrossRef]
50. Basu, P. *Biomass Gasification, Pyrolysis and Torrefaction: Pratical Design and Theory*, 3rd ed.; Academic Press: Cambridge, MA, USA, 2018. [CrossRef]

processes

MDPI

Article

Chemical and Functional Characterization of Extracts from Leaves and Twigs of *Acacia dealbata*

Ricardo Correia [1], Maria Paula Duarte [1], Elisabete Muchagato Maurício [2], João Brinco [3], José Carlos Quintela [4], Marco Gomes da Silva [5] and Margarida Gonçalves [1,6,*]

[1] MEtRICs/NOVA School of Science and Technology, Universidade NOVA de Lisboa, Campus de Caparica, 2829-516 Caparica, Portugal
[2] Faculty of Engineering/CBIOS, Universidade Lusófona, 1749-024 Lisboa, Portugal
[3] CENSE-Center for Environmental and Sustainability Research & CHANGE—Global Change and Sustainability Institute, NOVA School of Science and Technology, Universidade NOVA de Lisboa, Campus de Caparica, 2829-516 Caparica, Portugal
[4] Natac Biotech, C/Electrónica 7, 28923 Alcorcón, Madrid, Spain
[5] LAQV/REQUIMTE, Department of Chemistry, NOVA School of Science and Technology, Universidade NOVA de Lisboa, Campus de Caparica, 2829-516 Caparica, Portugal
[6] VALORIZA-Research Center for Endogenous Resource Valorization, Polytechnic Institute of Portalegre, 7300-555 Portalegre, Portugal
* Correspondence: mmpg@fct.unl.pt

Abstract: The purpose of this work was to evaluate the recovery of bioactive extracts from *Acacia dealbata* leaves and twigs and to characterize their chemical composition and functional properties. Fresh and air-dried samples were extracted by maceration at room temperature and by hot extraction at 60 °C using aqueous solutions of acetone, ethanol, and methanol. The highest extraction yields (14.8 and 12.0% for dried leaves and twigs, respectively) were obtained with 70% acetone, for both extraction procedures. Extracts were characterized for total phenolics content (TPC), total flavonoid content (TFC) and total proanthocyanidin content (TPrAC). Bioactive extracts with high TPC (526.4 mg GAE/g extract), TFC (198.4 mg CatE/g extract), and TPrAC (631.3 mg PycE/g extract) were obtained using maceration, a technically simple and low-energy process. The non-polar fraction of selected extracts was characterized using gas chromatography and time of flight mass spectrometry (GC-TOFMS). The main components detected were phytol, squalene, α-tocopherol, lupenone, and lupeol. The antioxidant activity of the extracts was characterized through DPPH and FRAP assays. Antimicrobial activity of the extracts against different bacteria was also determined. The highest DPPH and FRAP activities were obtained from dried twigs from Alcobaça (1068.3 mg TE/g extract and 9194.6 mmol Fe^{2+}/g extract, respectively). Extracts from both leaves and twigs showed antimicrobial properties against *Staphylococcus aureus*, *Staphylococcus epidermidis*, methicillin resistant *Staphylococcus aureus* (MRSA), *Enterococcus faecalis*, *Bacillus cereus*, *Streptococcus mutans*, and *Streptococcus mitis*. The results obtained demonstrate the feasibility of recovering valuable components from these biomass fractions that may be further valorized for energy production in a biorefinery concept.

Keywords: *Acacia dealbata*; leaves; twigs; antioxidant; antimicrobial; invasive species

1. Introduction

The genus *Acacia* comprises more than 1350 species distributed throughout tropical and warm temperate areas of the world [1]. Most of those species are native to Australia but spread all over the world due to a wide variety of useful applications such as sand and dunes stabilization, extraction of tannins, essences or gums, valorization as timber or fodder crop, and production of biofuels [2–4]. The ability to easily adapt to changing environments, the large seed production and accumulation of massive seed banks for long

periods, the high capacity for reproduction after fires and cuttings, and the allelopathic properties are some of the characteristics that contribute to the success of *Acacia* spp. as invaders, leading to negative impacts on ecosystem biodiversity [5–7].

A. dealbata is one of the most widespread *Acacia* species [7,8] and is classified as invasive in Portuguese territory [9]. Periodic removal operations to minimize its proliferation generate high amounts of biomass that is usually burned for energy production or landfilled, but these solutions are not economically sustainable due to the high costs of biomass collection and transportation. However, different fractions of *Acacia* spp. biomass have been evaluated as raw materials to produce functional extracts that can be used in the nutraceutical, cosmetic, or food industries. In fact, it is widely documented that bark, wood, leaves, flowers, pods, seeds or roots of *Acacia* spp. are rich in bioactive secondary metabolites (e.g., amines and alkaloids, cyanogenic glycosides, cyclitols, fatty acids and seed oils, gums, non-protein amino acids, terpenes, tannins and other flavonoids, and simple phenolics) [4,10] and have been used in traditional medicine for a wide range of ailments, such as diabetes, worm infection, dysmenorrhea, eczema, malaria, gout, jaundice, abdominal pain, kidney problems, constipation, leprosy, piles, pneumonia, rheumatism, fever, and cancer [11].

Plant extracts are known for their ability to act as antioxidants and reduce oxidative stress [12], a physiologic condition considered to play a key role in the pathogenesis of several degenerative diseases, such as cardiovascular diseases, diabetes neurodegeneration, or cancer [13]. Additionally, it has been reported that plant secondary metabolites also possess antimicrobial properties, which is important in the development of alternatives to antibiotics due to the increasing resistance to conventional antimicrobial agents [14]. Therefore, the production of bioactive extracts from *A. dealbata* biomass is an additional pathway for the valorization of these biomass materials, complementing energy applications and contributing to the sustainability of the forest cleaning and management actions, reducing the risk of fire, and improving the social-economic development of rural areas.

Extraction of value-added components from *Acacia* spp. has been focused mainly on the bark, flower, wood, and leaves as reviewed by Correia et al. [15]. Concerning the leaves fraction, antioxidant or antimicrobial activities have been determined for *A. farnesiana* [16], *A. karroo* [17–20], *A. longifolia* [21], *A. pycnantha* [22,23], *A. saligna* [24–27], or *A. nilotica* [28]. The antioxidant and antimicrobial activities of *A. dealbata* leaves were evaluated by Borges et al. [29], for acetonic and ethanolic extracts of fresh *A. dealbata* leaves, obtained with different extraction methods. Ethanolic extracts of dried *A. dealbata* leaves were also found to have antimicrobial activity against the food poisoning agent *Bacillus cereus* [30].

Research on extraction of functional components from twigs of *Acacia* spp. is scarce. Extracts of *A. nilotica* twigs were characterized for antimicrobial activity against oral pathogens [31–34], while extracts of *A. pennata* twigs were described as having some potential application in the prevention of Alzheimer's disease [35].

The extraction methods explored so far included solid-liquid extraction for a predetermined period under agitation at room temperature (1 h [29], 8 h [34], or 2 days [30,33]) ultrasound-assisted extraction [29], Soxhlet [29,35], microwave-assisted extraction [29], cold percolation [31], and supercritical fluid extraction [32,36]. Most of these methods are energy-consuming or involve high investment costs and may promote thermal degradation of the extract components [37].

This study aimed to investigate the production of bioactive extracts from leaves and twigs of *A. dealbata*, using maceration at room temperature, a method with low energy requirements and easy to implement on an industrial scale. Extraction with different aqueous solvents (acetone, ethanol, and methanol) was applied to fresh and dried biomass, collected in two different locations to evaluate the influence of solvent polarity, biomass water content, and geographic origin on the characteristics of the extracts, namely their yield, composition, and properties. To the best of our knowledge, this is also the first study on the production and characterization of bioactive extracts from *A. dealbata* twigs. The

extracts were characterized for mass yield, total phenolic content, total flavonoid content, total proanthocyanidins content, in vitro antioxidant activity tests, and antimicrobial activity against several bacteria and yeasts. To identify non-polar components that might contribute to the antioxidant or antimicrobial properties of the extracts, a representative set of leaves and twigs extracts were fractionated and characterized by GC-TOFMS.

2. Materials and Methods

2.1. Plant Material

Branches of at least ten different *A. dealbata* trees of Caparica (CAP) and Alcobaça (ALC) regions were collected. Samples of around 500 g of branches were collected from each tree and combined to obtain a composite sample from that geographical origin. For each composite sample, leaves were separated from the twigs and both fractions were analyzed separately. Fresh and dried leaves and twigs were manually cut into small pieces about 1 cm in length before impregnation with the solvent.

2.2. Chemicals and Reagents

Acetone, ethanol 96°, methanol, and petroleum ether used in the extraction processes were purchased from CarloErba Reagents (Val de Reuil, France). Folin-Ciocalteau reagent (Panreac, Barcelona, Spain), sodium carbonate (Labkem, Barcelona, Spain), and gallic acid (Merck, Darmstadt, Germany) were used to determine phenolics content. The reagents sodium nitrite ($NaNO_2$), sodium hydroxide (NaOH), and aluminium chloride ($AlCl_3$) used in the determination of flavonoids were all purchased from Merck (Darmstadt, Germany). Butanol (Panreac, Barcelona, Spain), ferrous sulfate heptahydrate ($FeSO_4 \cdot 7H_2O$) (Panreac, Barcelona, Spain), hydrochloric acid (Chem-Lab NV, Zedelgem, Belgium), and Pycnognol® (generously provided by Horphag Research Ltd, Geneva, Switzerland) were used in the acid-butanol assay. The reagent 2,2-diphenyl-1-picrylhydrazyl (DPPH) (Sigma-Aldrich, St. Louis, MO, USA) was used in the DPPH assay. The reagents 2,4,6-tris(2-pyridyl)-s-triazine (TPTZ), acetate buffer 3.6, iron (III) chloride ($FeCl_3$), and iron (II) sulfate ($FeSO_4$) used in the ferric reducing antioxidant power (FRAP) assay were also purchased from Merck (Darmstadt, Germany). Ketoconazole, ofloxacin and vancomycin were purchase from Sigma-Aldrich (St. Louis, MO, USA). Brain heart infusion agar (BHIA) was purchased from Merck (Darmstadt, Germany). Mueller-Hinton agar (MHA), Sabouraud dextrose agar (SDA) and Trypto casein-soy agar (TSA) were purchase from Biokar diagnostics (Allonne, France).

2.3. Extraction Procedure

A portion of leaves and twigs was processed in a fresh state, during the first 24 h from harvest, while the remaining biomass was left to dry in air, at room temperature, until a constant weight was attained. Two extraction methods were compared with the fresh and dried raw material: maceration at room temperature for 48 h in the case of the leaves and 24 h for the twigs; extraction times were selected for leaves and twigs as the maceration time necessary to achieve constant values of extract yield and extract composition according to a previous study (Supplementary Materials; Table S2). Hot extraction was performed at 60 °C for 1 h, for both leaves and twigs, to evaluate the effect of temperature in extract yield and properties. Higher temperatures were not selected to avoid thermal degradation of the extracts. Maceration and hot extraction were performed in a single step, at a biomass:solvent ratio of 1:6 (w:v), using 70% of aqueous acetone (70% ACE), 70% aqueous ethanol (70% ET), and 70% of aqueous methanol (70% MET) as extraction solvents. After the extraction period, the liquid extract was separated from the biomass by filtration and stored at −20 °C until analysis. An adequate aliquot was evaporated to dryness at reduced pressure to determine the mass yield (expressed as percentage, on a wet basis). The extraction process was made in duplicate for each one of the four biomass samples of leaves and twigs (fresh and dried material, from Caparica and Alcobaça).

Extraction of spent raw material was also assessed after the removal of lipophilic components by petroleum ether. Dried leaves and twigs were extracted with petroleum ether by maceration at room temperature using a biomass:solvent ratio of 1:5, and the lipophilic extracts were stored for subsequent analysis and not included in this study. The spent biomass was left to dry in air at room temperature and then submitted to extraction of polar components by maceration at room temperature with 70% ACE at the same conditions that were used for the raw leaves and twigs. Mass yields were determined as described above, and the extracts were stored at −20 °C until analysis.

2.4. Extracts Characterization

Total phenolic content (TPC) of the extracts was measured by the Folin-Ciocalteu method, following an adaptation of the method described by Singleton et al. [38]. Briefly, 0.5 mL of extract, 2 mL of distilled water, and 0.5 mL of Folin-Ciocalteu reagent were added to a test tube and allowed to stand for 5 min. Then, 2 mL of aqueous sodium bicarbonate (10% m/V) were added, and the mixture was incubated for 1 h in the dark. Absorbance was then measured at 760 nm and total phenolic content was determined using a calibration curve constructed with gallic acid standards. Results were expressed as gallic acid equivalents (mg GAE/g of dry extract, and mg GAE/g of fresh biomass).

Total flavonoid content was determined as described by Barros et al. [39]. Briefly, 0.5 mL of extract was mixed with 2 mL of distilled water and subsequently with 0.15 mL of $NaNO_2$ solution (5%). After 6 min, 0.15 mL of $AlCl_3$ solution (10%) was added and allowed to stand further 6 min. After this period 2 mL of NaOH solution (4%) was added to the mixture, and distilled water was then added to bring the final volume to 5 mL. Then, the mixture was completely mixed and allowed to stand for 15 min. Finally, absorbance was measured at 510 nm (Biochrom Libra S4). The results were expressed in catechin equivalents (mg CatE/g of dry extract, and mg CatE/g of fresh biomass). A calibration curve was also made using rutin as a standard for comparison of the results with the ones found in the literature expressed in rutin equivalents (mg RE/g of dry extract, and mg RE/g of fresh biomass).

Total proanthocyanidin content (TPrAC) was determined by the butanol-HCl assay, exactly as described by Skerget et al. [40]. Briefly, 5 mL of an acidic ferrous solution (77 mg $FeSO_4 \cdot 7H_2O$ in 500 mL HCl/BuOH (2/3)) was added to 0.5 mL of the extract. The tubes were covered and put in a water bath at 95 °C for 15 min. The absorbance was read at 540 nm (Biochrom Libra S4). The same procedure was made using a proanthocyanidin commercial extract (Pycnogenol®) to build a calibration curve, and the results were expressed as Pycnogenol® equivalents (mg PycE/g of dry extract, and mg PycE/g of fresh biomass).

Antioxidant activity was evaluated by the DPPH free radical scavenging assay and by the ferric reducing antioxidant power assay. For the DPPH assay [41], 0.5 mL of extract were mixed with 4 mL of DPPH solution (2,2-diphenyl-1-picrylhydrazyl at 45 mg/L in methanol), and then incubated at room temperature for 30 min. After incubation, absorbance was measured at 517 nm and the results were expressed in Trolox equivalents by using a calibration curve obtained with Trolox as a standard (mg TE/g of dry extract, and mg TE/g of fresh biomass).

The FRAP assay was carried out using the procedure of Benzie and Strain with slight modifications [42]. The FRAP reagent was prepared from 0.3 M acetate buffer (pH 3.6), 10 mM TPTZ solution in 40 mM HCl, and 20 mM iron (III) chloride solution in proportions of 10:1:1 (v/v), respectively. This reagent was freshly prepared before analysis and warmed to 37 °C in a water bath prior to use. One hundred microliters of sample were added to 3 mL of the FRAP reagent and the mixture was kept at 37 °C for 30 min. After this period, absorbance was recorded at 593 nm. A standard curve was made using iron (II) sulfate solution, and the results were expressed as mmol Fe(II)/g of dry extract and as mmol Fe(II)/g of fresh biomass.

In all these characterization assays, two replicates of each sample were analyzed in triplicate.

2.5. Antimicrobial Activity

Antimicrobial activity was assayed against Gram-negative bacteria (*Escherichia coli* ATCC® 8739™ and *Pseudomonas aeruginosa* ATCC® 9027™), Gram-positive bacteria (*Staphylococcus aureus* ATCC® 6538™, *Staphylococcus epidermidis* ATCC®12228™, methicillin resistant *Staphylococcus aureus* (MRSA) ATCC® 33591™, *Enterococcus faecalis* ATCC® 29212™, *Bacillus cereus* ATCC®11778™, *Streptococcus mutans* ATCC®25175™ and *Streptococcus mitis* NCIMB®13770) and a yeast (*Candida albicans* ATCC® 10231™). All microbial strains were kept at −70 °C in broth with glycerol (15% *v*/*v*). The antimicrobial activity was assessed by the well-diffusion assay, according to Pereira et al. [43]. Briefly, microorganisms were subcultured on TSA (*E. coli*, *P. aeruginosa*, *S. Choleraesuis*, *S. aureus*, MRSA, *S. epidermidis*, *E. faecalis* and *B. cereus*), BHIA (*S. mutans* and *S. mitis*) or SDA (*C. albicans*) and incubated at 30 ± 2 °C (*B. cereus* and *C. albicans*) or 35 ± 2 °C (remaining bacteria). Isolated colonies were suspended in saline medium (NaCl, 0.85% *w*/*v*), and the turbidity was adjusted to 0.5 on the McFarland scale (approx. 1–2 × 10^8 CFU/mL for bacteria and 1–5 × 10^6 CFU/mL for yeasts) (DEN-1B McFarland Densitometer, Grant-bio). Subsequently, microbial suspensions were spread on BHIA (*S. mutans* and *S. mitis*) or MHA (remaining microorganisms) Petri dishes, wells (6 mm in diameter) were aseptically punched, and 50 µL of extracts (10 mg/mL) were poured into the wells. The plates were incubated, in the dark, for 24 h at 30 ± 2 °C (*B. cereus* and *C. albicans*) or 35 ± 2 °C (remaining bacteria). Antimicrobial activity was evaluated by measuring the diameter of the growth inhibition zone (mm) around the well. Paper disks impregnated with vancomycin (Gram-positive bacteria), ofloxacin (Gram-negative bacteria) and ketoconazole (*C. albicans*) were used as positive controls. Ethanol (70% *w*/*v*) was used as a negative control. Data are presented as the mean ± standard deviation. All the determinations were performed in triplicates.

2.6. GC-TOFMS Analysis

The extracts selected for analysis of non-polar components were derivatized using a procedure adapted from Popova et al. [44]. Briefly, 2 mL of each extract was evaporated to dryness and the residue was diluted in 100 µL of pyridine and 100 µL of the derivatizing agent N,O-bis(trimethylsilyl)trifluoroacetamide (BSTFA); the mixture was incubated at room temperature for 12 h, diluted in petroleum ether (1.5 mL), dried with anhydrous sodium sulphate and kept at −5 °C until analysis. Analyses were performed with an Agilent 7890B (Palo Alto, CA, USA) gas chromatograph equipped with a multi-mode inlet. An Agilent HP-5MS UI fused silica capillary column (30 m × 0.25 mm i.d., 0.25 µm d f—film thickness) was used in all separations. An aliquot of the derivatized sample (1 µL) was injected via a LECO L-PAL3 autosampler fitted with a 10 µL syringe. The injector was operated in solvent vent mode, with the split valve opened at 100 mL/min for 25 s, and the injector at 70 °C. Then, the split valve was closed for 120 s, and the inlet temperature was raised to 300 °C at 700 °C/min. Finally, the split valve was opened again at 20 mL/min until the end of the run. The oven program was as follows: 50 °C for 1 min, then 7 °C/min until 100 °C, then 3 °C/min until 220 °C, and finally 10 °C/min until 295 °C, held for 8 min. The transfer line to the MS was kept at 300 °C. Detection was performed with a LECO Pegasus BT Time-of-Flight mass spectrometer (Saint Joseph, MI, USA). The MS was operated with the ion source at 250 °C, electron ionization at 70 eV, acquisition from m/z 40 to 550, 10 spectra per second and an acquisition delay of 480 s for liquid samples. Data acquisition, system control and spectra deconvolution were performed using LECO ChromaTOF version 5.40. NIST MS Search Program Version 2.3 g was used for spectra matching (NIST, 2015). Linear retention index (LRIs) values for sample peaks were calculated by analyzing the commercial alkane standard solution C8–C40, using the aforementioned chromatographic conditions [45].

2.7. Statistical Analysis

Statistical analysis of the results was performed using the SPSS software, version 23 (IBM Analytics, Armonk, NY, USA). Analysis of variance (ANOVA) was performed to

evaluate significant differences between averages, and the Tukey post hoc test ($p < 0.05$) was used to perform multiple comparisons between averages.

3. Results and Discussion

3.1. Extract Yield and Composition

The recovery of bioactive extracts from *A. dealbata* leaves and twigs was evaluated for different extraction methods (maceration at room temperature and hot extraction), different solvents (70% ACE, 70% ET, and 70% MET), different geographical origins (Caparica and Alcobaça) and for different biomass water contents (fresh biomass and dried biomass).

Leaves and twigs were collected in Alcobaça (39°36′36.5″ N; 8°59′45.0″ W, at 32–40 m of altitude) and Caparica (38°37′22.6″ N; 9°10′38.5″ W, at 44–48 m of altitude). Both locations are classified as Csb (Warm-summer Mediterranean climate) according to Köppen-Geiger's classification system for climate but with some differences between them. Monthly average daily temperatures are in similar ranges (10.6–20.4 °C for Alcobaça and 11.6–21.9 °C for Caparica), but Alcobaça is characterized by a higher level of annual rainfall (696 mm against 591 mm) and relative humidity (73–81% against 68–80%) [46,47]. The fresh leaves and twigs that were processed in the first 24 h from the collection had moisture contents in the ranges of 47.7–58.3% and 43.4–51.9%, respectively. After air-drying at room temperature, moisture contents were in the range of 8.1–9.3% for leaves and 8.8–11.2% for twigs.

Extraction yields and compositions (TPC, TFC, and TPrAC contents) for the extracts obtained leaves and twigs, and the different extraction conditions are presented in Table 1.

Making an overall analysis of this set of data, significantly higher extraction yields were obtained for dried raw material, and significantly higher TPC, TFC, and TPrAC contents were found in the extracts produced with 70% ACE (except for hot extraction from twigs). The TPC, TFC, and TPrAC contents of twigs extracts with 70% ACE were also higher than those contents in the leaves extracts obtained with the same solvent.

The extraction yield obtained for leaves with 70% ACE (10.5–15.8%, on a wet basis) was higher than the ones reported by Borges et al. for *A. dalbata* leaves, extracted with different solvents (water, methanol, ethanol, acetone, dichloromethane, and hexane) and extraction methods (maceration under agitation, Soxhlet, and the use of ultrasound and microwaves), and solvent-to biomass ratio of 1:10, that were in the range of 2.8–12.0% of fresh weight [29]. Extraction yields were also higher than those observed by Luís et al. [48] for ethanolic, hydroethanolic (1:1 in volume basis), methanolic, and acetonic extracts of aerial parts (wood, bark, and leaves) of *A. dealbata* (3.26–9.51% dry weight) using Soxhlet extraction and were in the same range of the described for *A. melanoxylon* aerial parts (11.88–15.41% dry weight) by the same authors. Concerning twigs, Lomarat et al. found an extraction yield of dried *A. pennata* twigs of 15.1%, obtained by Soxhlet extraction with methanol [35].

For the best extraction solvent (70% ACE), TPC in leaves and twigs extracts varied in the range 345.8–478.4 mg GAE/g extract and 367.1–526.5 mg GAE/g extract, respectively. These contents are higher than those found by Luís et al. [48] in extracts of aerial parts of *A. dealbata* (203.10–290.65 mg GAE/g extract) and *A. melanoxylon* (100.10–138.76 mg GAE/g extract), and higher than the reported for *A. farnesiana* leaves extracts (63.2–247.9 mg GAE/g extract) [49], similar to the TPC contents found for *A. mearnsii* (163.9–646.6 mg GAE/g extract) [50], *A. tortilis* (260.7–512.4 mg GAE/g extract) [49], *A. nilotica* (42.18–116.60 mg GAE/g extract) [51], and *A. ataxacantha* (63.26–115.57 mg GAE/g extract) [51] leaves extracts, but lower than the observed for *A. longifolia* leaves extracts (524.9–858.8 mg GAE/g extract) [49]. Leaves and twigs are important sources of phenolics, with contents of 36.2–71.2 mg GAE/g of fresh leaves and 30.1–59.9 mg GAE/g of fresh twigs, respectively (see full results in Supplementary Material, Table S1). These are in a similar range as what was observed by Ferreira-Santos et al. [52] with *Pinus pinaster* bark, a known source of phenolic compounds, which gave 65.1 and 68.2 mg GAE/g of bark by extraction with 70% and 50% aqueous ethanol, respectively.

Table 1. Extraction yields (%, wet basis), TPC (mg GAE/g extract), TFC (mg CatE/g extract), and TPrAC (mg PycE/g extract) of extracts from fresh and dried leaves and twigs from Alcobaça (ALC) and Caparica (CAP), using different extraction solvents and extraction methods; TPC, TFC, and TPrAC expressed relative to the mass of biomass are presented in the Supplementary Material, Table S1.

	Samples	Maceration at Room Temperature			Hot Extraction		
		70% ACE	70% ET	70% MET	70% ACE	70% ET	70% MET
Leaves							
Yield	Fresh (ALC)	12.2 ± 0.1^{h}	10.8 ± 0.1^{j}	11.6 ± 0.1^{i}	12.2 ± 0.1^{h}	11.0 ± 0.1^{j}	9.9 ± 0.1^{l}
	Fresh (CAP)	10.5 ± 0.2^{k}	10.0 ± 0.1^{l}	9.8 ± 0.1^{l}	12.3 ± 0.1^{i}	9.8 ± 0.1^{l}	9.9 ± 0.1^{l}
	Dried (ALC)	14.8 ± 0.1^{c}	14.4 ± 0.1^{de}	14.1 ± 0.1^{de}	15.8 ± 0.1^{a}	13.5 ± 0.1^{f}	13.0 ± 0.1^{g}
	Dried (CAP)	14.0 ± 0.1^{e}	14.3 ± 0.1^{de}	13.5 ± 0.1^{f}	15.6 ± 0.1^{a}	15.8 ± 0.1^{a}	15.2 ± 0.1^{b}
TPC	Fresh (ALC)	449.1 ± 8.0^{b}	338.9 ± 6.6^{ghi}	329.0 ± 7.6^{ijk}	428.4 ± 3.7^{c}	361.0 ± 5.9^{de}	336.7 ± 6.9^{hj}
	Fresh (CAP)	345.8 ± 4.0^{fgh}	295.8 ± 6.4^{m}	288.3 ± 3.4^{mn}	352.6 ± 5.8^{def}	324.5 ± 9.5^{kl}	314.7 ± 7.6^{l}
	Dried (ALC)	478.5 ± 4.5^{a}	324.9 ± 3.3^{jkl}	336.1 ± 3.2^{hijk}	450.6 ± 3.7^{b}	362.2 ± 3.6^{d}	351.3 ± 5.4^{def}
	Dried (CAP)	350.2 ± 4.4^{efg}	292.3 ± 4.3^{mn}	255.2 ± 5.3^{p}	352.6 ± 5.4^{def}	272.4 ± 4.4^{o}	282.4 ± 4.7^{no}
TFC	Fresh (ALC)	98.7 ± 2.5^{cde}	81.4 ± 2.5^{kl}	75.3 ± 2.6^{m}	90.7 ± 3.1^{gh}	83.1 ± 3.4^{ijkl}	77.7 ± 3.3^{lm}
	Fresh (CAP)	94.9 ± 2.4^{efg}	97.7 ± 3.4^{cde}	89.3 ± 3.7^{h}	106.5 ± 2.8^{b}	96.6 ± 3.9^{def}	95.7 ± 2.8^{defg}
	Dried (ALC)	114.8 ± 2.0^{a}	82.7 ± 1.8^{ijkl}	81.7 ± 1.3^{jkl}	103.2 ± 1.5^{bc}	88.2 ± 1.8^{hi}	87.0 ± 1.9^{hij}
	Dried (CAP)	105.4 ± 1.7^{b}	92.1 ± 1.8^{fgh}	78.9 ± 2.3^{klm}	101.2 ± 2.8^{bcd}	83.6 ± 2.3^{ijk}	82.1 ± 1.9^{jkl}
TPrAC	Fresh (ALC)	330.7 ± 7.9^{b}	192.4 ± 6.2^{h}	203.7 ± 9.3^{gh}	292.7 ± 9.4^{c}	191.0 ± 6.1^{h}	211.6 ± 8.4^{g}
	Fresh (CAP)	255.4 ± 5.5^{de}	140.2 ± 6.0^{j}	120.0 ± 5.1^{k}	263.6 ± 8.1^{d}	142.2 ± 8.3^{j}	146.4 ± 5.3^{j}
	Dried (ALC)	357.0 ± 8.0^{a}	201.5 ± 5.5^{gh}	189.4 ± 6.3^{hi}	331.5 ± 5.1^{b}	241.9 ± 8.8^{ef}	238.1 ± 7.8^{f}
	Dried (CAP)	279.3 ± 4.5^{c}	211.1 ± 4.9^{g}	133.5 ± 5.1^{jk}	280.0 ± 7.6^{c}	174.9 ± 8.5^{i}	198.2 ± 5.8^{gh}
Twigs							
Yield	Fresh (ALC)	7.9 ± 0.1^{h}	6.9 ± 0.1^{kl}	6.9 ± 0.1^{kl}	9.0 ± 0.1^{e}	$8,3 \pm 0.1^{g}$	7.7 ± 0.1^{hi}
	Fresh (CAP)	7.3 ± 0.1^{j}	6.7 ± 0.1^{l}	7.0 ± 0.1^{k}	8.0 ± 0.2^{g}	7.6 ± 0.1^{i}	7.0 ± 0.1^{k}
	Dried (ALC)	12.0 ± 0.1^{a}	10.7 ± 0.1^{b}	10.6 ± 0.1^{b}	8.8 ± 0.1^{ef}	7.1 ± 0.1^{k}	10.1 ± 0.1^{c}
	Dried (CAP)	9.0 ± 0.1^{e}	8.6 ± 0.1^{f}	10.1 ± 0.1^{c}	8.8 ± 0.1^{ef}	8.3 ± 0.1^{g}	9.5 ± 0.1^{d}
TPC	Fresh (ALC)	526.5 ± 4.5^{a}	406.6 ± 4.3^{g}	348.3 ± 6.3^{j}	514.6 ± 2.2^{b}	420.9 ± 3.3^{ef}	419.1 ± 3.0^{ef}
	Fresh (CAP)	412.6 ± 6.7^{fg}	294.2 ± 4.9^{n}	273.7 ± 7.9^{o}	367.1 ± 3.8^{i}	344.8 ± 5.3^{jk}	324.0 ± 6.1^{l}
	Dried (ALC)	499.0 ± 3.9^{c}	389.5 ± 7.3^{h}	329.0 ± 8.3^{l}	485.6 ± 3.5^{d}	412.5 ± 5.5^{fg}	402.6 ± 6.2^{g}
	Dried (CAP)	419.1 ± 3.7^{ef}	311.0 ± 6.5^{m}	251.6 ± 3.4^{p}	425.1 ± 5.8^{e}	341.5 ± 6.1^{jk}	334.9 ± 3.3^{kl}
TFC	Fresh (ALC)	166.2 ± 4.3^{cd}	139.1 ± 4.0^{ijkl}	130.9 ± 2.1^{m}	166.3 ± 3.9^{c}	137.6 ± 3.3^{jkl}	135.3 ± 2.6^{klm}
	Fresh (CAP)	178.7 ± 4.7^{b}	147.6 ± 2.3^{fgh}	130.0 ± 3.8^{mn}	153.0 ± 2.8^{f}	153.2 ± 2.4^{ef}	144.7 ± 4.5^{ghi}
	Dried (ALC)	166.3 ± 3.0^{c}	143.0 ± 3.4^{hij}	133.8 ± 2.0^{lm}	163.8 ± 1.7^{cd}	139.7 ± 2.8^{ijkl}	141.0 ± 2.9^{hijk}
	Dried (CAP)	198.4 ± 2.7^{a}	149.8 ± 3.3^{fg}	123.8 ± 2.4^{n}	201.0 ± 1.9^{a}	159.6 ± 1.4^{de}	151.5 ± 2.7^{f}
TprAC	Fresh (ALC)	585.8 ± 10.3^{b}	307.5 ± 7.1^{i}	286.4 ± 11.6^{j}	553.3 ± 7.0^{c}	375.2 ± 6.8^{g}	387.7 ± 9.0^{g}
	Fresh (CAP)	440.3 ± 9.1^{e}	94.2 ± 6.9^{m}	72.3 ± 6.3^{n}	388.3 ± 9.2^{g}	209.1 ± 7.8^{k}	142.1 ± 7.3^{l}
	Dried (ALC)	576.4 ± 5.5^{b}	340.3 ± 9.5^{h}	305.1 ± 6.9^{i}	516.9 ± 8.2^{d}	351.0 ± 8.1^{h}	384.6 ± 6.5^{g}
	Dried (CAP)	631.3 ± 7.9^{a}	379.9 ± 9.8^{g}	306.0 ± 7.2^{i}	614.3 ± 8.4^{a}	417.6 ± 6.1^{f}	432.4 ± 6.4^{ef}

Values (mean ± standard deviation) are average of two replicates of each sample, analyzed individually in triplicate (n = 2 × 3); different letters indicate significant differences of means within samples, for each determined parameter (one-way ANOVA, Tukey test at $p < 0.05$).

For 70% ACE, TFC in leaves and twigs extracts lied between 90.7 and 114.8 mg CatE/g extract and 153.0 to 198.4 mg CatE/g extract, respectively. A calibration curve was made using rutin as a standard for comparison purposes, giving 228.8–348.0 mg RE/g extract for leaves, and 375.5–601.4 mg RE/g extract (Supplementary Material, Table S3). TFC in leaves extracts were in the range observed by Tung et al. [53] with leaves of *A. nilotica* (2.3–355.3 mg RE/g extract), while TFC in twigs extracts were higher. The TFC values found in the extracts of *A. dealbata* twigs with 70% ACE were higher than those

observed in bark extracts of various *Acacia* spp. including *A. dealbata* (74.0–134.0 mg RE/g extract) [54], in leaves and bark extracts of *A. nilotica* and *A. ataxacantha* (0.34–49.90 mg RE/g extract) [51], or in *Pinus pinaster* bark extracts, a known source of flavonoids (77–161 mg CatE/g extract) [52]. Relatively to the mass of raw material, TFC contents varied in the range 9.9–17.0 mg CatE/g of leaves (30.2–51.4 mg RE/g of leaves), and 12.6–20.0 mg CatE/g of twig (38.2–60.5 mg RE/g of twig) (see full results in Supplementary Material, Table S4), which are much superior to the reported by Sowndhararajan et al. for the bark of *A. dealbata* and other *Acacia* spp. (2.4–15.5 mg RE/g of bark), and also other known sources of flavonoids such as yellow, green, and black teas (0.2–3.8 mg CatE/g of tea) [55], and red fruits (0.2–0.8 mg CatE/g of tea) [56].

Regarding TPrAC, the results were expressed relative to a standard source of proanthocyanidins, the commercial extract Pycnogenol®, a mixture of proanthocyanidins extracted from bark of Atlantic Pinus trees. As observed for TPC and TFC, the extracts with higher TPrAC contents were obtained with 70% ACE, with TPrAC values in the range of 255.4–357.0 mg PycE/g extract for leaves, and in the range of 388.3–631.3 mg PycE/g extract for twigs.

The results of this study showed that the leaves and twigs of *A. dealbata* from Caparica and from Alcobaça regions can be an abundant source of extracts rich in phenolics, especially flavonoids and proanthocyanidins, with average contents similar or higher than comparable extratcs described in the literature.

For a better interpretation of the impact of the extraction method (regardless of the drying status or the origin of the plant), the average of the measured variables for all extracts produced by maceration was compared with the average of all extracts produced by hot extraction for each solvent. The same approach was followed to evaluate the average values of the measured variables for all extracts obtained from fresh and dried leaves (regardless of other extraction parameters). The average values of the measured variables for the extracts obtained from a specific origin (Caparica or Alcobaça) were also determined and compared. These results were then subject to analysis of variance (ANOVA) followed by Tukey's test at $p < 0.05$ and are shown in Supplementary Material, Table S5.

For the extraction yield, statistically significant differences were only found between fresh and dried raw materials, as shown in the Figure 1. Yields in the range 13.9–15.0%, and 10.3–11.6% were found for dried and fresh leaves, respectively and yields in the range of 8.7–10.1%, and 7.2–8.1% were found for dried and fresh twigs, respectively.

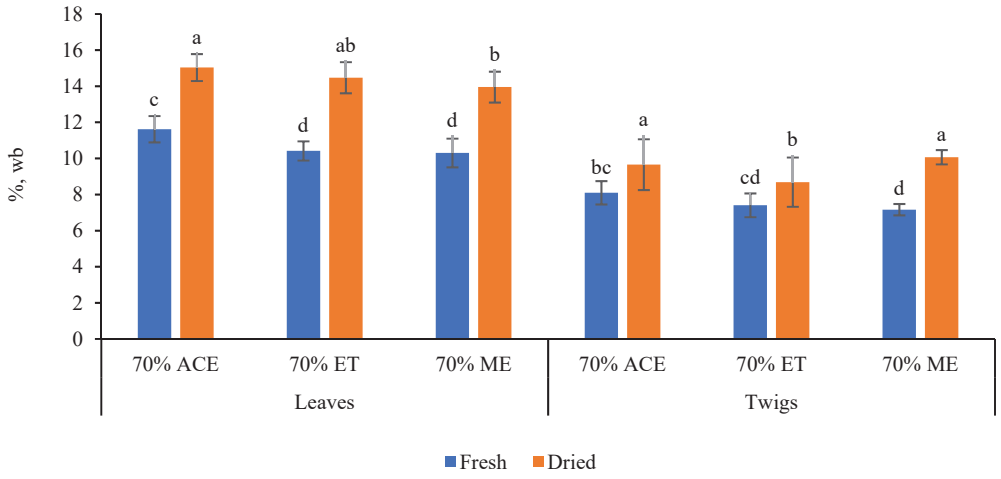

Figure 1. Comparison of the average extraction yields for fresh and dried leaves and twigs (regardless the extraction method and the provenience of the raw material); different letters indicate significant differences of means (one-way ANOVA, Tukey test at $p < 0.05$).

In what concerns the TPC, TFC, and TPrAC of the extracts, no significant differences were found between maceration and hot extraction, except for methanolic extracts that

presented slightly higher contents for hot extraction (Supplementary Material, Table S5). Figure 2 highlights differences coming from the drying status and origin of the raw material, for all determined composition parameters.

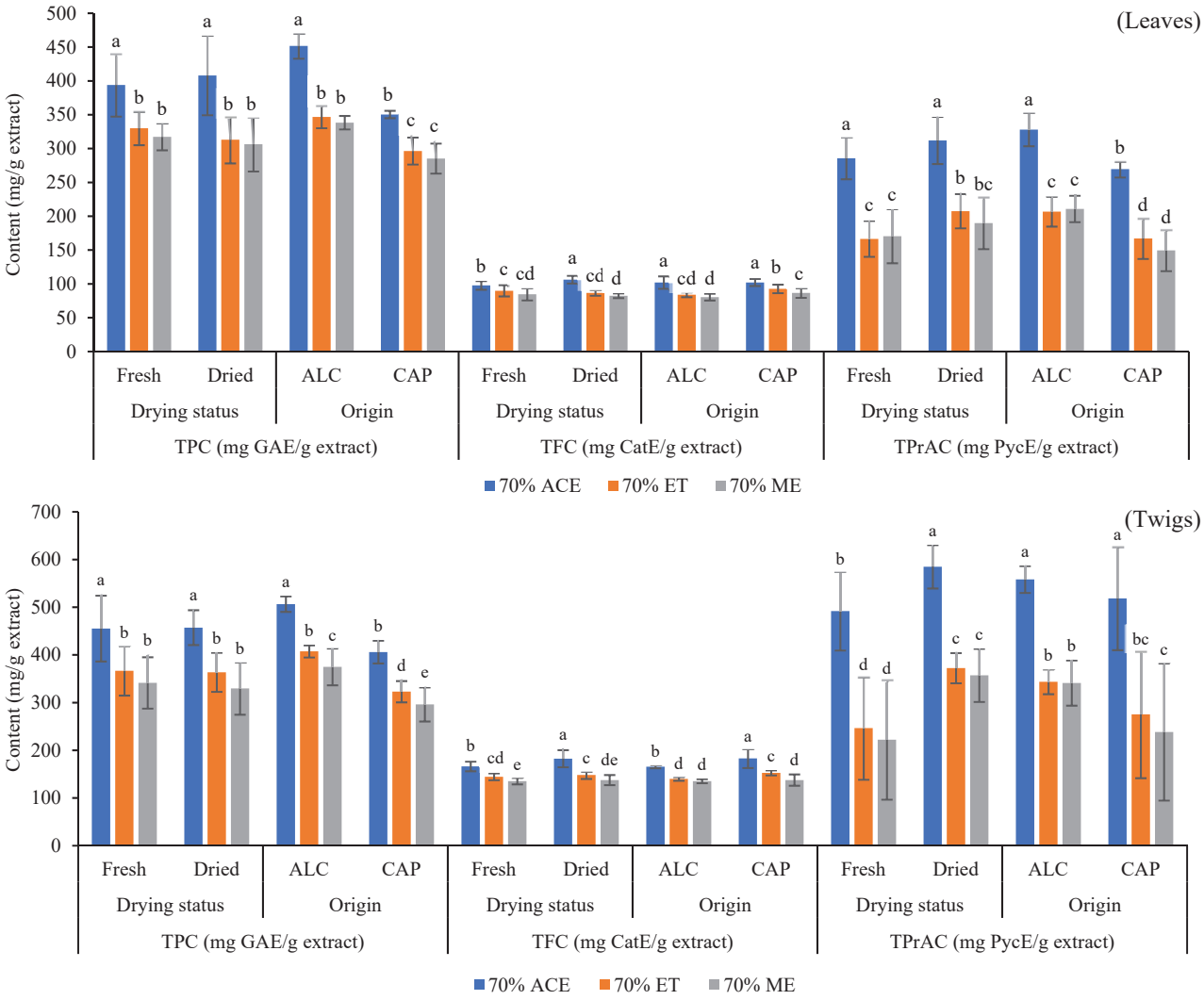

Figure 2. Comparison of the average values of TPC (mg GAE/g extract), TFC (mg CatE/g extract), and TPrAC (mg PycE/g extract) for fresh or dried material (regardless the extraction method and the provenience of the raw material), and for plants from Alcobaça (ALC) and Caparica (CAP) (regardless the extraction method and the drying status); different letters indicate significant differences of means (one-way ANOVA, Tukey test at $p < 0.05$).

Overall, it was confirmed that the higher average values for all the parameters considered were higher for the extracts obtained with 70% ACE. Regarding leaves, the extracts from the Alcobaça region had higher average values of TPC and TPrAC and higher average values of TFC (only for 70% ET and 70% ME extracts) than those from Caparica region. In the case of twigs, extracts from dried biomass had higher average values of TFC and TPrAC than those obtained from wet biomass with the same solvents. Extracts of twigs from Alcobaça region showed higher average values of TPC than those from the Caparica region. Differences in the average values comparing fresh and dried plants were most noticed in the extraction yield, TFC, and TPrAC, with dried material originating better results. The differences of extraction yield or extract composition between fresh or dried biomass may be explained by the change of the extraction solvent characteristics, since the presence of biomass moisture corresponds to a reduction of the concentration of the organic component (acetone, ethanol, or methanol). Differences coming from the plant origin can

be explained by the fact that secondary metabolites are synthesized by plants to protect them in adverse conditions from pathogens and environmental stresses, being influenced by several biotic and abiotic factors, such as water, drought, salinity, temperature, radiation, or chemical stresses [57]. Thus, differences in edaphoclimatic conditions between Alcobaça and Caparica can explain the differences observed.

3.2. Antioxidant Activity

The antioxidant activity of the extracts obtained from *A. dealbata* leaves and twigs was assessed by DPPH and FRAP assays, and the results are presented in Table 2.

Table 2. Results from DPPH (mg TE/g extract) and FRAP (mmol Fe^{2+}/g extract) of extracts from fresh and dried leaves and twigs from Alcobaça (ALC) and Caparica (CAP), using different extraction solvents and extraction methods; DPPH and FRAP results expressed relative to the mass of biomass are presented in Supplementary Material, Table S1.

	Samples	Maceration at Room Temperature			Hot Extraction		
		70% ACE	70% ET	70% MET	70% ACE	70% ET	70% MET
Leaves							
DPPH	Fresh (ALC)	740.8 ± 10.1 ^{b}	597.9 ± 8.3 ^{e}	535.8 ± 8.5 ^{i}	740.2 ± 6.1 ^{b}	636.7 ± 6.0 ^{d}	526.8 ± 5.3 ^{i}
	Fresh (CAP)	560.0 ± 7.2 ^{h}	348.5 ± 5.7 ^{n}	335.4 ± 5.9 ^{n}	540.0 ± 8.4 ^{gh}	428.4 ± 9.0 ^{k}	393.6 ± 7.2 ^{m}
	Dried (ALC)	893.4 ± 10.8 ^{a}	578.2 ± 6.5 ^{fg}	576.4 ± 8.2 ^{fg}	886.5 ± 7.5 ^{a}	634.3 ± 9.1 ^{d}	685.4 ± 5.5 ^{c}
	Dried (CAP)	446.3 ± 7.0 ^{j}	412.2 ± 5.6 ^{l}	337.0 ± 8.3 ^{n}	588.9 ± 5.5 ^{ef}	392.6 ± 7.3 ^{m}	406.6 ± 6.0 ^{lm}
FRAP	Fresh (ALC)	7664.1 ± 167.6 ^{b}	6285.3 ± 95.4 ^{ef}	5620.3 ± 118.5 ^{gh}	7702.8 ± 164.7 ^{b}	6501.3 ± 132.2 ^{de}	5423.2 ± 142.5 ^{hi}
	Fresh (CAP)	6612.1 ± 167.8 ^{d}	4386.9 ± 93.0 ^{l}	4403.9 ± 129.7 ^{l}	6015.2 ± 177.6 ^{def}	5072.4 ± 225.1 ^{jk}	4835.8 ± 178.6 ^{k}
	Dried (ALC)	8885.4 ± 93.1 ^{a}	6299.9 ± 71.9 ^{ef}	5334.0 ± 79.0 ^{ij}	6962.5 ± 63.4 ^{c}	6175.8 ± 138.3 ^{f}	3300.7 ± 98.7 ^{n}
	Dried (CAP)	5846.6 ± 90.7 ^{g}	4855.0 ± 58.6 ^{k}	3934.8 ± 103.5 ^{m}	5766.3 ± 81.2 ^{g}	4097.2 ± 124.8 ^{m}	4449.8 ± 82.2 ^{l}
Twigs							
DPPH	Fresh (ALC)	996.8 ± 6.7 ^{b}	757.2 ± 11.6 ^{e}	511.1 ± 11.3 ^{j}	994.7 ± 6.2 ^{bc}	778.8 ± 14.0 ^{d}	782.7 ± 8.1 ^{d}
	Fresh (CAP)	675.5 ± 11.0 ^{h}	254.2 ± 6.6 ^{q}	230.2 ± 9.2 ^{r}	596.3 ± 11.5 ^{i}	379.7 ± 11.8 ^{n}	358.4 ± 11.4 ^{o}
	Dried (ALC)	1068.3 ± 8.5 ^{a}	665.5 ± 11.2 ^{h}	514.2 ± 11.8 ^{j}	974.2 ± 6.4 ^{c}	791.2 ± 14.3 ^{d}	782.1 ± 7.1 ^{d}
	Dried (CAP)	731.3 ± 6.1 ^{f}	418.5 ± 7.9 ^{m}	321.3 ± 8.3 ^{p}	710.2 ± 5.2 ^{g}	474.5 ± 9.9 ^{k}	452.6 ± 8.5 ^{l}
FRAP	Fresh (ALC)	6852.4 ± 208.0 ^{de}	6546.5 ± 221.0 ^{e}	3989.4 ± 61.6 ^{j}	7829.9 ± 140.9 ^{c}	6851.8 ± 225.2 ^{de}	6554.3 ± 112.4 ^{e}
	Fresh (CAP)	6951.8 ± 146.0 ^{d}	3306.8 ± 109.3 ^{k}	3075.8 ± 75.0 ^{k}	6192.0 ± 53.1 ^{f}	4626.8 ± 255.7 ^{hi}	4461.1 ± 137.7 ^{i}
	Dried (ALC)	9194.6 ± 165.8 ^{a}	4770.3 ± 86.1 ^{h}	3783.0 ± 84.8 ^{j}	8804.2 ± 112.4 ^{b}	6987.7 ± 163.4 ^{d}	7098.5 ± 87.1 ^{d}
	Dried (CAP)	7754.4 ± 119.0 ^{c}	5354.9 ± 141.1 ^{g}	3969.0 ± 85.0 ^{j}	8003.8 ± 171.7 ^{c}	5585.2 ± 140.0 ^{g}	5429.1 ± 83.3 ^{g}

Values (mean ± standard deviation) are average of two replicates of each sample, analyzed individually in triplicate (n = 2 × 3); different letters indicate significant differences of means within samples, for each antioxidant determination method (one-way ANOVA, Tukey test at $p < 0.05$).

The highest antioxidant activity of extracts from leaves or twigs was observed when using 70% ACE as extraction solvent, regardless of the extraction method, drying status, or the geographical origin of the plant. When using this solvent, the antioxidant activity of twigs extracts was higher than the one of corresponding leaves extracts.

The DPPH assay measures the ability of extract components to act as free radical scavengers or hydrogen donors antioxidants [58]. For 70% ACE extracts, the values lied between 446.3–893.4 mg TE/g extract (58.6–132.1 mg TE/g of leaves) for leaves extract and between 596.3–1068.3 mg TE/g extract (49.0–128.3 mg TE/g of twigs). These values are higher than those reported by Zheleva-Dimitrova et al. for extracts from leaves (31.94–493.90 mg TE/g extract) and stem bark (8.51–349.17 mg TE/g extract) of *A. nilotica* and *A. ataxacantha* [51]. These results are also higher than the ones reported for known antioxidant sources such as yellow, green, and black teas (11.930–26.521 μmol TE/100 g, which corresponds to 0.030–0.066 mg TE/g of tea leaves) [55], red fruits (64.14–177.11 μmol TE/g, corresponding to 16.1–44.3 mg TE/g of fruit) [56], or pine bark (approximately between 50 and 350 mg TE/g of extract) [59].

The reducing power of the obtained extracts was measured through the FRAP assay, which evaluates the reduction of Fe^{3+} in the complex (Fe^{3+}-TPTZ) to a ferrous form

(Fe^{2+}-TPTZ), by donation of electrons from the antioxidants, resulting in stopping the free radical production chain [13,60,61]. For 70% ACE the FRAP values were in the range 5766.3–8885.4 μmol Fe^{2+}/g extract and 6192.0–9194.6 μmol Fe^{2+}/g extract, for leaves and twigs extracts, respectively. These values higher than those found in leaves (233.17 μmol Fe^{2+}/g extract), pods (254.42 μmol Fe^{2+}/g extract), and seed (178.14 μmol Fe^{2+}/g extract) extracts of *A. leucophloea* [62]. Values of 152 mg Fe^{2+}/g (corresponding to 2721.2 μmol Fe^{2+}/g extract) and 575 mg Fe^{2+}/g (corresponding to 10296.4 μmol Fe^{2+}/g extract) were found for *Pinus radiata* bark extract and standardized *Pinus pinaster* bark extract Pycnogenol®, respectively [63].

The extraction solvent significantly affected the antioxidant activity, with the best results being obtained when using 70% ACE, regardless of the origin and the drying status of the raw material. Higher antioxidant activities of extracts obtained with aqueous acetone solutions were also observed with stem bark extracts of *Butea monosperma* (Lam.) Kuntze [64], bark extracts of *A. leucophloea*, *A. ferruginea*, *A. dealbata* and *A. pennata* [54], and flower extracts of safflower (*Carthamus tinctorius* L.) [65].

A better understanding of the influence of the extraction method, drying status, and provenience of the plant on the antioxidant activity can be derived from the analysis of variance applied using the same approach as for the impact of these factors on the composition and extract yield. The results are presented in Table 3. Besides the confirmation of 70% ACE as the best extraction solvent for the removal of antioxidant compounds, it can be seen that the geographical origin of the plant had the major impact on the antioxidant activity of the produced extracts, since the extracts of leaves and twigs from Alcobaça showed significantly higher antioxidant activity than the corresponding extracts from biomass collected in the Caparica region. The extraction method only gave significant differences on methanolic and ethanolic extracts of twigs, with hot extraction giving the highest antioxidant activity by both DPPH and FRAP assays. The effect of using fresh or dried material was most reflected in the antioxidant activity of twigs given by the FRAP assay, with dried twigs extracted with 70% ACE originating a significantly higher value than the one obtained using fresh leaves.

Table 3. Average values of DPPH (mg TE/g extract) and FRAP (mmol Fe^{2+}/g extract) assays for extracts obtained by maceration and hot extraction (regardless drying status and origin), from fresh and dried material (regardless extraction method and origin), and from plants from Alcobaça (ALC) and Caparica (CAP) (regardless extraction process and drying status).

Samples	Leaves			Twigs		
	70% ACE	70% ET	70% MET	70% ACE	70% ET	70% MET
DPPH						
Maceration	660.1 ± 174.7 ^{a}	484.2 ± 109.0 ^{b}	446.1 ± 113.5 ^{b}	868.0 ± 171.5 ^{a}	523.8 ± 203.4 ^{bc}	394.2 ± 125.7 ^{c}
Hot extraction	696.2 ± 131.2 ^{a}	523.0 ± 115.9 ^{b}	503.1 ± 120.0 ^{b}	818.9 ± 174.4 ^{a}	606.0 ± 186.4 ^{b}	593.9 ± 195.7 ^{b}
Fresh	652.5 ± 90.2 ^{a}	502.9 ± 121.4 ^{b}	447.9 ± 88.0 ^{b}	815.8 ± 186.2 ^{a}	542.5 ± 235.1 ^{b}	470.6 ± 210.4 ^{b}
Dried	703.8 ± 197.2 ^{a}	504.3 ± 106.5 ^{b}	501.3 ± 140.5 ^{b}	871.0 ± 157.5 ^{a}	587.4 ± 152.6 ^{b}	517.5 ± 171.7 ^{b}
Alcobaça	815.2 ± 76.8 ^{a}	611.8 ± 26.2 ^{b}	581.1 ± 64.7 ^{bc}	1008.5 ± 37.0 ^{a}	748.2 ± 51.7 ^{b}	647.5 ± 138.1 ^{c}
Caparica	541.1 ± 57.3 ^{c}	395.4 ± 31.3 ^{d}	368.1 ± 33.6 ^{d}	678.3 ± 53.1 ^{c}	381.7 ± 83.2 ^{d}	340.6 ± 81.9 ^{d}
FRAP						
Maceration	7252.1 ± 1174.0 ^{a}	5456.8 ± 873.7 ^{b}	4823.3 ± 746.5 ^{bc}	7688.3 ± 969.5 ^{a}	4994.6 ± 1199.0 ^{c}	3704.3 ± 386.4 ^{d}
Hot extraction	6693.0 ± 746.5 ^{a}	5461.7 ± 981.1 ^{b}	4502.4 ± 801.6 ^{c}	7707.5 ± 976.6 ^{a}	6012.9 ± 1007.8 ^{b}	5885.8 ± 1046.0 ^{b}
Fresh	7079.9 ± 644.8 ^{a}	5561.5 ± 898.9 ^{b}	5070.8 ± 509.5 ^{b}	6956.5 ± 610.9 ^{b}	5333.0 ± 1491.8 ^{cd}	4520.2 ± 1306.5 ^{d}
Dried	6865.2 ± 1287.9 ^{a}	5357.0 ± 946.6 ^{b}	4254.8 ± 765.0 ^{c}	8439.3 ± 611.2 ^{a}	5674.5 ± 841.4 ^{c}	5069.9 ± 1364.5 ^{cd}
Alcobaça	7803.7 ± 715.8 ^{a}	6315.6 ± 159.6 ^{b}	4919.5 ± 966.2 ^{c}	8170.3 ± 940.4 ^{a}	6289.1 ± 926.3 ^{c}	5356.3 ± 1518.6 ^{d}
Caparica	6141.4 ± 380.2 ^{b}	4602.9 ± 412.3 ^{cd}	4406.1 ± 347.9 ^{d}	7225.5 ± 737.5 ^{b}	4718.4 ± 921.4 ^{de}	4233.7 ± 873.4 ^{e}

Different letters indicate significant differences of means within samples for each set of parameters (one-way ANOVA, Tukey test at $p < 0.05$).

3.3. Extraction of Spent Raw Material

Leaves and twigs of *Acacia* spp. contain lipophilic compounds such as terpenes, long-chain alcohols, fatty acids, sterols, aromatic compounds, among others [66]. These lipophilic components may be valorized in different application fields, and their presence might limit the access of polar solvents to the matrix, affecting extraction of the bioactive components. To test this hypothesis the dried leaves and twigs were treated with petroleum ether, to remove non-polar components and extraction with 70% ACE was performed on the spent leaves and twigs using equivalent conditions to those used with the raw biomass. The characterization of the lipophilic extracts will be addressed elsewhere.

The comparison of composition and antioxidant activity of extracts obtained from dried material macerated at room temperature with 70% ACE, and those of extracts obtained from spent material in similar conditions is shown in Table 4.

Table 4. Extract yield, composition, and antioxidant activity of extracts obtained from raw and spent leaves and twigs, using maceration at room temperature with 70% ACE as extraction solvent.

Sample		Yield	TPC	TFC	TPrAC	DPPH	FRAP
Leaves	Alcobaça-spent	15.5 ± 0.1	436.4 ± 11.1	116.1 ± 2.8	441.0 ± 6.8	796.0 ± 9.9	8807.8 ± 225.1
	Alcobaça-raw	14.8 ± 0.1	478.5 ± 4.5	114.8 ± 2.0	357.0 ± 8.0	893.4 ± 10.8	8885.4 ± 93.1
	Caparica-spent	14.5 ± 0.1	350.5 ± 2.4	97.0 ± 1.8	356.9 ± 1.6	661.7 ± 3.5	6431.1 ± 85.8
	Caparica-raw	14.0 ± 0.1	350.2 ± 4.4	105.4 ± 1.7	279.3 ± 4.5	446.3 ± 7.0	5846.6 ± 90.7
Twigs	Alcobaça-spent	12.9 ± 0.1	448.3 ± 8.0	152.8 ± 3.6	610.1 ± 5.8	838.6 ± 8.6	8171.1 ± 153.0
	Alcobaça-raw	12.0 ± 0.1	499.0 ± 3.9	166.3 ± 3.0	576.4 ± 5.5	1068.3 ± 8.5	9194.6 ± 165.8
	Caparica-spent	10.2 ± 0.1	389.0 ± 5.3	147.6 ± 2.2	544.2 ± 4.7	644.8 ± 9.6	7151.6 ± 160.4
	Caparica-raw	9.0 ± 0.1	419.1 ± 3.7	198.4 ± 2.7	631.3 ± 7.9	731.3 ± 6.1	7754.4 ± 119.0

The extracts produced from spent leaves and twigs had a slightly higher yield and slightly higher proanthocyanidin contents than those obtained from the raw dried materials. However, TPC and TFC, as well as the antioxidant activity, were slightly lower when using spent raw material. The removal of lipophilic compounds from the plant matrix may facilitate the penetration of the solvent, thus allowing obtaining higher extract yields. The slight decrease in the antioxidant activity may be explained by the previous removal of lipophilic components with antioxidant activity, such as terpenes or sterols. Despite this, it should be noted that the values are quite close and that this option allows more efficient use of this resource by obtaining a wider range of products from the same amount of raw material.

3.4. Correlations between Composition and Antioxidant Activity

The correlation analysis between TPC, TFC, TPrAC, and antioxidant activities by DPPH and FRAP assays for the extracts of fresh and spent flowers are given in Table 5.

All the correlations found in this work were statistically significant at $p < 0.01$, with the exception made for the correlation between TFC and antioxidant activity by the DPPH assay for leaves (non-significant) and twigs (significant at $p < 0.05$) and for the correlation between TFC and FRAP assay in the case of leaves (significant at $p < 0.05$). The Pearson's correlation coefficients found indicate very strong correlations between TPC and antioxidant activity given by DPPH and FRAP assays, and strong correlations between TPrAC and the same assays [67], for both leaves and twigs. Moderate correlation was found between TFC of leaves and twigs and both antioxidant assays. Ref. [68] also found strong correlations between TPC, TFC and DPPH values (r = 0.771 and r = 0.815), for extracts of *A. nilotica* leaves. However, [69] found non-significant correlation between TPC of extracts of different components (leaves, flowers, and pods) of three *Acacia* species (*A. nilotica*, *A. seyal*, and *A. laeta*) and DPPH results, having found a significant correlation between TFC and DPPH values instead. Significant and strong correlations between TPC and the DPPH and

FRAP results were found in *Pinus densiflora* bark extract [59] and in medicinal herbs and spices [70].

Table 5. Correlation analysis between total phenolics content (TPC), total flavonoid content (TFC), total proanthocyanidins content (TPrAC) and antioxidant activities given by DPPH and FRAP assays, for leaves extracts; significance of the correlations assessed at $p < 0.05$ and at $p < 0.01$ (two-tailed).

		TPC	TFC	TPrAC	DPPH	FRAP
Leaves	TPC	1				
	TFC	r = 0.563 ** p = 0.003	1			
	TPrAC	r = 0.801 ** p = 0.000	r = 0.553 ** p = 0.003	1		
	DPPH	r = 0.922 ** p = 0.000	r = 0.373 p = 0.061	r = 0.766 ** p = 0.000	1	
	FRAP	r = 0.864 ** p = 0.000	r = 0.490 * p = 0.011	r = 0.742 ** p = 0.000	r = 0.778 ** p = 0.000	1
Twigs	TPC	1				
	TFC	r = 0.511 ** p = 0.008	1			
	TPrAC	r = 0.754 ** p = 0.000	r = 0.671 ** p = 0.000	1		
	DPPH	r = 0.967 ** p = 0.000	r = 0.396 * p = 0.045	r = 0.765 ** p = 0.000	1	
	FRAP	r = 0.861 ** p = 0.000	r = 0.603 ** p = 0.011	r = 0.856 ** p = 0.000	r = 0.884 ** p = 0.000	1

** correlation is significant at $p < 0.01$ (two-tailed); * correlation is significant at $p < 0.05$ (two-tailed).

These findings demonstrate that phenolic compounds have an important role in the observed antioxidant activity given by DPPH and FRAP assays. Moreover, the abundance of these compounds in the produced extracts suggests that leaves and twigs have a strong potential to be explored for obtaining antioxidants for diverse applications, such as in nutraceutical or cosmetic industries.

3.5. Antimicrobial Activity

A representative group of extract samples was selected to assess antimicrobial activity against several microorganisms responsible for foodborne disease, skin infections, caries, and oral infections. Some of these microorganisms, namely *S. aureus*, *Enterococcus* spp., *P. aeruginosa*, *E. coli*, and *C. albicans*, are usually involved in hospital-acquired infections and have developed resistance to antibiotics, and virulence factors can exacerbate microbial drug resistances [71,72]. Antibiotic resistance is emerging as a serious worldwide problem and natural extracts with antimicrobial activity have been suggested as a solution to this problem [73]. Natural products from plants could also target microbial virulence factors and thus play an important role to combat microbial infections and overcoming antibiotic resistances [74]. Microbial virulence factors encompass a wide range of molecules produced by pathogens, such as toxins, enzymes, exopolysaccharides, cell surface structures such as capsules, lipopolysaccharides, glyco- and lipoproteins [75]. Moreover, natural extracts with antimicrobial activity could be an less polluting and more safe alternative to synthetic antimicrobial substances applied in food industry and in oral, cosmetics, and pharmacological formulations [43].

Both leaves and twigs extracts were able to inhibit the growth of Gram-positive bacteria but were inactive against Gram-negative bacteria and *C. albicans*. The inhibition zones against bacteria *S. aureus*, MRSA, *S. epidermis*, *E. faecalis*, *B. cereus, S. mutans and S. mitis* are presented in Table 6. Overall, extracts were more effective against *B. cereus* (inhibition zones in the range 11.0–12.1 mm for leaves extracts and 9.3–13.0 mm for twigs extracts), while *E. faecalis* showed a sensitivity lower than the remaining microorganisms

(inhibition zones in the range 8.3–8.8 mm for leaves extracts and 9.3–9.8 mm for twigs extracts).

Table 6. Inhibition zones (mm) of selected extracts of *A. dealbata* leaves and twigs against *S. aureus*, MRSA, *S. epidermis*, *E. faecalis*, *B. cereus*, *S. mutans* and *S. mitis*.

Samples (0.5 mg/well)	*S. aureus*	*MRSA*	*S. epidermidis*	*E. faecalis*	*B. cereus*	*S. mutans*	*S. mitis*
Leaves							
Dried-70%ACE-maceration (ALC)	10.3 ± 0.1	10.3 ± 0.0	9.8 ± 0.1	8.5 ± 0.1	12.1 ± 0.1	11.0 ± 0.0	11.3 ± 0.6
Dried-70%ET-maceration (ALC)	8.8 ± 0.0	9.5 ± 0.1	8.5 ± 0.1	8.0 ± 0.0	11.5 ± 0.0	10.0 ± 0.0	11.0 ± 0.0
Dried-70%MET-maceration (ALC)	8.5 ± 0.1	9.3 ± 0.1	8.0 ± 0.0	nd	11.0 ± 0.0	10.0 ± 0.0	nd
Dried-70%ACE-maceration (CAP)	9.3 ± 0.0	9.0 ± 0.0	8.5 ± 0.1	8.8 ± 0.0	11.0 ± 0.0	10.0 ± 0.0	9.0 ± 1.7
Dried-70%ACE-hot extraction (ALC)	9.5 ± 0.1	10.5 ± 0.1	9.5 ± 0.1	8.8 ± 0.1	12.0 ± 0.0	10.0 ± 0.0	nd
Fresh-70%ACE-maceration (ALC)	9.5 ± 0.1	9.8 ± 0.0	9.3 ± 0.1	8.3 ± 0.1	11.3 ± 0.0	10.0 ± 0.0	9.3 ± 0.6
Spent leaves-70%ACE-maceration (ALC)	10.5 ± 0.1	10.5 ± 0.1	9.3 ± 0.0	8.5 ± 0.1	11.8 ± 0.0	11.3 ± 0.0	nd
Twigs							
Dried-70%ACE-maceration (ALC)	10.8 ± 0.0	10.5 ± 0.0	10.3 ± 0.1	9.5 ± 0.1	12.5 ± 0.1	9.0 ± 0.0	12.0 ± 0.0
Dried-70%ET-maceration (ALC)	nd	7.8 ± 0.0	nd	nd	10.0 ± 0.0	9.0 ± 0.0	11.0 ± 0.0
Dried-70%MET-maceration (ALC)	nd	nd	nd	nd	9.3 ± 0.0	10.0 ± 0.0	10.0 ± 0.0
Dried-70%ACE-maceration (CAP)	11.0 ± 0.0	11.0 ± 0.0	10.0 ± 0.0	9.5 ± 0.1	13.0 ± 0.0	12.0 ± 0.0	10.0 ± 0.0
Dried-70%ACE-hot extraction (ALC)	10.0 ± 0.0	10.8 ± 0.1	9.8 ± 0.0	9.5 ± 0.1	13.0 ± 0.0	9.0 ± 0.0	11.0 ± 0.0
Fresh-70%ACE-maceration (ALC)	11.0 ± 0.0	10.7 ± 0.0	9.5 ± 0.1	9.3 ± 0.0	12.8 ± 0.1	11.0 ± 0.0	12.0 ± 0.0
Spent twigs-70%ACE-maceration (ALC)	11.0 ± 0.0	11.0 ± 0.0	9.5 ± 0.1	9.8 ± 0.0	12.1 ± 0.0	9.0 ± 0.0	10.0 ± 0.0
Positive control	12.5 ± 0.5 [a]	13.9 ± 0.7 [a]	15.7 ± 1.0 [a]	12.5 ± 0.5 [a]	16.4 ± 1.1 [a]	19.3 ± 0.6 [b]	25.7 ± 0.6 [b]

[a] Vancomycin (5.0 mg); [b] Vancomycin (50.0 mg); nd: not detected.

Comparing leaves and twigs, twigs originated slightly higher inhibition diameters than leaves extracts, whenever acetone was used as extraction solvent. 70% ACE was the best extraction solvent regarding antimicrobial activity, for both leaves and twigs extracts, having produced significantly higher inhibition diameters than 70% ET or 70% MET extracts.

The origin of the raw material had a marked influence in the case of leaves extracts, with extracts obtained with leaves from Alcobaça having better results with all microorganisms, except for *E. faecalis*. In the case of twigs extracts, the differences were not so visible but extracts from Caparica twigs gave better results, exception made against *S. epidermidis*, *E. faecalis*, and *S. mitis*.

For both leaves and twigs extracts, the extraction process (maceration versus hot extraction), as well as the drying state of the raw material (dried versus fresh raw material), and the use of dried versus spent raw material did not significantly affect the antimicrobial activity, with extracts producing very similar inhibition zones against the microorganisms. Regarding the obtention of antibacterial extracts, these are important findings, once it supports the suggestion of using a more sustainable process (maceration at room temperature), with facilitated logistics due to not having the necessity of using fresh raw material. Moreover, the results show the possibility of retrieving a broader range of products from the same amount of raw material, since the previous extraction with petroleum ether to get lipophilic compounds did not affect the antimicrobial activity of the extracts that were then obtained with 70% aqueous acetone.

Considering the concentration of 10 mg/mL used in the antimicrobial assays for comparison purposes, it can be observed that the leaves extracts obtained in this study produced similar effects on the microorganisms to the ones shown by other extracts from leaves of *Acacia* spp. reported in the literature with concentrations ranging from 5 mg/mL to 200 mg/mL. Antimicrobial effects of leaves extracts expressed by inhibition zones were already described against *S. aureus* with *A. dealbata* aqueous and ethanolic extract (10.0–10.2 mm of inhibition, at 5 mg/mL) [29], with *A. saligna* (15 mm by an ethyl acetate extract at 10 mg/mL [24], and 24.7 mm by an ethanolic extract at 200 mg/mL [26]), with extracts of *A. etbaica*, *A. laeta*, and *A. origena* (7.3–21.0 mm at 500 mg/mL) [23], with *A.*

pycnantha (10.2–21.0 mm at 500 mg/mL [23], and 9–12 mm by aqueous and ethanolic extracts, no concentration reported [22]), and with *A. rigidula* and *A. berlandieri* acetonic, methanolic, and acetic acid extracts (6–11.4 mm at 500 mg/mL); against MRSA with *A. saligna* ethanolic extract (22.7 mm at 200 mg/mL) [26]; against *S. epidermis* (6–10 mm by aqueous and ethanolic extracts, no concentration reported) [22]; against *E. faecalis* with *A. rigidula* and *A. berlandieri* acetonic, methanolic, and acetic acid extracts (6–12.1 mm at 500 mg/mL); and against *B. cereus* with *A. dealbata*, *A. melanoxylon*, *A. baileyana*, and *A. nicholli* aqueous, ethanolic, and methanolic extracts (6–19 mm at 10 mg/mL) [30], and with *A. saligna* ethyl acetate extract (inhibition zone of 16 mm at 10 mg/mL) [24].

Concerning twigs in particular, just a few studies on antimicrobial effects involving *Acacia* spp. were found in the literature, most of them involving *A. nilotica* twigs [31–34]. Antimicrobial activity of twigs extracts produced in this work was in a lower range than the reported by Kumari et al. for *A. nilotica* twigs against *S. aureus* (10.8–40.2 mm), *E. faecalis* (16.2–38.0 mm), and *C. albicans* (14.7–27.0 mm) [31]. However, these results were obtained by applying 2 mg of extract/well [31], while in this work only 0.5 mg of extract/well was applied, which can at least partially explain the differences observed. To the best of our knowledge, no results of antimicrobial effects against MRSA, *S. epidermidis*, or *B. cereus* for twigs extracts of other *Acacia* spp. have been reported in the literature.

It is known that Gram-negative bacteria are more resistant to plant extracts than Gram-positive bacteria, due to the protection of the lipopolysaccharide layer in the outer membrane [73]. *Candida albicans* was included in this study as a model to determine the antifungal activity of the extracts. Despite being a common commensal yeast fungus of the human oral, gastrointestinal, and genital mucosal surfaces and skin, under specific circumstances, such as perturbation of barrier integrity or host immune responses, *C. albicans* causes opportunistic infections that range from superficial infections of the skin to life-threatening systemic infections [76,77]. All tested samples revealed ineffective against Gram-negative *P. aeruginosa* and *E. coli*, which was equally reported by El-Toumy et al. with aqueous, methanolic, and ethyl acetate extracts of *A. saligna* leaves [24].The tested samples were also ineffective against *C. albicans* yeast, as observed by Silva et al. with aqueous and methanolic extracts of *A. dealbata* leaves [30], by Ramli et al. with ethanolic extract of *A. farnesiana* leaves [16], or by Cock and van Vuuren with aqueous and methanolic extracts of *A. karroo* leaves [17]. Antibacterial effects against Gram-negative *E. coli* bacteria [22,25,26,29,30] and *C. albicans* yeast [24,26,30,31] were detected in leaves extracts of *Acacia* spp., but, in some cases, using extract concentrations that were more than double [31] or even twenty times higher [26] than the ones used in this work. In general, a positive correlation was observed between the antimicrobial activity of extracts from leaves and twigs of *A.dealbata*, and their total phenolic content, but this association should be confirmed by additional quantitative studies.

3.6. Characterisation of the Non-Polar Components of the Extracts

To understand if the phenolic extracts also contained non-polar components with antioxidant or antimicrobial activities that might influence the properties of the extracts, a group of selected extracts were derivatized and fractionated to isolate these less polar components and analysed by GC-TOFMS. A total of 32 compounds were tentatively identified using the NIST mass spectra library matching (Supplementary Material, Table S6). Among them, phytol, squalene, α-tocopherol, lupeol, and lupenone (lup-20(29)-en-3-one) (Figure 3) are the most predominant, showing the highest peak areas. Phytol, squalene, lupeol, lupenone, and α-tocopherol have been previously identified in *A. dealbata* leaves [36,66,78].

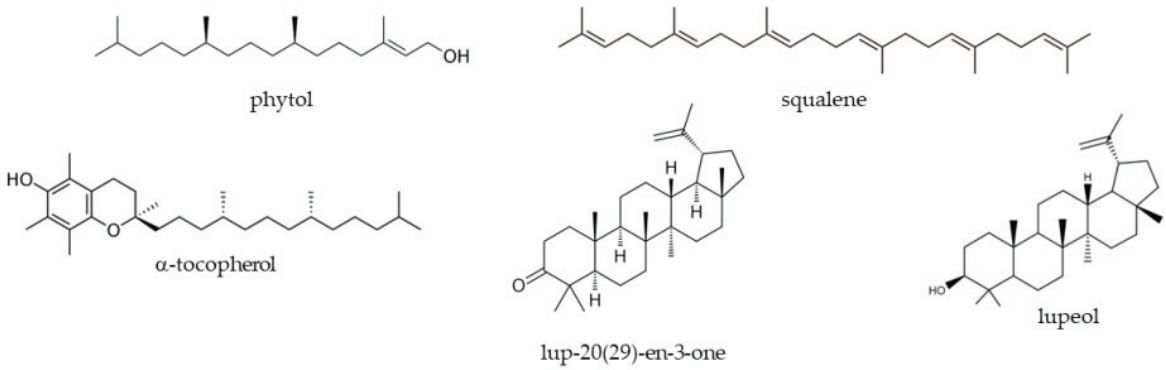

Figure 3. Chemical structures of phytol, squalene, α-tocopherol, lupenone (lup-20(29)-en-3-one), and lupeol.

Phytol is a diterpene known for its wide range of biological activities, such as antimicrobial, antioxidant, cytotoxic, anxiolytic, anticonvulsant, immunomodulatory, antinociceptive, and anti-inflammatory activities, besides its role in the induction of apoptosis and protective autophagy and in the treatment of metabolic disorders [79]. Phytol is the most abundant compound in the analyzed extracts, especially in the leaves fraction, with the extracts obtained from dried leaves showing higher content than the one obtained from fresh leaves (Figure 4).

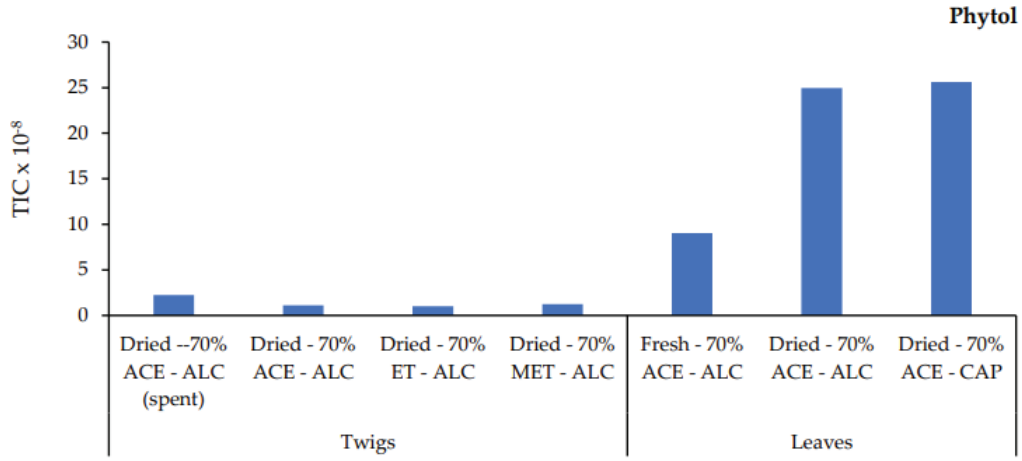

Figure 4. Absolute peak areas of phytol in the analyzed extracts; TIC: Total Ion Current.

Figure 5 shows the absolute peak areas of squalene, α-tocopherol, lupenone, and lupeol for the selected extracts.

Squalene is a triterpene with reported antioxidant, anti-inflammatory, and anti-atherosclerotic properties [80], as well as presenting the potential for cosmetic dermatology applications due to its emollient and antioxidant properties, and for hydration and its antitumor activities [81]. Squalene is more abundant in 70% ACE extracts than in 70% ET or 70% MET ones, with the highest amounts being observed in the dried leaves extracts.

α-Tocopherol is the main form of vitamin E, which has antioxidant, anti-inflammatory, and antitumor properties already described in the literature [82]. α-Tocopherol is not present in the 70% ET and 70% MET extracts, being particularly abundant in the dried leaves extracts.

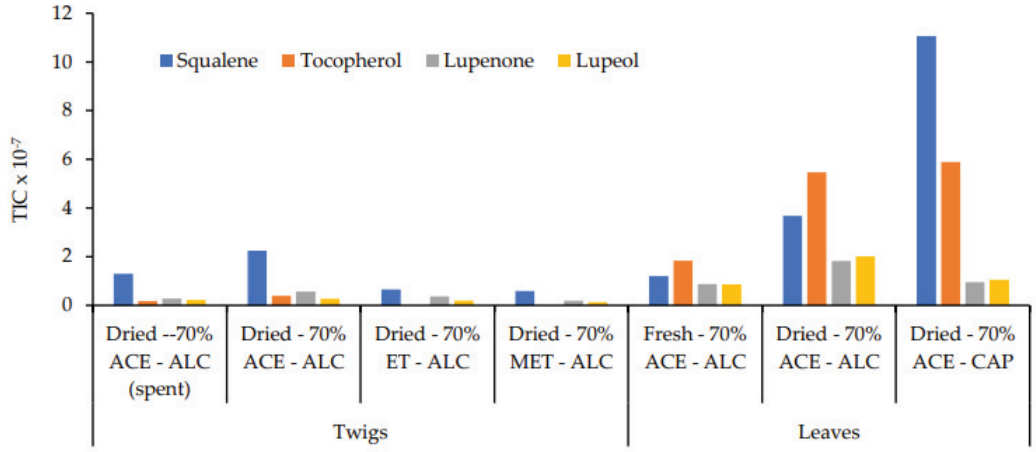

Figure 5. Absolute peak areas of squalene, α-tocopherol, lupenone (lup-20(29)-en-3-one), and lupeol in the analyzed extracts; TIC: Total Ion Current.

Lupenone and lupeol are pentacyclic triterpenes showing a broad spectrum of biological activities. For the former, its importance as a therapeutic and chemo preventive agent for the treatment of inflammation, virus infection, diabetes, cancer, and Chagas disease was already described in the literature [83]. For lupeol, antioxidant, antiprotozoal, anti-inflammatory, antitumor, and antimicrobial activities were previously reported, in addition to its cardio- and hepatoprotective effects and as a cancer chemo preventive agent [84]. Both compounds are more abundant in leaves extracts than in twigs extracts. These results show the ability of acetone to extract both polar and non-polar compounds, which occurred to a lesser extent when using aqueous ethanol or methanol, given the higher polarity of these solvents. The use of dry material favored the extraction of this non-polar fraction as well. The previous extraction of the raw material with petroleum ether naturally decreased the amount of these non-polar compounds in the extract obtained from spent material. The presence of these bioactive compounds in a higher amount in the leaves extracts does not agree with the highest antioxidant and antimicrobial effects observed in the twig's extracts, which suggests that these effects are predominantly due to the action of the more polar compounds present in the extracts. In fact, it was observed a strong positive correlation between TPC and antioxidant activity.

4. Conclusions

This investigation demonstrated the possibility of producing extracts rich in phenolic compounds with antioxidant and antimicrobial properties using leaves and twigs of Portuguese *A. dealbata* by a simple maceration process at room temperature. The highest values of extraction yield, TPC, TFC, and TPrAC as well as antioxidant activity measured by the DPPH and FRAP assays were obtained with 70% ACE using leaves and twigs from Alcobaça. The drying status of the raw material also affected some characteristics of the extracts, improving extraction yield, TFC, and TPrAC for dried leaves and twigs.

As a rule, better results were observed in extracts from the twigs than in the corresponding extracts from the leaves, except for extraction yield. This observation shows the possibility of using the entire fraction of the branches, where the leaves represent by far the highest weight fraction, without the necessity of separating the twigs from the leaves once they add quality to the produced extracts.

Moreover, this work showed the possibility of obtaining a wider range of products from the same amount of raw material via sequential extraction with petroleum ether to remove lipophilic compounds followed by the best extraction solvent to remove phenolic compounds, all without significantly decreasing the quality of the extract.

Significant and strong correlations between TPC and TPrAC and antioxidant activity by DPPH and FRAP assays shows that those phenolic components are the main responsible

for the antioxidant and antimicrobial properties of the extracts. Nevertheless, bioactive lipophilic components, such as phytol, squalene, α-tocopherol, lupenone, and lupeol were also detected, especially in the extracts of leaves. Therefore, this work demonstrates the possibility of obtaining high-value extracts with antioxidant and antimicrobial properties from fractions of *A. dealbata* biomass that can be collected regularly to reduce widespread dissemination of this species.

Supplementary Materials: The following supporting information can be downloaded at: https://www.mdpi.com/article/10.3390/pr10112429/s1, Table S1: TPC (mg GAE/g of biomass, wet basis), TFC (mg CatE/g of biomass, wet basis), and antioxidant activity by DPPH (mg TE/g of biomass) and FRAP (mmol Fe^{2+}/g of biomass) of extracts from fresh and dried leaves and twigs from Alcobaça and Caparica, using different extraction solvents and extraction methods; Table S2: Extraction yield, TPC and DPPH values for different times of maceration at room temperature, of plants collected in Caparica using 70% ACE as extraction solvent; Table S3: TFC (mg RE/g extract, wet basis) of extracts from fresh and dried leaves and twigs from Alcobaça and Caparica, using different extraction solvents and extraction methods; Table S4: TFC (mg RutE/g of raw material, wet basis) of extracts from fresh and dried leaves and twigs from Alcobaça and Caparica, using different extraction solvents and extraction methods; Table S5: Average values of extraction yield (%, wet basis), TPC (mg GAE/g extract), TFC (mg CatE/g extract) and TPrAC (mg PycE/g extract) for extracts obtained by maceration and hot extraction (regardless drying status and origin), from fresh and dried material (regardless extraction method and origin), and from plants from Alcobaça and Caparica (regardless extraction process and drying status); Table S6: Chromatographic peak areas of non-polar components co-extracted with phenolic compounds for a group of selected extracts obtained by maceration at room temperature; Figure S1: Chromatographic profile of the non-polar fraction of the extract obtained with 70% acetone by maceration of dried Acacia leaves collected in Alcobaça region. Part 1—Low retention time components; Figure S2: Chromatographic profile of the non-polar fraction of the extract obtained with 70% acetone by maceration of dried Acacia leaves collected in Alcobaça region. Part 2—High retention time components; Figure S3: Chromatographic profile of the non-polar fraction of the extract obtained with 70% methanol by maceration of dried Acacia twigs collected in Alcobaça region. Part 1—Low retention time components.

Author Contributions: Conceptualization, R.C. and M.G.; methodology, R.C. and M.G.; investigation, R.C., E.M.M. and J.B.; writing—original draft preparation, R.C.; writing—review and editing, M.G., M.P.D., J.C.Q., M.G.d.S. and R.C.; supervision, M.G., M.P.D., M.G.d.S. and J.C.Q. All authors have read and agreed to the published version of the manuscript.

Funding: This work was supported by national funds through the Fundação para a Ciência e a Tecnologia, I.P. (Portuguese Foundation for Science and Technology) by the project (UIDB/04077/2020-2023 and UIDP/04077/2020-2023) of Mechanical Engineering and Resource Sustainability Center—MEtRICs, by the project UIDB/05064/2020 of VALORIZA—Research Centre for Endogenous Resource Valorization), by the project (PTDC/CTA-AMB/6587/2020) of CENSE "Center for Environmental and Sustainability Research" and by the project (UID/QUI/50006/2020) of LAQV/REQUIMTE; human resources were also supported by the PhD grants SFRH/BD/133300/2017 and UI/BD/150867/2021.

Data Availability Statement: Not applicable.

Acknowledgments: The authors acknowledge Fundação para a Ciência e a Tecnologia, I.P. (Portuguese Foundation for Science and Technology) for financing the projects (UIDB/04077/2020-2023 and UIDP/04077/2020-2023), UIDB/05064/2020, (PTDC/CTA-AMB/6587/2020) and (UID/QUI/50006/2020) that support the activities of the research units that participated in this work. The authors also acknowledge Fundação para a Ciência e a Tecnologia, I.P. for the PhD grants SFRH/BD/133300/2017 and UI/BD/150867/2021.

Conflicts of Interest: The authors declare no conflict of interest.

References

1. Maslin, B.R. Synoptic overview of *Acacia* sensu lato (Leguminosae: Mimosoideae) in East and Southeast Asia. *Gard. Bull. Singap.* **2015**, *67*, 231. [CrossRef]
2. Breton, C.; Guerin, J.; Ducatillion, C.; Médail, F.; Kull, C.A.; Bervillé, A. Taming the wild and "wilding" the tame: Tree breeding and dispersal in Australia and the Mediterranean. *Plant Sci.* **2008**, *175*, 197–205. [CrossRef]
3. Kull, C.A.; Shackleton, C.M.; Cunningham, P.J.; Ducatillon, C.; Dufour-Dror, J.-M.; Esler, K.J.; Friday, J.B.; Gouveia, A.C.; Griffin, A.R.; Marchante, E.; et al. Adoption, use and perception of Australian acacias around the world. *Divers. Distrib.* **2011**, *17*, 822–836. [CrossRef]
4. Seigler, D.S. Phytochemistry of *Acacia—Sensu lato*. *Biochem. Syst. Ecol.* **2003**, *31*, 845–873. [CrossRef]
5. Fuentes-Ramírez, A.; Pauchard, A.; Cavieres, L.A.; García, R.A. Survival and growth of *Acacia dealbata* vs. native trees across an invasion front in south-central Chile. *For. Ecol. Manag.* **2011**, *261*, 1003–1009. [CrossRef]
6. Le Maitre, D.C.; Gaertner, M.; Marchante, E.; Ens, E.J.; Holmes, P.M.; Pauchard, A.; O'Farrell, P.J.; Rogers, A.M.; Blanchard, R.; Blignaut, J.; et al. Impacts of invasive Australian acacias: Implications for management and restoration. *Divers. Distrib.* **2011**, *17*, 1015–1029. [CrossRef]
7. Lorenzo, P.; González, L.; Reigosa, M.J. The genus *Acacia* as invader: The characteristic case of *Acacia dealbata* Link in Europe. *Ann. For. Sci.* **2010**, *67*, 101. [CrossRef]
8. Richardson, D.M.; Rejmánek, M. Trees and shrubs as invasive alien species—A global review. *Divers. Distrib.* **2011**, *17*, 788–809. [CrossRef]
9. Ministério do Ambiente. *Ministério do Ambiente Decreto-Lei n.º 565/99 de 21 de Dezembro*; Série-A. N.º 295—31-12-1999; Diário da República: Lisboa, Portugal, 1999; pp. 9100–9115.
10. Jæger, D.; O'Leary, M.C.; Weinstein, P.; Møller, B.L.; Semple, S.J. Phytochemistry and bioactivity of *Acacia sensu stricto* (Fabaceae: Mimosoideae). *Phytochem. Rev.* **2019**, *18*, 129–172. [CrossRef]
11. Subhan, N.; Burrows, G.E.; Kerr, P.G.; Obied, H.K. Phytochemistry, Ethnomedicine, and Pharmacology of *Acacia*. In *Studies in Natural Products Chemistry*; Elsevier B.V.: Amsterdam, The Netherlands, 2018; Volume 57, pp. 247–326. ISBN 9780444640574.
12. Miguel-Chávez, R.S. Phenolic Antioxidant Capacity: A Review of the State of the Art. In *Phenolic Compounds—Biological Activity*; IntechOpen: London, UK, 2017; pp. 59–74.
13. Santos-Sánchez, N.F.; Salas-Coronado, R.; Villanueva-Cañongo, C.; Hernández-Carlos, B. Antioxidant Compounds and Their Antioxidant Mechanism. In *Antioxidants*; IntechOpen: London, UK, 2019; pp. 1–28.
14. Ghannoum, M.A.; Rice, L.B. Antifungal Agents: Mode of Action, Mechanisms of Resistance, and Correlation of These Mechanisms with Bacterial Resistance. *Clin. Microbiol. Rev.* **1999**, *12*, 501–517. [CrossRef]
15. Correia, R.; Quintela, J.C.; Duarte, M.P.; Gonçalves, M. Insights for the valorization of biomass from portuguese invasive *Acacia* spp. in a biorefinery perspective. *Forests* **2020**, *11*, 1342. [CrossRef]
16. Ramli, S.; Harada, K.I.; Ruangrungsi, N. Antioxidant, antimicrobial and cytotoxicity activities of *Acacia farnesiana* (L.) Willd. Leaves ethanolic extract. *Pharmacogn. J.* **2011**, *3*, 50–58. [CrossRef]
17. Cock, I.E.; van Vuuren, S.F. South African food and medicinal plant extracts as potential antimicrobial food agents. *J. Food Sci. Technol.* **2015**, *52*, 6879–6899. [CrossRef]
18. Nielsen, T.R.H.; Kuete, V.; Jäger, A.K.; Meyer, J.J.M.; Lall, N. Antimicrobial activity of selected South African medicinal plants. *BMC Complement. Altern. Med.* **2012**, *12*, 74. [CrossRef]
19. Nyila, M.A.; Leonard, C.M.; Hussein, A.A.; Lall, N. Activity of South African medicinal plants against *Listeria monocytogenes* biofilms, and isolation of active compounds from *Acacia karroo*. *S. Afr. J. Bot.* **2012**, *78*, 220–227. [CrossRef]
20. Priyanka, C.; Kumar, P.; Bankar, S.P.; Karthik, L. In vitro antibacterial activity and gas chromatography–mass spectroscopy analysis of *Acacia karoo* and Ziziphus mauritiana extracts. *J. Taibah Univ. Sci.* **2015**, *9*, 13–19. [CrossRef]
21. Lima, C.P.; Cunico, M.M.; Auer, C.G.; Miguel, O.G.; Miguel, M.D.; da Silva, C.B.; Andrade, C.A.; Kerber, V.A. Potencial alelopático e antifúngico do extrato das folhas de *Acacia longifolia* (Andr.) Willd. *Visão Acadêmica* **2013**, *14*, 16–25. [CrossRef]
22. Edrah, S.M.; Alafid, F.; Shmeala, H.; Abobaker, D.M. Phytochemical analysis and antibacterial activity of *Acacia pycnantha* from Alkhums Libya. In Proceedings of the 2nd Annual Conference on Theories and Applications of Basic and Biosciences, Bali, Indonesia, 11–12 April 2019; pp. 704–712.
23. Mahmoud, M.F.; Alrumman, S.A.; Hesham, A.E.L. Biological activities of some *Acacia* spp. (Fabaceae) against new clinical isolates identified by ribosomal RNA gene-based phylogenetic analysis. *Pak. J. Pharm. Sci.* **2016**, *29*, 221–229.
24. El-Toumy, S.A.; Salib, J.Y.; Mohamed, W.M.; Morsy, F.A. Phytochemical and antimicrobial studies on *Acacia saligna* leaves. *Egypt. J. Chem.* **2010**, *53*, 705–717. [CrossRef]
25. Noreen, I.; Iqbal, A.; Rabbi, F.-; Muhammad, A.; Shah, Z.; Rahman, Z.U. Antimicrobial activity of different solvents extracts of *Acacia cyanophylla*. *Pak. J. Weed Sci. Res.* **2017**, *23*, 79–90.
26. Gumgumjee, N.M.; Hajar, A.S. Antimicrobial efficacy of *Acacia saligna* (Labill.) HL Wendl. and *Cordia sinensis* Lam. leaves extracts against some pathogenic microorganisms. *Int. J. Microbiol. Immunol. Res* **2015**, *3*, 51–57.
27. Gedara, S.R.; Galala, A.A. New cytotoxic spirostane saponin and biflavonoid glycoside from the leaves of *Acacia saligna* (Labill.) H.L. Wendl. *Nat. Prod. Res.* **2014**, *28*, 324–329. [CrossRef] [PubMed]
28. Fowora, M.A.; Onyeaghasiri, F.U.; Olanlege, A.L.O.; Edu-Muyideen, I.O.; Adebesin, O.O. In Vitro Susceptibility of Dermatophytes to Anti-Fungal Drugs and Aqueous *Acacia nilotica* Leaf Extract in Lagos, Nigeria. *J. Biomed. Sci. Eng.* **2021**, *14*, 74–82. [CrossRef]

29. Borges, A.; José, H.; Homem, V.; Simões, M. Comparison of techniques and solvents on the antimicrobial and antioxidant potential of extracts from *Acacia dealbata* and *Olea europaea*. *Antibiotics* **2020**, *9*, 48. [CrossRef]
30. Silva, E.; Fernandes, S.; Bacelar, E.; Sampaio, A. Antimicrobial activity of aqueous, ethanolic and methanolic leaf extracts from *Acacia* spp. and Eucalyptus nicholii. *Afr. J. Tradit. Complement. Altern. Med.* **2016**, *13*, 130–134. [CrossRef] [PubMed]
31. Kumari, R.; Mishra, R.C.; Yadav, A.; Yadav, J.P. Screening of traditionally used medicinal plants for their antimicrobial efficacy against oral pathogens and GC-MS analysis of acacia nilotica extract. *Indian J. Tradit. Knowl.* **2019**, *18*, 162–168.
32. Kumari, R.; Mishra, R.C.; Yadav, J.P. Preparation and in vitro antimicrobial activity of supercritical fluid extracts of selected Indian plants against oral pathogens and their phytochemicals and statistical analysis. *Int. J. Green Pharm.* **2020**, *14*, 146–154. [CrossRef]
33. Kumari, R.; Mishra, R.C.; Sheoran, R.; Yadav, J.P. Fractionation of antimicrobial compounds from *Acacia nilotica* twig extract against oral pathogens. *Biointerface Res. Appl. Chem.* **2020**, *10*, 7097–7105. [CrossRef]
34. Arshad, M.S.; Hussain, I.; Mahmood, M.S.; Khan, M.N. Evaluation of antimicrobial potential of *Acacia nilotica* (Kikar) against oral pathogens associated with caries and periodontitis. *Pak. J. Agric. Sci.* **2017**, *54*, 423–430. [CrossRef]
35. Lomarat, P.; Chancharunee, S.; Anantachoke, N.; Kitphati, W.; Sripha, K.; Bunyapraphatsara, N. Bioactivity-guided separation of the active compounds in *Acacia pennata* responsible for the prevention of Alzheimer's disease. *Nat. Prod. Commun.* **2015**, *10*, 1431–1434. [CrossRef]
36. Rodrigues, V.H.; De Melo, M.M.R.; Portugal, I.; Silva, C.M. Extraction of added-value triterpenoids from *Acacia dealbata* leaves using supercritical fluid extraction. *Processes* **2021**, *9*, 1159. [CrossRef]
37. Azwanida, N.N. A Review on the Extraction Methods Use in Medicinal Plants, Principle, Strength and Limitation. *Med. Aromat. Plants* **2015**, *4*, 3–8. [CrossRef]
38. Singleton, V.L.; Orthofer, R.; Lamuela-Raventós, R.M. Analysis of total phenols and other oxidation substrates and antioxidants by means of Folin-Ciocalteu reagent. *Methods Enzymol.* **1999**, *299*, 152–178. [CrossRef]
39. Barros, L.; Carvalho, A.M.; Morais, J.S.; Ferreira, I.C.F.R. Strawberry-tree, blackthorn and rose fruits: Detailed characterisation in nutrients and phytochemicals with antioxidant properties. *Food Chem.* **2010**, *120*, 247–254. [CrossRef]
40. Škerget, M.; Kotnik, P.; Hadolin, M.; Hraš, A.R.; Simonič, M.; Knez, Ž. Phenols, proanthocyanidins, flavones and flavonols in some plant materials and their antioxidant activities. *Food Chem.* **2005**, *89*, 191–198. [CrossRef]
41. Blois, M.S. Antioxidant Determinations by the Use of a Stable Free Radical. *Nature* **1958**, *181*, 1199–1200. [CrossRef]
42. Benzie, I.F.F.; Strain, J.J. Hormonelle Beeinflussung des experimentellen Portiocarcinoms. *Anal. Biochem.* **1996**, *239*, 70–76. [CrossRef]
43. Pereira, P.; Mauricio, E.M.; Duarte, M.P.; Lima, K.; Fernandes, A.S.; Bernardo-Gil, G.; Cebola, M.-J. Potential of supercritical fluid myrtle extracts as an active ingredient and co-preservative for cosmetic and topical pharmaceutical applications. *Sustain. Chem. Pharm.* **2022**, *28*, 100739. [CrossRef]
44. Popova, V.; Ivanova, T.; Stoyanova, A.; Nikolova, V.; Hristeva, T.; Zheljazkov, V.D. GC-MS composition and olfactory profile of concretes from the flowers of four *Nicotiana* species. *Molecules* **2020**, *25*, 2617. [CrossRef]
45. van Den Dool, H.; Kratz, P.D. A generalization of the retention index system including linear temperature programmed gas—Liquid partition chromatography. *J. Chromatogr. A* **1963**, *11*, 463–471. [CrossRef]
46. Climate-Data.org. Clima Alcobaça. Available online: https://pt.climate-data.org/europa/portugal/alcobaca/alcobaca-882351/ (accessed on 1 April 2021).
47. Climate-Data.org. Clima Almada. Available online: https://pt.climate-data.org/europa/portugal/almada/almada-7111/ (accessed on 1 April 2021).
48. Luís, A.; Gil, N.; Amaral, M.E.; Duarte, A.P. Antioxidant activities of extracts from *Acacia melanoxylon*, *Acacia dealbata* and *Olea europaea* and alkaloids estimation. *Int. J. Pharm. Pharm. Sci.* **2012**, *4*, 225–231.
49. Gabr, S.; Nikles, S.; Maria, E.; Wenzig, P.; Ardjomand-woelkart, K.; Hathout, R.M.; El-ahmady, S.; Abdel, A.; Singab, A.; Bauer, R. Characterization and optimization of phenolics extracts from *Acacia* species in relevance to their anti-inflammatory activity. *Biochem. Syst. Ecol.* **2018**, *78*, 21–30. [CrossRef]
50. Xiong, J.; Grace, M.H.; Esposito, D.; Wang, F.; Lila, M.A. Phytochemical characterization and anti-inflammatory properties of *Acacia mearnsii* leaves. *Nat. Prod. Commun.* **2016**, *11*, 649–653. [CrossRef]
51. Zheleva-Dimitrova, D.; Sinan, K.I.; Etienne, O.K.; Ak, G.; Sharmeen, J.B.; Dervisoglu, G.; Ozdemir, F.A.; Mahomoodally, M.F.; Zengin, G. Comprehensive chemical characterization and biological evaluation of two *Acacia* species: *A. nilotica* and *A. ataxacantha*. *Food Chem. Toxicol.* **2021**, *156*, 112446. [CrossRef] [PubMed]
52. Ferreira-Santos, P.; Genisheva, Z.; Botelho, C.; Santos, J.; Ramos, C.; Teixeira, J.A.; Rocha, C.M.R. Unravelling the biological potential of *Pinus pinaster* bark extracts. *Antioxidants* **2020**, *9*, 334. [CrossRef] [PubMed]
53. Tung, Y.T.; Wu, J.H.; Hsieh, C.Y.; Chen, P.S.; Chang, S.T. Free radical-scavenging phytochemicals of hot water extracts of *Acacia confusa* leaves detected by an on-line screening method. *Food Chem.* **2009**, *115*, 1019–1024. [CrossRef]
54. Sowndhararajan, K.; Joseph, J.M.; Manian, S. Antioxidant and free radical scavenging activities of Indian acacias: *Acacia leucophloea* (Roxb.) Willd., *Acacia ferruginea* Dc., *Acacia dealbata* Link. and *Acacia pennata* (l.) Willd. *Int. J. Food Prop.* **2013**, *16*, 1717–1729. [CrossRef]
55. Kopjar, M.; Tadić, M.; Piližota, V. Phenol content and antioxidant activity of green, yellow and black tea leaves. *Chem. Biol. Technol. Agric.* **2015**, *2*, 1. [CrossRef]

56. Sariburun, E.; Şahin, S.; Demir, C.; Türkben, C.; Uylaşer, V. Phenolic content and antioxidant activity of raspberry and blackberry cultivars. *J. Food Sci.* **2010**, *75*, 328–335. [CrossRef]
57. Verma, N.; Shukla, S. Impact of various factors responsible for fluctuation in plant secondary metabolites. *J. Appl. Res. Med. Aromat. Plants* **2015**, *2*, 105–113. [CrossRef]
58. Kedare, S.B.; Singh, R.P. Genesis and development of DPPH method of antioxidant assay. *J. Food Sci. Technol.* **2011**, *48*, 412–422. [CrossRef] [PubMed]
59. Venkatesan, T.; Choi, Y.-W.; Kim, Y.-K. Impact of Different Extraction Solvents on Phenolic Content and Antioxidant Potential of *Pinus densiflora* Bark Extract. *Biomed Res. Int.* **2019**, *2019*, 3520675. [CrossRef] [PubMed]
60. Sadiq, M.B.; Tharaphan, P.; Chotivanich, K.; Tarning, J.; Anal, A.K. In vitro antioxidant and antimalarial activities of leaves, pods and bark extracts of *Acacia nilotica* (L.) Del. *BMC Complement. Altern. Med.* **2017**, *17*, 372. [CrossRef] [PubMed]
61. Afsar, T.; Razak, S.; Shabbir, M.; Khan, M.R. Antioxidant activity of polyphenolic compounds isolated from ethyl—Acetate fraction of *Acacia hydaspica* R. Parker. *Chem. Cent. J.* **2018**, *12*, 5. [CrossRef]
62. Zia-Ul-Haq, M.; Cavar, S.; Qayum, M.; Khan, I.; Ahmad, S. Chemical composition and antioxidant potential of *Acacia leucophloea* Roxb. *Acta Bot. Croat.* **2013**, *72*, 133–144. [CrossRef]
63. Astuya, A.; Ziehe, J.; Rivera, A.; Ortiz, S.; Ulloa, V.; Roeckel, M.; Aspé, E.; Fernández, K. Antioxidant and anti-inflammatory activities of *Pinus radiata* bark extract in salmonid cell lines. *Aquac. Res.* **2016**, *48*, 3568–3578. [CrossRef]
64. Salar, R.K.; Seasotiya, L. Free radical scavenging activity, phenolic contents and phytochemical evaluation of different extracts of stem bark of *Butea monosperma* (Lam.) Kuntze. *Front. Life Sci.* **2011**, *5*, 107–116. [CrossRef]
65. Salem, N.; Msaada, K.; Hamdaoui, G.; Limam, F.; Marzouk, B. Variation in Phenolic Composition and Antioxidant Activity during Flower Development of Safflower (*Carthamus tinctorius* L.). *J. Agric. Food Chem.* **2011**, *59*, 4455–4463. [CrossRef]
66. Oliveira, C.S.D.; Moreira, P.; Resende, J.; Cruz, M.T.; Pereira, C.M.F.; Silva, A.M.S.; Santos, S.A.O.; Silvestre, A.J.D. Characterization and cytotoxicity assessment of the lipophilic fractions of different morphological parts of *Acacia dealbata*. *Int. J. Mol. Sci.* **2020**, *21*, 1814. [CrossRef]
67. Akoglu, H. User's guide to correlation coefficients. *Turk. J. Emerg. Med.* **2018**, *18*, 91–93. [CrossRef]
68. Yadav, A.; Yadav, M.; Kumar, S.; Sharma, D.; Yadav, J.P. In vitro antioxidant activities and GC-MS analysis of different solvent extracts of *Acacia nilotica* leaves. *Indian J. Pharm. Sci.* **2018**, *80*, 892–902. [CrossRef]
69. Abdel-Farid, I.B.; Sheded, M.G.; Mohamed, E.A. Metabolomic profiling and antioxidant activity of some *Acacia* species. *Saudi J. Biol. Sci.* **2014**, *21*, 400–408. [CrossRef] [PubMed]
70. Ulewicz-Magulska, B.; Wesolowski, M. Total Phenolic Contents and Antioxidant Potential of Herbs Used for Medical and Culinary Purposes. *Plant Foods Hum. Nutr.* **2019**, *74*, 61–67. [CrossRef] [PubMed]
71. Zeng, X.; Su, W.; Zheng, Y.; Liu, H.; Li, P.; Zhang, W.; Liang, Y.; Bai, Y.; Peng, W.; Yao, H. UFLC-Q-TOF-MS/MS-based screening and identification of flavonoids and derived metabolites in human urine after oral administration of exocarpium citri grandis extract. *Molecules* **2018**, *23*, 895. [CrossRef]
72. Jenkins, D.R. Nosocomial infections and infection control. *Medicine* **2017**, *45*, 629–633. [CrossRef]
73. Ganaie, H.A.; Ali, M.N.; Ganai, B.A.; Meraj, M.; Ahmad, M. Antibacterial activity of 14, 15-dihydroajugapitin and 8-o-acetylharpagide isolated from *Ajuga bracteosa* Wall ex. Benth against human pathogenic bacteria. *Microb. Pathog.* **2017**, *103*, 114–118. [CrossRef]
74. Wu, S.-C.; Liu, F.; Zhu, K.; Shen, J.-Z. Natural Products That Target Virulence Factors in Antibiotic-Resistant *Staphylococcus aureus*. *J. Agric. Food Chem.* **2019**, *67*, 13195–13211. [CrossRef]
75. Leitão, J.H. Microbial Virulence Factors. *Int. J. Mol. Sci.* **2020**, *21*, 5320. [CrossRef]
76. Mayer, F.L.; Wilson, D.; Hube, B. *Candida albicans* pathogenicity mechanisms. *Virulence* **2013**, *4*, 119–128. [CrossRef]
77. Lopes, J.P.; Lionakis, M.S. Pathogenesis and virulence of *Candida albicans*. *Virulence* **2022**, *13*, 89–121. [CrossRef]
78. Pereira, F.B.M.; Domingues, F.M.J.; Silva, A.M.S. Triterpenes from *Acacia dealbata*. *Nat. Prod. Lett.* **1996**, *8*, 97–103. [CrossRef]
79. Islam, M.T.; Ali, E.S.; Uddin, S.J.; Shaw, S.; Islam, M.A.; Ahmed, M.I.; Chandra Shill, M.; Karmakar, U.K.; Yarla, N.S.; Khan, I.N.; et al. Phytol: A review of biomedical activities. *Food Chem. Toxicol.* **2018**, *121*, 82–94. [CrossRef] [PubMed]
80. Lou-Bonafonte, J.M.; Martínez-Beamonte, R.; Sanclemente, T.; Surra, J.C.; Herrera-Marcos, L.V.; Sanchez-Marco, J.; Arnal, C.; Osada, J. Current Insights into the Biological Action of Squalene. *Mol. Nutr. Food Res.* **2018**, *62*, 1800136. [CrossRef] [PubMed]
81. Huang, Z.R.; Lin, Y.K.; Fang, J.Y. Biological and pharmacological activities of squalene and related compounds: Potential uses in cosmetic dermatology. *Molecules* **2009**, *14*, 540–554. [CrossRef] [PubMed]
82. Szewczyk, K.; Chojnacka, A.; Górnicka, M. Tocopherols and tocotrienols—Bioactive dietary compounds; what is certain, what is doubt? *Int. J. Mol. Sci.* **2021**, *22*, 6222. [CrossRef]
83. Xu, F.; Huang, X.; Wu, H.; Wang, X. Beneficial health effects of lupenone triterpene: A review. *Biomed. Pharmacother.* **2018**, *103*, 198–203. [CrossRef]
84. Wal, P.; Wal, A.; Sharma, G.; Rai, A.K. Biological activities of lupeol. *Syst. Rev. Pharm.* **2011**, *2*, 96–103. [CrossRef]

processes

MDPI

Article

Poplar Wood Pretreatment Using Deep Eutectic Solvents for Promoting Enzymatic Hydrolysis

Xuyang Zhao, Ying Zhan, Lihua Han, Xiaoran Sun, Tianyu Zhang and Zheng Zhao *

College of Chemical Engineering, North China University of Science and Technology, Tangshan 063210, China; a15736973753@163.com (X.Z.); zhanying0326@163.com (Y.Z.); tshlh@ncst.edu.cn (L.H.); xiaoranhb@yeah.net (X.S.); a13786654504@163.com (T.Z.)

* Correspondence: buctzhaozheng@163.com; Tel.: +86-315-8805-460

Abstract: Bioethanol produced from lignocellulose is a renewable energy substitute for traditional fossil fuels. Poplar wood as forest waste is popular in bioethanol production. Nonetheless, the complex structure of lignocellulose leads to low reducing sugar and ethanol yields. Thus, lignocellulose pretreatment is necessary to promote enzymatic hydrolysis. Deep eutectic solvents (DESs) have good dissolution capacity, low vapor pressure, a simple synthesis procedure, low synthesis cost and low toxicity. More and more researchers have begun paying attention to the application of DESs in lignocellulose pretreatment. In this work, poplar wood was pretreated using a series of basic DESs based on diol. The effects of the DES species, the basicity of the solvents, the pretreatment temperature and the pretreatment time on the effectiveness of pretreatment and enzyme hydrolysis for poplar wood were investigated, and characterization analysis (Fourier transform infrared spectroscopy, X-ray diffraction and scanning electron microscopy) of poplar wood was carried out to reveal the pretreatment mechanism. The best pretreatment effect was obtained from K: 1, 2-PG, which removed 89.2% and 71.6% of the lignin and hemicellulose, respectively, while preserving 97.5% of the cellulose at 130 °C for 7 h. This enhanced the reducing sugar yield to 82.5% relative to that of the raw sample (3.3%) after 72 h of hydrolysis. The results of the characterization analysis demonstrated that lignin and hemicellulose were removed. Therefore, the DES based on K: 1, 2-PG is a promising solvent for poplar wood pretreatment, and could improve the industrial production of reducing sugar and bioethanol.

Keywords: deep eutectic solvents; diol; poplar wood; pretreatment; enzymatic hydrolysis

1. Introduction

Bioethanol, a source of renewable energy, can replace traditional fossil fuels and, thus, resolve two energy problems. The main sources of lignocellulosic biomass include agricultural and forestry wastes. In particular, a huge amount of forest waste originates from deforestation, timber processing and forest pruning, i.e., about 400 million tons of standard coal annually in China [1]. Nevertheless, the complex structure of lignocellulose hinders the transformation of cellulose into bioethanol. Lignocellulosic biomass contains lignin, hemicellulose and cellulose. Hemicelluloses adhere to the surface of cellulose through van der Waals forces and hydrogen bonds, and connect lignin through ether bonds and glycoside bonds to form a stable network structure [2]. Therefore, it is necessary to pretreat lignocellulosic biomass by removing lignin and hemicellulose in order to improve the reducing sugar and ethanol yields.

Many common traditional pretreatment methods, such as dilute acid, dilute alkali, organic solvent and biological methods [3–7], have one or several disadvantages, including high energy consumption, high toxicity, harsh conditions, corrosion equipment or a long pretreatment time. Therefore, the majority of scientific research workers have begun to look at green solvent ionic liquids (ILs). ILs have the characteristics of high thermal stability,

low steam pressure, non-flammability and non-volatilization [8], making them suitable for lignocellulose pretreatment. Nonetheless, the greenness of ILs has been questioned and the industrial application of IL pretreatment technology has been hindered because they possess several drawbacks, such as high synthetic cost, complex synthetic steps and high toxicity in ILs.

Recently, the application of deep eutectic solvents (DESs) in lignocellulosic biomass pretreatment has attracted extensive attention. DESs usually consist of two or more hydrogen bond donors (HBDs) and hydrogen bond acceptors (HBAs). Otherwise, the melting points of DESs are lower than those of individual components. The most important point is that DESs have a few similar properties to ILs and possess merits such as a low cost of synthesis, a simple synthesis procedure, low toxicity and good biocompatibility, which compensate for the shortcomings of ILs. Lee et al. [9] used choline chloride: glycerol, choline chloride: lactic acid and choline chloride: urea to pretreat oil palm empty fruit bundles under ultrasound with 210 W at 50 °C for 15 min. As a result, reducing sugar yields of 35.3%, 36.7% and 35.8%, respectively, were obtained after the pretreated residues were enzymatically hydrolyzed for 72 h. Sai et al. [10] used chloride: lactic acid (molar ratio was 1:10) to pretreat empty fruit bunches at 100 °C for 1 h. After residue hydrolysis for 48 h, 51.1% of the reducing sugar yield was obtained. Li et al. [11] compared the pretreatment capacity of choline chloride: lactic acid and choline chloride: glycine. The research results showed that choline chloride: lactic acid removed 90.4% of the lignin, but choline chloride: glycine only removed 58.4% of the lignin during poplar wood pretreatment at suitable pretreatment conditions (temperature: 120 °C, time: 12 h). Wu et al. [12] reported that the continuous pretreatment of 0.75% (*w*/*w*) NaOH and choline chloride: lactic acid for sorghum straw exhibited high pretreatment efficiency. Firstly, 0.75% (*w*/*w*) NaOH pretreated sorghum straw at 121 °C for 1 h. Then, choline chloride: lactic acid was used to pretreat sorghum straw at 140 °C for 40 min. As a result, 78.4% lignin and 67.6% hemicellulose were removed, respectively. After the enzymatic hydrolysis of pretreated residue for 72 h, 94.9% of the reducing sugar yield was obtained. However, several problems, such as the larger proportions of cellulose loss and low reducing sugar yield, have yet to be resolved in the current DES pretreatment method. Our research group [13,14] has reported that basic DESs have the capacity to selectively remove the lignin and hemicellulose while retaining the majority of the cellulose in wheat straw. Otherwise, the basic DESs pretreatment method is less studied; in addition, the studies are not extensive and the pretreatment mechanism lacks depth, so it is necessary to conduct systematic research on basic DES pretreatment.

In this paper, a series of basic DESs based on diol (i.e., sodium hydroxide: ethylene, sodium hydroxide: polyethylene glycol-200, potassium hydroxide: polyethylene glycol-300, lithium hydroxide: polyethylene glycol-400, sodium hydroxide: polyethylene glycol-600, sodium hydroxide: 1,4-butyl glycol and potassium hydroxide: 1,2-propylene glycol) were screened to pretreat poplar wood. The effects of the DES species, the basicity of the solvents, the pretreatment temperature (i.e., 70 °C, 90 °C, 110 °C, 130 °C, 150 °C) and the pretreatment time (i.e., 7 h, 9 h, 11 h, 13 h, 15 h, 17 h) on the composition and reducing sugar yield of poplar wood were investigated. Moreover, the crystal structure, surface morphology and chemical structure of poplar biomass were also analyzed via Fourier transform infrared spectroscopy (FT-IR), X-ray diffraction (XRD) and scanning electron microscopy (SEM) to clarify the mechanism of basic DESs based on diol pretreating poplar wood.

2. Materials and Methods

2.1. Materials

Sodium hydroxide, potassium hydroxide (purity: 95%), ethylene glycol, lithium hydroxide (purity: 98%), 1,2-propanediol, 1,4-butanediol (purity: 99%), polyethylene glycol-600, polyethylene glycol-400, polyethylene glycol-300, polyethylene: glycol-200 and cellulase (enzymatic activity: 10,000 U·g^{-1}, C805042) were utilized. All of the aforementioned reagents were purchased from Maclean. Poplar wood was obtained from

Shijiazhuang Farm. The poplar wood was milled using a pulverizer and then screened to the desirable particles with a 50–80 mesh. After Soxhlet extraction was performed using ethanol and water for 24 h, the poplar wood particles was airdried and stored at 4 °C.

2.2. Preparation of DESs

The HBAs and HBDs were mixed with a specific molar ratio. Subsequently, the mixture was magnetically stirred at 80 °C until transparent and homogeneous solutions formed [15,16]. Table 1 lists the compositions of prepared DESs and the molar ratios of HBA to HBD in DESs.

Table 1. The preparation of DESs.

HBA	HBD	Molar Ratio (HBA:HBD)	Abbreviation
Sodium hydroxide	Ethylene glycol	1:4	Na: EG
Sodium hydroxide	Polyethylene glycol-200	1:2	Na: PEG-200
Potassium hydroxide	Polyethylene glycol-300	1:4	K: PEG-300
Lithium hydroxide	Polyethylene glycol-400	1:10	Li: PEG-400
Sodium hydroxide	Polyethylene glycol-600	1:4	Na: PEG-600
Sodium hydroxide	1,4-Butyl glycol	1:5	Na: 1,4-BDO
Potassium hydroxide	1,2-Propylene glycol	1:2	K: 1,2-PG

2.3. Pretreatment Process

Firstly, a 50–80 mesh of poplar wood was mixed with DESs at 1:20 (w/w), then stirred magnetically at a certain temperature for a set length of time. Next, the pretreatment liquid was diluted using hot water, then centrifuged (3000 r·s^{-1}) and filtered to separate the solid from the liquid. When the separation step was completed, the solid was washed further using deionized water. Centrifuging and washing were repeated until the scrubbing solution was neutral. In the end, the solid residue was freeze-dried for 72 h, then weighed and stored at 25 °C.

2.4. Enzymatic Hydrolysis

Firstly, the dipotassium hydrogen phosphate–citrate buffer solution was adjusted to pH = 4.8. Then, a mixture of 52.5 mL of ready-prepared buffer solution, 7.5 mL of cellulase solution and 0.4 g of the poplar wood sample was shaken in 72 h at 120 r/min and 45 °C. Additionally, 0.6 mL of hydrolysate was withdrawn at regular intervals, and the enzymatic hydrolysis reaction was terminated in a boiling water bath. According to the DNS method, the reducing sugar concentration was determined using the standard curve for reducing sugar ($y = 1.68x - 0.075$, $R^2 = 0.9998$). The reducing sugar yield was calculated based on the reducing sugar concentration [17].

2.5. Components Analysis

2.5.1. Determination of Lignin Content

Firstly, the 72% (w/w) sulfuric acid (10 mL) hydrolyzed a 0.3 g poplar wood sample for 1.5 h. Afterwards, the filtration of the suspension liquid was carried out to obtain liquids and solids (hydrolysis residue). The deionized water was used to wash the solid until the scrubbing solution was neutral. After filtering, the solid containing acid-insoluble lignin and ash was dried and calcined to determine the acid-insoluble lignin content [18]. The absorbance of the liquid was measured at 205 nm to determine the acid-soluble lignin content. The total lignin content in the poplar wood sample consisted of the acid-soluble lignin content and the acid-insoluble lignin content. According to Equation (1), the lignin removal was calculated.

$$R_l = [1 - (R \times w_{rl})/w_l] \quad (1)$$

R_l—lignin removal (%), R—residue recovery (%), w_{rl}—lignin content of pretreated poplar wood (%) and w_l—lignin content of untreated poplar wood (%).

2.5.2. Determination of Cellulose and Hemicellulose Content

First, 5 mL of 4 mg·mL^{-1} KOH solution (containing 1 mg·mL^{-1} $NaBH_4$) was used to treat 0.1 g of the poplar wood sample for 1 h in a water bath shaker at 25 °C. Next, 10 mL of deionized water and an equal volume of 4 mg·mL^{-1} KOH solution were added to the treatment liquid for washing and diluting. The supernatant and the absorbances were measured at 660 nm (xylose) and 620 nm (glucose), respectively. Then, the concentrations of xylose and glucose were calculated based on the absorbances and the standard curves of xylose ($y = 300.97x - 0.016$, $R^2 = 0.9994$) and glucose ($y = 102.75x + 0.0075$, $R^2 = 0.9992$) [19].

Afterwards, the 72% (w/w) sulfuric acid (4 mL) treated the residue, which was obtained from the above alkali treatment process, in a water bath shaker at 25 °C for 1 h. Then, the treatment liquid was filled to 30 mL by adding deionized water. The absorbances of the supernatant were also measured in order to calculate the concentrations of xylose and glucose, as described above.

Lastly, the cellulose content of the poplar wood sample was calculated according to the dehydration coefficient of glucose (0.90) and the glucose concentration obtained from the acid treatment process. The hemicellulose content in the poplar wood sample was determined according to the dehydration coefficient of glucose (0.90) and xylose (0.88), while the glucose and xylose concentrations were determined during the base treatment process and the xylose concentration was determined during the acid treatment process. According to Equations (2) and (3), the hemicellulose removal and cellulose reservation were calculated, respectively.

$$R_{\mathrm{h}} = [1 - (R \times w_{rh})/w_h] \quad (2)$$

R_{h}—hemicellulose removal (%), R—residue recovery (%), w_{rh} —hemicellulose content in poplar wood residue (%) and w_h —hemicellulose content in untreated poplar wood (%).

$$R_{\mathrm{c}} = [1 - (R \times w_{rc})/w_c] \quad (3)$$

R_{c}—cellulose reservation (%), R—residue recovery (%), w_{rc}—cellulose content in pretreated poplar wood (%) and w_c —lignin content in untreated poplar wood (%).

2.6. SEM Analysis

The crushed poplar wood sample was evenly dispersed on a disc coating with the conductive glue, and then spray-gold treatment was performed. Afterwards, the surface morphology of poplar wood samples before and after pretreatment by DESs was observed using a JSM-IT100 (A) type SEM [20].

2.7. FT-IR Analysis

Firstly, the mixture of the poplar wood sample and potassium bromide, with a mass ratio of 100:1, was pressed into a tablet. Then, a Vertex 80 V spectrometer was used to scan the tablet for 32 s (resolution: 2 cm^{-1}) in order to carry out the chemical structural analysis of the poplar wood sample. The wavenumber ranged from 4000 cm^{-1} to 400 cm^{-1} [21].

2.8. XRD Analysis

The poplar wood sample was scanned from 10° to 50° at a rate of 5°/min, using a Bruker D8 Advanced diffractometer to analyze the crystallinity in the poplar wood. The intensity of the spectrum peaks was used to calculate the crystallinity index, as shown in Equation (4) [21].

$$CrI = \frac{I_{002} - I_{\mathrm{am}}}{I_{002}} \times 100 \quad (4)$$

CrI—crystallinity index, I_{002}—peak intensity of crystalline region (2θ = 22.5°) and I_{am}—peak intensity of amorphous region (2θ = 18°).

3. Results and Analysis

3.1. Effect of DES Type on Pretreatment of Poplar Wood

Figure 1 shows the results of different DESs pretreating poplar wood at 90 °C for 11 h. As depicted in Figure 1, the pretreatment effects of diol monomer-based DESs were better than those of PEG-based DESs. The lignin and hemicellulose removal of Na: EG, Na: 1,4-BDO and K: 1,2-PG (diol monomer based DESs) pretreated residues ranged from 56.6% to 76.4% and from 54.1% to 69.5%, respectively, while Na: PEG-200, K: PEG-300, Li: PEG-400 and Na: PEG-600 (PEG based DESs) only removed 37.6–56.2% of the lignin and 24.3–60.9% of the hemicellulose. It is worth noting that K: 1,2-PG exhibited the best pretreatment capacity for poplar wood; for example, 76.4% lignin and 69.5% hemicellulose were removed, but 97.3% cellulose was preserved during K: 1,2-PG pretreatment of poplar wood.

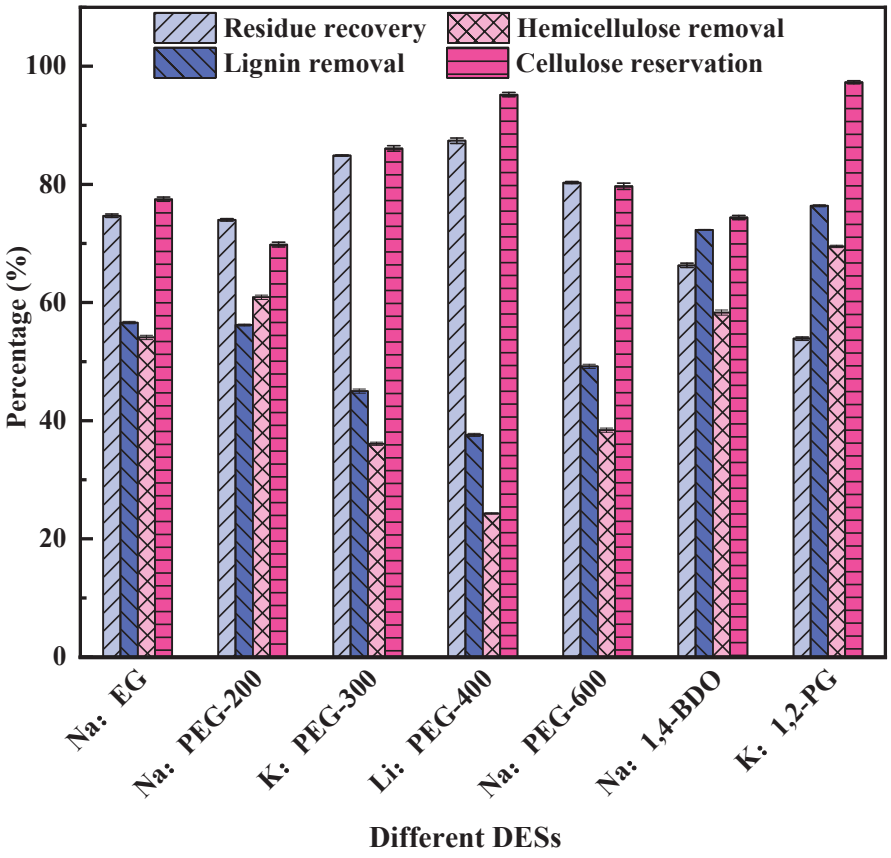

Figure 1. Effect of DES type on pretreatment of poplar wood (pretreatment conditions: 90 °C, 11 h).

The pH values of different DESs were measured as depicted in Figure 2. From Figure 2, we can observe a phenomenon: the pH values of the seven DESs were all greater than 11, which suggests that all of the DESs were basic solvents. In particular, K: 1,2-PG had the strongest basicity among these DESs, with the highest pH value being 13.3. Our previous studies [13,22] have proven that basic solvents can dissolve lignin and hemicellulose, but little cellulose. This explains the phenomenon by which a larger amount of lignin and hemicellulose than cellulose was removed by K: 1,2-PG.

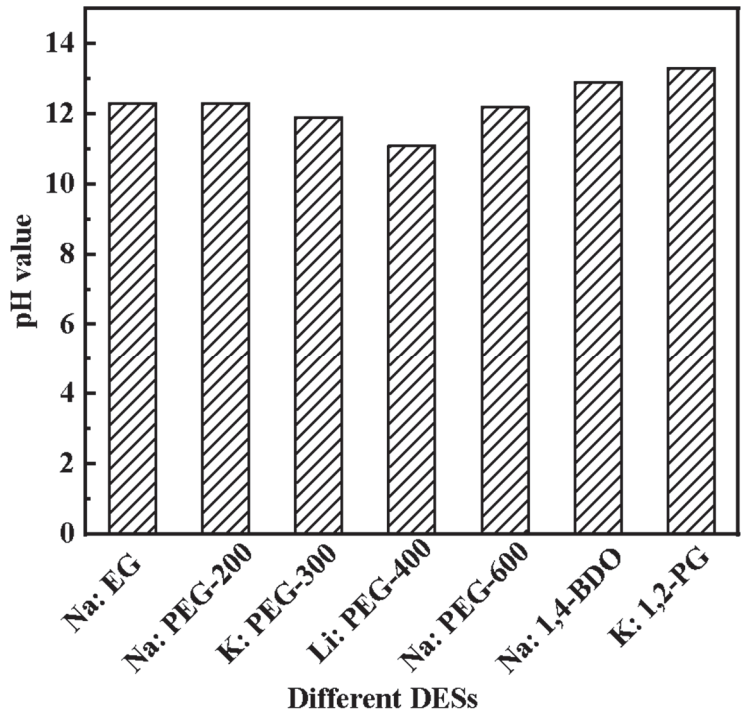

Figure 2. pH values of different DESs (the pH values were obtained by measuring 0.1 mol·L^{-1} DES aqueous solutions).

In addition, the pH values of DESs influence the pretreatment effects. Figure 3 illustrates the relationship between the pH values of DESs and the results of lignin or hemicellulose removal. As shown in Figure 3, the higher the pH values of DESs, the greater the amount of lignin and hemicellulose that is removed. Therefore, K: 1,2-PG can remove more lignin and hemicellulose than other DESs, which can be explained by our previous study, in which the lignin–carbohydrate complex and deacetylation of hemicellulose were destroyed by removing the carbonyl group in hemicellulose and cutting off the ester bond between lignin and hemicellulose during basic DES pretreatment [13].

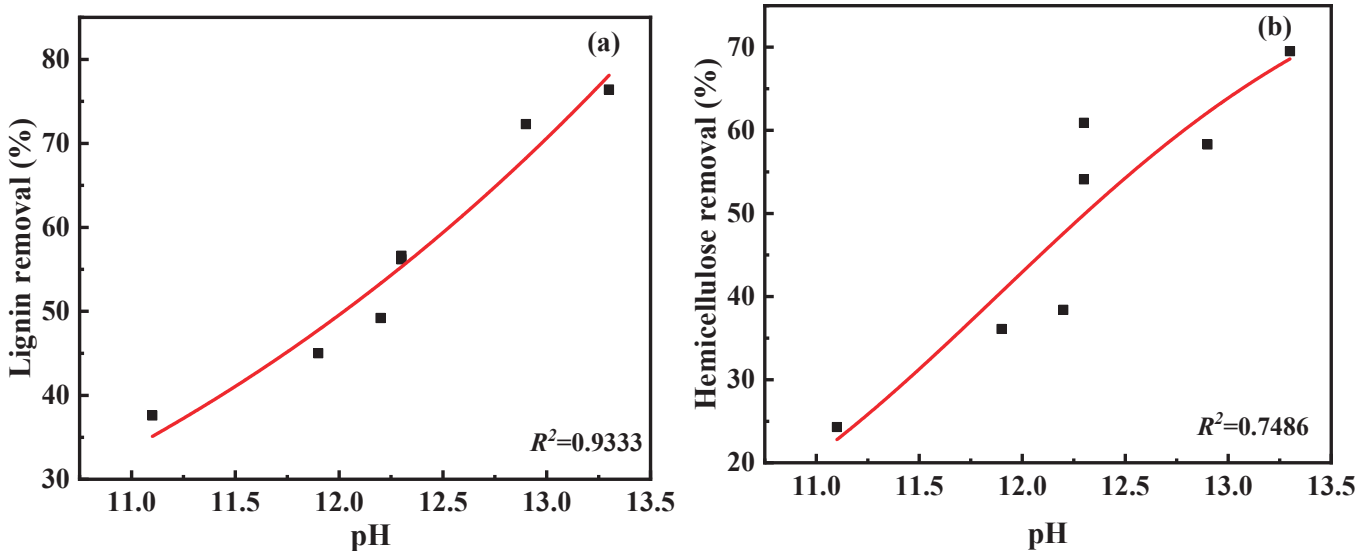

Figure 3. The relationship of lignin removal (**a**) and hemicellulose removal (**b**) with the pH values of different DESs.

Figure 4 shows the influence of DES species on the initial saccharification rate and the reducing sugar yield during the enzyme-catalyzed hydrolysis of poplar wood. According to Figure 4a, the initial saccharification rates of Na: EG-, Na: PEG-200-, K: PEG-300-, Li: PEG-400- and Na: PEG-600-pretreated residues were similar to that of untreated poplar wood (2.7–3.6 mg·mL^{-1}·h^{-1} vs. 2.6 mg·mL^{-1}·h^{-1}) during enzymatic hydrolysis. However, the Na: 1,4-BDO and K: 1,2-PG pretreatment process for poplar wood can significantly increase the initial saccharification rate, i.e., 5.7 mg·mL^{-1}·h^{-1} and 7.5 mg·mL^{-1}·h^{-1}. In particular, the initial saccharification rate of K: 1,2-PG-pretreated residues was its maximum, which is in agreement with the results obtained from pretreatment in Figure 1.

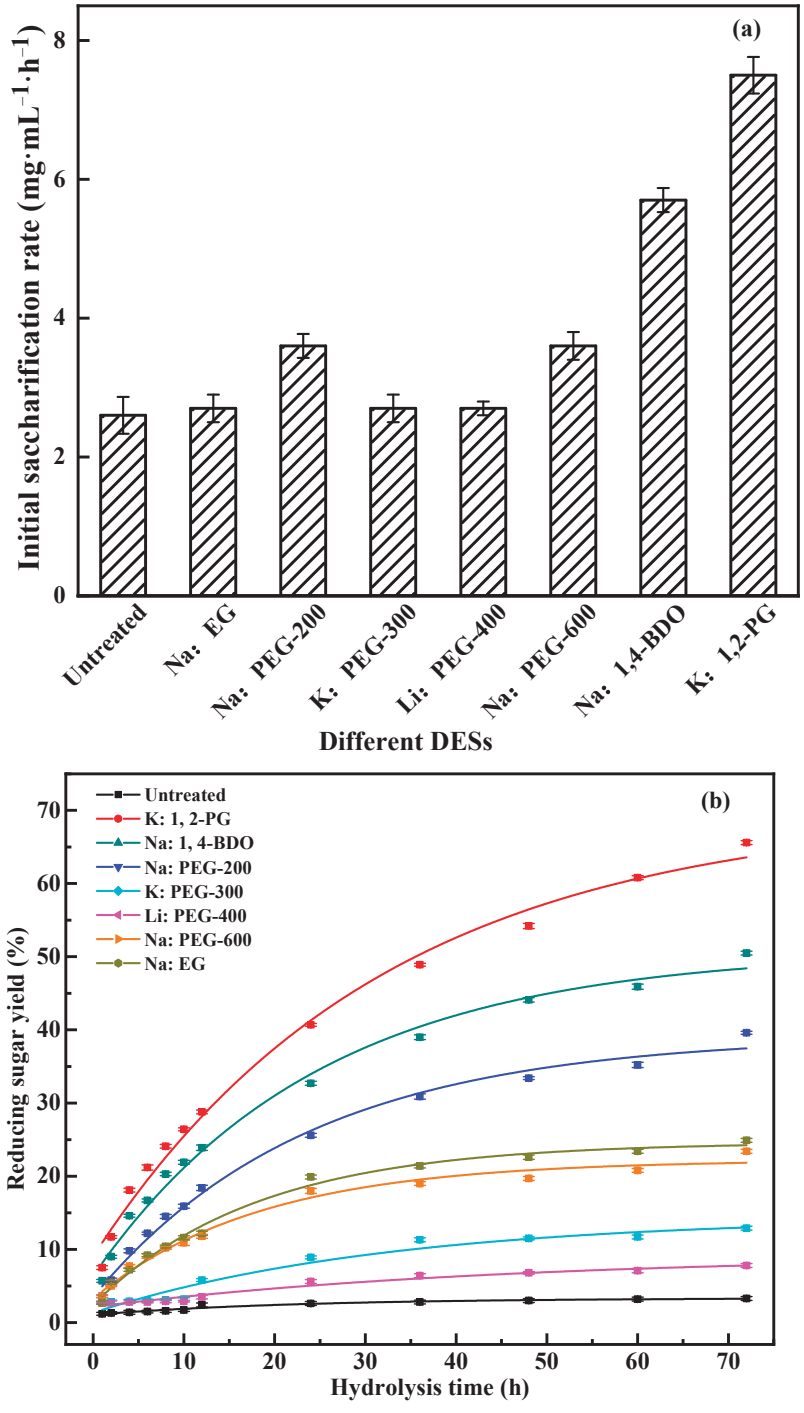

Figure 4. Effect of DES types on enzymatic hydrolysis: (**a**) initial saccharification rate; (**b**) reducing sugar yield.

As observed from Figure 4b, except for Na: EG, the other two diol-based DESs more effectively promoted the production of reducing sugar than PEG-based DESs did. For instance, compared with untreated poplar wood, the reducing sugar yield of Na: PEG-200-, K: PEG-300-, Li: PEG-400- and Na: PEG-600-pretreated residues did not increase significantly (3.3% vs. 7.8–39.6%), while the reducing sugar yields of Na: 1,4-BDO- and K: 1,2-PG-pretreated residues after hydrolysis for 72 h were 15.3 and 19.9 times higher, respectively, than that of untreated poplar wood (i.e., 3.3% vs. 50.5% and 65.6%). This is because the removal of both lignin and hemicellulose has a positive relationship with the reducing sugar yield, as shown in Figure 5. The more lignin and hemicellulose was removed, the higher the obtained reducing sugar yield was, indicating that the removal of lignin and hemicellulose is beneficial to enzyme hydrolysis. From Figures 1 and 4, the pretreatment and hydrolysis results of K: 1,2-PG-pretreated residue were the best of the seven DES-pretreated residues. The lignin and hemicellulose removal reached 76.4% and 69.5%, respectively. About 65.6% of reducing sugar was produced during hydrolysis for 72 h. As a consequence, K: 1,2-PG was determined to be the most effective solvent promoting enzymatic hydrolysis among these seven DESs.

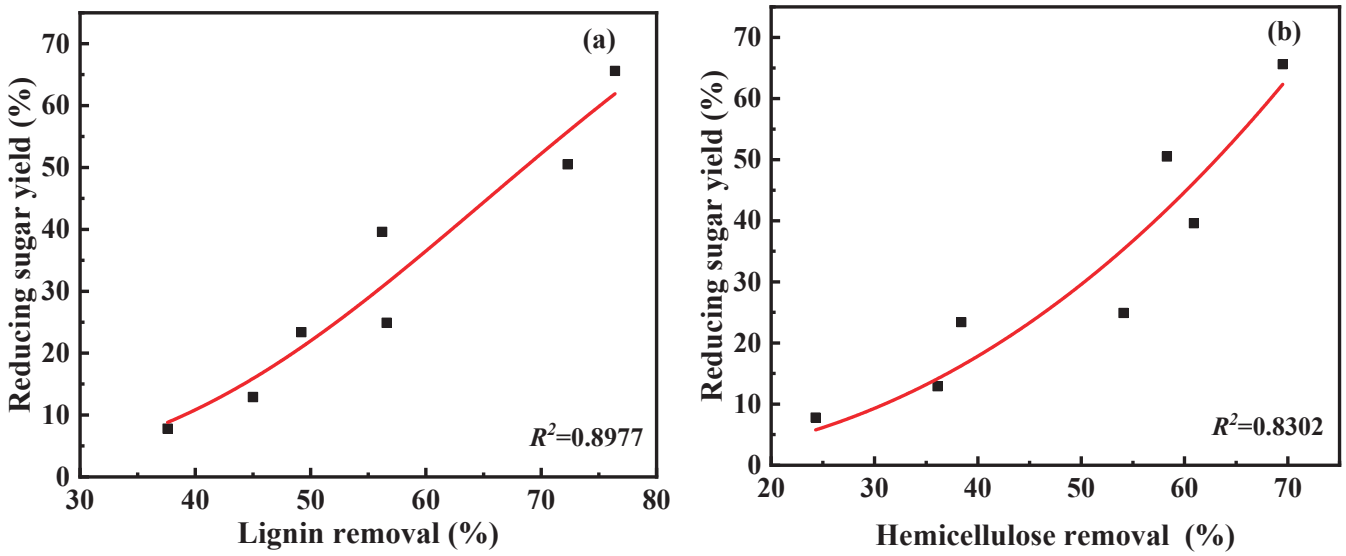

Figure 5. The relationship of reducing sugar yield (72 h) with lignin removal (**a**) or hemicellulose removal (**b**).

3.2. Influence of Pretreatment Temperature on Pretreatment of Poplar Wood

Figure 6 illustrates the effect of the pretreatment temperature on the pretreatment of poplar wood. It can be observed from Figure 6 that, as the temperature increased, the lignin and hemicellulose removal gradually increased from 48.1% to 97.4% and from 48.3% to 91.2%, respectively. This indicates that a high pretreatment temperature contributes to the removal of lignin and hemicellulose. The reason may be that the viscosity of K: 1,2-PG decreases with increasing temperature, and the lower the viscosity, the more diffusible the solute is in the solvent, increasing the contact opportunities between poplar wood and K: 1,2-PG. In addition, there was no obvious change in the lignin removal when the pretreatment temperature was elevated from 130 °C to 170 °C (e.g., 91.1–97.4%). However, cellulose preservation gradually decreased with the increase in the pretreatment temperature. Notably, there was a significant decrease in cellulose preservation from 93.8% to 39.2% when the pretreatment temperature increased from 130 °C to 170 °C, which indicates that an excessive pretreatment temperature causes the degradation of cellulose, resulting in a significant loss of cellulose. Therefore, the balance between the lignin and hemicellulose removal and the cellulose loss should be considered comprehensively. From the perspective of the pretreatment effect, 130 °C can be selected as the suitable pretreatment temperature.

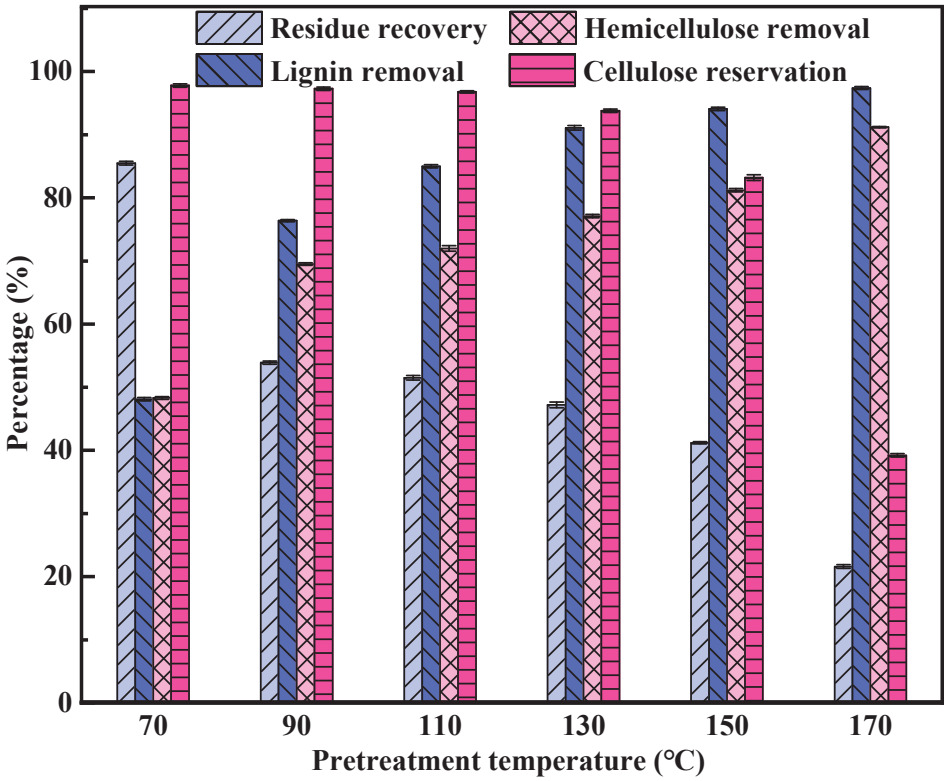

Figure 6. Influence of pretreatment temperature on pretreatment of poplar wood.

Figure 7 exhibits the influence of pretreatment temperature on the hydrolysis results. As shown in Figure 7, the reducing sugar yields and initial saccharification rates of residues obtained from pretreatment at different temperatures all increased in comparison with untreated poplar wood. With the increase in the pretreatment temperature, the reducing sugar yield and initial saccharification rate after hydrolysis for 72 h first gradually increased and then gradually decreased. When the pretreatment temperature was elevated from 70 °C to 130 °C, the reducing sugar yield (hydrolysis for 72 h) and initial saccharification rate increased from 34.1% to 82.6% and from 3.2 $mg \cdot mL^{-1} \cdot h^{-1}$ to 11.7 $mg \cdot mL^{-1} \cdot h^{-1}$, respectively. Nonetheless, when the pretreatment temperature increased from 130 °C to 170 °C, the reducing sugar yield and initial saccharification rate began to decrease gradually from 82.6% to 81.6% and from 11.7 $mg \cdot mL^{-1} \cdot h^{-1}$ to 4.9 $mg \cdot mL^{-1} \cdot h^{-1}$, respectively. This is because degradation products such as organic acids, furfural and phenolic compounds, which were produced during the pretreatment of poplar wood at an excessive pretreatment temperature, may inhibit the cellulase activity, resulting in a low reducing sugar yield and initial saccharification rate.

Consequentially, 130 °C was chosen as the best pretreatment temperature for further investigation. As a result, 91.1% of lignin and 77.1% of hemicellulose were removed, and 93.8% of cellulose was preserved during the pretreatment of poplar wood using K: 1,2-PG at 130 °C for 11 h. The reducing sugar yield reached 82.6% after 72 h of enzymatic hydrolysis.

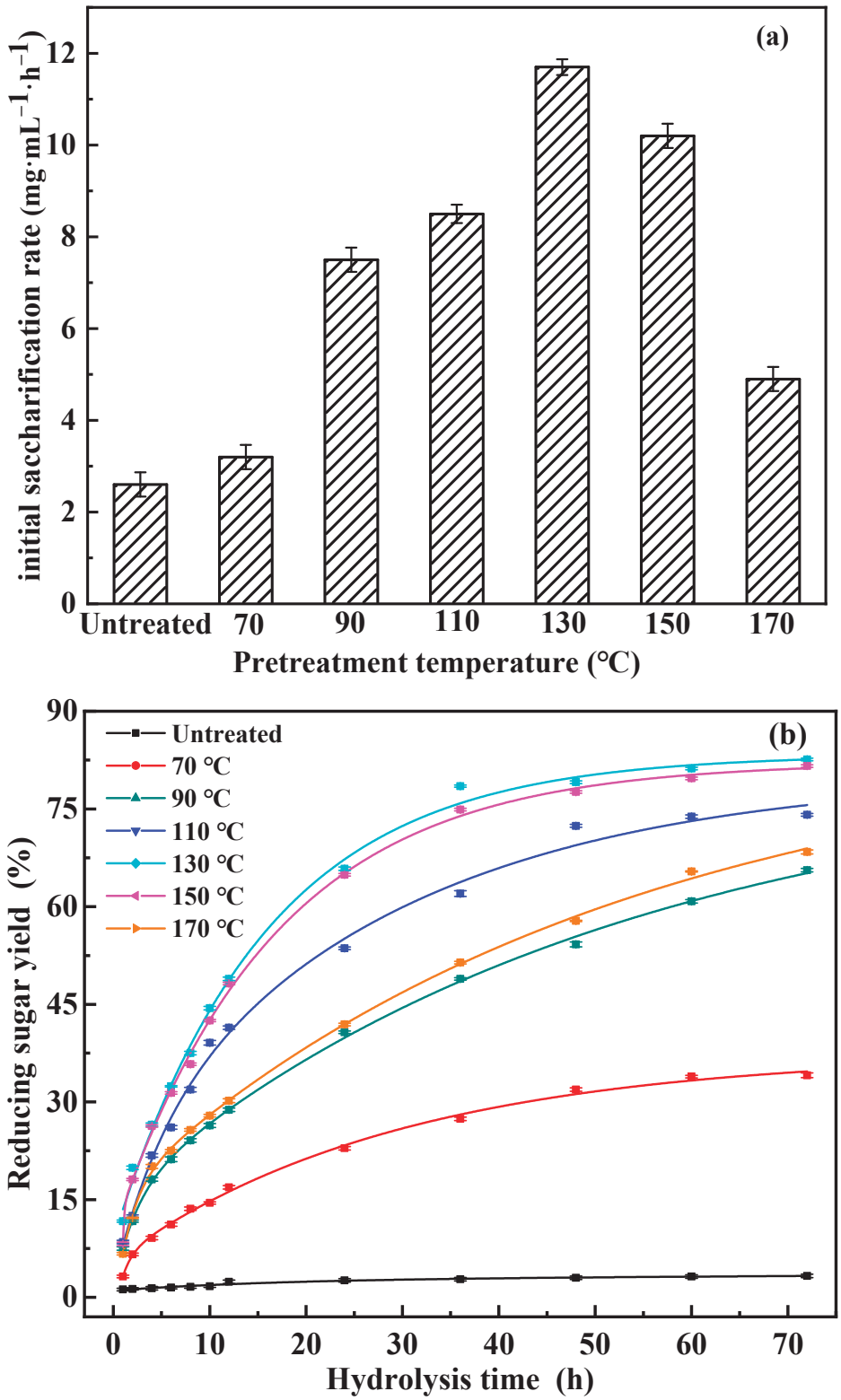

Figure 7. Influence of pretreatment temperature on enzymatic hydrolysis: (**a**) initial saccharification rate; (**b**) reducing sugar yield.

3.3. Influence of Pretreatment Time on Pretreatment of Poplar Wood

Figure 8 depicted the influence of pretreatment time on the residue recovery, lignin removal, hemicellulose removal and cellulose preservation of poplar wood. Figure 8 shows that the residue recovery and cellulose reservation slowly decreased from 50.6% to 46.3%

and from 97.5% to 92.7% with the increase in pretreatment time, respectively, while when the operation time increased, the lignin removal slowly increased from 89.2% to 93.9% and the hemicellulose removal increased from 71.6% to 77.1%. These results indicate that pretreatment time has little effect on poplar wood.

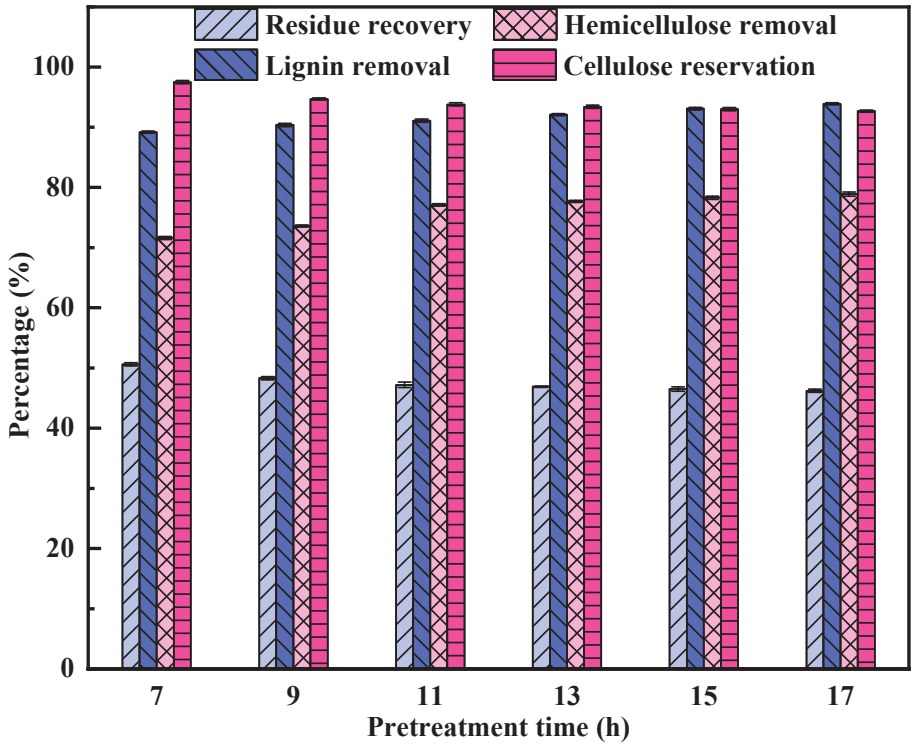

Figure 8. Influence of pretreatment time on the pretreatment of poplar wood.

Figure 9 shows the influence of pretreatment time on the hydrolysis efficiency of poplar wood. As observed from Figure 9, both the reducing sugar yield (72 h) and initial saccharification rate of poplar wood residue for enzymatic hydrolysis were higher than those of untreated poplar wood (82.5~87.3% vs. 3.3% and 10.2–13.2 $mg \cdot mL^{-1} \cdot h^{-1}$ vs. 2.6 $mg \cdot mL^{-1} \cdot h^{-1}$). These phenomena demonstrate that the removal of lignin and hemicellulose promoted the hydrolysis of poplar wood. Furthermore, the reducing sugar yield (72 h) and initial saccharification rate slowly increased from 82.5% to 87.3% and from 10.2 $mg \cdot mL^{-1} \cdot h^{-1}$ to 13.2 $mg \cdot mL^{-1} \cdot h^{-1}$ as the pretreatment time increased from 7 h to 17 h. The lower hydrolysis results indicate that enzymatic hydrolysis efficiency is not sensitive to pretreatment time.

Therefore, 7 h was chosen as the best pretreatment time. The lignin and hemicellulose removal rates were 89.2% and 71.6%, and the cellulose preservation rate was 97.5% when the poplar wood was pretreated with K: 1,2-PG at 130 °C for 7 h. While the pretreated poplar wood was hydrolyzed by enzymes for 72 h, the reducing sugar yield reached 82.5%.

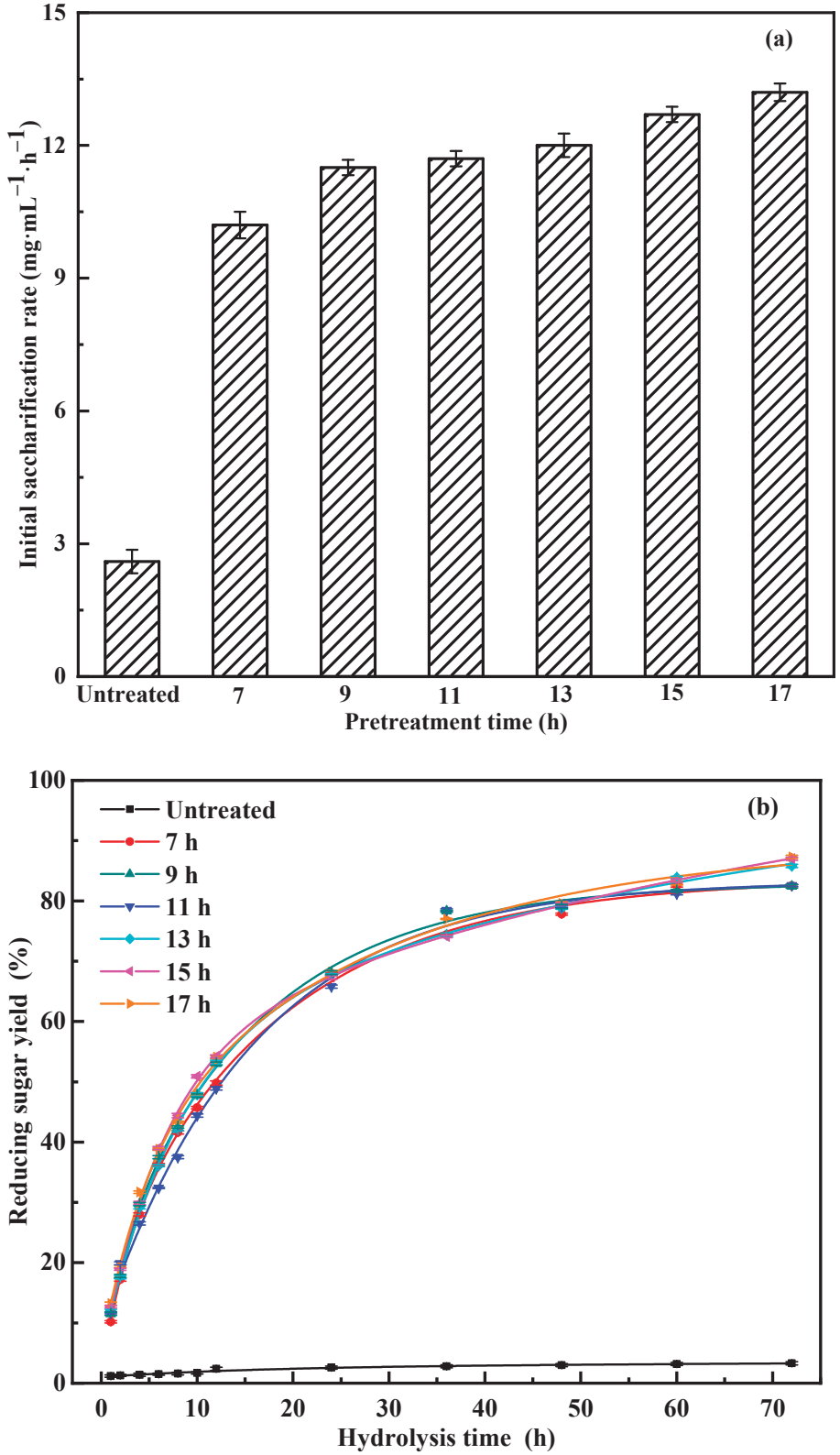

Figure 9. Influence of pretreatment time on enzymatic hydrolysis: (**a**) initial saccharification rate; (**b**) reducing sugar yield.

3.4. Comparison of Different Pretreatment Methods

Figure 10 compares the different methods of poplar wood pretreatment. The pretreatment efficiency of K: 1,2-PG was superior to that of choline chloride: guaiacol: aluminum

chloride (molar ratio 25: 50:1, C:G:A) [23], choline chloride:lactic acid (molar ratio 1:8, C:L) [24] and 1-ethyl-3-methyl-imidazolium acetate ([C_2mim][OAc]) [25]. For example, K: 1,2-PG removed the greatest amount of lignin and the lowest amount of cellulose of the four pretreatment solvents (89.2% vs. 58.0–88.0% and 97.5% vs. 87.5–94.1%). More significantly, the reducing sugar yield of poplar wood pretreated with K: 1,2-PG exhibited values higher than or similar to those of poplar wood pretreated with the other two DESs, or [C_2mim][OAc], after enzymatic hydrolysis for 72 h (82.5% vs. 32.6–88.2%).

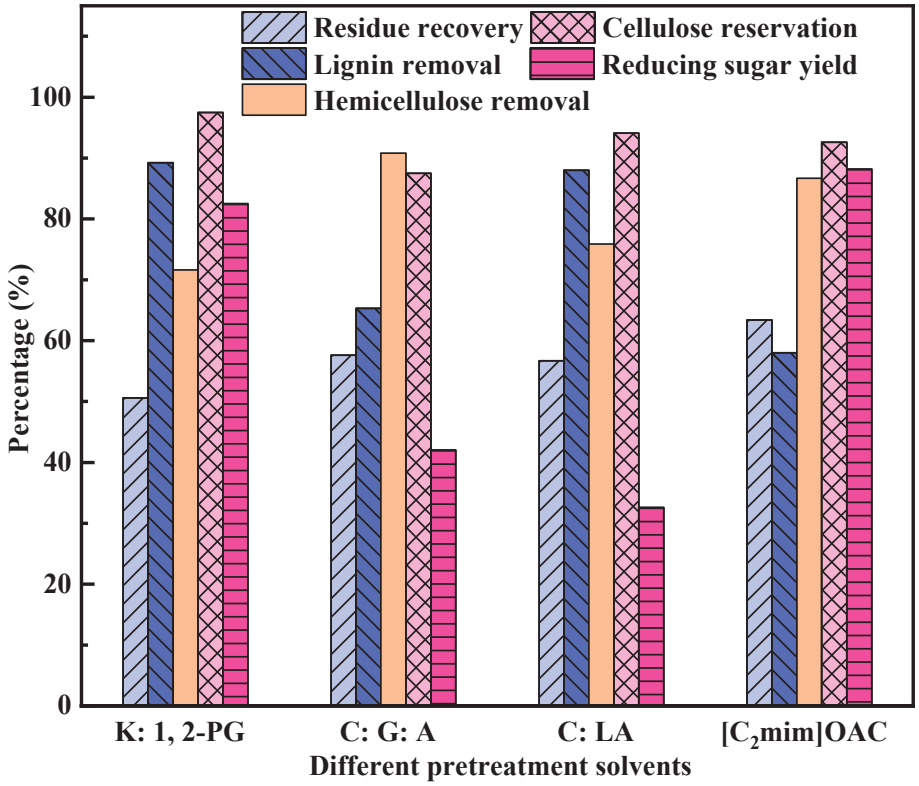

Figure 10. Comparison of different methods of poplar wood pretreatment.

3.5. Structural Characterization of Poplar Wood

3.5.1. XRD

Figure 11 shows the XRD pattern of poplar wood samples before and after pretreatment. From Figure 11, we can observe that the change in the cellulose crystal structure (CrI value) of poplar wood before and after pretreatment with K: 1,2-PG was investigated. The CrI value of K: 1,2-PG-pretreated poplar wood was significantly higher than that of untreated poplar wood (e.g., 57.1 vs. 48.3). This indicates that the crystallinity of pretreated poplar wood significantly increased compared with untreated poplar wood. The increased crystallinity was due to K: 1,2-PG, which has a stronger capacity to remove amorphous structures, i.e., lignin and hemicellulose, than that of structurally ordered cellulose. For example, 89.2% of lignin and 71.6% of hemicellulose were removed, while only 2.5% of cellulose was lost during the pretreatment process with K: 1,2-PG at 130 °C for 7 h.

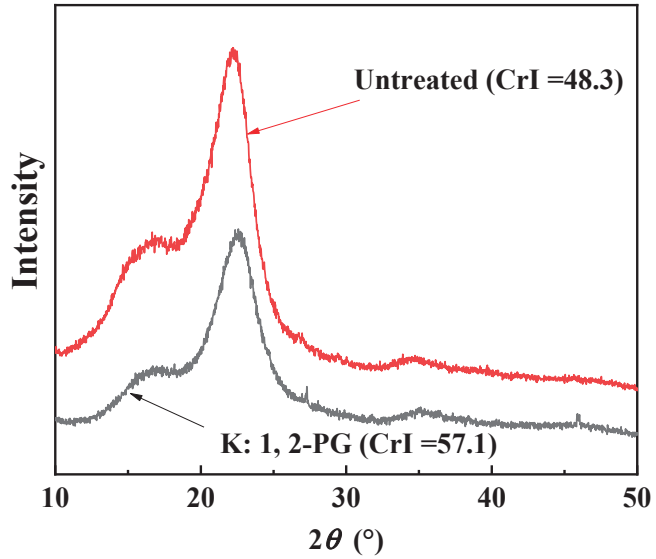

Figure 11. XRD pattern of poplar wood samples before and after K: 1,2-PG pretreatment (pretreatment conditions: 130 °C, 7 h).

3.5.2. FT-IR

Figure 12 depicts the FT-IR spectra of the poplar wood sample before and after K: 1,2-PG pretreatment. As shown in Figure 12, the peaks of K: 1,2-PG-pretreated poplar wood at 1737 cm^{-1}, 1602 cm^{-1}, 1510 cm^{-1} and 1245 cm^{-1} almost disappeared compared with untreated poplar wood. The peak at 1737 cm^{-1} represents the C=O stretching vibration peak in the carbonyl or ester groups. The disappearance of this peak demonstrates that K: 1,2-PG removed the carbonyl group in hemicellulose and cut off the ester bond between lignin and hemicellulose. The peaks at 1602 cm^{-1}, 1510 cm^{-1} and 1245 cm^{-1} represent the aromatic ring skeleton vibration peaks of lignin. The near-disappearance of these peaks illustrates that K: 1,2-PG destroyed the aromatic ring structure of lignin [26–29]. The results obtained from the FT-IR spectra, which were in accordance with the results of pretreatment, confirmed the removal of lignin and hemicellulose.

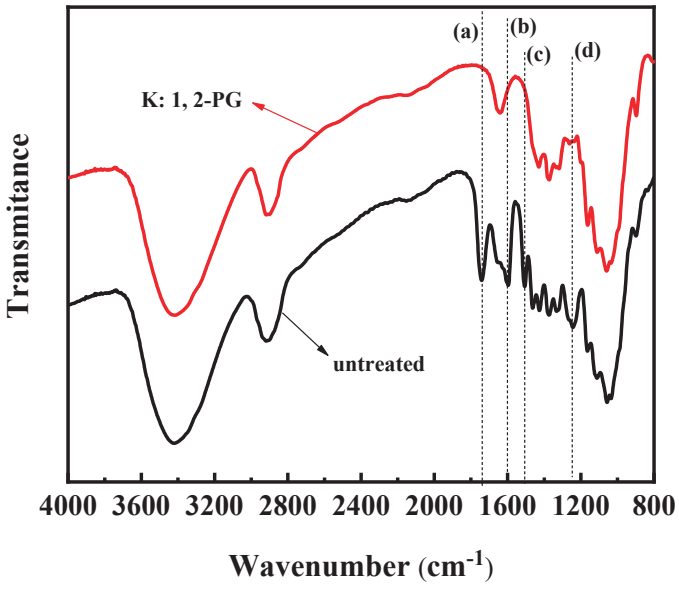

Figure 12. FT-IR spectra of poplar wood samples before and after K: 1,2-PG pretreatment: (**a**) 1737 cm^{-1}, (**b**) 1602 cm^{-1}, (**c**) 1510 cm^{-1} and (**d**) 1245 cm^{-1}.

3.5.3. SEM

Figure 13 illustrates the surface morphology of poplar wood before and after K: 1,2-PG pretreatment. As observed from Figure 13a,b, the intact surface of the untreated poplar wood was displayed, and as a result, it was difficult to see the internal cellulose structure. Figure 13c,d show that many pore structures appeared on the surface of K: 1,2-PG-pretreated residue, and a large number of fiber bundles were distributed in a disorganized manner, which greatly improved the contact area between the enzyme and the cellulose. The broken structure was caused by the removal of lignin and hemicellulose. Hence, the variations in the surface morphology between the untreated and pretreated poplar wood confirm that the removal of lignin and hemicellulose resulted from K: 1,2-PG pretreatment of poplar wood.

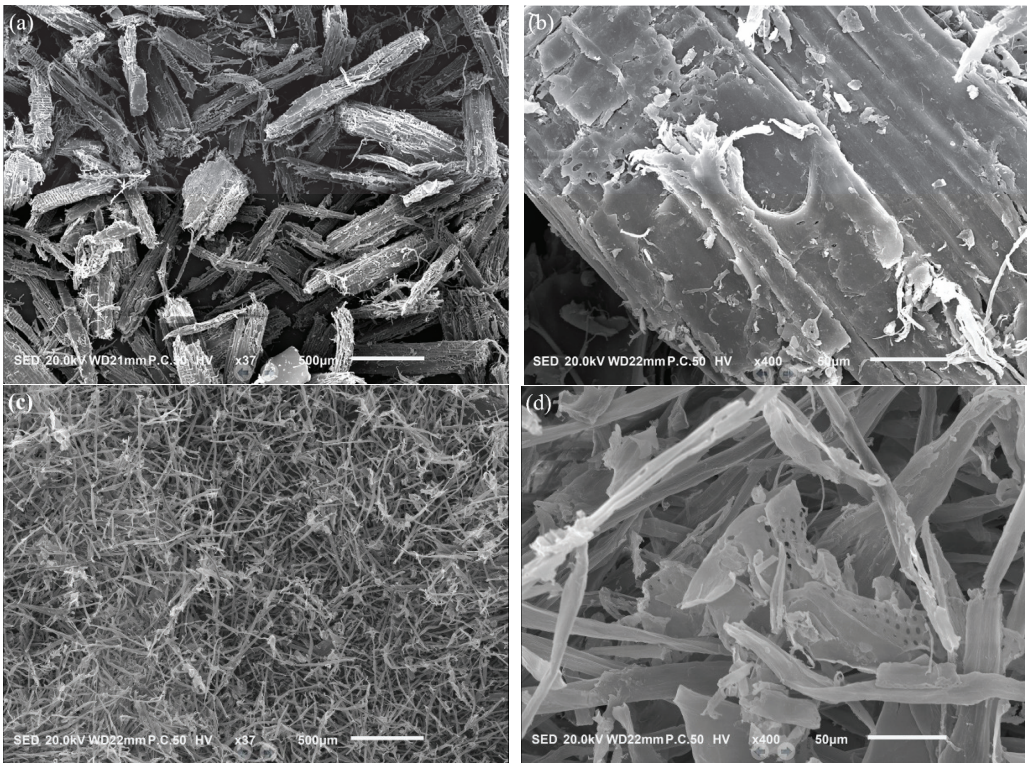

Figure 13. Surface morphology of poplar wood before and after K: 1,2-PG pretreatment: (**a**) untreated poplar wood × 37, (**b**) untreated poplar wood × 400, (**c**) K: 1,2-PG-pretreated poplar wood × 37 and (**d**) K: 1,2-PG-pretreated poplar wood × 400.

4. Conclusions

Seven basic DESs based on diol were screened for their ability to improve enzymatic hydrolysis in poplar wood pretreatment. Among these DESs, the pretreatment effects of diol monomer-based DESs were better than those of PEG-based DESs. The best pretreatment and hydrolysis results were obtained using a K: 1,2-PG pretreatment process (pretreatment conditions: 130 °C, 7 h), which furthered the enzymatic hydrolysis process (hydrolysis time: 72 h). As a result, the higher the pH of the DES, the greater the amounts of lignin and hemicellulose that were removed. For instance, the lignin and hemicellulose removal rates were 89.2% and 71.6%, the cellulose preservation rate was 97.5% and the reducing sugar yield reached 82.5%. Otherwise, the results of the FT-IR, XRD and SEM analyses all confirmed the removal of lignin and hemicellulose and revealed the pretreatment mechanism by which K: 1,2-PG removes lignin and hemicellulose by cutting the ester bond between lignin and hemicellulose, breaking the carbonyl group of hemicellulose and the aromatic ring structure of lignin. Thus, the establishment of this new pretreatment system will promote enzymatic hydrolysis in poplar wood.

Author Contributions: Conceptualization, X.Z. and Z.Z.; formal analysis, X.Z., Z.Z. and Y.Z.; investigation, X.Z., Z.Z., Y.Z. and T.Z.; project administration, Z.Z.; resources, L.H., X.S. and Z.Z.; supervision, L.H., X.S. and Z.Z.; writing—original draft, X.Z., Z.Z., Y.Z. and T.Z.; writing—review and editing, Y.Z. and Z.Z. All authors have read and agreed to the published version of the manuscript.

Funding: This research was funded by the Basic Scientific Research Project of Colleges and Universities of the Hebei Province, grant number JQN2022011, and the Key Program of Hebei Province Department of Science and Technology, grant number 20373805D.

Data Availability Statement: The data are listed in this paper.

Conflicts of Interest: The authors declare no conflict of interest.

References

1. Shang, Z.J. *Risk Management Study of HNJY Biomass Cogeneration Project*; Shandong University: Jinan, China, 2021.
2. Mosier, N.; Wyman, C.; Dale, B.; Elander, R.; Lee, Y.Y.; Holtzapple, M.; Ladisch, M. Features of promising technologies for pretreatment of lignocellulosic biomass. *Bioresour. Technol.* **2005**, *96*, 673–686. [CrossRef] [PubMed]
3. Zhang, L.; Xu, C.C.; Champagne, P. Overview of recent advances in thermo-chemical conversion of biomass. *Energ. Convers. Manag.* **2010**, *51*, 969–982. [CrossRef]
4. Prasad, S.; Malav, M.K.; Kumar, S.; Singh, A.; Pant, D.; Radhakrishnan, S. Enhancement of bio-ethanol production potential of wheat straw by reducing furfural and 5-hydroxymethylfurfural. *Bioresour. Technol.* **2018**, *4*, 50–56. [CrossRef]
5. Haque, M.A.; Barman, D.N.; Kang, T.H.; Kim, M.K.; Kim, J.; Kim, H.; Yun, H.D. Effect of dilute alkali on structural features and enzymatic hydrolysis of barley straw (Hordeum vulgare) at boiling temperature with low residence time. *J. Microbiol. Biotech.* **2012**, *22*, 1681–1691. [CrossRef] [PubMed]
6. Te, M.T.D.; Kersten, S.R.; Lange, J.P.; Ruiz, M.P. Cellulosic glycols: An integrated process concept for lignocellulose pretreatment and hydrogenolysis. *Biofuels Bioprod. Biorefining* **2021**, *15*, 1725–1736.
7. Luo, J.; Xu, Y. Comparison of biological and chemical pretreatment on coproduction of pectin and fermentable sugars from apple pomace. *Appl. Biochem. Biotech.* **2020**, *190*, 129–137. [CrossRef]
8. Peleteiro, S.; Rivas, S.; Alonso, J.L.; Santos, V.; Parajo, J.C. Utilization of ionic liquids in lignocellulose biorefineries as agents for separation, derivatization, fractionation, or pretreatment. *J. Agric. Food Chem.* **2015**, *63*, 8093–8102. [CrossRef]
9. Lee, K.M.; Hong, J.Y.; Tey, W.Y. Combination of ultrasonication and deep eutectic solvent in pretreatment of lignocellulosic biomass for enhanced enzymatic saccharification. *Cellulose* **2021**, *28*, 1513–1526. [CrossRef]
10. Sai, Y.W.; Lee, K.M. Enhanced cellulase accessibility using acid-based deep eutectic solvent in pretreatment of empty fruit bunches. *Cellulose* **2019**, *26*, 9517–9528. [CrossRef]
11. Li, L.; Yu, L.; Wu, Z.; Hu, Y. Delignification of poplar wood with lactic acid-based deep eutectic solvents. *Wood Res.* **2019**, *64*, 499–514.
12. Wu, M.; Gong, L.; Ma, C.; He, Y.C. Enhanced enzymatic saccharification of sorghum straw by effective delignification via combined pretreatment with alkali extraction and deep eutectic solvent soaking. *Bioresour. Technol.* **2021**, *340*, 125695. [CrossRef] [PubMed]
13. Zhao, Z.; Chen, X.; Ali, M.F.; Abdeltawab, A.A.; Yakout, S.M.; Yu, G. Pretreatment of wheat straw using basic ethanolamine-based deep eutectic solvents for improving enzymatic hydrolysis. *Bioresour. Technol.* **2018**, *263*, 325–333. [CrossRef] [PubMed]
14. Zhao, X.; Han, L.; Ma, X.; Sun, X.; Zhao, Z. Enhanced Enzymatic Hydrolysis of Wheat Straw to Improve Reducing Sugar Yield by Novel Method under Mild Conditions. *Processes* **2023**, *11*, 898. [CrossRef]
15. Chen, J.; Ali, M.C.; Liu, R.; Munyemana, J.C.; Li, Z.; Zhai, H.; Qiu, H. Basic deep eutectic solvents as reactant, template and solvents for ultra-fast preparation of transition metal oxide nanomaterials. *Chin. Chem. Lett.* **2020**, *31*, 1584–1587. [CrossRef]
16. Ali, M.C.; Liu, R.; Chen, J.; Cai, T.; Zhang, H.; Li, Z.; Qiu, H. New deep eutectic solvents composed of crown ether, hydroxide and polyethylene glycol for extraction of non-basic N-compounds. *Chin. Chem. Lett.* **2019**, *30*, 871–874. [CrossRef]
17. Li, Y.; Zhuo, J.; Liu, P.; Chen, P.; Hu, H.; Wang, Y.; Zhou, S.; Tu, Y.; Peng, L.; Wang, Y. Distinct wall polymer deconstruction for high biomass digestibility under chemical pretreatment in Miscanthus and rice. *Carbohydr. Polym.* **2018**, *192*, 273–281. [CrossRef]
18. Sluiter, A.; Hames, B.; Ruiz, R.; Scarlata, C.; Sluiter, J.; Templeton, D.; Crocker, D.L.A.P. Determination of structural carbohydrates and lignin in biomass. *Lab. Anal. Proced.* **2008**, *1617*, 1–16.
19. Fry, S.C. *The Growing Plant Cell Wall: Chemical and Metabolic Analysis*; The Blackburn Press: Caldwell, NJ, USA, 1988.
20. Hossain, M.A.; Rahaman, M.S.; Yelle, D.; Shang, H.; Sun, Z.; Renneckar, S.; Dong, J.; Tulaphol, S.; Sathitsuksanoh, N. Effects of polyol-based deep eutectic solvents on the efficiency of rice straw enzymatic hydrolysis. *Ind. Crops Prod.* **2021**, *167*, 113480. [CrossRef]
21. Mamilla, J.L.K.; Novak, U.; Grilc, M.; Likozar, B. Natural deep eutectic solvents (DES) for fractionation of waste lignocellulosic biomass and its cascade conversion to value-added bio-based chemicals. *Biomass Bioenergy* **2019**, *120*, 417–425. [CrossRef]
22. Zhao, Z.; Yang, Y.; Abdeltawab, A.A.; Yakout, S.M.; Chen, X.; Yu, G. Cholinium amino acids-glycerol mixtures: New class of solvents for pretreating wheat straw to facilitate enzymatic hydrolysis. *Bioresour. Technol.* **2017**, *245*, 625–632. [CrossRef]

23. Huang, C.; Zhan, Y.; Cheng, J.; Wang, J.; Meng, X.; Zhou, X.; Ragauskas, A.J. Facilitating enzymatic hydrolysis with a novel guaiacol-based deep eutectic solvent pretreatment. *Bioresour. Technol.* **2021**, *326*, 124696. [CrossRef] [PubMed]
24. Su, Y.; Huang, C.; Lai, C.; Yong, Q. Green solvent pretreatment for enhanced production of sugars and antioxidative lignin from poplar. *Bioresour. Technol.* **2021**, *321*, 124471. [CrossRef] [PubMed]
25. Yuan, T.Q.; Wang, W.; Xu, F.; Sun, R.C. Synergistic benefits of ionic liquid and alkaline pretreatments of poplar wood. Part 1: Effect of integrated pretreatment on enzymatic hydrolysis. *Bioresour. Technol.* **2013**, *144*, 429–434. [CrossRef] [PubMed]
26. Francisco, M.; Van, D.B.A.; Kroon, M.C. New natural and renewable low transition temperature mixtures (LTTMs): Screening as solvents for lignocellulosic biomass processing. *Green Chem.* **2012**, *14*, 2153–2157. [CrossRef]
27. Nor, N.A.M.; Mustapha, W.A.W.; Hassan, O. Deep eutectic solvent (DES) as a pretreatment for oil palm empty fruit bunch (OPEFB) in sugar production. *Procedia Chem.* **2016**, *18*, 147–154. [CrossRef]
28. Han, Y.; Bai, Y.; Zhang, J.; Liu, D.; Zhao, X. A comparison of different oxidative pretreatments on polysaccharide hydrolyzability and cell wall structure for interpreting the greatly improved enzymatic digestibility of sugarcane bagasse by delignification. *Bioresour. Bioprocess.* **2020**, *7*, 24. [CrossRef]
29. Sun, F.F.; Wang, L.; Hong, J.; Ren, J.; Du, F.; Hu, J.; Zhou, B. The impact of glycerol organosolv pretreatment on the chemistry and enzymatic hydrolyzability of wheat straw. *Bioresour. Technol.* **2015**, *187*, 354–361. [CrossRef]

MDPI AG
Grosspeteranlage 5
4052 Basel
Switzerland
Tel.: +41 61 683 77 34

Processes Editorial Office
E-mail: processes@mdpi.com
www.mdpi.com/journal/processes

MDPI

Academic Open
Access Publishing

mdpi.com

ISBN 978-3-7258-6004-3